JOHANNES GUTENBERG UNIVERSITÄT MAINZ

Development and Evaluation of Radiotracers for Tumor Imaging via Positron Emission Tomography

Dissertation

zur Erlangung des Grades eines
"Doktor rerum naturalium (Dr. rer. nat.)"
im Promotionsfach Chemie

Am Fachbereich Chemie, Pharmazie und Geowissenschaften
der Johannes Gutenberg-Universität Mainz

Kathrin Kettenbach

geboren in Mainz

Mainz, im Februar 2017

Dekan:

Erster Berichterstatter:

Zweiter Berichterstatter:

Tag der mündlichen Prüfung: 06.06.2017

Die vorliegende Arbeit wurde in der Zeit von 2013 bis 2017 am Institut für Kernchemie der Johannes Gutenberg-Universität Mainz angefertigt.

„I hereby declare that I wrote the dissertation submitted without any unauthorized external assistance and used only sources acknowledged in this work. All textual passages which are appropriated verbatim or paraphrased from published and unpublished texts as well as information obtained from oral sources are duly indicated and listed in accordance with bibliographical rules. In carrying out this research, I complied with the rules of standard scientific practice as formulated in the statutes of Johannes Gutenberg-University Mainz to insure standard scientific practice."

Mainz, Februar 2017

Abstract

Positron emission tomography (PET) enables the non-invasive imaging of metabolical processes in the human body. Thus, the use of radiolabeled cancer-specific targeting vectors can facilitate early diagnosis of tumors. A robust and reliable attachment of the radionuclide to the bioactive compound without major influences on its pharmacokinetic behavior is mandatory for routine PET imaging. In the herein presented work two different ^{18}F-prosthetic groups for the radiolabeling of biomolecule-azides via click chemistry were evaluated.

First, a strained prosthetic group based on (aza)dibenzocyclooctyne (DBCO) was developed to enable copper-free strain-promoted alkyne-azide cycloadditions (SPAAC) with biomolecule-azides. The radiolabeling conditions were evaluated and optimized providing [^{18}F]fluoro-DBCO in good radiochemical yields and within a suitable synthesis time. Click reactions with various azides (cRGD, ɲMSH peptides, maltohexaose, PDGF-ɴ peptide) showed very high yields under mild conditions, which proved the general feasibility of this novel prosthetic group for the labeling of sensitive biomolecules with fluorine-18.

The oxidized form of folic acid (5,6,7,8-tetrahydrofolate, THF) plays an important role as one-carbon donor during DNA synthesis. The reduced folate carrier (RFC) provides sufficient supply of THF for normal cell proliferation. Tumors additionally (over)express the folate receptor (FR) due to their increased proliferation rate. This makes the FR an ideal oncological target for diagnosis and therapy. Most of the ^{18}F-labeled folate derivatives until now suffer from either insufficient radiolabeling or unfavorable *in vivo* behavior. Especially the need of cytotoxic copper during click radiolabeling might hinder the application of [^{18}F]fluoro-click-folates for human use. On one hand the novel [^{18}F]fluoroDBCO was used for the copper-free radiofluorination of a folate-azide. On the other hand, the recently reported [^{18}F]fluoro-alakyne was applied to the same folate-azide to improve its pharmacokinetic behavior. Both [^{18}F]fluoro-folates were available in good radiochemical yields and showed high affinities to the FR. Unfortunately, the DBCO-moiety increased the overall lipophilicity of this novel folate-based radiotracer. Thus, high unspecific binding was observed in cell studies and the tumor was not visible in µPET imaging studies due to high abdominal background. In contrast, the [^{18}f]fluoro-alafolate showed a much more favorable lipophilitity reducing the unspecific binding *in vitro* and provided moderate tumor accumulation combined with a suitable tumor-to-background contrast.

In a second part of this work, [^{18}F]fluoro-alakyne was evaluated as a tumor imaging candidate. Tumors in general show a high demand on amino acids due to an increased protein synthesis rate. Most of the amino acid based radiotracers suffer from unwanted accumulation in the abdominal region, limiting the application of these radiotracers for the detection of brain tumors. [^{18}F]fluoro-alakyne showed low accumulation in non-small cell lung cancer xenografts but no unspecific binding in other organs

combined with an exclusively renal excretion pathway. Therefore, despite the low tumor uptake a good tumor visibility was achieved. These findings enable a 2in1 approach where [^{18}F]fluoro-alakyne cannot only be used as a polar ^{18}F-prosthetic group but also as a highly potential tumor imaging radiotracer. This approach broadens the application range of [^{18}F]fluoro-alakyne for various different tumor types.

In the last part of this work, a microbody with specificity to the fibroblast activation protein (FAP) was derivatized with a DOTA chelator and labeled with gallium-68. *In vitro* cell studies with [^{68}Ga]Ga-DOTAMC-FA-012 showed high specific accumulation in huFAP-positive cells compared to huFAP-negative cells. In addition, the multivalency approach was evaluated with a microbody neutrAvidin-biotin tetramer, showing an enhanced uptake compared to the monomer and increased specificity. This proved the high potential of this novel microbody for the imaging of epithelial cancers (breast, lung or colorectal).

Zusammenfassung

Die Positronen-Emissions-Tomographie (PET) ermöglicht die nicht-invasive Bildgebung metabolischer Prozesse im menschlichen Körper. Durch die Verwendung radiomarkierter krebsspezifischer Zielstrukturen wird damit die frühzeitige Diagnose von Tumoren ermöglicht. Eine robuste und verlässliche Anbindung des Radionuklids an die biologisch aktive Komponente ohne nennenswerten Einfluss auf sein pharmakologisches Verhalten ist dabei unabdingbar für routinemäßige PETMessungen. In der vorliegenden Arbeit wurden zwei unterschiedliche ^{18}F-prosthetische Gruppen für die Radiomarkierung von Biomolekül-Aziden via Click-Chemie evaluiert.

Als erstes wurde eine gespannte prosthetische Gruppe basierend auf (Aza)dibenzocyclooctin entwickelt, um die kupferfreie spannungsvermittelte Alkin-Azid-Cycloaddition (SPAAC) zu ermöglichen. Die Radiomarkierungbedingungen wurden evaluiert und optimiert, um [^{18}F]Fluor-DBCO in guten radiochemischen Ausbeuten und innerhalb einer angemessenen Synthesezeit zugänglich zu machen. Clickreaktionen mit verschiedenen Aziden (cRGD, ɲ-MSH Peptide, Maltohexaose, PDGF-ɴ Peptid) zeigten sehr gute radiochemische Ausbeuten unter äußerst milden Bedingungen, was die generelle Anwendbarkeit dieser innovativen, prosthetischen Gruppe für die Markierung von sensiblen Biomolekülen mit Fluor-18 bestätigte.

Die oxidierte Form der Folsäure (5,6,7,8-Tetrahydrofolat, THF) spielt eine wichtige Rolle als Kohlenstoff-Baustein-Donor während der DNA-Synthese. Der Folattransporter 1 (Reduced Folate Carrier, RFC) gewährleistet die ausreichende Versorgung normal proliferierender Zellen mit THF.
Tumore überexprimieren auf Grund ihrer erhöhten Proliferationsrate zusätzlich den Folatrezeptor (FR). Das macht den FR zum idealen Zielobjekt für die Tumordiagnose und –therapie. Die meisten ^{18}Fmarkierten Folatderivate weisen bisher entweder eine unzureichende Radiomarkierung oder eine unvorteilhafte Bioverteilung im Körper auf. Vor allem die Notwendigkeit eines zytotoxischen Kupferkatalysators während der Radiomarkierung könnte die Anwendbarkeit solcher [^{18}F]Fluor-ClickFolate für die Tumordiagnose beim Patienten erschweren. Auf der einen Seite wurde daher das neue [^{18}F]Fluor-DBCO für die kupferfreie Radiofluorierung eines Folat-Azids verwendet. Auf der anderen Seite sollte das kürzlich publizierte [^{18}F]Fluor-Alakin für das gleiche Folat-Azid verwendet werden, um sein pharmakologisches Verhalten zu verbessern. Beide [^{18}F]Fluor-Folate wurden in guten radiochemischen Ausbeuten erhalten und zeigten eine hohe Affinität zum FR. Leider erhöhte die DBCO-Einheit die Lipophilie des neuen Folat-basierten Radiotracers so sehr, dass *in vitro* eine hohe unspezifische Bindung beobachtet wurde und der Tumor in µPET Studien durch den hohen abdominalen Hintergrund nicht erkennbar war. Im Gegensatz dazu zeigte das [^{18}F]Fluro-Ala-Folat eine vielversprechend niedrige Lipophilie, wodurch die unspezifische Bindung *in vitro* reduziert und eine

moderate Tumoranreicherung in Kombination mit einem geeigneten Tumor-zu-HintergrundVerhältnis erzielt werden konnte.

Im zweiten Teil dieser Arbeit wurde [^{18}F]Fluor-Alakin für die Tumorbildgebung evaluiert. Tumor haben auf Grund ihrer erhöhten Proteinsyntheserate (PSR) generell einen hohen Bedarf an Aminosäuren. Die meisten Aminosäure-basierten Radiotracer weisen allerdings eine unerwünschte Anreicherung im Abdomen auf, was ihre Anwendung auf die Diagnose von Gehirntumoren beschränkt. [^{18}F]Fluro-Alakin zeigte eine geringe Anreicherung im Tumor, aber auch keine unspezifische Anreicherung in anderen Organen kombiniert mit einer ausschließlich renalen Ausscheidung. Dadurch konnte trotz des geringen Tumoruptakes eine gute Bildgebung des Tumors erzielt werden. Diese positiven Ergebnisse ermöglichen einen 2in1 Ansatz, wobei das [^{18}F]Fluro-Alakin nicht nur als polare, prosthetische Gruppe sondern auch als äußerst vielversprechender Radiotracer verwendet werden kann. Dies bietet ein breiteres Spektrum der Anwendbarkeit des [^{18}F]Fluro-Alakins auf verschiedenste Tumorarten.

Im letzten Teil dieser Arbeit wurde ein Fibroblasten-Aktivierungs-Protein (FAP) spezifischer Microbody mit einem DOTA-Chelator derivatisiert und mit Gallium-68 radiomarkiert. *In Vitro* Zellstudien mit [^{68}Ga]Ga-DOTA-MC-FA-012 zeigte eine hochspezifische Anreicherung in huFAP-positiven Zellen im Vergleich zu huFAP-negativen Zellen. Zusätzlich wurde ein Multivalenz-Ansatz mit einem MicrobodyneutrAvidin-Biotin-Tetramer evaluiert. Dabei zeigte sich eine erhöhte Anreicherung im Vergleich zum Monomer kombiniert mit einer höheren Spezifizität. Diese Ergebnisse bestätigen das große Potential dieses neuen Microbody für die Bildgebung epitheler Karzinome, wie z.B. Brust-, Lungen- oder kolorektaler Tumore.

Für meine Lieben

Table of Contents

List of Abbreviations

AAZTA	6-[Bis(carboxymethyl)amino]-1,4bis(carboxymethyl)-6-methyl-1,4-diazepane	FCS	fluorescence correlation spectroscopy
Arg	arginine	FDG	fluorodeoxyglucose
Asp	asparagine	Fe	iron
ATDD	acoustic targeted drug delivery	FET	2-fluoroethyltyrosine
BBB	blood brain barrier	FLT	fluoro-3´-deoxy-3´-L-fluorothymidine
BCH	2-aminobicyclo[2.2.1]heptane-2-carboxylic acid	fMRI	functional magnetic resonance imaging
BGO	bismuth germanate	FMT	fluoro-ɲ-methyltyrosine
BOLD	blood-oxygen-level-dependent	g	gram
Bq	bequerel	Gd	gadolinium
c.a.	carrier added	Gly	glycine
$CDCl_3$	deuterated chloroform	h	hour
c.f.	carrier free	HBED	*N,N*-bis(2-hydroxybenzyl)ethylenediamine*N,N*-diacetic acid
CT	computed tomography	HMPAO	hexamethylpropylene amine oxime
CuAAC	copper(I)-catalyzed azide-alkyne cycloaddition	HOMO	highest occupied molecule orbital
d	doublet (NMR)	HPLC	high performance liquid chromatography
DATA	6-amino-1,4-diazepine-triacetic acid	HSAB	hard and soft acids and bases, Pearson concept
DBCO	dibenzocyclooctyne	IC_{50}	half maximal inhibitory concentration
d.c.	decay corrected	ID	injected dose
DFO	deferoxamine	L	liter
DMF	dimethylformamide	LUMO	lowest unoccupied molecule orbital
DMSO	dimethyl sulfoxide	LSO	lutetiumoxyorthosilicate
DNA	deoxyribonucleic acid	i.v.	intravenous
DOTA	1,4,7,10-tetraazacyclododecanetetraacetic acid	m	multiplet (NMR)
DTPA	diethylenetriaminepentaacetic acid	M	molar
EC	electron capture	max.	maximum
EDTA	ethylenediaminetetraacetic acid	MC1R	melanocortin-1 receptor
EETI-II	*Echallium elaterium* trypsin inhibitor	MeCN	acetonitrile
FACBC	1-amino-3-fluoro-cyclobutane-1-carboxylic acid	Met	methionine
FAHep	2-amino-7-fluoro-heptanoicacid	MeOH	methanol
FAMHep	2-amino-7-fluoro-2-methyl-heptanoicacid	MeV	mega electronvolt
FAP	fibroblast activation protein, Seprase	min	minute
FBA	fluorobenzylamine	MIP	maximum intensity projection
MR	magnetic resonance	Ti	titanium

MRI	magnetic resonance imaging
MSH	melanocyte-stimulating hormone
n	neutron
NaCl	sodium chloride
NaI	sodium iodide
n.c.a.	no carrier added
n.d.	not determined
n.d.c.	not decay corrected
NFP	4-nitrophenyl-2-fluoropropionate
Nle	norleucine
NMR	nuclear magnetic resonance
NOTA	1,4,7-triazacyclononane-triacetic acid
nsclc	non-small cell lung cancer
o-/p-Ps	*ortho-/para*-positronium
OEG	oligo ethylene glycole
p	proton
PBS	phosphate buffered saline
PET	positron emission tomography
Phe	phenylalanine
p.i.	post injection
PSR	protein synthesis rate
q	quartett (NMR)
RCY	radiochemical yield
RNA	ribonucleic acid
ROI	region of interest
s	singulet (NMR)
sec	second
SFB	*N*-succinimidyl-4-fluorobenzoate
SHMT	serine hydroxymethyl transferase
SPECT	single photon emission computed tomography
SUV	standardized uptake value
THF	tetrahydrofolate
THF	tetrahydrofuran
Tl	thallium
TLC	thin layer chromatography
US	ultra sound
µPET	small animal PET
Z	atomic number

1. Introduction

1. Introduction

In 2012, almost 480.000 people in Germany came down with any form of cancer and this observation shows a tendency to rise. [1] Cancer describes an abnormal cell growth and a potential to invade and spread to other parts of the body. This enhanced cellular proliferation results in the formation of tumors, which can be classified in either malignant or benign, referring to its nature. Malignant tumor cells proliferate more aggressively than benign tumor cells. Besides this they are known to infiltrate other organs and tissues, such as the liver, lymph nodes and lungs. This metastasis usually occurs at a progressed point of the disease and declines the chance of survival of the patient seriously. [2] Therefore, diagnosis in an early stage of cancer disease is most important for the chance of recovery or prolonged survival of the patient.

Since most malignancies show a very fast proliferation rate, they need an enhanced supply of nutrients, such as folic acid and amino acids. Besides, specific growth factors and nuclear receptors are (over)expressed on highly proliferating cells. These characteristics can be used for molecular imaging via near-infrared optical imaging, magnetic resonance imaging, positron emission tomography (PET) and single-photon emission computed tomography (SPECT). Various targeting structures have been modified to visualize structures on the cell surface such as vascular endothelial growth factors and integrins [3] as well as folate derivatives addressing the folate receptor. [4–6] Nevertheless, there is still a remarkable need for selective and effective compounds to target the tumor tissue for diagnostic as well as for therapeutic approaches.

1.1. Non-invasive Imaging

Non-invasive imaging, which can be differentiated between structural and functional imaging, became a very popular diagnostic tool in clinical routine in the past few decades. Structural imaging such as magnetic resonance imaging (MRI), computed tomography (CT) and ultrasound (US) enables detection of morphological changes in tissue with high spatial resolution, which can be associated with diseases and infections. Unfortunately, structural imaging provides only static images, whereas many diseases come along with pathological malfunctions and metabolic pathways. Areas with enhanced metabolism in the human body can be visualized via functional imaging such as single photon emission computed tomography (SPECT) and positron emission tomography (PET). These imaging methods enable early stage diagnosis long time before symptoms occur by visualizing pharmacokinetics and –dynamics of certain radioactive compounds. But only the combination of PET/MRI or CT and SPECT/CT provides both, functional and anatomical information, which is very important for exact localization of tumors and metastases.

Structural Imaging (MRI, CT, US)

MRI, CT and US technology enables early diagnosis of morphological abnormalities in tissue at mm scale by static images. The whole process takes only a few minutes and is already part of daily clinical routine.

MRI

Magnetic resonance imaging (MRI) is based on the principle of nuclear magnetic resonance (NMR) of certain atomic nuclei when they are placed in a strong external magnetic field. Depending on the nature of these atomic nuclei and their chemical environment the relaxation rate varies when removing the magnetic field. In the human body these atomic nuclei are mostly hydrogen atoms found in water and fat. Therefore, MRI scans mainly provide a map of location of water and fat in the body, a picture of different tissues based on different relaxation rates. [7] In 1988, Magnevist®, the first gadolinium (Gd)-based contrast agent, was approved for human use in the USA. In the following years three more of these "first-generation" Gd-contrast agents have been approved, followed by some "second-generation" agents with improved properties (scheme 1). Furthermore, an iron particulate agent and a manganese-based agent have been developed. [8]

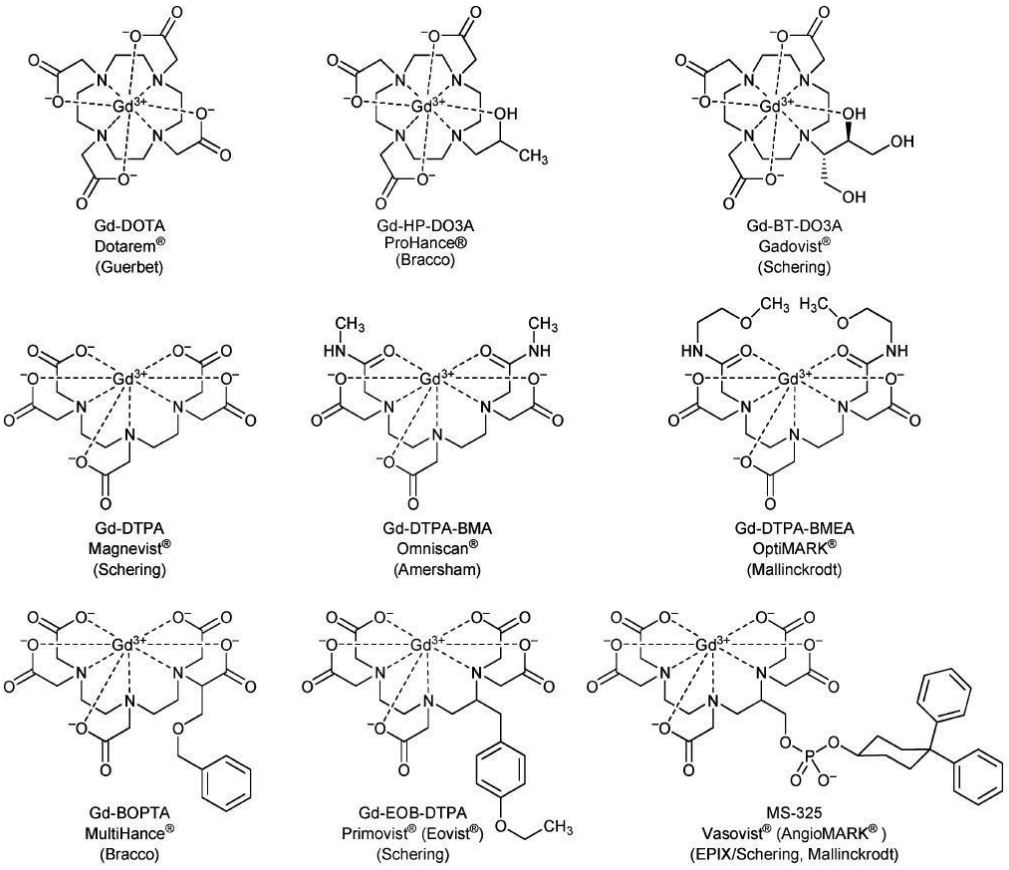

Scheme 1: Clinical used Gd-based contrast agents for MRI. [9]

In general, all of these agents contain paramagnetic nuclei, which can change the relaxation rate of protons. Gd^{3+}-complexes exhibit seven unpaired electrons (highly paramagnetic) and therefore show a slow relaxation of electron spins. Dipole-dipole interactions between the local magnetic field coming from the unpaired electrons and the proton nuclear spins affect an increased relaxation rate of water protons enhancing the contrast of the MRI images.

Functional MRI (fMRI) uses external stimuli or passive activity to visualize the corresponding brain functions (*brain mapping*). This imaging technique is based on the fact that cerebral blood flow and neuronal activation are linked. Using the blood-oxygen-level-dependent (BOLD) contrast a map of neural activity in the brain can be created. Nowadays fMRI is mainly used for behavioral and cognitive research and neurosurgery planning. [10, 11]

CT

Computed tomography (CT), also known as X-ray CT, uses X-ray images taken from different angles to produce cross-sectional images ("slices") of different areas of the human body. Compared to conventional X-ray, CT provides a higher spatial resolution and 3-dimensional images can be reconstructed. [12] Due to the higher resolution, tissues with differences in their physical density of less than 1 % can be distinguished. CT scans are mainly used to detect structural changes such as broken bones, bleedings and inflammations. Based on the degree of X-ray absorption a tissue map consisting of fluids, bones and tissue can be reconstructed. [13] One great disadvantage of CT compared with conventional X-ray is the 100 to 1000 times higher radiation dose delivered to the human body. This radiation dose may damage body cells and cause DNA single or double strand breaks, which can cause cancer development. [14] It is estimated that 0.4 % of all current cancers in the US are due to CT scans and that this number may increase up to 2 % in the following years. [15]

To improve the visibility of internal physical structures, iodine or barium compounds can be used as contrast agents. Sometimes it is very difficult to identify the interface between two adjacent tissues, for example liver and tumor or to image soft tissue. In these cases, contrast agents can increase CT sensitivity and provide specific information. [16] Elements with a higher atomic number like iodine (Z = 53) can effect a higher level of attenuation for the tissue where the contrast agent accumulates compared to other biological tissues. Iodinated contrast agents can be separated into "ionic" and "non-ionic" molecules. Due to their higher osmolality ionic iodinated contrast agents are known to have more side-effect than non-ionic ones. [17] While these iodinated contrast agents are mainly used for intravascular imaging angiography or venography (figure 1), barium sulfate is the most frequently used agent for imaging the gastrointestinal tract. [18] To increase the blood circulation time and to reduce the rate of renal clearance, nanoparticulate contrast agents are under current investigation. [19]

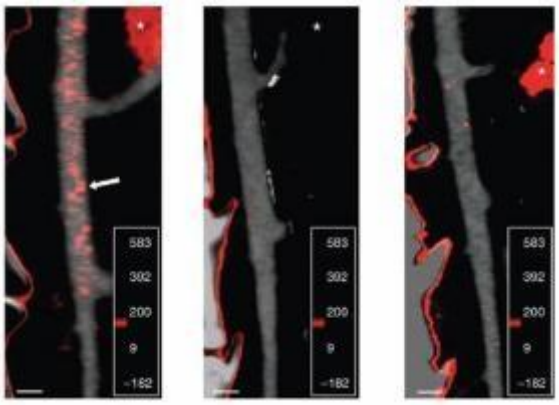

Figure 1: *In vivo* CT imaging of atherosclerosis. Intense red spots representing high CT number detected in atherosclerotic plaques after administration of N1177, a crystalline iodinated particle (left), but not in atherosclerotic plaques after administration of a conventional contrast agent (middle), nor in the aortic wall of a normal rabbit after injection of N1177 (right). [20]

Furthermore, nanocapsules can encapsulate both drugs and one or even more contrast agents or radioactive labeled compounds at a same time. These multifunctional blood pool contrast media can then be used for multimodal imaging methods like the combination of CT and PET. [21, 22] *US*

Medical ultrasound uses sound waves with frequencies above audible limit of humans (ш 20kHz), typically in the range of 1 to 18 MHz. These sound waves are reflected, scattered and absorbed by tissues and fluids in the human body producing echoes, which can be recorded and displayed as an image. Ultrasound imaging has some great advantages compared to other structural imaging methods like MRI or CT. It is significantly more cost-efficient and most importantly it does not deliver any radiation dose to the patient. Besides it provides real-time images and can be brought even to outlying areas. Ultrasound is mainly used for diagnostic application in different fields of medicine such as angiology (arterial and venous diseases), cardiology (echocardiography) [23], emergency medicine (trauma) [24, 25] and gynecology (control during pregnancy). But ultrasound can also be used for therapeutic approaches such as destroying kidney stones and gallstones (lithotripsy) [26, 27], to deliver chemotherapeutic agents and other drugs to tissues (acoustic targeted drug delivery (ATDD)) [28] or in dental hygiene.

Functional Imaging (SPECT, PET)

In 1913 Georg de Hevesy described for the first time the so called “tracer principle” during tea time with Moseley at Rutherford´s institute. He was very interested in tracing the way of the compounds of tea through the human body. [29] In 1923 he investigated the absorption of lead by plants using

lead212 as a radiotracer. His idea was to apply toxic lead in such small amounts that no pharmacological effect was observed. [30] Nowadays this principle is the basis for visualization of biochemical and physiological processes in the human body by PET and SPECT imaging using radiotracer.

Three different major types of primary radioactive decay are known: ɲ-decay (emission of particles, He nuclei) and ɴ-decay (emission of particles, electrons or positrons). In the case the primary transformation product exhibits excited nuclear levels, œ-emission may occure as a secondary effect. According to the type of decay we can define two different imaging methods: SPECT and PET. Both imaging methods are non-invasive, using radioactive labeled compounds, which are applied in trace amounts to the human body. For SPECT imaging these molecules, which are part of the metabolic pathway we are interested in, carry a photon-emitting (e.g. ^{99m}Tc, ^{123}I) nuclide. For PET imaging the molecules need to be labeled with a positron emitter (e.g. ^{11}C ,^{18}F, ^{68}Ga).

SPECT

Single photon emission computed tomography (SPECT) is a non-invasive imaging method which allows the visualization of biochemical processes in the human body. A gamma camera, which detects gamma photons occurring after excitation in consequence of a decay or isomeric transition, is rotated around the patient. This gamma camera consist of a collimator, a scintillation crystal (NaI(Tl)), photomultiplier types, amplifiers and an analyzer. The centerpiece of a conventional gamma camera is still the same than reported already in 1958. [31] SPECT technique is very similar to planar imaging using a gamma camera. Due to the rotation of two or three cameras around the patient a 3dimensional projection can be created. Besides further investigation of existing gamma cameras to provide a higher spatial resolution, there is also a high demand on developing organ-specific SPECT systems, for example in the field of cardiology. To image a specific organ only a very small field-of-view is necessary. Most of these cardiac SPECT systems use cadmium (zinc) telluride detector modules, which lead to an improved sensitivity of the system for photons up to 200 keV energy. [32, 33]

SPECT cameras do not directly detect the decay of a radionuclide, but photon emission of a previous primary decay. These excited nuclides may convert to lower-energetic nuclear states or to the nuclear ground state via photon emission, inner conversion or inner pair production. The most prominent photon emitting radionuclide used in SPECT imaging is technetium-99m with a half-life of 6 h. [34] The great advantage of this SPECT nuclide is that it is available from a generator and can be used for kittype preparation of ^{99m}Tc-radiopharmaceuticals, which makes them readily accessible for nuclear medicine practice. Furthermore it provides a high œ-yield of 83.3 % and a œ-energy of 140 keV. [35]

SPECT is for example used in functional cardiac imaging for the diagnosis of ischemic heart disease. Therefore, [^{99m}Tc]Tc-tetrofosmin (Myoview, GE healthcare) and [^{99m}Tc]Tc-Sestamibi, cardiac specific radiopharmaceuticals are applied followed by an induced myocardial stress. [36, 37] By comparing the stress image with another sets of images at rest a diagnosis can be obtained (figure 2). [38]

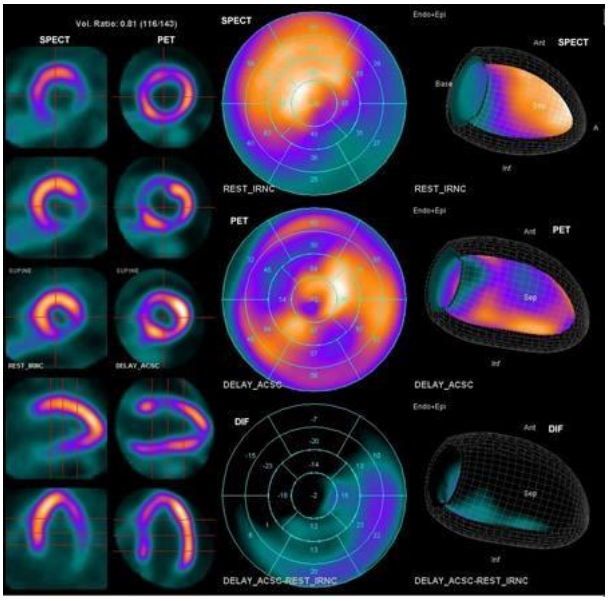

Figure 2: Assessment of myocardial feasibility in a patient with infero-lateral infarction. A serve detect (ч 50 %) may be observed in such region by myocardial perfusion SPECT with [^{99m}Tc]Tc-tetrofosmin; both in tomographic view as in polar maps, and the positive uptake with [^{18}F]fluorodeoxyglucose-PET. In the inferior polar map, the extension of the mismatching territory between both scans is shown. [39]

For imaging the cerebral blood flow [^{99m}Tc]Tc-HMPAO (hexamethylpropylene amine oxime) can be used. The blood flow of the brain is proportional to the brain metabolism and therefore this allows the diagnosis of dementia and Alzheimer´s disease. [40, 41, 42] Another method for brain imaging is given by PET using [^{18}F]fluorodeoxyglucose ([^{18}F]FDG). By visualizing local brain glucose metabolism information about brain damage can be obtained. [43, 44]

PET

Positron emission tomography (PET) is based on the emission of a positron during β^+-decay of proton rich radionuclides. A proton is converted into a neutron, a positron (β^+-particle) and an electron neutrino (Scheme 4).

□□□´ □□ +□+□+□+□ + ħ+□

□□□□´ □□□□□□□□ □□ □□ ħ□

Equation 1: Decay equation of positron emission.

Depending on its energy, the emitted positron can travel a certain distance before it pairs with an electron forming a positronium. The ν⁺-energy has a crucial influence on the resolution of the PET image, because the higher the ν⁺-energy the longer the way the positron travels reducing its kinetic energy. Two ground states of positronium, *para*- and *ortho*-positronium having different spin states of the electron and the positron, are known. Table 1 gives an overview of the two positronium types and their properties. Only the annihilation of the *para*-positronium can be used for PET imaging, because two photons with an angle of nearly 180° and energy of 511 keV each are emitted. In contrast to this, the *ortho*-positronium annihilates under a continuous œ-spectrum, where coincident detection is impossible. The probability of *ortho*-annihilation is much higher (75 %) than the one of *para*annihilation (25 %), but *ortho*-positronium can be transferred into *para*-positronium by interaction with the environment of dense matter. [45, 46]

Table 1: Comparison between *ortho*- and *para*-Positronium.

	ortho-Positronium	*para*-Positronium
State	triplet	singlet
Impulse (J)	1	0
Life-time (free Positronium)	1.4×10^{-7} s	1.25×10^{-10} s
Annihilation	$E_{œ1} + E_{œ2} + E_{œ3} = 1.02$ MeV	2 x 0.511 keV = 1.02 MeV
Angle	statistically	180°

To detect the coincident annihilation of both 511 keV photons, the patient is surrounded by a PET scanner consisting of 6 to 70 million detector pairs. Inorganic crystals, such as lutetiumoxyorthosilicate (LSO, Lu_2SiO_5) [47] doped with cerium, or bismuth germanate (BGO) are used providing a spatial resolution of 2-5 mm. Small animal-PET-scanners can even reach a resolution of under 1 mm. [48] A computer is used for the reconstruction of the origin of both photons, lying on the line which connects the co-incident photons. Using this data, a three-dimensional image can be created (Figure 3).

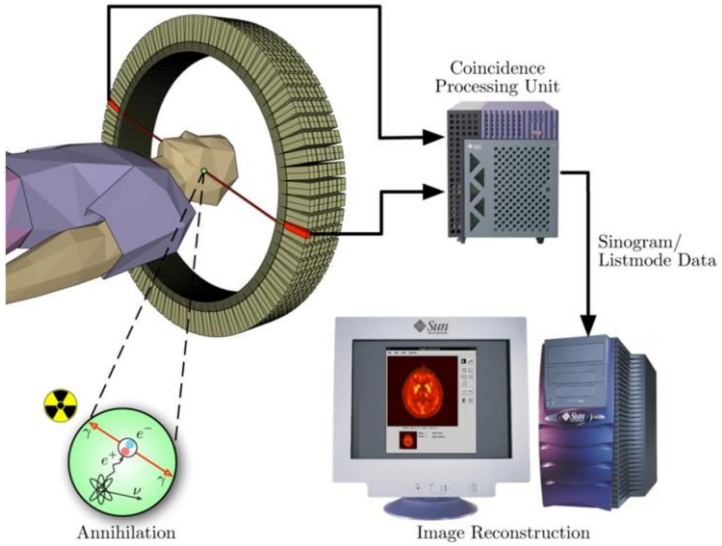

Figure 3: PET acquisition process. [49]

Based on the principle of PET, only β^+-emitting radionuclides can be used. The radionuclides can be either cyclotron-produced (e.g. oxygen-15, fluorine-18, carbon-11, nitrogen-13) or available from a generator (gallium-68, scandium-44). [50–54] To choose the most suitable radionuclide for a specific application, some characteristics need to be considered: the half-life of the radionuclide should be long enough for a multi-step radiosynthesis followed by purification and quality control. On the other hand, the radiation exposure for the patient should be as low as possible. Very short living radionuclides such as oxygen-15 ($t_{1/2'}$ = 2.04 min) and nitrogen-13 ($t_{1/2'}$ = 9.97 min) can only be used for easy accessible radiotracer like $[^{15}O]H_2O$ and $[^{13}N]NH_3$ and imaging rapid biological processes (myocardial perfusion). [55] To visualize for example the metabolism of tumor cells, radionuclides with longer half-lifes such as fluorine-18, gallium-68 or iodine-124 can be used. As mentioned before, the β^+-energy is another very important selection criterion, determining the spatial resolution of the PET image. [56] Most proton-rich radionuclides cannot only decay via β^+-emission, but can also perform electron capture (EC). This transformation does not provide a positron and therefore radionuclides with a high ratio of EC are not suitable for PET application.

Table 2: Overview of some important positron emitters for PET. [57]

Nuclide	$t_{1/2}$	Decay [%]	$E_{\beta+max}$ [MeV]	Production
^{18}F	109.7 min	β^+ (97)	0.63	$^{18}O(p,n)^{18}F$
^{15}O	2.03 min	β^+ (99.9)	1.73	$^{14}N(d,n)^{15}O$ $^{15}N(p,n)^{15}O$
^{11}C	20.30 min	β^+ (99.8)	0.96	$^{10}B(d,n)^{11}C$ $^{14}N(p,\alpha)^{11}C$
^{13}N	9.97 min	β^+ (100)	1.20	$^{16}O(p,\alpha)^{13}N$

^{124}I	4.2 h	β^+ (23), EC (77)	2.14	^{124}Te(p,n)^{124}I
^{44}Sc	3.97 h	β^+ (94)	1.48	^{44}Ti/^{44}Sc generator ^{44}Ca(p,n)^{44}Sc
^{68}Ga	67.7 min	β^+ (89), EC (11)	1.90	^{68}Ge/^{68}Ga generator

Table 2 gives an overview of common PET radionuclides. Fluorine-18 shows ideal nuclear-physical characteristics: a half-life of 110 min enables a multi-step radiosynthesis and transportation from cyclotron to hospital, with a low radiation exposure of the patient. Compared with other PET radionuclides fluorine-18 provides a very low β^+-energy of only 0.63 MeV resulting in a good spatial resolution. [58] Fluorine-18 needs to be produced on a cyclotron through the bombardment of oxygen-18 enriched water with protons (equation 2).

□□□□ + □ ´ □□□□ + □

Equation 2: Nuclear reaction of oxygen-18 enriched water to produce fluorine-18.

The specific activity should also be considered when choosing a radionuclide. We differ between carrier free (c.f.), no carrier added (n.c.a.) and carrier added (c.a.), in which the carrier free produced radionuclides provide the best specific activity. Working with naturally occurring elements, this state is not possible, because other isotopes are omnipresent, calling this situation no carrier added. Cyclotron production delivers n.c.a. fluorine-18 with specific activities of 3.7 x 10^5 GBq/mmol. [59, 60]

Chemically speaking, PET radionuclides can be divided into metals and non-metals resulting in some basic differences in their attachment to tracer molecules. Metal radionuclides such as gallium-68, copper-64 and scandium-44 require a chelator molecule attached to the targeting vector. The most prominent chelator currently is DOTA (1,4,7,10-Tetraazacyclododecane-1,4,7,10-tetraacetic acid) and its derivatives. Whereas non-metal radionuclides like fluorine-18, carbon-11, nitrogen-13 and oxygen15 can be attached covalently to the biomolecule using basic organic chemistry. The van-der-Waals radius of fluorine-18 is very similar to te one of hydrogen, whereas the electronegativities are quite different. Therefore the bond length is more similar to the one of a hydroxyl group.

The main field of application for PET is still the clinical oncology, with [^{18}F]fluorodeoxyglucose ([^{18}F]FDG) being the most prominent radiopharmaceutical. This glucose analog tracer is taken up by tissues with increased glucose metabolism, such as brain, liver and most cancers (figure 4). [61, 62]

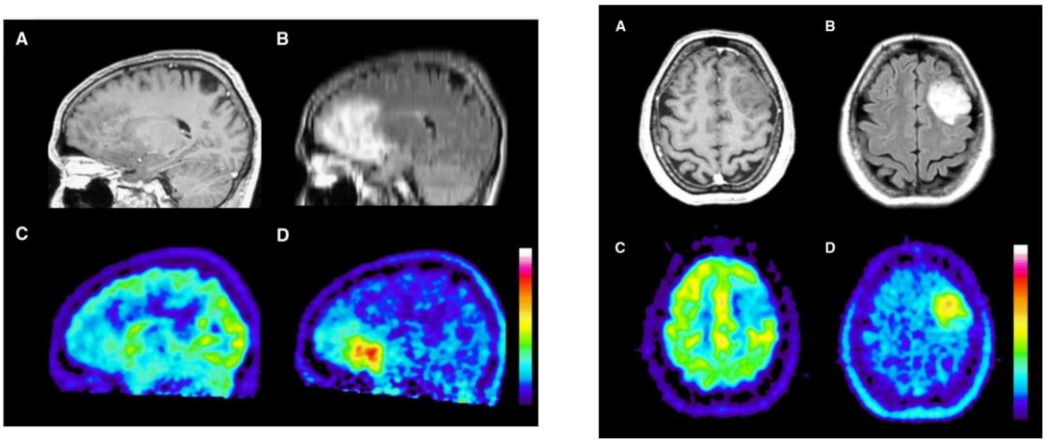

Figure 4: Anaplastic oligoastrocytoma WHO Grade III in the frontal lobe (left) and diffuse astrocytoma WHO Grade II in the left lobe (right). (A) Contrast-enhanced, T1-weighted MRI. (B) MRI FLAIR (fluid-attenuated inversion recovery)-sequence. (C) [^{18}F]FDG PET. (D) [^{18}F]FET PET. [62]

Numerous studies already showed, that radiolabeled amino acids such as *O*-(2-[^{18}]fluoroethyl)-Ltyrosine ([^{18}F]FET) or [^{11}C]methionine are superior over [^{18}F]FDG for clinical management of glioma patients. [63] For neuroimaging [^{18}F]FDG is more or less only used in the diagnosis and differentiation of Alzheimer´s disease from other dementing processes. Furthermore, it is applied for the diagnosis of tumors (others than brain tumors) and inflammations. [64]

The combination of PET with CT allows a much more precise diagnosis as well as staging and monitoring of cancer treatment. [65, 66]

1.2. Melanocortin-1 receptor and ɲ-MSH peptides

Malignant melanoma develops from the pigment-containing cells also known as melanocytes and is one of the most aggressive and therapy-resistant types of cancer. In 2015, there have been 20.820 new cases and 2.875 deaths caused by melanoma in Germany. [67] Melanomas cannot only occur in the skin, but also in the mouth, the intestines or the eye and are mainly caused by ultraviolet light (UV) from the sun or tanning devices. [68] Due to UV radiation the cells start to produce melanin, which accumulates in the melanocytes and kerationocytes. The high invasiveness of melanoma makes surgical treatment very low efficient, and chemotherapy shows only limited success. [69] Currently, non-invasive methods of imaging melanoma include the use of [^{18}F]FDG for PET or [^{99m}Tc]Tc-MIBI ([^{99m}Tc]Tc-Sestamibi) for scintigraphy. [70, 71] However, both radiotracers suffer from relatively high false positive rates. [72] Therefore, the investigation of specific markers and signaling pathways for developing targeted diagnosis and (immuno)therapy is of great interest. [73] During malignant transformation of melanocytes various growth factors (fibroblast growth factor, transforming growth factors alpha and beta, stem cell factors) are produced and receptors (Melanocortin-1 receptor, MC1R) are expressed, which are absent on normal melanocytes. Researchers specialy focused on the human

melanocortin-1 receptor (MC1R), which is one of the five members of the subfamily of melanocortin receptors (MCRs) belonging to the family of G-protein coupled receptors (GPCR). [74] The interaction of G-proteins with extracellular parts of the receptor is activated by ligand binding and plays an important role in signal cascades leading to cell proliferation and growth. [75] The MC1R is expressed on melanocytes and melanoma and is normally responsible for skin pigmentation by regulation of pigment production. In 1961, Lerner and McGuire found that the application of ɲ-MSH ;ɲ-melanocyte-stimulating hormone), the agonist of the MC1R, resulted in skin darkening. [76] The ɲMSH binds selectively to the MC1R with nanomolar to subnanomolar affinities. [77] Many different derivatizations based on the naturally occurring ɲ-MSH have been tested to improve the binding affinity, biological half-life and enzymatic stability. The conversion of Phe^7 into D-Phe^7 and the substitution of Met^4 by Nle^4 resulted in the development of Melanotan I ([Nle^4, *D*-Phe^7]-ɲMSH, NDP-ɲMSH). [78] Further shortening and cyclization resulted in stabilization of the binding sequence and produced Melanotan II (Ac-Nle-*cyclo*[Asp-His-*D*Phe-Trp-Lys]-NH_2). [79] The development of Melanotan I and II led to a broad variety of radiolabeled ɲ-MSH analogues. Various SPECT tracers radiolabeled with technetium-99m, indium-111 or gallium-67 have been synthesized within the last decades. Especially derivatives with a lactam bridge showed improved *in vivo* stability and a very good tumorto-normal tissue contrast. [80, 81] Due to the fact that PET offers considerable advantages over SPECT in terms of sensitivity, resolution and quantification, there is a high demand on developing ɲ-MSH analogues radiolabeled with positron emitters. Currently, there are two classes of ɲ-MSH peptides showing promising *in vivo* characteristics. The first group consists of linear NAPamide-based peptides (Ac-Nle-Asp-His-*D*Phe-Arg-Trp-Gly-Lys-NH_2), which have already been radiolabeled with fluorine-18 [82] and copper-64. [83] Unfortunately, the [^{18}F]FB-NAPamide showed only moderate tumor uptake and retention in B16F10 xenografts, whereas the [^{64}Cu]Cu-DOTA-NAPamide provided clear tumor localization. The second group of promising candidates for *in vivo* imaging of melanoma is given by ɲMSH analogues cyclized via the transition metal rhenium (ReO[$Cys^{3,4,10}$,*D*Phe^7.Arg^{11}ɲ-MSH_{3-13}. Because of their resistance to proteolytic degradation, these derivatives show high tumor uptake and long tumor retention. Again, these derivatives have been labeled with both, fluorine-18 [84] and copper64, showing great potential to detect malignant melanoma. [85] Nevertheless, there is still a high demand on developing (cyclic) ɲ-MSH peptides with high affinities to the MC1R applicable in PET imaging.

However, it should be mentioned, that all of the above mentioned studies are based on the evaluation of radiotarcers in animal models. The actual expression of the target on the human melanoma is in disput. This hampered the translation of radiolabeled ɲ-MSH peptides to the patient until now.

1.3. Microbodies

To further improve the thermal and proteolytic stability of peptides, cysteine-knot microbodies also known as “knottins” based on 30-50 amino acids have been developed within the last years. [86, 87] The remarkable chemical and thermal stability of these polypeptides is caused by a unique knotted topology of three disulfide bonds. The internal knot-structure is created by the inter-connection of the backbone due to the penetration of one disulfide bridge through a macrocycle formed by two other disulfide bonds. [88–90] Additionally, the antiparallel ɴ-strands are connected by a network of hydrogen bonds. [91, 92] Therefore, cysteine-knot peptides are very promising candidates for peptidebased pharmaceuticals for imaging and therapy, combining bioactivity and high stability. [90] The general structure of knottins is displayed in figure 5. The different loop regions consist of various amino acids, which can be modulated to create recognition structures.

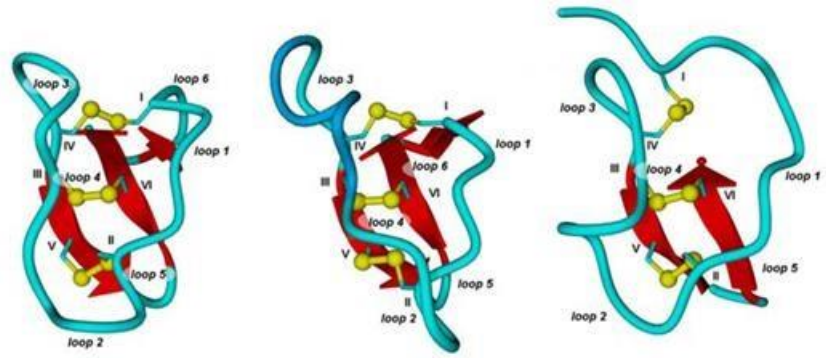

Figure 5: Cartoon diagrams of prototypical cysteine knots. Loops are depicted in light blue and numbered according to their appearance in the sequence, ɲ- helices in dark blue, ɴ-sheets in red and cysteines in yellow with Roman numerals according to their appearance in the sequence. [93]

Microbodies can be produced via either chemical synthesis (solid phase peptide synthesis) or recombinant expression. Due to their small size these polypeptides generally provide fast tumor targeting and a short *in vivo* half-life compared to for example monoclonal antibodies, but exhibit high binding affinities such as antibodies. [94] Standardized data on sequences and structures of known knottins are provided by the KNOTTIN database. [95]

The first engineered cysteine knot peptide was reported by Kimura *et al.* in 2009. The *Echallium elaterium* trypsin inhibitor (EETI-II) is a knottin peptide from the family of protease inhibitors, binding to integrins. They substituted the 6-amino acid trypsin binding loop by an 11-amino acid loop containing the Arg-Gly-Asp integrin binding motif and screened the libraries to identify mutants that bind to the integrin $\alpha_V\beta_3$. Receptor specific assays showed that the engineered peptides do not only bind to $\alpha_V\beta_3$ integrins but also to $\alpha_V\beta_5$ integrins and one peptide (2.5 D) even to $\alpha_5\beta_1$. [96, 97] Later on, optical (Cy5.5) and positron emission tomography (copper-64) imaging probes have been conjugated to these engineered peptides showing a good tumor uptake of around 5 %ID/g tissue and low

unspecific kidney and liver uptake. [98, 99] The same group also developed a dual-labeled knotting peptide (Cy5.5 and copper-64), which can be used for multimodal imaging using near-infrared and PET. Conjugation of Cy5.5 increased kidney uptake and retention, but also a decreased tumor washout compared to the [^{64}Cu]Cu-DOTA knottin peptide was observed. This strategy cannot only be used for site-specific coupling of two imaging labels but also to attach an imaging label and a therapeutic moiety for diagnosis and therapy. [100] As these engineered knottin peptides show high potential as new imaging agents, the peptide 2.5 D was further radiolabeled with fluorine-18 to evaluate its clinical translation ability. For site-specific labeling through the peptide N-terminus, [^{18}F]fluoro-*N*succinimidyl-4-fluorobenzoate ([^{18}F]SFB) was used. In U87MG tumor bearing mice [^{18}F]SFB-2.5 D showed a moderate tumor uptake and a fast blood clearance providing an excellent tumor-to-normaltissue contrast. [94] The engineered knottin mutants have also been radiofluorinated using 4nitrophenyl-2-[^{18}F]fluoropropionate ([^{18}F]NFP) and evaluated in U87MG tumor bearing mice. A reduced uptake in the gallbladder was observed for [^{18}F]NFP-2.5 D and [^{18}F]NFP-2.5 F than previously reported for [^{18}F]SFB-2.5 D while maintaining the high integrin-specific tumor uptake. [101] In 2011, first preliminary studies using ^{177}Lu-labeled knottin peptides (2.5 D and 2.5 F) for integrin receptormediated radionuclide therapy have been reported. Knottin [^{177}Lu]Lu-DOTA-2.5 F showed higher tumor uptake and better tumor-to-blood ratios compared to [^{177}Lu]Lu-DOTA-2.5 D, making it a promising candidate for radionuclide therapy of integrin-positive tumors. [102] The latest approach deals with tumor-targeted drug delivery using knottin peptides conjugated to gemcitabine, a chemotherapeutic agent. The EETI-2.5Z-Val-Ala-PAB-gemcitabine showed selective binding to tumorassociated integrins and releases its cytotoxic payload inside the tumor. Therefore, this modified knottin peptide has great potential as inhibitor of tumor growth. [103]

1.4. Fibroblast activation protein (FAP)

The human fibroblast activation protein ɲ, also known as seprase, is a 170 kDa transmembrane serine protease with closest homology (50 %) to dipeptidyl peptidase IV (DPP IV), which is ubiquitously expressed and both being members of the S9b peptidase family. [104, 105] DPP IV plays an important role in T-cell stimulation, glucose metabolism and tumorigenesis. [106] In contrast, FABɲ is only expressed in reactive stromal fibroblasts of human epithelial cancers (breast, lung and colorectal), in granulation of healing wounds and in bone and soft tissue sarcomas. [105, 107] In general, FAB is expressed in ɯ 90 % of all human tumors. Moreover it shows no expression in benign epithelial tumors and normal adult tissues (FABɲ negative). It is suggested that FABɲ promotes tumor growth and proliferation and furthermore, indicates the invasiveness of the tumor. [108] Therefore, FABɲ shows great potential as immunodiagnostic tool and as target for immunotherapy.

FABɲ was first identified in 1986 in cultured fibroblasts using the monoclonal antibody F19 and named F19 Cell Surface Antigen. [105, 109, 110] During the following years, many malignant epithelial cancers were found to be F19 negative, wherefore the F19 Cell Surface Antigen was renamed as Fibroblast Activation Protein ɲ in 1994. [111] Simultaneously, a 170 kDa gelatinase was identified in the cell line LOX (human malignant melanoma) and named Seprase. [112] This glycoprotein peptidase was found in stromal fibroblasts of more than 90 % of all epithelial cancers and its expression correlated with the invasiveness of human melanoma and carcinoma cells. [105, 113] Only a few years later it turned out, that FABɲ and Seprase are the same cell surface serine protease. [113 –116]

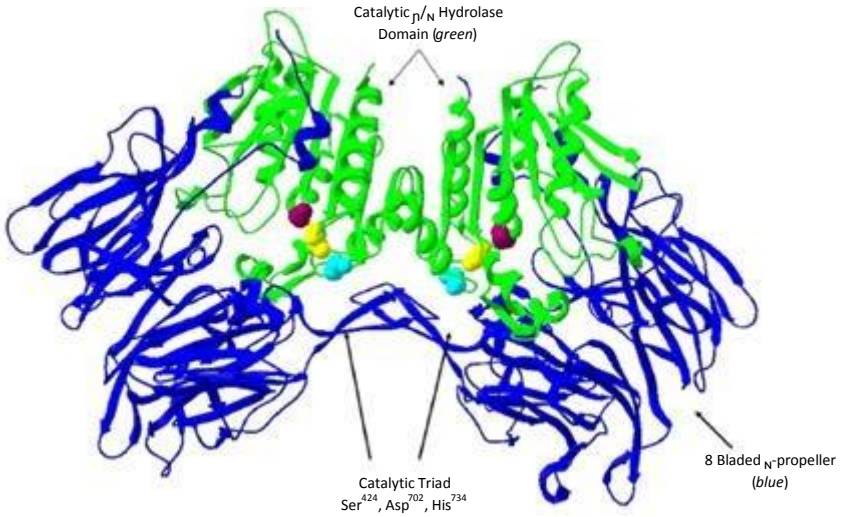

Figure 6: Structure of Seprase. The ribbon diagram illustrates the dimeric structure of Seprase. The extracellular domain consists of two domains, an eight bladed ɴ-propeller (blue) and an ɲɴ hydrolase domain (green) that contains the catalytic triad. The catalytic residues are shown in purple (Serine 624), cyan (Aspartic Acid 702) and yellow (Histidine 734). [117]

In 2005, Aertgeerts *et al.* reported the crystral structure (figure 6) of FABɲ and investigated the molecular parameters that are responsible for its specificity. [104] Seprase is a 170 kDa homodimer protein that consists of 760 amino acids and contains two *N*-glycosylated 97 kDa subunits. The structure of the Seprase monomer is basically composed of three parts: a large *C*-terminal extracellular domain, a hydrophobic transmembrane segment and a short cytoplasmic tail, which consist of six amino acids. Furthermore, the enzyme functionality is given by five potential *N*glycosylation sites and 13 cysteine residues. [115] The subunits are composed of an eight bladed ɴpropeller and a catalytic ɲɴ hydrolase domain, on which interface the catalytic triad (Ser^{624}, Asp^{702}, His^{734}) is located. The ɴ-propeller is located on top of the catalytic triad and controls selectively the access of proteins to the triad: the oscillating bladder lets small peptide substrates into the active site, while large proteins are excluded which prevents accidental proteolysis in the cytosol. [118]

Already in 1994, a ^{131}I-labeled murine monoclonal antibody ([^{131}I]I-mAbF19) with selectivity to the fibroblast activation protein was reported in a proof-of-principle study. [119] They demonstrated

stromal targeting by selective accumulation of ^{131}I-mAbF19 in tumor stroma tissue. Furthermore, [^{131}I]I-mAbF19 was evaluated in 2001 as a potential antitumor agent in two phase I studies in cancer patients. The pharmacokinetics of antistromal mAbF19 have been well defined in these studies and the monoclonal antibody showed no binding to normal tissue or blood cells. Nevertheless, the total number of patients was small in these studies and a larger study might reveal other effects. [120] If patients get repeated doses of this murine antibody this might lead to the formation of anti-mouse antibodies in the patient. Therefore, sibrotuzumab, a human monoclonal antibody was developed from F19. Several phase I and II studies have been carried out with ^{131}I-labeled or non-labeled sibrotuzumab demonstrating the safe and well-tolerated administration of repeated infusion. [121] Anyway, sibrotuzumab failed a clinical trial including 25 patients with metastatic colorectal cancer in 2003 because the minimum of at least one complete or partial remission of 4 patients with stable disease was not met. [122] Nevertheless, the fibroblast activation protein still displays a high potential target for diagnosis and therapy of various cancer types, such as breast, lung and colorectal cancer. Currently, Rollinger *et al.* are holding a patent in which they describe the use of seprase as a tumor marker not only for a single type of cancer. [123]

The highly selective expression of the fibroblast activation protein at various epithelial cancer types compared to normal tissue makes FAP a very promising target for highly precise diagnosis and very effective therapy. Therefore, more suitable targeting vectors such as microbodies need to be identified and evaluated as radiolabeled derivatives.

1.5. ^{68}Ga-labeling

Gallium-68 is one of three radioisotopes of the element gallium and decays via a β^+-decay into zinc-68. With a high positron yield of 89 %, maximum positron energy of 1.9 MeV and a half-life of 67.71 min gallium-68 provides good characteristics for PET. Gallium-68 can easily be obtained from the ^{68}Ge/^{68}Ga generator, which is based on the radiochemical equilibrium between a mother (M) and a daughter nuclide (T). Germanium-68 can be produced in a (p,2n)-reaction from the stable isotope gallium-69 using a cyclotron, and has a half-life of 270.8 d. It decays to gallium-68 via electron capture (EC).

We generally differ between two different equilibria based on the proportion of half-life respectively decay constant of mother and daughter. If the half-life of the mother nuclide is greater than ten times the half-life of the daughter, we call this a *transient equilibrium*. The ^{68}Ge/^{68}Ga-generator is based on the *secular equilibrium*, because the half-life of germanium-68 is much greater than the one of gallium-68 (5700-times). Therefore it is supposed, that for a period of time (e.g. ten half-lifes of daughter) the amount of mother atoms is constant respectively that the decay of the mother nuclide can be neglected.

□□□□(□) □ □□□□□□(□) *Transient equilibrium* □□□□(□)ب □□□□□□(□) *Secular equilibrium*

^{68}Ge/^{68}Ga-generators are already known since 1960, when they were called a “positron cow” because the gallium-68 can be milked from the generator. [124] Commercially available generators mostly use TiO_2 or SnO_2 as a matrix to immobilize the mother nuclide and reached market authorization as medical product or GMP certification. Latest developments in ^{68}Ge/^{68}Ga-genereator design use polymer-based matrix materials. Due to the 67.7 min half-life of gallium-68, the generator can be eluted 2-4 times a day.

To remove common impurities such as co-eluted germanium-68 (mother nuclide breakthrough), zinc68 (decay product of the daughter), Ti^{4+} (from the matrix) and Fe^{3+} (from the hydrochloride acid for elution), a post-processing procedure must be performed (Figure 7). [125] Several purification methods have been developed within the last decades including the fractionation of the gallium-68 eluate in small volumes. [126] Furthermore, ion exchange resins (cationic or anionic) can be used to selectively trap, wash and elute the gallium-68. Using the anionic method the activity is trapped as a tetrachloro ^{68}Ga-complex and water is used for elution. [127] For the cationic resin, there are three methods available for elution: the acetone post-processing, the ethanol post-processing and a postprocessing, that uses an acidified NaCl solution. Since acetone is not approved for *in vivo* application, it needs to be removed before or after the radiolabeling reaction. To overcome this problem, Roesch *et al.* investigated a novel post-processing method, in which acetone is replaced by ethanol. [128] After optimizing the ratios of ethanol and hydrochloride acid, similar results were obtained compared to the acetone post-processing. The third method uses only acidified sodium chloride solution to elute the gallium-68 while the impurities remain on the resin. [129] Optimizing a radiolabeling reaction also includes evaluation of the suitable post-processing method.

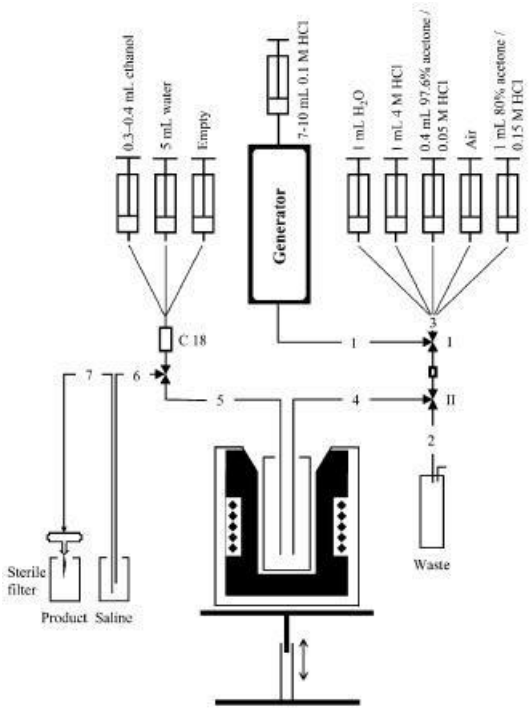

Figure 7: Schematic diagram of elution and post-processing of gallium-68 and generator-associated synthesis of ^{68}Ga-labeled compounds. [130]

The element gallium is located at the thirteenth group in the periodic table. Its electron configuration [Ar]$4s^2 3d^{10} 4p^1$ suggests that its most stable oxidation state is +3. Based on the HSAB concept of Pearson, Ga^{3+} with a small ionic radius (0.62 Å) and its high charge can be classified as a hard acid. Consequently, it prefers hard basic donors to form stable octahedral complexes. These six dative bonds can be located on either nitrogen or anionic oxygen. A suitable chelator should allow on one side a stable complexation of $^{68}Ga^{3+}$ and on the other side there must be a further functional group for the attachment of the chelator to a targeting vector. These molecules are than called bifunctional chelators.

In general, we differ between acyclic and cyclic chelators. The first generation chelators EDTA, DTPA, Citrate or DFO are acyclic and complex a wide range of metal ions (scheme 2). Therefore, very good radiochemical yields were achieved already at room temperature, but these chelators showed also a very high transmetalation and decomplexation rate. Especially, on the transchelation of Ga^{3+} with transferrin needs to be paid special attention.

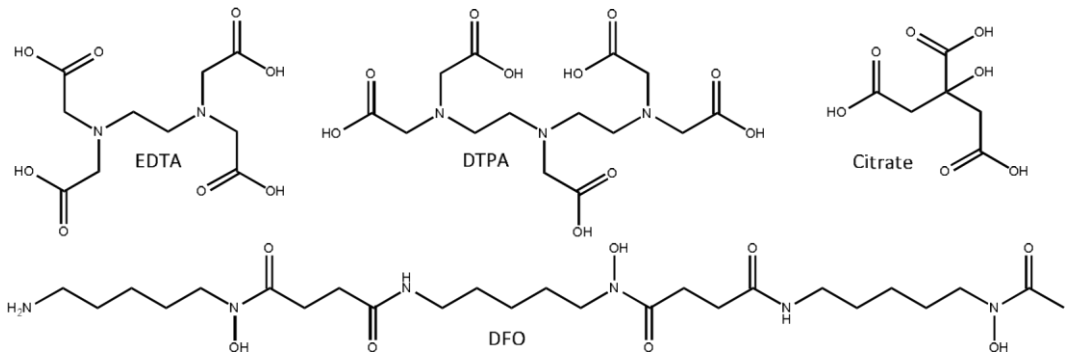

Scheme 2: First generation acyclic chelators for the complexation of gallium-68. [131]

To overcome these stability problems, cyclic chelators have been developed (scheme 3). But these cyclic chelators are often less flexible than acyclic ones, which has in some cases a negative influence on the radiolabeling efficiency. Furthermore, DOTA was originally designed to complex lanthanides with an ionic radius of around 1 Å (MRT contrast agents). [132] Therefore harsh labeling conditions of around 95 °C and pH 3-4 are required to form a stable complex. A much better suited geometry and cage size is provided by triazacyclononan-based chelators, which offer a much more efficient radiolabeling. NOTA exhibits only six coordination ligands, which are essential for a stable complexation of gallium-68. This makes the attachment of a targeting vector very challenging. To overcome these issues, derivatives such as NODAGA have been developed.

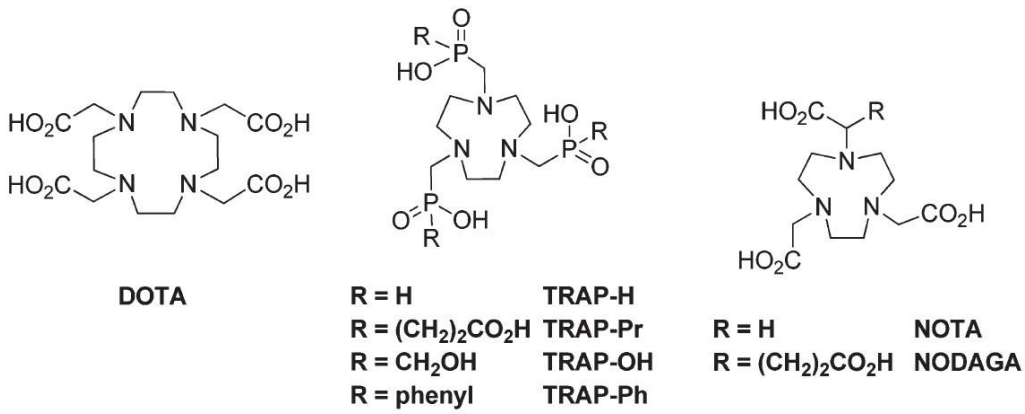

Scheme 3: Next generation cyclic chelators for the complexation of gallium-68. [134]

With its much lower radiolabeling temperature of only 50 °C, NOTA is especially suitable for sensitive biomolecules. [133, 134] If even milder reaction conditions are required, AAZTA- , DATA- and THPderivatives can be used (scheme 4). The novel AAZTA- and DATA-chelators combine the advantages of an acyclic (fast labeling) and a macrocyclic chelator (high stability). For the complexation two nitrogen atoms from a 1,4-diazepine ring and one exocyclic nitrogen atom are used. Due to the high flexibility of this molecule, radiolabeling can already be performed at room temperature. [135, 136]

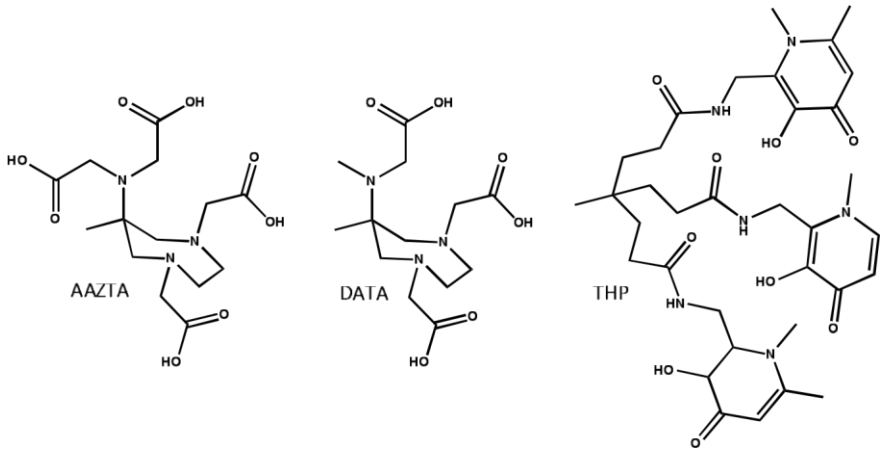

Scheme 4: Novel chelators, which combine the advantages of acyclic and macrocyclic chelators.

1.6. Folic acid

Folic acid also known as vitamin B_9 is an essential nutrient required by the human body. Since the human body is not able to synthesize folic acid and folates by itself, we need to take it up through food. One derivative of folic acid, 5-methyl-5,6,7,8-tetrahydrofolate (5-methyl-THF) plays an important role as an one-carbon donor for the built-up synthesis of purines during deoxyribonucleic acid (DNA) replication. [137] Purines (adenine and guanine) and pyrimidines (thymidine and cytosine), which are four types of nucleobases, are attached to the phosphate-backbone of each twisted double-stranded helix of DNA. During proliferation of chromosomes in the human body, every part of the cells needs to be doubled in certain intervals. [138] Since folic acid and folates are essential for these DNA replications, the human body uses several receptors (e.g. folate receptor) and carriers (reduced folate carrier, proton-coupled transporter) to ensure sufficient supply of these molecules. [139] A folic acid deficiency during pregnancy is related to malformations such as *spina bifida* because insufficient onecarbon units are provided for cell growth. [140, 141]

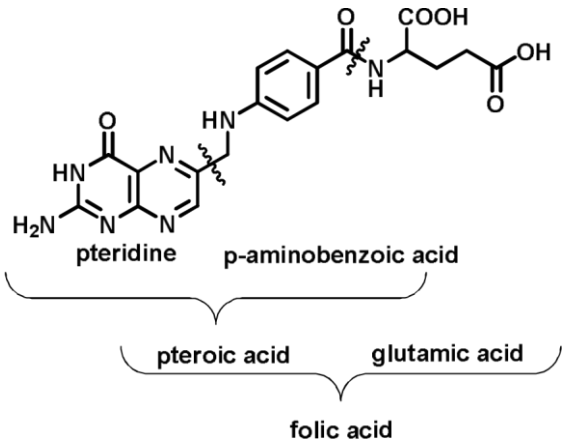

Scheme 5: Chemical structure of folic acid.

The chemical structure (scheme 5) of folic acid consists of pteridine, *p*-aminobenzoic acid and glutamic acid. The connection between pteridine and aminobenzoic acid is called pteroic acid. This pteroate part is responsible for the binding of folic acid to the folate receptor. [142]

At the beginning of the folate cycle, also known as one-carbon metabolism (figure 8), folic acid is transported through the cell membrane mainly by reduced folate carriers (RFC). In the first step folic acid is reduced to tetrahydrofolate (THF), which is then converted to 5,10-methylene-THF by serine hydroxymethyl transferase (SHMT). Subsequently 5-methyl-THF, the most common form of folic acid in the plasma, is formed and acts as an important one-carbon-unit donor for DNA replication and repair mechanisms. [143] Therefore, the kidneys ensure strict recycling of folic acid and folates via reduced folate carriers (RFCs), ɲ-folate receptors (ɲ-FRs), proton-coupled folate transporters (PCFTs) and other organic transporters as well as proteins. In 2013, the first crystal structure of the folate receptor was reported providing a much better understanding of binding mechanisms. [144]

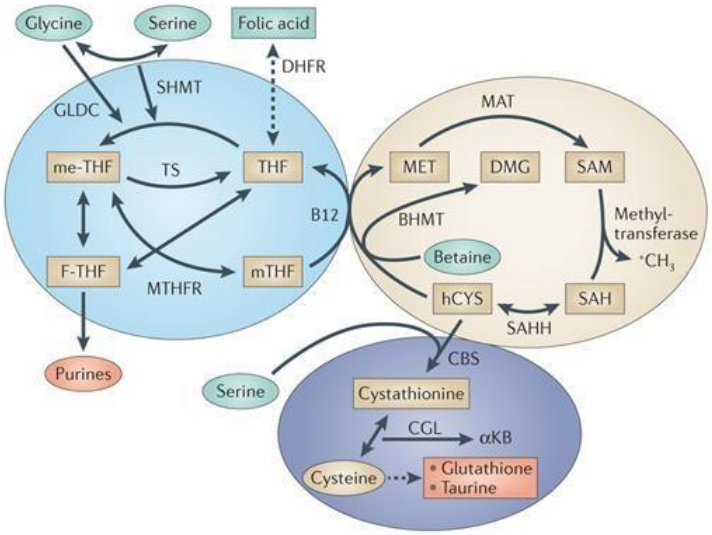

Figure 8: Folate and methionine metabolism constitute one-carbon metabolism. THF = tetrahydrofolate, DHFR = dihydrofolate reductase, mTHF = 5-methyltetrahydrofolate, me-THF = 5,10-methylene-tetrahydrofolate, F-THF = 10formyltetrahydrofolate, SHMT = serine hydroxymethyl transferase, GLDC = glycine decarboxylase, TS = thymidylate synthase, MTHFR = methylenetetrahydrofolate reductase. [143]

1.7. The folate receptor as target

To ensure sufficient supply of folic acid and folates, tetrahydrofolate is transported via the anionic reduced folate carrier across the cellular membrane. This reduced form of folic acid (5-methyl-THF) plays an important role for normal cell proliferation. [145] Recently, a transporter was discovered which can provide folate transportation under acidic conditions. This proton-coupled folate transporter (PCFT) is mainly found in the intestines. [139, 146, 147] These transport systems can easily be reached by folates circulating in the blood stream. In contrast to this, there is another family of receptors divided in three subtypes: ɲ-folate receptor (ɲ-FR), ɴ-folate receptor (ɴ-FR) and œ-folate receptor (œ-FR). These receptors provide receptor-mediated transportation of the oxidized form of folic acid via endocytosis into the cells. [148] The lower pH value inside the cell causes opening of the receptor (FR), especially to the ɲ-FR (IC_{50} of 0.1 nM, $k_D \sim 1$ nM). High proliferating cells such as cancer vesicle and releases folic acid into the cytosol. [149] Folic acid shows very high affinities to the folate cells (over)express the folate receptor to ensure sufficient folic acid supply. Therefore, the folate receptor can be found on various tumor types, especially ovarian, lung and breast cancer, providing an excellent target for diagnosis and therapy. In general, (over)expression of this receptor can be found on more than 50 % of all human tumors. On the other hand, the ɴ-FR plays an important role in inflammatory and autoimmune diseases due to its expression on activated macrophages. [150, 151,152] However, in healthy tissue the expression of the FR is strictly limited to a few sites such as the kidneys, choroid plexus, lung, salivary glands and the placenta making it an ideal oncological target for imaging and therapy. [153–155]

1.8. Folic acids and folates in diagnosis and therapy

The essential role of folic acid in DNA and RNA synthesis makes folate derivatives promising candidates for tumor diagnosis and therapy. The development of folate-based radiotracers for tumor diagnosis began in 1996 with the radiolabeling of a deferoxamine-functionalized folic acid derivative with gallium-67. [156–158] In the following years several other SPECT-tracers based on folate derivatives have been developed, mostly labeled with technetium-99m. [159–163] The comparison between radiolabeled folate and pteroate derivatives in 2006 by Mueller *et al.* showed that the pteroic acid moiety is the pharmacophoric relevant region of the folic acid molecule. [164] One very promising folate derivative for diagnosis was reported by Endocyte in 2002. [165] [^{99m}Tc]Tc-EC20 (*Etarfolatide*^{TM}) is mainly used for diagnosis of ovarian cancer, especially the *cis*-platinum resistant types. The folate-based chemotherapeutic *Vintafolide*^{TM} enables treatment of ovarian cancer. [166]

1.9. PET-folates

The first PET-folate derivative labeled with fluorine-18, [^{18}F]fluorobenzylamine(FBA)-folate, was reported in 2006 by Bettio *et al.* showing a moderate tumor uptake of around 6 % ID/g tissue and predominant hepatobiliary elimination. [167] Furthermore, only an isomeric mixture of ɲœ-[^{18}F]FBAfolate was obtained during labeling reaction. The click approach was applied to ^{18}F-labeled folate derivatives in 2008, but unfortunately this [^{18}F]fluoro-click-folate showed pronounced hepatobiliary excretion due to an increased hydrophobicity. [168] In 2010, Ross *et al.* reported a direct labeled [^{18}F]fluoro-folate derivative with very good affinities to the folate receptor (K_i=1.8 ± 0.1 nM). This radiotracer showed fast renal clearance and only a moderate hepatobiliary elimination, but unfortunately direct labeling resulted in very poor overall radiochemical yields. [169] This problem was overcome by replacing the phenyl ring of the folic acid molecule by a less electron-rich pyridine ring. Higher RCYs up to 9 % (d.c.) were achieved and even the tumor uptake was increased to around 12 %ID/g tissue. [170] Further improvements of *in vivo* properties were achieved with a [^{18}F]FDG(click)-folate in 2012, which combines the click approach with the idea to use the most important PET-tracer [^{18}F]FDG as a prosthetic group. [6] Also in 2012 Jammaz *et al*. published a [^{18}F]FDG-folate where the [^{18}F]FDG was attached via oxime ligation to the folate derivative. They observed only a moderate tumor uptake of around 3 %ID/g tissue and a very low and unexpected kidney uptake of below 2 %ID/ g tissue. The exact reason for this low uptake remained unclear but might be due to the overall negative charge of the radiotracer. [171] Another click-folate with increased hydrophilic character was published in 2013 by Schieferstein *et al*., but unfortunately the [^{18}F]fluoro-oligoethyleneglycol(OEG)-folate showed only a moderate tumor uptake. [172] The problem of hepatobiliary excretion was already overcome in 2011 by the introduction of polar ligands for radiometal complexation. [144] The combination of therapeutic radionuclides with existing folate derivatives for therapeutic approach was not possible until 2013 due to high kidney uptake. Only the introduction of an albumin moiety into a [^{177}Lu]Lu-folate derivative resulted in a reduced kidney uptake in animal models allowing further therapeutic studies. [173] This approach was also applied to ^{18}F-labeled folates, increasing the tumor-to-kidney-ratio to a value of around 1. The albumin-binding[^{18}F]FDG-folate showed the highest ever published tumor uptake in KB tumor bearing mice (15.2 ± 0.53 %ID/g, 4h p.i.). [174] To overcome the mostly long labeling reaction times and to simplify the synthesis Chen *et al.* recently published a NOTA-Al[^{18}F]F-folate, which can be produced within 37 min with a RCY of 19 %. [175] Almost all folate-based radiopharmaceuticals have been prepared via derivatization at the œ-position. In 2015 Boss *et al.* published a comparative study between three pairs of ɲ- and œ-conjugated folic acid derivatives labeled with fluorine-18. For all six derivatives IC_{50} values in the range of 1.4 to 2.2 nM were

determined and therefore the authors concluded that the site of derivatization has no dramatic influence on the binding affinities. [176] The recently published crystal structure of the ɲ-folate receptor in complex with folic acid agrees with these findings, because it shows that the pteroate moiety is buried in the FR and the glutamate part sticks out of the binding pocket. [177] These results are also confirmed by the work of Bettio *et al.* [178], Leamon *et al. [179]* and Mueller *et al.*. [180] The ɲ- and œ- derivatives showed also similar tumor uptake, but for the ɲregioisomers a lower liver uptake and therefore a lower hepatobiliary excretion was observed. The authors assumed that this might be due to the proton-coupled folate transporter (PCFT), which is mainly expressed in the liver, but the exact reason remained unclear.

Table 3 gives an overview of several [^{18}F]fluoro-folate derivatives including radiochemical yields, preparation time, specific activity and *in vivo* accumulation.

Table 3: Details and results of the radiolabeling and *in vivo* behavior of different [^{18}F]fluoro-folate derivatives.

Compound	RCY [%]	Time [min]	SA [GBq/µmol]	Tumor [%ID/g]	Kidney [%ID/g]	Liver [%ID/g]	Lit.
ɲœ- [^{18}F] FBAfolate	~ 5	135	7 - 24	6.6±1.8 125 min	40.7±12.8	2.4±0.4	[178]
[^{18}F]fluoroclick-folate	35	90	160±70	3.1±0.8 45 min p.i.	16.5±2.2	1.7±0.1	[169]
2´-[^{18}F]fluoro folic acid	4	80	24±12	9.4±1.8	46.1±13.4	7.8±1.2	[5]
3´-Aza-2´[^{18}F]fluorofolic acid	9	110	35-127	12.6±1.8 90 min p.i.	57.3±8.4	10.3±2.4	[170]
[^{18}F]FDG-folate	35	70	ш9	3.3±0.3	1.5±0.05	0.7±0.6	[171]
[^{18}F]FDG(click)folat	25	180	90 ± 38	10.0±1.1 60 min p.i.	42.9±2.0	9.5±1.1	[6]
[^{18}F]fluoro-OEG-folate	8.7	90		3.5±0.7 90 min p.i.	41.0±7.0	2.3±0.5	[172]
Albumin-[^{18}F]FDG-folate	1-2	180	20-50	15.2±0.5 4 h p.i.	18.1±0.41	5.6±0.6	[174]
Folate-NOTA-Al[^{18}F]F	18.6±4.5	37	69 ± 20	10.9±2.7 120 p.i.	78.6±5.1	5.3±0.5	[175]
ɲ-[^{18}F]FDG (click)-folate	3-10		30-170	10.9±0.5 90 min	52.9±4.2	3.0±0.5	[6]
œ-[^{18}F]FDG (click)-folate	5-25			9.1±2.1 90 min	27.1±1.5	3.4±1.2	[176]
ɲ-[^{18}F]FE(click)-folate	2-4		25-122	12.5±1.0	32.7±3.5	2.8±0.6	[176]
œ-[^{18}F]FE(click)folate	n.d.			7.2±1.0	16.9±1.2	8.7±1.2	[176]
ɲ-[^{18}F]FB(click)-folate	20-23		63-196	3.7±0.6	44.2±4.0	0.9±0.2	[176]

Œ-[^{18}F]FB(click)folate	19-21		3.2±1.1	32.9±1.7	2.3±0.2	[176]
[^{18}F]fluoro-ala-Folate	21 ± 3	150	1.7±1.1	14.4±1.0	1.7±1.0	*curr. work*
[^{18}F]fluoro-DBCO-Folate	3.2 ± 1.8	120	0.5±0.1	4.8±0.9	0.2±0.1	*curr. work*

Some [^{18}F]fluoro-click-folates show strong hepatobiliary excretion due to the high lipophilicity of the prosthetic groups. To compare the lipophilicity of different [^{18}F]fluoro-folates, the capacity factor (k´value) determined by the same reversed-phase HPLC system and eluent can be used. The comparison with examples from the literature (table 4) can give an idea about the extent of liver uptake, hepatobiliary excretion and abdominal background of new [^{18}F]fluoro-folate derivatives.

Table 4: Relative lipophilicity (k´ values) of several [^{18}F]fluoro-folate derivatives.

Folate derivative	k´ value (relative lipophilicity)	Literature
[^{19}F]fluoro-ala-folate	0.27 (0.40*)	*current work*
native folic acid	0.30	[168]
[^{19}F]fluoro-TEG-DBCO-TEG-FS	0.50 ± 0.10 (0.88 ± 0.13*)	*current work*
2´[^{19}F]fluorofolic acid	0.53	[169]
[^{19}F]fluoro-benzyl-FS	0.67	[168]
[^{19}F]fluoro-TEG-triazol-TEG-FS	1.12	[172]
[^{19}F]fluoro-propyl-triazol-FS	2.28	[168]

*determined at pH 7.4

1.10. Amino acid transporter

Peptides and proteins are built out of so called proteinogenic amino acids by a step-by-step addition using ribosome. [181] Nine of these 22 proteinogenic amino acids are “essential” (phenylalanine, valine, threonine, tryptophan, methionine, leucine, isoleucine, lysine and histidine), which means they must be taken up by food, because they cannot be produced by the human body from other compounds. [182] Other amino acids are only essential in some certain ages or medical condition and pregnancy. Amino acids do not only play an important role for protein synthesis, but also in brain as neurotransmitters (glutamic acid, gamma-amino-butyric acid “GABA”) [183] and for the synthesis of porphyrins used in the red blood cells (glycine). Therefore, the transportation of amino acids into the cells and across the blood brain barrier is very important for the human body. Furthermore, highly

proliferating cells such as tumor cells have an even higher demand on amino acids for protein synthesis.

In general, solute carrier transporter (SCL) can be classified based on their substrate-specificity and Na^+-dependence. Heterodimeric amino acid transporters consist of a light chain (SLC7, Na^+independent family) [184] and a heavy chain (SLC3) [185, 186], which are covalently linked via a disulfide-bridge. [187, 188] The interaction between different heavy and light chains forms various different amino acid transport systems. For example, system L is formed by the interaction of the heavy chain 4F2hc with LAT1 and LAT2. Table 5 provides an overview of the different interactions of heavy and light chains and their substrates.

Table 5: Classification of the heterodimeric amino acids transporter. [189] *BCH = 2-aminobicyclo[2.2.1]heptane-2-carbocylic acid

Heavy chain	Light chain	Transport system	Na^+-dependence	Substrates
rBAT	$b^{0,+}$, AT	$b_{0,+}$	independent	basic, large and small neutral amino acids
	Y^+LAT1	Y^+L	dependent	neutral amino acids
			independent	basic amino acids
	Y^+LAT2	Y^+L	dependent	neutral amino acids
			independent	basic amino acids
	xCT	X_{c-}	independent	acidic amino acids
4F2hc	asc1	asc	independent	basic and small neutral amino acids
	LAT1	L	independent	large neutral amino acids and BCH
	LAT2	L	independent	large and small neutral amino acids and BCH*

System L was first identified in 1963 [190] and transports large neutral, branched and aromatic acids into the cells. The first light chain subunit of this transporter system was reported in 1998 and named LAT1. [187, 188] Within the following years three more systems (LAT2, LAT3 and LAT4) have been identified. [191–194] All four transporter systems have in common that they are Na^+-independent and are inhibited by 2-aminobicyclo[2.2.1]heptane-2-carboxylic acid (BCH). In contrast, LAT3 and LAT4 are not heterodimeric, which means they do not need co-expression of the heavy chain 4F2hc. [189]

For Na^+-dependent transporters, the electrochemical gradient across the cell membrane can be used to transport amino acids into the cells. Since LAT1 and LAT2 are Na^+-independent, they transport amino acids by an 1:1 exchange of another amino acids into the cell (figure 9). Therefore, a second transporter system and a substrate for both transporters are needed. This substrate should provide low influx

affinity and high efflux activity for the LAT1 or LAT2 transporter. In 2001, L-glutamine [195] and in 2002, L-methionine were proposed to act as shared substrates between LAT1 and Na^+dependent transporters. [196, 197]

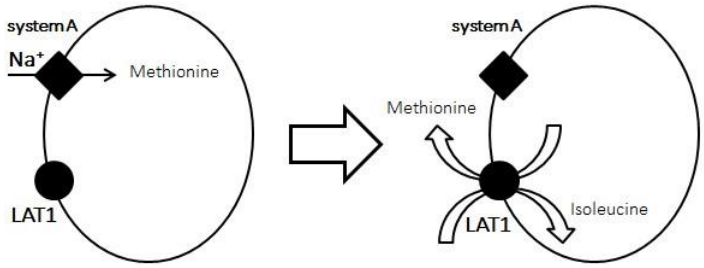

Figure 9: Schematic overview of the influx of isoleucine and efflux of methionine by LAT1. In the first step, L-methionine is transported into the cells via system A transporter followed by exchange to L-isoleucine. [189]

LAT1 transports mainly large neutral amino acids such as leucine, isoleucine, valine, phenylalanine, tyrosine, tryptophan, methionine and histidine [186, 188], whereas LAT2 in general provides a broader substrate specificity. It transports also smaller amino acids as for example glycine, alanine, serine, threonine, cysteine, glutamine and aspartate, but shows in general lower affinities than LAT1. [194]

The main responsibility of LAT1 is the transportation of amino acids into growing cells and across the blood brain barrier. Therefore, it is primary expressed in tumors, the placenta [188] and in the brain [198] whereas LAT2 is mainly found in the kidneys, the colon and the intestines. [199, 200] Since fast growing cells have a very high demand on amino acids, LAT1 is overexpressed on many tumor cells to ensure sufficient supply. [185, 188, 195]

In 2000, Fukasawa *et al*. described ASC-1 as a novel protein with high affinities to small neutral amino acids such as glycine, L-serine, D-serine, alanine and cysteine. Western blot analyses confirmed that ASC-1 and its heavy chain 4F2hc are linked via a disulfide bond. ASC-1 shows the highest structural similarity to LAT2, whereas ASC-1 in contrast to LAT2 prefers the transportation of small amino acids and shows no inhibition by BCH. A particularity of ASC-1 is the fact that it also accepts D-amino acids and amino acid-related compounds such as alanine-methylester, N-alanine and 2-aminoisobutyric acid. Efflux experiments with preloaded [^{14}C]alanine indicated an exchange transport as well as a facilitated diffusion for ASC-1, in which the exchange mode is preferred. [201] Detection of RNA by gene expression studies reveals the expression of ASC-1 in lung, small intestines, but mainly the brain. In 2003, Helboe *et al.* studied in detail the distribution of ASC-1 expression in rodent brain. The fact, that ASC-1 expression was mainly found in the same areas with high D-serine concentrations indicated a regulation of serine by this transporter. Highest expression was found in the cerebral cortex, hippocampus, striatum and the limbic forebrain. [202]

1.11. ^{18}F-labeled amino acids for tumor imaging

In general, malignant cells show a higher demand on amino acids due to their increased proliferation rate, which results also in a higher protein synthesis rate (PSR). [203] It is thought, that tumors can upregulate the amino acid transporter expression to ensure sufficient supply of nutrients. [204] Therefore, radiolabeled amino acids can be used to investigate the incorporation of amino acids into proteins by measuring the PSR (L-[^{11}C]leucine) [205] or only the tumor uptake using PET. [206–208] However, compared to the total amount of amino acids taken up by the cells, the fraction of incorporated amino acids into proteins is quite low. Furthermore, amino acid uptake in general proceeds very fast (within 20 min), while the imaging of the PSR takes up to 60 min. Due to their easy labeling properties mainly ^{11}C-labeled amino acids have been the research focus for many years. [205] L-[^{11}C]methionine is the most investigated amino acid usable for PET imaging of brain, head and neck, lung and breast cancer. Unfortunately, it shows a high uptake in the liver, the pancreas and the intestines, what hampers the imaging of tumors in the abdominal and bladder/prostate region. [209] Since cyclotrons are not available at every research site or clinic and the very short half-life of carbon11 does not allow the transportation of ^{11}C-labeled radiotracers, the interest in radiopharmaceuticals labeled with fluorine-18 increased. Distinct research activities focused on ^{18}F-labeled tyrosine derivatives, such as L-2-[^{18}F]fluorotyrosine [210, 211], L-3-[^{18}F]fluoro-ɲ-methyl tyrosine [212, 213] and *O*-(2-[^{18}F]fluoroethyl)- L-tyrosine. [206, 214] Coenen *et al.* reported the incorporation of L-2[^{18}F]fluorotyrosine into proteins in mouse cerebral tissue, which was proven by SDS gel electrophoresis. Therefore, they concluded that L-2-[^{18}F]fluorotyrosine can be used to image the PSR. However, in contrast to this, studies in patients showed that the tumor accumulation is mainly due to the increased amino acid transportation rate. [211] Furthermore this radiotracer showed a low stability and a high amount of fluoride was measured in the plasma (23 % after 40 min p.i.). Since fluoride is not able to cross the blood brain barrier this is not a problem for brain imaging, but harms the application of this tracer for imaging other organs due to accumulation of fluoride in the bones. L3-[^{18}F]fluoro-ɲ-methyl tyrosine ([^{18}F]FMT) showed a higher stability combined with a rapid blood clearance and fast brain uptake. In general, [^{18}F]FMT showed a higher uptake in all organs compared to 2-[^{18}F]fluorodeoxyglucose ([^{18}F]FDG), especially a high accumulation was observed in the pancreas and the kidneys. [213] In 1999, Wester *et al.* reported the synthesis and evaluation of *O*-(2[^{18}F]fluoroethyl)- L-tyrosine ([^{18}F]FET). They also overserved a high uptake in the pancreas and the kidneys. The fact, that the activity from plasma, brain and tumor samples was not acid precipitable lead to the conclusion, that [^{18}F]FET is not incorporated into proteins. [206] Furthermore, some radiotracers based on phenylalanine have been developed. 6-[^{18}F]fluoro- L-dihydroxyphenylalanine

(6[^{18}F]FDOPA) is mainly used to study the doparminergic brain system, [215] while the reduced liver uptake of L-2-[^{18}F]fluorophenylalanine compared to [^{11}C]methionine makes it preferable for wholebody scans. [209] Critically for the visualization of brain tumors is the ability of the radiotracer to cross the blood brain barrier. Therefore, especially substrates for system L, which is active at the blood brain barrier and upregulated in many tumors, such as [^{11}C]methionine, [^{18}F]FET and [^{18}F]FDOPA are promising brain tumor imaging candidates. Recently, 5-[^{18}F]fluoroleucine has been reported by Chin *et al.* showing high uptake in breast cancer cell lines via LAT1 transporter. Further evaluation in specific LAT1 overexpressing tumors, such as prostate cancer are to be investigated. [216]

Despite glucose, glutamine is one of the major sources for carbon and energy for tumor growth and proliferation. Although [^{18}F]FDG is widely used in PET imaging, it has some limitations due to nonspecificity towards inflammation and due to increased glucose metabolism in brain and heart. [217] Therefore, Koglin *et al.* published in 2011 an ^{18}F-labeled glutamate derivative, which is a substrate for system x_c^-. [218] This system is overexpressed in many tumors, ensuring increased access to L-cysteine. Since this system is not able to discriminate between L-cysteine and L-glutamate, fluorinated derivatives of glutamate promise high potential as tumor imaging candidates. Because the former 4-[^{18}F]fluoro L-glutamate showed defluorination in humans [219] (4S)-4-(3-[^{18}F]fluoropropyl)- L-glutamate, alias [^{18}F]FSPG, has been developed. This novel radiotracer was then evaluated in cell competition assays concerning its interaction with system x_c^-, showing strong inhibition with Lglutamate and L-cystine. [218] Furthermore, this derivative showed high uptake in several tumor cell lines and although no intracellular metabolism was observed a high retention in the tumor cells was achieved. In PET studies, the radiotracer showed fast and high tumor uptake compared with a rapid blood clearance. Clinical studies with [^{18}F]FSPG in comparison with [^{18}F]FDG with non-small cell lung cancer (nsclc) patients showed that they were able to identify all nsclc and that 59 of 67 (88 %) [^{18}F]FDG lesions were detected. [220] This proves the high potential of this novel amino acid-based radiotracer for tumor diagnosis using PET.

Besides these natural amino acids, a few synthetic analogues have been investigated as tumor imaging candidates. These analogues such as 1-aminocyclopentane carboxylic acid or 1-amino-3[^{18}F]fluorocyclobutane-1-carboxylic acid ([^{18}F]FACBC) [208] are not expected to be incorporated into proteins. [207] Recently, Bouhlel *et al.* reported the synthesis and evaluation of two novel long chain fluoroalkyl amino acids, (S)-2-amino-7-[^{18}F]fluoro-2-methylheptanoic acid ([^{18}F]FAMHep) and (S)-2amino-7-[^{18}F]fluoroheptanoic acid ([^{18}F]FAHep]. [221] They observed that the ɲ-methyl group plays an important role for the recognition of these amino acids by system L amino acid transporters. *In vitro* and *in vivo* studies showed, that only [^{18}F]FAHep is a substrate for system L, although the availability of ɲ-methyl substituted radiolabeled amino acids in the brain is reported.

1.12. ^{18}F-radiolabeling methods

A convenient ^{18}F-labeling strategy should provide the desired ^{18}F-radiotracer in good overall yields and within a short reaction time. Special attention needs to be paid at precursor design and synthesis for direct ^{18}F-fluorination: a suitable leaving group for nucleophilic substitution needs to be inserted into the molecule and often protecting groups are required to prevent issues during radiolabeling. Additionally, several problems can occur during deprotection of these groups after the radiolabeling reaction, such as decomposition of the molecule or incomplete deprotection. Furthermore, especially the harsh conditions during direct ^{18}F-labeling (high temperature, basic conditions) pose an exceeding challenge for the radiolabeling of sensitive biomolecules. [222, 223] To circumvent these problems, ^{18}F-labeling of such sensitive molecules can be performed using ^{18}F-prosthetic groups. These small molecules allow a sensitive and bioorthogonal ^{18}F-labeling, which treats a multitude of functional groups of those bioactive compounds with respect, without the need of protection chemistry. There are several methods for the attachment of the ^{18}F-prosthetic group to the biomolecule requiring different functional groups on both molecules. Click reactions fulfill all criteria mentioned above. High specificity and excellent yields can be achieved performing the Cu(I)-catalyzed variation of the Huisgen 1,3-dipolar cycloaddition (copper-catalyzed alkyne-azide cycloaddition, CuAAC) between terminal alkynes and azides giving a 1,2,3-triazole. [224] The reaction can be performed using a copper(I) species such as CuI or CuBr, but works much better with a copper(II) catalyst (e.g. $CuSO_4$ or copper acetate) and a reducing agent (sodium ascorbate), which produces Cu(I) *in situ*. Furthermore, an excess of sodium ascorbate prevents the formation of oxidative homo coupling products. A wide variety of protic and aprotic solvents including water and miscible organic solvents can be used for the click reaction. The resulting 1,2,3-triazole exhibits a high chemical stability and shows an aromatic character.

The copper catalyst is needed to decrease the activation energy for the reaction between the alkyne and the azide. First, a υ-complex is formed between the triple bond of the terminal alkyne and the copper species, which results in an ϻ-bond copper acetylide. Deprotonation of the alkyne is now possible, because the coordination between the metal and the alkyne decreases the pk_s value. Thus a second copper atom can be coordinated onto the triple bond via a υ-complex. [225] This catalytic complex is now able to bind the azide reversibly, which enables the ring closure as shown in scheme 6.

[226] The final product is formed by protonation, whereby the former alkyne proton is used.

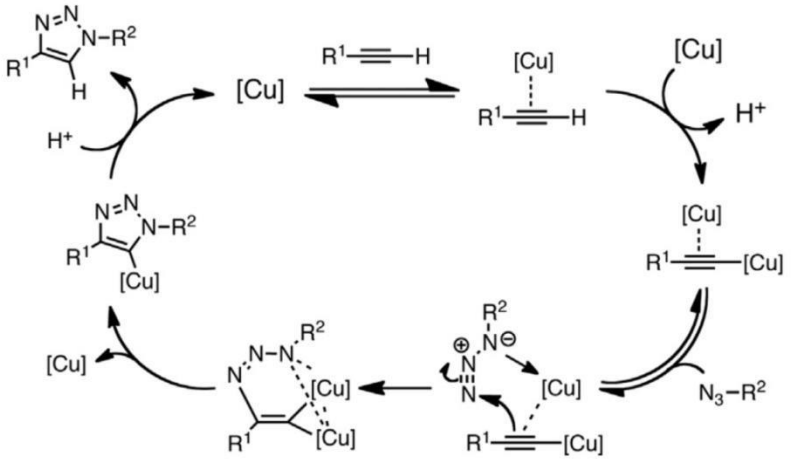

Scheme 6: Mechanistic overview of the copper-catalyzed azide-alkyne cycloaddition (CuAAC). [227]

Nevertheless, the need of cytotoxic copper [228] during radiosynthesis limits the application range of copper-catalyzed labeled radiotracers for clinical use. Therefore, within the last decade more and more strained prosthetic groups for the labeling via copper-free click reactions (strain-promoted alkyne-azide cycloaddition, SPAAC) have been developed. These molecules exhibit a much higher reactivity due to cyclic stress, whereby no catalyst is needed for the cycloaddition of an azide. In 2010, Kuzmin *et al.* published the synthesis of an aza-dibenzocyclooctyne, which was used for surfacefunctionalization via catalyst-free click reaction. [229] In contrast to the very reactive cyclooctyne derivatives, dibenzocyclooctynes (DBCO) are synthetically much more accessible. Furthermore, the substitution of one saturated carbon in the cyclooctyne ring improves its reactivity and eases the synthesis. [230–232] Electron withdrawing groups next to the alkyne function further increase the reaction rate. In 2007, Baskin *et al.* reported a difluorinated cyclooctyne with a second-order rate constant much greater than observed for the Staudinger ligation or any other previously reported strain-promoted cycloaddition. [232, 233] The propargylic fluorine atoms lower the LUMO (lowest unoccupied molecule orbital) and thus increase the interaction with the HOMO (highest occupied molecule orbital) of the azide. To increase the hydrophilic character of dibenzocyclooctynes, either, alcohol or amine functions are inserted. Furthermore, this eases the derivatization of these molecules for example for the use as prosthetic groups for radiolabeling reactions. The only drawback can be seen in the relatively low reaction rate of the dibenzocyclooctynes with azides (0.05 $M^{-1}s^{-1}$). [234–237] This is not a handicap for the use of DBCO-modified prosthetic groups for the radiolabeling of molecules with for example fluorine-18, but for the application as *in vivo* click agents.

The strain-promoted cycloaddition between alkynes and azides does not require a copper cataylst, wherefore the activation energy must be reduced by another effect. In 2008, Ess *et al.* analyzed the transition states for 1,3-dipolar cycloadditions between phenyl azide and acetylene, cyclooctyne and difluorocyclooctyne by density function theory. [238]

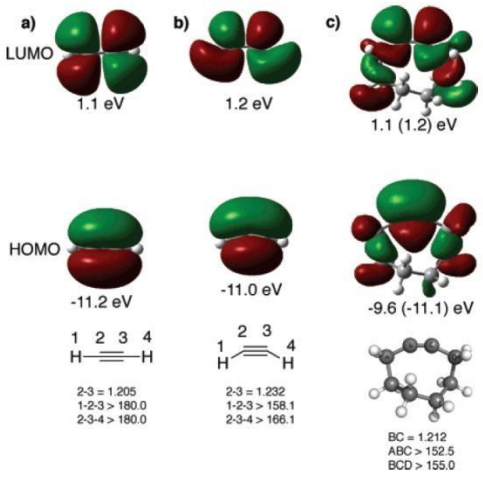

Figure 10: Geometries and frontiers orbitals of (a) acetylene, (b) distorted acetylene and (c) cyclooctyne. [238]

Figure 10 shows H-C-C angles and frontier orbitals of linear acetylene, distorted acetylene and the ground state of cyclooctyne. The linear acetylene deforms to angles of 158° and 166° in the transition state. Cyclooctyne exhibits already in the ground state lower angles of 153° and 155°, which decreases the barrier of the reaction with an azide from 16.2 kcal/mol for acetylene to 8.0 kcal/mol (figure 10). Fluorine atoms next to the alkyne function of the cyclooctyne further decrease the activation energy to 6 kcal/mol (figure 11). The activation energy is the sum of destabilizing distortions and stabilizing interactions ($\Delta E^{\ddagger} = \Delta E_d^{\ddagger} + \Delta E_i^{\ddagger}$). For the cyclooctyne not only the distortion energy for the alkyne is lower, but also for the 1,3-dipole due to an earlier transition state of this reaction. Therefore the rate enhancement (factor 10^6) is not due to orbital interaction effects but to the cyclic stress of the alkyne. The transition states are slightly earlier for cyclooctyne compared to acetylene with longer C-N bonds and larger N-N-N dipole angles (142° compared to 138°). This results in lower distortion energy for the reaction of an azide with cyclooctyne and explains again why the SPAAC occurs without a copper catalyst.

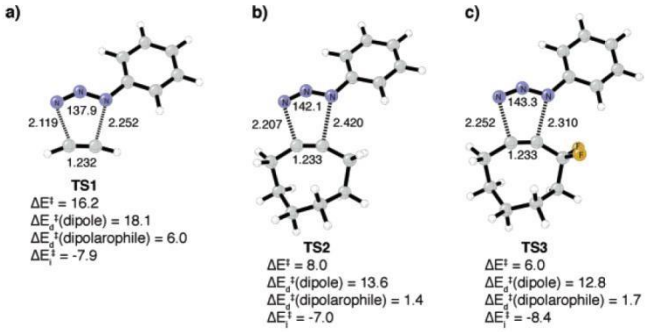

Figure 11: Density function theory calculations for the activation energy ($\Delta E^{\ddagger}$), the distortion energy ($\Delta E_d^{\ddagger}$) for the dipole and the alkyne and the stabilizing interaction energy ($\Delta E_i^{\ddagger}$) for the concerted transition structures of phenyl azide cycloaddition with (a) acetylene, (b) cyclooctyne and (c) difluorocyclootyne (kcal/mol). [238]

1.13. References

[1] Robert Koch Institut, “krebs_in_deutschland_2015.pdf”. (27.01.2017)

[2] *www.krebsinformationsdienst.de.* (27.01.2017)

[3] S. Liang, Y. Ma, J. Guo, R. Guo, and H. Wang, "^{18}F-radiolabeled analogs of peptide RGD-A7R for simultaneous PET imaging of both $\beta_V N_3$ and VEGF in tumors," *Journal of Radioanalytical and Nuclear Chemistry*, vol. 303, no. 3, pp. 1891-96, 2014.

[4] C. R. Fischer, C. Müller, J. Reber, A. Müller, S. D. Krämer, S. M. Ametamey, and R. Schibli, "[^{18}F]Fluoro-Deoxy-Glucose Folate: A Novel PET Radiotracer with Improved in Vivo Properties for Folate Receptor Targeting," *Bioconjugate Chemistry*, vol. 23, no. 4, pp. 805–813, 2012. [5] T. L. Ross, M. Honer, P. Y. Lam, T. L. Mindt, V. Groehn, R. Schibli, P. A. Schubiger, and S. M. Ametamey, "Fluorine-18 click radiosynthesis and preclinical evaluation of a new ^{18}F-labeled folic acid derivative," *Bioconjugate Chemistry*, vol. 19, no. 12, pp. 2462–2470, 2008.

[6] H. Schieferstein, A. Kelsch, A. Reibel, K. Koynov, M. Barz, H. G. Buchholz, N. Bausbacher, O. Thews, R. Zentel, and T. L. Ross, "^{18}F-Radiolabeling, preliminary evaluation of folate-pHPMA conjugates via PET," *Macromolecular Bioscience*, vol. 14, no. 10, pp. 1396–1405, 2014.

[7] R. R. Edelmann, and S. Warach, "Magnetic Resonance Imaging," *The New England Journal of Medicine*, vol. 328, pp. 708-16, 1993.

[8] S.-P. Lin, and J. J. Brown, "MR contrast agents: physical and pharmacologic basics," *Journal of Magnetic Resonance Imaging*, vol. 25, no. 5, pp. 884–899, 2007.

[9] P. Hermann, J. Kotek, V. Kubicek, and I. Lukes, "Gadolinium(III) complexes as MRI contrast agents: ligand design and properties of the complexes," *Dalton transactions*, no. 23, pp. 3027–3047, 2008.

[10] C. Giussani, F. E. Roux, J. Ojemann, E. P. Sqanzerla, D. Pirilli, and C. Papagno, "Is preoperative functional magnetic resonance imaging reliable for language areas mapping in brain tumor surgery? Review of language functional magnetic resonance imaging and direct cortical stimulation correlation studies," *Neurosurgery*, vol. 66, no. 1, pp. 113–120, 2010.

[11] D. J. Heeger, and D. Ress, "What does fMRI tell us about neuronal activity?," *Nature Reviews. Neuroscience*, vol. 3, no. 2, pp. 142–151, 2002.

[12] G. T. Herman, "Fundamentals of Computerized Tomography: Image reconstruction from projection," *Springer*, 2nd edition, New York, USA, 2009.

[13] W. R. Hendee, and E. R. Ritenour, "Medical imaging physics," *Wiley*, 4th edition, John & Sons, New York, USA, 2002.

[14] J. D. Mathews, A. V. Forsythe, Z. Brady, M. W. Butler, S. K. Goergen, G. B. Byrnes, G. G. Giles, A. B. Wallace, P. R. Anderson, T. A. Guiver, P. McGale, T. M. Cain, J. G. Dowty, A. C. Bickerstaffe, and S. C. Darby, "Cancer risk in 680,000 people exposed to computed tomography scans in childhood or adolescence: data linkage study of 11 million Australians," *British Medical Journal*, vol. 346, f2360, 2013.

[15] D. J. Brenner, and E. J. Hall, "Computed tomography: an increasing source of radiation exposure," *The New England Journal of Medicine*, vol. 357, no. 22, pp. 2277–2284, 2007.

[16] R. F. Mattrey, and D. A. Aguirre, "Advances in Contrast Media Research," *Academic Radiology*, no. 10, pp. 1450–1460, 2003.

[17] C. Christiansen, "X-ray contrast media - an overview," *Toxicology*, vol. 209, no. 2, pp. 185–187, 2005.

[18] H. Lusic, and M. W. Grinstaff, "X-ray-computed tomography contrast agents," *Chemical Reviews*, vol. 113, no. 3, pp. 1641–1666, 2013.

[19] F. Hallouard, N. Anton, P. Choquet, A. Constantinesco, and T. Vandamme, “Iodinated blood pool contrast media for preclinical X-ray imaging applications - a review,” *Biomaterials*, vol. 31, no. 24, pp. 6249–6268, 2010.

[20] N. Lee, S. H. Choi, and T. Hyeon, “Nano-sized CT contrast agents,” *Advanced Materials*, vol. 25, no. 19, pp. 2641–2660, 2013.

[21] X.-L. Wang, T. Nguyen, D. Gillespie, R. Jensen, and Z.-R. Lu, “A multifunctional and reversibly polymerizable carrier for efficient siRNA delivery,” *Biomaterials*, vol. 29, no. 1, pp. 15–22, 2008.

[22] J. Zheng, J. Liu, M. Dunne, D. A. Jaffray, and C. Allen, “In vivo performance of a liposomal vascular contrast agent for CT and MR-based image guidance applications,” *Pharmaceutical Research*, vol. 24, no. 6, pp. 1193–1201, 2007.

[23] K. K. Poh, R. A. Levine, J. Solis, L. Shen, M. Flaherty, Y. J. Kang, J. L. Guerrero, and J. Hung, “Assessing aortic valve area in aortic stenosis by continuity equation: a novel approach using real-time three-dimensional echocardiography,” *European Heart Journal*, vol. 29, no. 20, pp. 2526–2535, 2008.

[24] J. R. Marin, N. S. Zuckerbraun, and J. M. Kahn, “Use of emergency ultrasound in united states pediatric emergency medicine fellowship programs in 2011,” *Journal of Ultrasound in Medicine*, vol. 31, no. 9, pp. 1357-63, 2012.

[25] N. Razim, D. Fischer, M. Michaelson, A. Engel, and D. Gaitini, “The Ulitilty of focused assessment with sonography for traume as a triage tool in multiple-casualty incidents during the second Lebanon war,” *Journal of Ultrasound in Medicine*, vol. 26, no. 9, pp. 1149-56, 2007.

[26] A. Srisubat, S. Potisat, B. Lojanapiwat, V. Setthawong, and M. Laopaiboon, “Extracorporeal shock wave lithotripsy (ESWL) versus percutaneous nephrolithotomy (PCNL) or retrograde intrarenal surgery (RIRS) for kidney stones,” *The Cochrane Database of Systematic Reviews*, vol. 11, CD007044, 2014.

[27] K. G Baker, V. J Robertson, and F. A Duck, “A review of therapeutic ultrasound biophysical effects,” *Physical Therapy*, vol. 81, no. 7, pp. 1351-8, 2001.

[28] G. K Lewis, W. L Olbricht, and G. K. Lewis, “Acoustically enhanced evans blue dye perfusion in neurological tissues,” *The Journal of the Acoustical Society of America,* vol. 2, no. 1, pp. 200017, 2010.

[29] S. Niese, “George de Hevesy (1885–1966), founder of radioanalytical chemistry,” *Czechoslovak Journal of Physics*, vol. 56, no. 1, D3-D11, 2006.

[30] G. de Hevesy, "The Absorption and Translocation of Lead by Plants," *Biochemical Journal*, vol. 17, no. 4-5, pp. 439-45, 1923.

[31] H. O. Anger, “Scintillation Camera,” *Review of Scientific Instrumts*, vol. 29, no. 1, p. 27, 1958.

[32] J. W. Scuffham, M. D. Wilson, P. Seller, M. C. Veale, and P. J. Sellin, “A CdTe detector for hyperspectral SPECT imaging,” *Journal of Instrumentation*, vol. 7, no. 08, P08027-P08027, 2012.

[33] S. S. Gambhir, D. S. Berman, J. Ziffer, M. Nagler, M. Sandler, J. Patton, B. Hutton, T. Sharir, and S. B. Haim, “A novel high-sensitivity rapid-acquisition single-photon cardiac imaging camera,” *Journal of Nuclear Medicine*, vol. 50, no. 4, pp. 635–643, 2009.

[34] G. Mariani, L. Bruselli, T. Kuwert, E. E. Kim, A. Flotats, O. Israel, M. Dondi, and N. Watanabe, “A review on the clinical uses of SPECT/CT,” *European Journal of Nuclear Medicine and Molecular Imaging*, vol. 37, no. 10, pp. 1959–1985, 2010.

[35] Klaus Schwochau, “Technetium: Chemistry and Radiopharmaceutical Applications,” *WileyVCH*, p. 446, 2000.

[36] J D. Kelly, A. M. Forster, B. Hihley, C. M. Archer, F. S. Booker, L. R. Canning, K. W. Chiu, B. Edwards, H. K. Gill, M. McPartlin, K. R. Nagle, I. A. Latham, R. D. Picklet, A. E. Storey, and P. M. Webbon, "Technetium-99m-Tetrofosmin as a new radiopharmaceutical for myocardial perfusion imaging," *Journal of Nuclear Medicine*, vol. 34, no. 2, pp.222-7, 1993.

[37] D. S. Berman, R. Hachamovitch, H. Kiat, I. Cohen, J. A. Cabico, F. P. Wang, J. D. Friedman, G. Germano, K Van Train, and G. A. Diamond,"Incremental value of prognostic testing in patients with known or suspected ischemic heart disease: A basis for optimal utilization of exercise technetium-99m sestamibi nyocardial perfusion single-photon emission computed tomography," *Journal of American College of Cardiology*, vol. 26, no. 3, pp. 639-47, 1995.

[38] A. Elhendy, J. Bax, and D. Poldermans, "Dobutamine stress myocardial perfusion imaging in coronary artery disease," *Journal of Nuclear Chemistry*, vol. 43, no. 12, pp. 1634-46, 2002.

[39] J. Candell-Riera, "Present and future of nuclear cardiology. Where We Come From and Where We Are Going," *Revista Federación Argentina Cardiologia*, vol. 43, no. 2, pp. 64-70, 2014.

[40] F. J. Bonte, T. S. Harris, L. S. Hynan, E. H. Bigio, and C. L. 3. White, "Tc-99m HMPAO SPECT in the differential diagnosis of the dementias with histopathologic confirmation," *Clinical Nuclear Medicine*, vol. 31, no. 7, pp. 376–378, 2006.

[41] N. J. Dougall, S. Bruggink, and K. P. Ebmeier, "Systematic Review of the Diagnostic Accuracy of ^{99m}Tc-HMPAO-SPECT in Dementia," *American Journal of Geriatric Psychiatry*, vol. 12, no. 6, pp. 554–570, 2004.

[42] T. A. Henderson, "The diagnosis and evaluation of dementia and mild cognitive impairment with emphasis on SPECT perfusion neuroimaging," *CNS Spectrums*, vol. 17, no. 4, pp. 176–206, 2012.

[43] D. H. S. Silverman, "Brain ^{18}F-FDG PET in the diagnosis of neurodegenerative dementias comparison with perfusion SPECT," *Journal of Nuclear Medicine*, vol. 45, no. 4, pp. 594-607, 2004.

[44] A. van der Gucht, L. C. de Langavant, O. Bélissant, C. Rabu, A.-S. Cottereau, E. Evangelista, J. Chalaye, S. Bonnot-Lours, Gilles Fénelon, and E. Itti., "Brain ^{18}F-FDG, ^{18}F-Florbetaben PET/CT, ^{123}I-FP-CIT SPECT and Cardiac ^{123}I-MIBG Imaging for Diagnosis of a "Cerebral Type" of Lewy Body Disease," *Nuclear Medicine and Molecular Imaging*, vol. 50, no. 3, pp. 258-260, 2016.

[45] S. J. Tao, "Positronium Annihilation in Molecular Substances," *The Journal of Chemical Physics*, vol. 56, no. 11, p. 5499-5510, 1972.

[46] H. Herzog, and F. Rösch, "PET- und SPECT-Technik: Chemie und Physik der Bildgebung," *Pharmazie in unserer Zeit*, vol. 34, no. 6, pp. 468–473, 2005.

[47] C. L. Melcher, "Scintillation crystals for PET," *Journal of Nuclear Medicine*, vol. 41, no. 6, pp. 1051-5, 2000.

[48] M. Piel, I. Vernaleken, and F. Rosch, "Positron emission tomography in CNS drug discovery and drug monitoring," *Journal of Medicinal Chemistry*, vol. 57, no. 22, pp. 9232–9258, 2014.

[49] J. Langer, "Development of a Parallel Computing Optimized Head Movement Correction Method in Positron-Emission-Tomography," *Dissertation,* University of Applied Sciences Dresden, 2003.

[50] G. J. Ehrhardt, and M. J. Welch, "A New Germanium-68/Gallium-68-Generator," *Journal of Nuclear Medicine*, vol. 19, no. 8, pp. 925-9, 1978.

[51] K. Zhernosekow, "^{68}Ga-Generator," US 20120252981 A1, *Patent*, 2012.

[52] F. Rösch, "Past, present and future of ^{68}Ge/^{68}Ga generators," *The International Journal of Applied Radiation and Isotopes*, vol. 76, pp. 24-30, 2013.

[53] H. Arino, and H. H. Kramer, "Fission Product ^{99m}Tc Generator," *The International Journal of Applied Radiation and Isotopes*, vol. 26, no. 5, pp. 301-3, 1975.

[54] F. Rösch, "Maturation of a Key Resource - The Germanium-68/Gallium-68 Generator," *Current Radiopharmaceuticals*, vol. 5, no. 3, pp. 202-11, 2012.

[55] H. J. Harms, P. Knaapen, and S. Haan, "Automatic generation of absolute myocardial blood flow imaging using [^{15}O]H_2O and a clinical PET/CT," *European Journal of Nuclear Medicine and Molecular Imaging*, vol. 38, no. 5, pp. 930-9, 2011.

[56] M. E. Phelps, E. J. Hoffmann, S.-C. Huang, and M. M. Ter-Pogossian, "Effect of positron range on spatial resolution," *Journal of Nuclear Medicine*, vol. 16, no. 7, pp. 649-52, 1975.

[57] F. Rösch, "Handbook of Nuclear Chemistry: Radiochemistry and Radiopharmaceutical Chemistry in Life Science," *Kluwer Academic Publishers*, the Netherlands, 2003.

[58] J. Ermert, and H. H. Coenen, "Methods of ^{11}C- and ^{18}F-labeling of amino acids and derivatives for positron emission tomography," *Journal of Labelled Compounds and Radiopharmaceuticals*, vol. 56, no. 3-4, pp. 225-36, 2013.

[59] B. S. Gopal, "Cyclotron and Production of PET Radionuclides," *Springer*, 2nd edition, New York, USA, 2010.

[60] B. S. Gopal, "Basics of PET Imaging: Physics, Chemistry and Regulations," S*pringer*, 2nd edition, New York, USA, 2005.

[61] W. Chen, T. Cloughesy, N. Kamdar, N. Satyamurthy, M. Bergsneider, L. Liau, P. Mischel, J. Czernin, M. E Phelps, and D. H. Silverman, "Imaging Proliferation in Brain Tumors with ^{18}F-FLT PET: Comparison with ^{18}F-FDG," *Journal of Nuclear Medicine*, vol. 46, no. 6, pp. 945-52, 2005.

[62] D. Pauleit, G. Stoffels, A. Bachofner, F. W. Floeth, M. Sabel, H. Herzog, L. Tellmann, P. Jansen, G. Reifenberger, K. Hamacher, H. H. Coenen, and K.-J. Langen, "Comparison of ^{18}F-FET and ^{18}FFDG PET in brain tumors," *Nuclear Medicine and Biology*, vol. 37, no. 7, pp. 779-87, 2009.

[63] K. Van Laere, S. Ceyssens, F. Van Calenbergh, T. de Groot, J. Menten, P. Flamen, G. Bormans, and L. Mortelmans, "Direct comparison of ^{18}F-FDG and ^{11}C-methionine PET in suspected recurrence of glioma: sensitivity, interobserver variability and prognostic value," *European Journal of Nuclear Medicine and Molecular Imaging*, vol. 32, pp. 39-51, 2005.

[64] J. T. O´Brien, M. J. Firbank, C. Davison, N. Barnett, C. Bamford, C. Donaldson, K. Olsen, K. Herholz, D. Williams, and J. Lloyd, "^{18}F-FDG PET and perfusion SPECT in the diagnosis of Alzheimer and Lewy body dementias," *Journal of Nuclear Medicine*, vol. 55, no. 12, pp. 195965, 2014.

[65] C. Cohade, M. Osman, J. Leal, and R. L. Wahl, "Direct Comparison of ^{18}F-FDG PET and PET/CT in Patients with Colorectal Carcinoma," *Journal of Nuclear Medicine*, vol. 44, no. 11, pp. 1797803, 2003.

[66] D. Delbeke, R. E. Coleman, M. J. Guiberteau, M. L. Brown, H. D. Royal, B. A. Siegel, D. W. Townsend, L. L. Berland, J. A. Parker, K. Hubner, M. G. Stabin, G. Zubal, M. Kachelriess, V. Cronin, and S. Holbrook, "Procedure Guideline for Tumor Imaging with ^{18}F-FDG OET/CT 1.0," *Journal of Nuclear Medicine,* vol. 47, no. 5, pp. 885-95, 2006.

[67] *www.krebsdaten.de/Krebs/DE/Content/Krebsarten/Melanom/melanom_inhalt.html.* (13.02.2017)

[68] A. A. Rosenkranz, T. A. Slastnikova, M. O. Durymanov, and A. S. Sobolev, "Malignant melanoma and melanocortin 1 receptor," *Biochemistry,* vol. 78, no. 11, pp. 1228–1237, 2013.

[69] B. Lee, N. Mukhi, and D. Liu, "Current management and novel agents for malignant melanoma," *Journal of Hematology & Oncology*, vol. 5, no. 3, pp. 1-7, 2012.

[70] U. Hofmann, M. Szedlak, W. Rittgen, E. G. Jung, and D. Schadendorf, "Primary staging and follow-up in melanoma patients - monocenter evaluation of methods, costs and patient survival," *British Journal of Cancer*, vol. 87, no. 2, pp. 151–157, 2002.

[71] O. Alonso, M. Martínez, L. Delgado, A. De León, D. De Boni, G. Lago, M. Garcés, F. Fontes, J. Espasandín, and J. Priario, "Staging of Regional Lymph Nodes in Melanoma Patients by Means of ^{99m}Tc-MIBI Scintigraphy," *Journal of Nuclear Medicine*, vol. 44, no. 10, pp. 1561-5, 2003. [72] A. Dimitrakopoulou-Strauss, L. G. Strauss, and C. Burger, "Quantitative PET Studies in Pretreated Melanoma Patients: A Comparison of 6-[^{18}F]Fluoro-L-Dopa with ^{18}F-FDG and ^{15}OWater Using Compartment and Noncompartment Analysis," *Journal of Nuclear Medicine*, vol. 42, no. 2, pp. 248-56, 2001.

[73] A. M. M. Eggermont, "Advances in systemic treatment of melanoma," *Annals of Oncology*, vol. 21, Suppl 7, vii339-44, 2010.

[74] A. N. Eberle, "Studies on melanotropan (MSH) receptors of melanophores and melanoma cells," *Biochemical Society Transactions*, vol. 9, no. 1, pp. 37-9, 1981.

[75] D. M. Rosenbaum, S. G. F. Rasmussen, and B. K. Kobilka, "The structure and function of Gprotein-coupled receptors," *Nature*, vol. 459, no. 7245, pp. 356–363, 2009.

[76] A. B. Lerner, and J. S. McGuire, "Effect of alpha- and beta-melanocyte stimulating hormones on the skin colour of man," *Nature*, vol. 189, pp. 176-9, 1961.

[77] T. K. Sawyer, D. J. Staples, A. M. Castrucci, M. E, Hadley, F. A. al-Obeidi, W. L. Cody, and V. J. Hruby, "Alpha-Melanocyte Stimulating Hormone Message and Inhibitory Sequences: Comparative Structure-Activity Studies on Melanocytes," *Peptides*, vol. 11, no. 2, pp. 351-7, 1990.

[78] S. O. Uqwu, J. Blanchard, R. T. Dorr, N. Levine, C. Brooks, M. E. Hadley, M. Aichin, and V. J. Bruby, "Skin Pigmentation and Pharmacokinetics of Melanotan-I in Humans," *Biopharmaceuticals & Drug Disposition*, vol. 18, no. 3, pp. 259–269, 1997.

[79] R. T. Dorr, R. Lines, N. Levine, C. Brooks, L. Xiang, V. J. Hruby, and M. E. Hadley, "Evaluation of Melanotan-II, a superpotent cyclic melanotropic peptide in a pilot phase-I clinical study," *Life Sciences*, vol. 58, no. 20, pp. 1777–1784, 1996.

[80] H. Guo, F. Gallazzi, and Y. Miao, "Design and evaluation of new ^{99m}Tc-labeled lactam bridgecyclized alpha-MSH peptides for melanoma imaging," *Molecular Pharmaceutics*, vol. 10, no. 4, pp. 1400–1408, 2013.

[81] H. Guo, F. Gallazzi, and Y. Miao, "Gallium-67-labeled lactam bridge-cyclized alpha-MSH peptides with enhanced melanoma uptake and reduced renal uptake," *Bioconjugate Chemistry*, vol. 23, no. 6, pp. 1341–1348, 2012.

[82] Z. Cheng, L. Zhang, E. Graves, Z. Xiong, M. Dandekar, X. Chen, and S. S. Gambhir, "Small-animal PET of melanocortin-1 receptor expression using a ^{18}F-labeled alpha-melanocyte-stimulating hormone analog," *Journal of Nuclear Medicine*, vol. 48, no. 6, pp. 987–994, 2007.

[83] Z. Cheng, Z. Xiong, M. Subbarayan, X. Chen, and S. S. Gambhir, "^{64}Cu-labeled alphamelanocyte-stimulating hormone analog for microPET imaging of melanocortin 1 receptor expression," *Bioconjugate Chemistry*, vol. 18, no. 3, pp. 765–772, 2007.

[84] G. Ren, Z. Liu, Z. Miao, H. Liu, M. Subbarayan, F. T. Chin, L. Zhang, S. S. Gambhir, and Z. Cheng, "PET of malignant melanoma using ^{18}F-labeled metallopeptides," *Journal of Nuclear Medicine*, vol. 50, no. 11, pp. 1865–1872, 2009.

[85] P. McQuade, Y. Miao, J. Yoo, T. P. Quinn, M. J. Welch, and J. S. Lewis, "Imaging of melanoma using ^{64}Cu- and ^{86}Y-DOTA-ReCCMSH(Arg11), a cyclized peptide analogue of alpha-MSH," *Journal of Medicinal Chemistry*, vol. 48, no. 8, pp. 2985–2992, 2005.

[86] A. Heitz, O. Avrutina, D. Le-Nquyen, U. Diedrichsen, J. F. Hernandez, J. Gracy, H. Kolmar, and L. Chiche, "Knottin cyclization: impact on structure and dynamics," *BMC structural biology*, vol. 8, p. 54, 2008.

[87] D. Le-Nguyen, A. Heitz, L. Chiche, B. Castro, R. A. Boigegrain, A. Favel, and M. A. Colettipreviero, "Molecular recognition between serine proteases and new bioactive microproteins with a knotted structure," *Biochimie*, vol. 72, no. 6-7, pp. 431-5, 1990.

[88] S. J. Moore, C. Lun Leung, and J. R. Cochran, "Knottins: disulfide-bonded therapeutic and diagnostic peptides," *Drug Discovery Today*, vol. 9, no. 1, e1-e70, 2012.

[89] L. Thorstholm, and D.J. Craik, "Discovery and applications of naturally occurring cyclic peptides," *Drug Discovery Today*, vol. 9, no. 1, e1-e70, 2012.

[90] S.L. Carney Editor, "Peptides or modified peptides as drug molecules," *Drug Discovery Today*, vol. 9, no. 1, e1-e70, 2012.

[91] D. J. Craik, M. Cemazar, C. K. L. Wang, and N. L. Daly, "The cyclotide family of circular miniproteins: nature's combinatorial peptide template," *Biopolymers*, vol. 84, no. 3, pp. 250–266, 2006.

[92] C. K. Wang, S. H. Hu, J. L. Martin, T. Sjögren, J. Hajdu, L. Bohlin, P. Cleson, U. Göransson, K. J. Rosengren, J. Tang, N. H. Tan, and D. J. Craik., "Combined X-ray and NMR analysis of the stability of the cyclotide cystine knot fold that underpins its insecticidal activity and potential use as a drug scaffold," *The Journal of Biological Chemistry*, vol. 284, no. 16, pp. 10672–10683, 2009.

[93] M. Reinwarth, D. Nasu, H. Kolmar, and O. Avrutina, "Chemical synthesis, backbone cyclization and oxidative folding of cystine-knot peptides: promising scaffolds for applications in drug design," *Molecules*, vol. 17, no. 11, pp. 12533–12552, 2012.

[94] Z. Miao, G. Ren, H. Liu, R. H. Kimura, L. Jiang, J. R. Cochran, S. S. Gambhir, and Z. Cheng, "An engineered knottin peptide labeled with 18F for PET imaging of integrin expression," *Bioconjugate Chemistry*, vol. 20, no. 12, pp. 2342–2347, 2009.

[95] J.-C. Gelly, J. Gracy, Q. Kaas, D. Le-Nquyen, A. Heitz, and L. Chiche., "The KNOTTIN website and database: a new information system dedicated to the knottin scaffold," *Nucleic Acids Research*, vol. 32, D156-9, 2004.

[96] R. H. Kimura, A. M. Levin, F. V. Cochran, and J. R. Cochran, "Engineered cystine knot peptides that bind alpha$_v$beta$_3$, alpha$_v$beta$_5$, and alpha$_5$beta$_1$ integrins with low-nanomolar affinity," *Proteins*, vol. 77, no. 2, pp. 359–369, 2009.

[97] A. P. Silverman, A. M. Levin, J. L. Lahti, and J. R. Cochran, "Engineered cystine-knot peptides that bind alpha$_v$beta$_3$ integrin with antibody-like affinities," *Journal of Molecular Biology*, vol. 385, no. 4, pp. 1064–1075, 2009.

[98] R. H. Kimura, Z. Cheng, S. S. Gambhir, and J. R. Cochran, "Engineered Knottin Peptides: A New Class of Agents for Imaging Integrin Expression in Living Subjects," *Cancer Research*, vol. 69, no. 6, pp. 2435–2442, 2009.

[99] L. Jiang, R. H. Kimura, Z. Miao, A. P. Silverman, G. Ren, H. Liu, P. Li, S. S. Gambhir, J. R. Cochran, and Z. Cheng, "Evaluation of a ^{64}Cu-labeled cystine-knot peptide based on agouti-

related protein for PET of tumors expressing alpha$_v$beta$_3$ integrin," *Journal of Nuclear Medicine*, vol. 51, no. 2, pp. 251–258, 2010.

[100] R. H. Kimura, Z. Miao, Z. Cheng, S. S. Gambhir, and J. R. Cochran, "A Dual-labeled knottin pepdtide for PET and near-infrared fluorescence imaging of intregrin expression in living subjects," *Bioconjugate Chemistry*, vol. 21, no. 3, pp. 436-44, 2010.

[101] S. Liu, H. Liu, G. Ren, R. H. Kimura, J. R. Cochran, and Z. Cheng, "PET Imaging of integrin positive tumors using 18F labeled knottin peptides," *Theranostics*, vol. 1, pp. 403-12, 2011.

[102] L. Jiang, Z. Miao, R. H. Kimura, H. Liu, J. R. Cochran, C. S. Culterm A. Bao, P. Li, and Z. Cheng, "Preliminary evaluation of ^{177}Lu-labeled knottin peptides for integrin receptor-targeted radionuclide therapy," *European Journal of Nuclear Medicine and Molecular Imaging*, vol. 38, no. 4, pp. 613–622, 2011.

[103] N. Cox, J. R. Kintzing, M. Smith, G. A. Grant, and J. R. Cochran, "Integrin-Targeting Knottin Peptide-Drug Conjugates Are Potent Inhibitors of Tumor Cell Proliferation," *Angewandte Chemie International Edition*, vol. 55, no. 34, pp. 9894–9897, 2016.

[104] P. Garin-Chesa, L. J. Old, and W. J. Rettig, "Cell surface glycoprotein of reactive stromal fibroblasts as a potential antibody target in human epithelial cancers," *Proceedings of the National Academy of Sciences of the USA*, vol. 87, no. 18, pp. 7235-9, 1990.

[105] K. Aertgeerts, I. Levin, L. Shi, G. P. Snell, A. Jennings, G. S. Prasad, Y. Zhang, M. L. Kraus, S. Salakian, V. Sridhar, R. Wijnands, and M. G. Tennant, "Structural and Kinetic Analysis of the Substrate Specificity of Human Fibroblast Activation Protein," *Journal of Biological Chemistry*, vol. 280, no. 20, pp. 19441–19444, 2005.

[106] I. de Meester, S. Korom, J. van Damme, and S. Scharpé, "CD26, let it cut or cut it down," *Immunology Today*, vol. 20, no. 8, pp. 367–375, 1999.

[107] W. J. Rettig, P. Garin-Chesa, H. R. Beresford, H. F. Oettgen, M. R. Melamed, and L. J. Old, "Cellsurface glycoproteins of human sarcomas differential expression in normal and malignant tissues and cultured cells," *Proceedings of the National Academy of Sciences of the USA*, vol. 85, no. 9, pp. 3110-4, 1988.

[108] M. T. Levy, G. W. Mcaughan, C. A. Abbott, J. E. Park, A. M. Cunningham, E. Müller, W. J. Rettig, and M. D. Gorrell, "Fibroblast activation protein: a cell surface dipeptidyl peptidase and gelatinase expressed by stellate cells at the tissue remodelling interface in human cirrhosis," *Hepatology*, vol. 29, no. 6, pp. 1768–1778, 1999.

[109] W. J. Rettig, P. Garin-Chesa, J. H. Healey, S. L. Su, H. L. Ozer, M. Schwab, A. P. Albino, and L. J. Old, "Regulation and Heteromeric Structure of the Fibroblast Activation Protein in Normal and Transformed Cells of Mesenchymal and Neuroectodermal origin," *Cancer Research*, vol. 53, no. 14, pp. 3327-35, 1993.

[110] W. J. Rettig, P. Garin-Chesa, H. R. Beresford, H.-J. Feickert, and M. T. Jennings, "Differential Expression of Cell Antigens and Glial Fibrillary Acidic Protein in Human Astrocytoma Subsets," *Cancer Research*, vol. 46, no. 12, pp. 6406-12, 1986.

[111] W. J. Rettig, P. Garin-Chesa, H. R. Beresford, H. F. Oettgen, M. R. Melamed, and L. J. Old, "Cellsurface glycoproteins of human sarcomas: Differential expression in normal and malignant tissues and cultured cells," *Proceedings of the National Academy of Sciences of the USA*, vol. 85, pp. 3110-4, 1999.

[112] W. L. Monsky, C. Y. Lin, A. Aoyama, T. Kelly, S. K. Akiyama, S. C. Mueller, and W. T. Chen., "A potential marker protease of invasiveness,seprase, is localized on invadopodis of human malignant melanoma cells," *Cancer Research*, vol. 54, no. 21, pp. 5702-10, 1994.

[113] M. L. Pineiro-Sanchez, L. A. Goldstein, J. Dodt, L. Howard, Y. Yeh, H. Tran, W. S. Argraves, and W. T. Chen, "Identification of the 170-kDa Melanoma Membrane-bound Gelatinase (Seprase) as a Serine Integral Membrane Protease," *Journal of Biological Chemistry*, vol. 272, no. 12, pp. 7595–7601, 1997.

[114] S. Mathew, M. J. Scanlan, B. K. Mohan Rai, V. V. Murty, P. Garin-Chesa, L. J. Old, W. L. Rettig, and R. S. Chaganti., "The gene for fibroblast activation protein ɲ (FAP), a putative cell surface-
bound serine protease expressed in cancer stroma and wound healing, maps to chromosome band 2q23," *Genomics*, vol. 25, no. 1, pp. 335–337, 1995.

[115] W.-T. Chen, and T. Kelly, "Seprase complexes in cellular invasiveness," *Cancer Metastasis Review*, vol. 22, no. 2-3, pp. 259-69, 2003.

[116] M. J. Scanlan, B. K. Rai, B. Calvo, P. Garin-Chesa, M. P. Sanz-Moncasi, J. H. Healey, L. J. Old, and W. J. Rettig, "Molecular cloning of fibroblast activation protein alpha, a member of the serine protease family selectively expressed in stromal fibroblasts of epithelial cancers," *Proccedings of the National Academy of Sciences of the USA*,vol. 91, no. 12, pp. 5657-61, 1994.

[117] N. Guex, and M. C. Peitsch, "SWISS-MODEL and the Swiss-PdbViewer: an environment for comparative protein modeling," *Electrophoresis*, vol. 18, no. 15, pp. 2714–2723, 1997.

[118] P. O'Brien, and B. F. O'Connor, "Seprase: an overview of an important matrix serine protease," *Biochimica et Biophysica Acta*, vol. 1784, no. 9, pp. 1130–1145, 2008.

[119] S. Welt, C. R. Divgi, A. M. Scott, P. Garin-Chesa, R. D. Finn, M. Graham, E. A. Carswell, A. Cohen,
S. M. Larson, and L. J. Old, "Antibody Targeting in Metastatic Colon Cancer: A Phase I Study of Monoclonal Antibody F19 Against a Cell-Surface Protein of Reactive Tumor Stromal Fibroblasts," *Journal of Clinical Oncology*, vol. 12, no. 6, pp. 1193-203 1994.

[120] P. Tanswell, P. Garin-Chesa, W. J. Rettig, S. Welt, C. R. Divgi, E. S. Casper, R. D. Finn, S. M. Larson, L. J. Old, and A. M. Scott, "Population pharmacokinetics of antifibroblast activation protein monoclonal antibody F19 in cancer patients," *British Journal of Clinical Pharmacology*, vol. 51, no. 2, pp. 177-180, 2001.

[121] A. M. Scott, G. Wiseman, S. Welt, A. Adjei, F. T. Lee, W. Hopkins, C. R. Dicgi, L. H. Hanson, P. Mitchell, D. N. Gansen, S. M. Larson, J. N. Ingle, E. W. Hoffman, P. Transwell, G. Ritter, L. S. Cohen, P. Bette, L. Arvay, A. Amelsberg, D. Vlock W. J. Rettig, and L. J. Old, "A Phase I Doseescalation study of sibrotuzumab in patients with advanced or metastatic fibroblast activation protein positive cancer," *Clinical Cancer Research*, vol. 9, no. 5, pp. 1639-47, 2003.

[122] R.-D. Hofheinz, S. E. al-Batran, F. Hartmann, G. Hartung, D. Jäger, C. Renner, P. Transwell, U. Kunz, A. Amelsberg, H. Kuthan, and G. Stehle, "Stromal antigen targeting by a humanised monoclonal antibody: an early phase II trial of sibrotuzumab in patients with metastatic colorectal cancer," *Onkologie*, vol. 26, no. 1, pp. 44–48, 2003.

[123] W. Rollinger, J. Kurl, J. P. Kochan, M. Ressler, and M. Tacke, "Methods for providing diagnosis of cancer using seprase as a marker," US 8980573, *Patent*, 2007.

[124] F. Roesch, “Maturation of a Key Resource – The Germanium-68/Gallium-68 Generator: Development and New Insights,” *Communication Research & Practice*, vol. 5, no. 3, pp. 202–211, 2012.

[125] F. Rosch, “Past, present and future of ^{68}Ge/^{68}Ga generators,” *Applied Radiation and Isotopes*, vol. 76, pp. 24–30, 2013.

[126] D. Mueller, I. Kletter, R. P. Baum, M. Gottschaldt, M. K. Schultz, and W. A. P. Breeman, “Simplified NaCl based ^{68}Ga concentration and labeling procedure for rapid synthesis of ^{68}Ga radiopharmaceuticals in high radiochemical purity,” *Bioconjugate Chemistry*, vol. 23, no. 8, pp. 1712–1717, 2012.

[127] E. Boros, C. L. Ferreira, D. T. Yapp, R. K. Gill, E. W Price, M. J. Adam, and C. Orvig, “RGD conjugates of the H2dedpa scaffold: synthesis, labeling and imaging with ^{68}Ga,” *Nuclear Medicine and Biology*, vol. 39, no. 6, pp. 785–794, 2012.

[128] E. Eppard, M. Wuttke, P. L. Nicodemus, and F. Rosch, “Ethanol-Based Post-processing of Generator-Derived ^{68}Ga Toward Kit-Type Preparation of ^{68}Ga-Radiopharmaceuticals,” *Journal of Nuclear Medicine*, vol. 55, no. 6, pp. 1023–1028, 2014.

[129] W. A. P. Breeman, M. de Jong, E. de Blois, B. F. Bernard, M. Konijnenberg and E. P. Krenning, “Radiolabelling DOTA-peptides with ^{68}Ga,” *European Journal of Nuclear Medicine and Molecular Imaging*, vol. 32, no. 4, pp. 478–485, 2005.

[130] K. P. Zhernosekov, M. V. Filosofov, R. P. Baum, P. Aschoff, H. Bihl, A. A. Razbash, M. Jahn, M. Jennewein, and F. Rösch, “Processing of Generator-Produced ^{68}Ga for Medical Application,” *Journal of Nuclear Medicine*, vol. 48, no. 10, pp. 1741-8, 2007.

[131] M. A. Green, and M. J. Welch, “Gallium Radiopharmaceutical Chemistry,” *International Journal of Radiation Applications and Instrumentation*, vol. 16, no. 5, pp. 445-8, 1989.

[132] É. Tóth, E. Brücher, I. Lázár, and I. Tóth, “Kinetics of Formation and Dissociation of Lanthanide (III)-DOTA Complexes,” *Inorganic Chemistry*, vol. 33, no. 18, pp. 4070-6, 1994.

[133] S. C. Ghosh, K. L. Pinkston, H. Robinson, B. R. Harvey, N. Wilganowski, K. Goe, E. M. SevickMuraca, and A. Ashdarinia, “Comparison of DOTA and NODAGA as chelators for (64)Cu-labeled immunoconjugates,” *Nuclear Medicine and Biology*, vol. 42, no. 2, pp. 177–183, 2015.

[134] J. Simecek, H.-J. Wester, and J. Notni, "Copper-64 labelling of triazacyclononanetriphosphinate chelators," *Dalton Transactions*, vol. 41, pp. 13803-6, 2012.

[135] J. Seemann, B. P. Waldron, F. Roesch, and D. Parker, “Approaching 'Kit-Type' Labelling with ^{68}Ga: The DATA Chelators,” *ChemMedChem*, vol. 10, no. 6, pp. 1019–1026, 2015.

[136] J. Seemann, E. Eppard, B. P. Waldron, T. L. Ross, and F. Roesch, “Cation exchange-based postprocessing of ^{68}Ga-eluate: a comparison of three solvent systems for labelling of DOTATOC, NO2AP^{BP} and DATA^{m},” *Applied Radiation and Isotopes*, vol. 98, pp. 54–59, 2015.

[137] V. Schirch, and W. B. Strong, “Interaction of Folylpolyglutamates with enzymes in one-carbon metabolism,” *Archives of Biochemistry and Biophysics*, vol. 269, no. 2, pp. 371-80, 1989.

[138] J. Koolman, "Taschenatlas der Biochemie," 3rd edition, *Thieme*, Stuttgart, 2003.

[139] S. K. Desmoulin, Z. Hou, A. Gangjee, and L. H. Matherly, “The human proton-coupled folate transporter,” *Cancer Biology & Therapy*, vol. 13, no. 14, pp. 1355–1373, 2014.

[140] C. A. M. Atta, K. M. Fiest, A. D. Frolkis, N. Jette, T. Pringsheim, C. St Germaine-Smith, T. Rajapakse, G. G. Kaplan, and A. Mctcalfe, “Global Birth Prevalence of Spina Bifida by Folic Acid Fortification Status: A Systematic Review and Meta-Analysis,” *American Journal of Public Health*, vol. 106, no. 1, pp. e24-e34, 2016.

[141] L. H. Matherly, Z. Hou, and Y. Deng, "Human reduced folate carrier: Translation of basic biology to cancer etiology and therapy," *Cancer Metastasis Review*, vol. 26, no. 1, pp. 111–128, 2007.

[142] C. Chen, J. Ke, X. E. Zhou, W. Yi, J. S. Brunzelle J. Li, E. L. Yong, H. E. Xu, and K. Melcher, "Structural basis for molecular recognition of folic acid by folate receptors," *Nature*, vol. 500, no. 7463, pp. 486–489, 2013.

[143] J. W. Locasale, "Serine, glycine and one-carbon units: Cancer metabolism in full circle," *Nature Reviews Cancer*, vol. 13, no. 8, pp. 572–583, 2013.

[144] M. Fani, X. Wang, G. Nicolas, C. Medina, I. Raynal, M. Port, and H. R. Maecke, "Development of new folate-based PET radiotracers: preclinical evaluation of ^{68}Ga-DOTA-folate conjugates," *European Journal of Nuclear Medicine and Molecular Imaging*, vol. 38, no. 1, pp. 108–119, 2011.

[145] J. R. Whetstine, R. M. Flatley, and L. H. Matherly, "The human reduced folate carrier gene is ubiquitously and differentially expressed in normal human tissue: identification of seven noncoding exons and characterization of a novel promoter," *Biochemical Journal*, vol. 367, no. 3, pp. 629-40, 2002.

[146] S. S. Date, C.-Y. C. Chen, Y. Chen, and M. Jansen, "Experimentally optimized threading structures of the proton-coupled folate transporter," *FEBS Open Bio*, vol. 6, no. 3, pp. 216–230, 2016.

[147] R. Zhao, and I. D. Goldman, "The molecular identity and characterization of a Proton-Coupled Folate Transporter—PCFT; biological ramifications and impact on the activity of pemetrexed," *Cancer Metastasis Review*, vol. 26, no. 1, pp. 129–139, 2007.

[148] C.-Y. Ke, C. J. Mathias, and M. A. Green, "The folate receptor as a molecular target for tumorselective radionuclide delivery," *Nuclear Medicine and Biology*, vol. 30, no. 8, pp. 811–817, 2003.

[149] John J. Turek, Christopher P. Leamon, and Philip S. Low, "Endocytosis of folate-protein conjugates: ultrastructural localisation in KB cells," *Journal of Cell Science*, vol. 106, no. 1, pp. 423-30, 1993.

[150] J. W. van der Heijden, R. Oerlemans, B. A. Dijkmans, H. Qi, C. J. van der Laken, W. E. Lems, A. L. Jackman, M. C. Kraan, P. P. Tak, M. Ratnam, and G. Jansen, "Folate receptor beta as a potential delivery route for novel folate antagonists to macrophages in the synovial tissue of rheumatoid arthritis patients," *Arthritis and Rheumatism*, vol. 60, no. 1, pp. 12–21, 2009.

[151] P. S. Low, W. A. Henne, and D. D. Doorneweerd, "Discovery and development of folic-acidbased receptor targeting for imaging and therapy of cancer and inflammatory diseases," *Accounts of Chemical Research*, vol. 41, no. 1, pp. 120–129, 2008.

[152] E. I. Sega, and P. S. Low, "Tumor detection using folate receptor-targeted imaging agents," *Cancer Metastasis Reviews*, vol. 27, no. 4, pp. 655–664, 2008.

[153] N. Parker, M. J. Turk, E. Westrick, J. D. Lewis, P. S. Low, and C. P. Leamon, "Folate receptor expression in carcinomas and normal tissues determined by a quantitative radioligand binding assay," *Analytical Biochemistry*, vol. 338, no. 2, pp. 284–293, 2005.

[154] S. D. Weitmann, A. G. Weinberg, L. R. Coney, V. R. Zurawski, D. S. Jennings, and B. A. Kamen, "Cellular Localisation of the Folate Receptor: Potential Role in Drug Toxicity and Folate Homeostasis," *Cancer Research*, vol. 52, no. 23, pp. 6708-11, 1992.

[155] S. D. Weitmann, R. H. Lark, L. R. Coney, D. W. Fort, V. Frasca, and V. R. Zurawski, "Distribution of the Folate Receptor GP38 in Normal and Maligant Cell Lines and Tissues," *Cancer Research*, vol. 52, no. 12, pp. 3396-401, 1992.

[156] C. J. Mathias, D. Hubers, P. S. Low, and M. A. Green, "Synthesis of [^{99m}Tc]DTPA-Folate and Its Evaluation as a Folate-Receptor-Targeted Radiopharmaceutical," *Bioconjugate Chemistry*, vol. 11, no. 2, pp. 253–257, 2000.

[157] C. J. Mathias, S. Wang, P. S. Low, D. J. Waters, and M. A. Green, "Receptor-mediated targeting of ^{67}Ga-Deferoxamine-Folate to folate-receptor-positive human KB tumor xenografts," *Nuclear Medicine and Biology*, vol. 26, no. 1, pp. 23–25, 1999.

[158] S. Wang, R. J. Lee, C. J. Mathias, M. A. Green, and P. S. Low, "Synthesis, purification, and tumor cell uptake of ^{67}Ga-deferoxamine-folate - a potential radiopharmaceutical for tumor imaging," *Bioconjugate Chemistry*, vol. 7, no. 1, pp. 56–62, 1996.

[159] C. P. Leamon, M. A. Parker, I. R. Vlahov, L. C. Xu, J. A. Reddy, M. Vetzel, and N. Douglas*,* "Synthesis and Biological Evaluation of EC20: A New Folate-Derived, ^{99m}Tc-Based Radiopharmaceutical," *Bioconjugate Chemistry*, vol. 13, no. 6, pp. 1200–1210, 2002.

[160] H. Guo, J. Yang, F. Gallazzi, and Y. Miao, "Effects of the Amino Acid Linkers on the Melanoma-Targeting and Pharmacokinetic Properties of ^{111}In-Labeled Lactam Bridge-Cyclized MSH Peptides," *Journal of Nuclear Medicine*, vol. 52, no. 4, pp. 608–616, 2011.

[161] C. Müller, C. Dumas, U. Hoffmann, P. A. Schubiger, and R. Schibli, "Organometallic ^{99m}Tctechnetium(I)- and Re-rhenium(I)-folate derivatives for potential use in nuclear medicine," *Journal of Organometallic Chemistry*, vol. 689, no. 25, pp. 4712–4721, 2004.

[162] S. Ilgan, D. J. Yang, T. Hiquchi, F. Zareneyrizi, H. Bayhan, E. E. Kim, and D. A. Podoloff, "^{99m}TcEthylenedicysteine-Folate: A new tumor imaging agent. Synthesis, Labeling and evaluation in animals," *Cancer Biotherapy and Radiopharmaceuticals*, vol. 13, no. 6, pp. 427-35, 1998.

[163] David P. Trump, C. J. Mathias, Z. Yang, R. S. Low, M. Marmion, and M. A. Green, "Synthesis and evaluation of ^{99m}Tc$(CO)_3$-DTPA-Folate as a folate-receptor targeted radiopharmaceutical," *Nuclear Medicine and Biology*, vol. 29, no. 5, pp. 569-73, 2002.

[164] C. Müller, A. Hohn, P. A. Schubiger, and R. Schibli, "Preclinical evaluation of novel organometallic ^{99m}Tc-folate and ^{99m}Tc-pteroate radiotracers for folate receptor-positive tumour targeting," *European Journal of Nuclear Medicine and Molecular Imaging*, vol. 33, no. 9, pp. 1007–1016, 2006.

[165] C. P. Leamon, M. A. Parker, I. R. Vlahov, L. C. Xu, J. A. Reddy, M. Vetzel, and N. Douglas*,* "Synthesis and Biological Evaluation of EC20: A New Folate-Derived, ^{99m}Tc-Based Radiopharmaceutical," *Bioconjugate Chemistry*, vol. 13, no. 6, pp. 1200–1210, 2002.

[166] Committee for Medicinal Products for Human Use, "Folcepri - etarfolatide," *European Medicines Agency and Science Medicines Health*, 2014.

[167] A. Bettio, M. Honer, C. Müller, M. Brühlmeier, U. Müller, R. Schibli, V. Groehn, A. P. Schubiger, and S. M. Ametamey, "Synthesis and Preclinical Evaluation of a Folic Acid Derivative Labeled with ^{18}F for PET Imaging of Folate Receptor-Positive Tumors," *Journal of Nuclear Medicine*, vol. 47, no. 7, pp. 1153-60, 2006.

[168] T. L. Ross, M. Honer, P. Y. Lam, T. L. Mindt, V. Groehn, R. Schibli, P. A. Schubiger, and S. M. Ametamey*,* "Fluorine-18 click radiosynthesis and preclinical evaluation of a new ^{18}F-labeled folic acid derivative," *Bioconjugate Chemistry*, vol. 19, no. 12, pp. 2462–2470, 2008.

[169] T. L. Ross, M. Honer, C. Müller, V. Groehn, R. Schibli, and S. M. Ametamey, "A new ^{18}F-labeled folic acid derivative with improved properties for the PET imaging of folate receptor-positive tumors," *Journal of Nuclear Medicine*, vol. 51, no. 11, pp. 1756–1762, 2010.

[170] T. Betzel, C. Müller, V. Groehn, A. Müller, J. Reber, C. R. Fischer, S. D. Krämer, R. Schibli, and S. M. Ametamey, "Radiosynthesis and preclinical evaluation of 3'-Aza-2'-[^{18}F]fluorofolic acid: a novel PET radiotracer for folate receptor targeting," *Bioconjugate Chemistry*, vol. 24, no. 2, pp. 205–214, 2013.

[171] I. Al Jammaz, B. Al-Otaibi, S. Amer, N. Al-Hokbany, and S. Okarvi, "Novel synthesis and preclinical evaluation of folic acid derivatives labeled with ^{18}F-FDG for PET imaging of folate receptor-positive tumors," *Nuclear Medicine and Biology*, vol. 39, no. 6, pp. 864–870, 2012.

[172] H. Schieferstein, T. Betzel, C. R. Fischer, and T. L. Ross, "^{18}F-click labeling and preclinical evaluation of a new 18 F-folate for PET imaging," *European Journal of Nuclear Medicine and Molecular Imaging Research*, vol. 3, no. 1, p. 68, 2013.

[173] C. Muller, H. Struthers, C. Winiger, K. Zhernosekov, and R. Schibli, "DOTA conjugate with an albumin-binding entity enables the first folic acid-targeted ^{177}Lu-radionuclide tumor therapy in mice," *Journal of Nuclear Medicine*, vol. 54, no. 1, pp. 124–131, 2013.

[174] C. R. Fischer, V. Groehn, J. Reber, R. Schibli, S. M. Ametamey, and C. Müller, "Improved PET imaging of tumors in mice using a novel ^{18}F-folate conjugate with an albumin-binding entity," *Molecular Imaging and Biology*, vol. 15, no. 6, pp. 649–654, 2013.

[175] Q. Chen, X. Meng, P. McQuade, D. Rubins, A.-A. Lin, Z. Zeng, H. Haley, P. Müller, D. G. Trotter, and P. S. Low, "Synthesis and Preclinical Evaluation of Folate-NOTA-Al^{18}F for PET Imaging of Folate-Receptor-Positive Tumors," *Molecular Pharmaceutics*, vol. 13, no. 5, pp. 1520–1527, 2016.

[176] S. D. Boss, T. Betzel, C. Müllr, C. R. Fischer, S. Haller, J. Reber, V. Groehn, R. Schibli, and S. M. Ametamey, "Comparative Studies of Three Pairs of ɲ- and œ-Conjugated Folic Acid Derivatives Labeled with Fluorine-18," *Bioconjugate Chemistry*, vol. 27, no. 1, pp. 74–86, 2016.

[177] C. Chen, J. Ke, X. E. Zhou, W. Yi, J. S. Brunzelle, J. Li, E. L. Yong, H. E. Xu, and K. Melcher, "Structural basis for molecular recognition of folic acid by folate receptors," *Nature*, vol. 500, no. 7463, pp. 486–489, 2013.

[178] Andrea Bettio, M. Honer, C. Müller, M. Brühlmeier, U. Müller, R. Schibli, V. Groehn, A. P. Schubiger, and S. M. Ametamey, "Synthesis and Preclinical Evaluation of a Folic Acid Derivative Labeled with ^{18}F PET Imaging of Folate Receptor-Positive Tumors," *Journal of Nuclear Chemistry*, vol. 47, no. 7, pp. 1153-60, 2006.

[179] C. P. Leamon, R. B. Deprince, and W. Hendren, "Folate-mediated Drug Delivery: Effect of alternative Conjugation Chemistry," *Journal of Drug Targeting*, vol. 7, no. 3, pp. 157-69, 1999.

[180] C. Muller, A. Hohn, P. A. Schubiger, and R. Schibli, "Preclinical evaluation of novel organometallic ^{99m}Tc-folate and ^{99m}Tc-pteroate radiotracers for folate receptor-positive tumour targeting," *European Journal of Nuclear Medicine and Molecular Imaging*, vol. 33, no. 9, pp. 1007–1016, 2006.

[181] M. V. Rodnina, M. Beringer, and W. Wintermeyer, "How ribosomes make peptide bonds," *Trends in Biochemical Sciences*, vol. 32, no. 1, pp. 20-6, 2007.

[182] World Health Organization, Food and Agriculture Organization of the United Nations, "Protein and Amino Acid Requirements in Human Nutrition," 2007.

[183] O. A. C. Petroff, "GABA and Glutamate in the Human Brain" *Neuroscientist*, vol. 8, no. 6, pp. 562-73, 2002.

[184] F. Verrey, E. Closs, C. Wagner, M. Palacin, H. Endou, and Y. Kanai, "CATs and HATs: the SLC7 family of amino acid transporters" *Pflugers Archiv*, vol. 447, no.5, pp. 532-42, 2004.

[185] Y. Kanai, and H. Endou, "Heterodimeric Amino Acid Transporter: Molecular Biology and Pathological and Pharmacological Relevance" *Current Drug Metabolism*, vol. 2, no. 4, pp. 33954, 2001.

[186] C. A. Wagner, F. Lang, and S. Bröer, "Function and structure of heterodimeric amino acid transporters," *American Journal of Physiology and Cell Physiology*, vol. 281, no. 4, pp. C107793, 2001.

[187] Y. Kanai, H. Segawa, K. Miyamoto, H. Uchino, E. Takeda, and H. Endou , "Expression Cloning and Characterization of a Transporter for Large Neutral Amino Acids Activated by the Heavy Chain of 4F2 Antigen (CD98)," The *Journal of Biological Chemistry*, vol. 273, no. 37, pp. 2362932, 1998.

[188] L. Mastroberadino, B. Spindler, R. Pfeiffer, P. J. Skelly, J. Loffing, C. B. Shoemaker, and F. Verrey, "Amino-acid transport by heterodimers of 4F2hc/CD98 and members of a permease family," *Nature*, vol. 395, no. 6699, pp. 288-91, 1998.

[189] E. M. del Amo, A. Urtti, and M. Yliperttula, "Pharmacokinetic role of L-type amino acid transporters LAT1 and LAT2" *European Journal of Pharmaceutical Science*, vol. 35, no. 3, pp. 161-74, 2008.

[190] D. L. Oxender, and H. N. Christensen, "Evidence for two types of mediation of neutral aminoacid transport in ehrlich cells," *Nature*, vol. 197, pp. 765-7, 1963.

[191] M. Pineda, E. Fernandez, D. Torrents, R. Estevez, C. Lopez, M. Camps, J. lloberas, A. Zorzano, and M. Palacin, "Identification of a Membrane, LAT2, that co-expresses with a 4F2 Heavy Chain L-type amino acid transporter," The *Journal of Biological Chemistry*, vol. 274, no. 28, pp. 19738-44, 1999.

[192] H. Segawa, Y. Fukasawa, K. Miyamoto, E. Takeda, H. Endou, and Y. Kanai, ”Identification and functional characterization of a Na-independent neutral amino acid transporter with broad substrate selectivity," *The Journal of Biological Chemistry*, vol. 274, no. 28, pp. 19745-51, 1999. [193] E. Babu, Y. Kanai, A. Chairoungdua, D. K. Kim, Y. Iribe, S. Tangtrongsup, P. Jutabha, Y. Li, N. Ahmend, S. Sakamoto, N. Anzai, S. Nagamori, and H. Endou , "Identification of a novel system L amino acid transporter structurally distinct from heterodimeric amino acids transporters," *The Journal of Biological Chemistry*, vol. 278, no. 44, pp. 43838-45, 2003.

[194] S. Bodoy, L- Martin, A. Zorzano, M. Palacin, R. Estevez, and J. Bertran, "Identification of LAT4, a novel amino acid transporter with system L activity," *The Journal of Biological Chemistry*, vol. 280, pp. 12002-11, 2005.

[195] O. Yanagida, Y. Kanai, A. Chairoungdua, D. K. Kim, H. Segawa, T. Nii, S. Ho Cha, H. Matsuo, J.-i. Fukushima, Y. Fukasawa, Y. Tani, Y. Taketani, H. Uchino, J. Y. Kim, J. Inatomi, I. Okayasu, K.-i. Miyamoto, E. Takeda, T. Goya, and H. Endou, "Human L-type amino acid transporter 1 (LAT1): characterization of function and expression in tumor cell lines," *Biochimica et Biophysisa Acta*, vol. 1514, no. 2, pp. 291-302, 2001.

[196] F. Verrey, "System L: heterodimeric exchangers of large, neutral amino acids involved in directional transport," *Pflugers Archiv*, vol. 445, no. 5, pp. 529-33, 2003.

[197] C. Meier, Z. Ristic, S. Klauser, and F. Verrey , "Activation of system L heterodimeric amino acid exchangers by intracellular substrates," *EMBO Journal*, vol. 21, no. 4, pp. 580-9, 2002.

[198] R. Duelli, B. Enerson, D. Z. Gerhart, and L. R. Drewes, "Expression of large amino acid transporter LAT1 in rat brain endothelium," *Journal of Cerebral Blood Flow & Metabolism*, vol. 20, no. 11, pp. 1557-62, 2000.

[199] G. Rossier, C. Meier, C. Bauch, V. Summa, B. Sordat, F. Verrey, and L. C. Kuhn, "LAT2, a new basolateral 4F2hc/CD98-associated amino acid transporter of kidney and intestines," *The Journal of Biological Chemistry*, vol. 274, no. 49, pp. 34948-54, 1999.

[200] E. Nakamura, M. Sato, H. Yang, F. Miyagawa, M. Harasaki, K. Tomita, S. Matsuoka, A. Noma, K. Iwai, and N. Minato, "4F2 (CD98) heavy chain is associated covalently with an amino acid transporter and controls intracellular trafficking and membrane topology," *The Journal of Biological Chemistry*, vol. 274, no. 5, pp. 3009-16, 1999.

[201] Y. Fukasawa, H. Segawa, J. Y. Kim, A. Chairoungdua, D. K. Kim, H. Matsuo, S. H. Cha, H. Endou, and Y. Kanai, "Identification and Characterization of a Na^+-independent Neutral Amino Acid Transporter That Assiciates with the 4F2 Heavy Chaina and Exhibits Substrate Selectivity for Small Neutral D- and L- Amino Acids," *Journal of Biological Chemistry*, no. 13, pp. 9690–9698, 2000.

[202] L. Helboe, J. Egebjerg, M. Moller, and C. Thomsen, "Distribution and pharmacology of alanineserine-cysteine transporter 1 (asc-1) in rodent brain," *European Journal of Neuroscience*, no. 18, pp. 2227–2238, 2003.

[203] A. L. Lehninger, "Biochemistry", 2nd edition, *Worth*, New York, USA, 1976.

[204] T. Miyagawa, T. Oku, H. Uehara, R. Desai, B. Neattie, J. Tjuvajev, and R. Blasberg*.,* ""Facilitated" amino acid transport is upregulated in brain tumors," *Journal of Cerebral Blood Flow & Metabolism*, vol. 18, no. 5, pp. 500–509, 1998.

[205] W. Vaalburg, H. H. Coenen, C. Crouzel, P. H. Elsinga, B. Lanström, C. Lemaire, and G. J. Meyer*,* "Amino acids for the measurement of protein synthesis in vivo by PET," *International Journal of Radiation Applications and Instrumentation*, vol. 19, no. 2, pp. 227–237, 1992.

[206] T. M. Shoup, J. Olson, J. M. Hoffman, J. Votaw, D. Eshima, V. M. Camp, M. Stabin, D. Votaw, and M. M. Goodman*,* "Synthesis and evaluation of ^{18}F-1-Amino-3-fluorocyclobutane-1carboxylic acid to image brain tumors," *The Journal of Nuclear Medicine*, no. 40, pp. 331–338, 1999.

[207] H. Uehara, T. Miyagawa, J. Tjuvajev, R. Joshi, B. Beattie, T. Oku, R. Finn, and R. Blasberg*,* "Imaging experimental brain tumors with 1-aminocyclopentane carboxylic acid and alphaaminoisobutyric acid: comparison to fluorodeoxyglucose and diethylenetriaminepentaacetic acid in morphologically defined tumor regions," *Journal of Cerebral Blood Flow & Metabolism*, vol. 17, no. 11, pp. 1239–1253, 1997.

[208] H. J. Wester, M. Herz, W. Weber, P. Heiss, R. Senekowitsch-Schmidtke, M. Schwaiger, and G. Stöcklin*,* "Synthesis and Radiopharmacology of O-(2-[^{18}F)fluoroethyl-L-tyrosine for tumor imaging," *The Journal of Nuclear Medicine*, vol. 1999, no. 205-212, 40.

[209] K. Kubota, K. Ishiwata, R. Kubota, S. Yamada, J. Takahashi, Y. Abe, H. Fukuda, and T. Ido*,* "Feasibility of Fluorine-18-Fluorophenylalanne for Tumor Imaging Compared with Carbon-11L-Methionine," *The Journal of Nuclear Medicine*, no. 37, pp. 320–325, 1996.

[210] H. H. Coenen, P. Kling, and G. Stöcklin, "Cerebral Metabolism of L-2-[^{18}F]Fluorotyrosine, a new PET tracer of protein synthesis," *The New England Journal of Medicine*, no. 30, pp. 1367–1372, 1989.

[211] K. Wienhard, K. Herholz, H. H. Coenen, J. Rudolf, P. Kling, G. Stöcklin, and W. D. Heiss., "Increased Amino Acid Transport into Brain Tumors Measured by PET of L-2-[^{18}F]Fluorotyrosine," *The Journal of Nuclear Medicine*, no. 32, pp. 1338–1346, 1991.

[212] T. Inoue, K. Tomiyoshi, T. Hiquichi, K. Ahmed, M. Sarwar, K. Aoyagi, S. Amano, S. Alyafei, H. Zhang, and K. Endo., "Biodistribution Studies on L-3-[^{18}F]Fluoro-alpha-methyl tyrosine," *The Journal of Nuclear Medicine*, no. 39, pp. 663–667, 1998.

[213] T. Inoue, T. Shibasaki, N. Oriuchi, K. Aoyagi, K. Tomiyoshi, S. Amango, M. Mikuni, I. Ida, J. Aoki, and K. Endo, "^{18}F-ɲ-methy tyrosine PET studies in patients with brain tumors," *The Journal of Nuclear Medicine*, no. 40, pp. 399–405, 1999.

[214] P. Heiss, S. Mayer, M. Herz, H. J. Wester, M. Schwaiger, and R. Senekowitsch-Schmidtke, "Investigation of Transport Mechanism and Uptake Knietics of O-2-^{18}F-Fluoroethyl-L-tyrosine in vitro and in vivo," *The Journal of Nuclear Medicine*, no. 40, pp. 1367–1373, 1999.

[215] J. R. Barrio, S. C. Huang, and M. E. Phelps, "Biological imaging and the molecular basis of dopaminergic diseases," *Biochemical Pharmacology*, vol. 54, no. 3, pp. 341–348, 1997.

[216] B. Chin, D. McDougald, D. Weitzel, T. Hawk, R. Reiman, M. Zalutsky, and G. Vaidyanathan., "Synthesis and preliminary evaluation of 5-[^{18}F]fluoroleucine: a novel LAT1 substrate," *The Journal of Nuclear Medicine*, no. vol. 57, suppl 2, p. 1390, 2016.

[217] P. D. Shreve, Y. Anzai, and R. L. Wahl, "Pitfalls in oncologic diagnosis with FDG PET imaging: physiologic and benign variants," *Radiographics*, vol. 19, no. 1, pp. 61-77, 1999.

[218] N. Koglin, A. Mueller, M. Berndt, H. Schmitt-Willich, L. Toschi, A. W. Stephens, V. Gekeler, M. Friebe, and L. M. Dinkelborg "Specific PET imaging of xC- transporter activity using a ^{18}Flabeled glutamate derivative reveals a dominant pathway in tumor metabolism," *Clinical Cancer Research*, vol. 17, no. 18, pp. 6000–6011, 2011.

[219] R. N. Krasikova, O. F. Kuznetsova, O. S. Fedorova, Y. N. Belokon, V. I. Maleev, S. M. Ametamey, P. A. Schubiger, M. Friebe, M. Berndt, N. Koglin, A. Mueller, K. Graham, L. Lehmann, and L. M. Dinkelborg., "4-[^{18}F]fluoroglutamic acid (BAY 85-8050), a new amino acid radiotracer for PET imaging of tumors: synthesis and in vitro characterization," *Journal of Medicinal Chemistry*, vol. 54, no. 1, pp. 406–410, 2011.

[220] S. Baek, C. M. Choi, S. H. Ahn, J. W. Lee, G. Gong, J. S. Ryu, S. J. Oh, C. Bacher-Stier, L. Fels, N. Koglin, C. Hultsch, C. A. Schatz, L. M. Dinkelborg, E. S. Mittra, S. S. Gambhir, and D. H. Moon, "Exploratory clinical trial of (4S)-4-(3-[^{18}F]fluoropropyl)-L-glutamate for imaging xC-transporter using positron emission tomography in patients with non-small cell lung or breast cancer," *Clinical Cancer Research*, vol. 18, no. 19, pp. 5427–5437, 2012.

[221] A. Bouhlel, W. Alyami, A. Li, L. Yuan, K. Rich, and J. McConathy, "Synthesis and characterization of the novel amino acid (S)-[^{18}F]FAHep for brain tumor imaging: effect of alpha-carbon substitution on brain availability," *The Journal of Nuclear Medicine*, no. 57, suppl 2, p. 443, 2016.

[222] J. Becaud, L. Mu, M. Karramkam, P. A. Schubiger, S. M. Ametamey, K. Graham, T. Stellfeld, L. Lehmann, S. Borkowski, D. Berndorff, L. Dinkelborg, A. Srinivasan, R. Smits, and B. Koksch, "Direct one-step ^{18}F-labeling of peptides via nucleophilic aromatic substitution," *Bioconjugate Chemistry*, vol. 20, no. 12, pp. 2254–2261, 2009.

[223] H. H. Coenen, "Fluorine-18 Labeling Methods: Features and Possibilities of Basic Reactions," *Ernst Schering Research Foundation Workshop*, vol. 62, pp. 15-50, 2007.

[224] R. Huisgen, "1.3-Dipolare Cycloadditionen Rückschau und Ausblick," *Angewandte Chemie*, vol. 13, pp. 604-37, 1963.

[225] F. Himo, T. Lovell, R. Hilgraf, V. V. Rostovtsev, L. Noodleman, K. B. Sharpless, and V. V. Fokin., "Copper(I)-catalyzed synthesis of azoles. DFT study predicts unprecedented reactivity and intermediates," *Journal of the American Chemical Society*, vol. 127, no. 1, pp. 210–216, 2005.

[226] B. T. Worrell, J. A. Malik, and V. V. Fokin, "Direct evidence of a dinuclear copper intermediate in Cu(I)-catalyzed azide-alkyne cycloadditions," *Science*, vol. 340, no. 6131, pp. 457–460, 2013.

[227] C. S. McKay and M. G. Finn, "Click chemistry in complex mixtures: bioorthogonal bioconjugation," *Chemistry & Biology*, vol. 21, no. 9, pp. 1075–1101, 2014.

[228] L. Gaetke and C. K. Chow, "Copper toxicity, oxidative stress, and antioxidant nutrients," *Toxicology*, vol. 189, no. 1-2, pp. 147–163, 2003.

[229] Alexander Kuzmin, Andrei Poloukhtine, Margreet A. Wolfert, and Vladimir V. Popik, "Surface Functionalization using catalyst free azide alkyne cycloaddition," *Bioconjugate Chemistry*, vol. 21, no. 11, pp. 2076-85, 2010.

[230] Jeremy M. Baskin, Jennifer A. Prescher, Scott T. Laughlin, Nicholas J. Agard, Pamela V. Chang, Isaac A. MIller, Anderson Lo, Julian A. Codelli, and Carolyn R. Bertozzi, "Copper-free click chemistry for dynamic in vivo imaging," *Proceedings of the National Academy of Science of the USA*, vol. 104, no. 43, pp. 16793-7, 2007.

[231] Ellen M. Sletten and Carolyn R. Bertozzi, "A Hyrophilic Azacyclooctyne for Cu-free click chemistry," *Organic Letters*, vol. 10, no. 14, pp. 3097-99, 2008.

[232] John C. Jewett, Ellen M. Sletten and Carolyn R. Bertozzi, "Rapid Cu-free click chemistry with readily synthesized biarylazacycloocytnones," *Journal of the American Chemical Society*, vol. 132, pp. 3688-90, 2010.

[233] Julian A. Codelli, Jeremy M. Baskin, Nicholas J. Agard, and Carolyn R. Bertozzi, "Secondgeneration difluorinated cyclooctynes for copper-free click chemistry," *Journal of the American Chemical Society*, vol. 130, no. 34, pp. 11486-93, 2008.

[234] A. James Link, Mandy K. S. Vink, Nicholas J. Agard, Jennifer A. Prescher, Carolyn R. Bertozzi, and David A. Tirell, "Discovery of aminoacyl-tRNA synthetase activity through cell-surface display of noncanonical amino acids," *Proceedings of the National Academy of Sciences of the USA*, vol. 103, no. 27, pp. 10180-5, 2006.

[235] M. Fernandez-Suarez, H. Baruah, L. Martínez-Hernández, K. T. Xie, J. M. Baskin, C. R. Bertozzi, and A. Y. Ting, "Redirecting lipoic acid ligase for cell surface protein labeling with smallmolecule probes," *Nature Biotechnology*, vol. 25, no. 12, pp. 1483–1487, 2007.

[236] Y. Zou, and J. Yin, "Cu-free cycloaddition for identifying catalytic active adenylation domains of nonribosomal peptide synthetases by phage display," *Bioorganic & Medicinal Chemistry Letters*, vol. 18, no. 20, pp. 5664–5667, 2008.

[237] M. A. Nessen, G. Kramer, J. W. Back, J. M. Baskin, L. E. J. Smeenk, L. J. de Koning, J. H. van Maarseveen, L. de Jong, C. R. Bertozzi, H. Hiemstra, and C. G. de Koster, "Selective enrichement of azide-containing peptides from complex mixtures," *Journal of Proteome Research*, vol. 8, no. 7, pp. 3702-11, 2009.

[238] D. H. Ess, G. O. Jones, and K. N. Houk, "Transition states of strain-promoted metal-free click chemistry: 1,3-dipolar cycloadditions of phenyl azide and cyclooctynes," *Organic Letters*, vol. 10, no. 8, pp. 1633–1636, 2008.

1.14. List of illustrations

^{18}F-labeling using click cycloadditions

Kathrin Kettenbach[1], Hanno Schieferstein[1], Tobias L. Ross[1,2]

[1] Institute of Nuclear Chemistry, Johannes Gutenberg-University Mainz, 55128 Mainz, Germany

[2] Radiopharmaceutical Chemistry, Department of Nuclear Medicine, Hannover Medical School, 30625 Hannover, Germany

Abstract

Due to expanding applications of positron emission tomography (PET) there is a demand for developing new techniques to introduce fluorine-18 ($t_{1/2}$= 109.8 min). Considering that most novel PET-tracers are sensitive biomolecules and that direct introduction of fluorine-18 often needs harsh conditions, the insertion of ^{18}F in those molecules poses an exceeding challenge. Two major challenges during ^{18}F-labeling are a regioselective introduction and a fast and high yielding way under mild conditions. Furthermore, attention has to be paid to functionalities, which are usually present in complex structures of the target molecule. The Cu-catalyzed azide-alkyne cycloaddition (CuAAC) and several copper-free click reactions represent such methods for radiolabeling of sensitive molecules under the above-mentioned criteria. This mini review will provide a quick overview about the development of novel ^{18}F-labeled prosthetic groups for click cycloadditions and will summarize recent trends in copper-catalyzed and copper-free click ^{18}F-cycloadditions.

Introduction

For the application in positron emission tomography (PET) [1], fluorine-18 provides ideal nuclear physical characteristics for *in vivo* imaging. Fluorine-18 offers a half-life of 110 min, β^+-branch of 97 % and especially a low β^+-energy of 635 keV, which is responsible for a very high spatial resolution. [2] The challenges for researchers are to develop convenient ^{18}F-labeling strategies, which include short reaction times and applicability for sensitive biomolecules. Especially the harsh conditions during direct ^{18}F-labeling pose an exceeding challenge. [3,4] Therefore, most of the radiolabeling strategies focus on ^{18}F-containing prosthetic groups, which allow a sensitive and bioorthogonal ^{18}F-labeling treating the multitude of functional groups in those bioactive compounds with respect.

The most established method, which fulfills all mentioned criteria, is given by click reactions. Especially the Cu(I)-catalyzed variant of the Huisgen 1,3-dipolar cycloaddition of terminal alkynes and azides offers a very powerful reaction with high specificity and excellent yields under mild conditions. [5] As a result, numerous PET-tracers have been synthesized using CuAAC in a widespread spectrum of structural varieties of the prosthetic group within the last decade. One of the latest investigations deals with an amino acid-based prosthetic group to further improve the pharmacokinetic properties of radiotracers, particularly suitable for peptides and proteins. [6] In contrast to structurally different prosthetic groups, a minimized influence on the pharmacological behavior of the molecule with an amino acid based labeling system is expected.

However, the need of cytotoxic copper during CuAAC has led to the necessity of alternative fast and copper-free click reaction strategies for radiofluorination and additionally enabling pre-targeting approaches in living systems. Those so-called strain-promoted click reactions can be carried out

between cyclooctyne derivatives and azides (strain-promoted azide-alkyne cycloaddition, SPAAC) [7-13] or tetrazines (tetrazine-trans-cyclooctne (TTCO) ligation) [14],[15],[16],[17] as well as between norbornene derivatives and tetrazines. [18] Especially, the TTCO ligation showed promising reaction rates, which makes this click reaction concept very suitable for ^{18}F-labeling, but also for *in vivo* application in living systems. Very recently, new versions of ^{18}F-click cycloadditions are added to the range of reactions. [19-21] In this line, the first ^{18}F-labeled ɴ-lactames became available via a new *radio*-Kinugasa reaction. [21]

As a consequence, click cycloaddition is one of the most frequently applied methods for ^{18}F-labeling of new bioactive compounds, with or without a catalytic system. This can be impressively illustrated by the fact, that over 50 original papers have been published in this research area within the last eight years.

Table 1 – 3 give an overview of the ^{18}F-prosthetic groups, the reaction conditions and reaction partners applied for copper-catalyzed, copper free and new developments in click ^{18}F-fluorination. The most important lead structures of those prosthetic groups are shown in figure 1, 3 and 5.

Copper-catalyzed ^{18}F-click cycloadditions

In the last decade, the copper-catalyzed azide alkyne cycloaddition (CuAAC), which has first been reported independently by Sharpless *et al.* [22] and Meldal *et al.* [23] in 2002, has spread over almost all fields of chemistry [24-28], biology [29-31], and material science. [32,33] The great advantage of this method is given by its outstanding efficiency, its regiospecificity and fast formation of 1,4disubstituted 1,2,3-triazoles at ambient temperatures, which is particularly suitable for ^{18}F-labeling of sensitive biomolecules. In particular, the CuAAC enables incorporation of fluorine-18 via a prosthetic group under mild and bioorthogonal conditions. [34-37] 1,2,3-triazoles were first introduced by Arthur Michael, who described the formation of a 1,2,3-triazole from a phenylazide in 1893. [38] Following this pioneering work, Dimroth, Fester and Huisgen described this type of reaction as a 1,3-dipolar cycloaddition for the first time in 1963. [5]

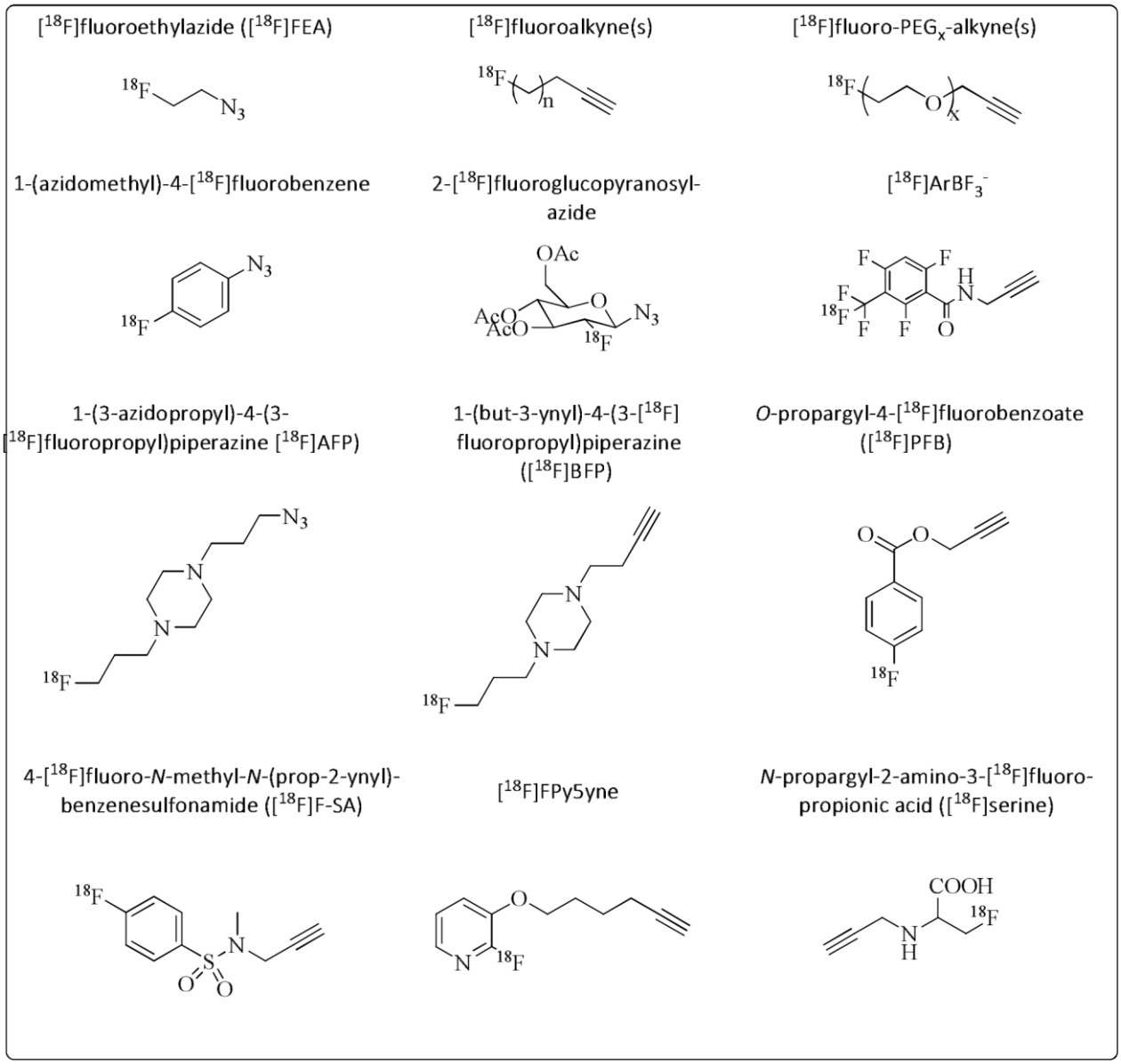

FIGURE 1: Lead structures of the most important ^{18}F-prosthetic groups applied for copper-catalyzed click ^{18}F-fluorination.

In 2006, Marik and Sutcliffe published the application of the CuAAC as an ^{18}F-labeling strategy for the first time. [39] They radiolabeled three different alkyne precursors in radio chemical yields (RCY) of 36 – 81 %. Afterwards they reacted them with azido-functionalized peptides in RCY of 54 – 99 % and an overall reaction time of 30 min. Thus, they could show a new, very fast, efficient and mild ^{18}F-labeling strategy for complex compounds, especially appropriate for sensitive biomolecules. Only two years later, the suitability of this approach was demonstrated for the ^{18}F-labeling of a folate derivative for *in vivo* tumor imaging with the same prosthetic group, 6-[^{18}F]fluorohexyne. [40] The radiofolate was obtained in RCY of 25 – 35 % and was applied to KB-tumor bearing mice. A specific tumor accumulation could be observed by using the folate receptor (FR) targeting concept. Furthermore, Kim *et al.* used ^{18}F-labeled alkynes as prosthetic groups for the ^{18}F-labeling of 2,3,4,6-tetra-O-acetyl-E-Dglucopyranosyl azide [41], which in turn was employed to label the $\alpha_V\beta_6$ specific peptide A20FMDV2.

[42]
Considering all known clickable prosthetic groups for ^{18}F-labeling, [^{18}F]fluoroethyl azide ([^{18}F]FEA) is certainly one of the most investigated clickable ^{18}F-prosthetic groups. Until today, about twenty different manuscripts deal with [^{18}F]FEA to radiolabel a broad variety of biomolecules and compounds. In 2007, Glaser *et al.* [43] mentioned for the first time the preparation of [^{18}F]FEA with a RCY of 55 % using 2-azidoethyl-4-toluenesulfonate as precursor. As a proof-of-concept, they reacted [^{18}F]FEA with different terminal alkynes in very good to excellent RCY of 61 – 98 %. In respect to the catalytic system copper sulfate in combination with ascorbic acid or sodium ascorbate has mainly been used, whereas only in a few approaches copper(I) iodide was used. [44,45] It has been shown that addition of bathophenanthroline disulfonate (Cu^{I} stabilizing agent) accelerates the 1,3-dipolar cycloaddition [4648]. The very good access to [^{18}F]FEA led to the development of a variety of radiotracers labeled with this prosthetic group, like ^{18}F-deoxyuridine [44], [^{18}F]fluoro-oxothymidine ([^{18}F]FOT) or [^{18}F]fluorothiothymidine ([^{18}F]FTT) [49] as well as apoptosis markers [46] and several peptide systems. [50-52] In 2012, Glaser *et al.* [49] described the reduction of [^{18}F]FEA using copper wire under acidic conditions, which is a possible explanation of the poor yields during some click reactions.

In 2007, Sirion *et al.* [53] reported for the first time [^{18}F]fluoro-PEG$_x$-derivatives (x = various polyethylenglycol (PEG) ratios) as new ^{18}F-labeled prosthetic click-groups. These compounds showed a reduced volatility and increased polarity compared with other ^{18}F-labeled prosthetic groups like [^{18}F]FEA or [^{18}F]fluoroalkynes. These properties ease their handling as well as improve the *in vivo* behavior of the labeled compounds. The compounds showed a longer circulation time and a reduced renal clearance making them very suitable for *in vivo* application. Sirion *et al.* described the preparation of different aliphatic and aromatic [^{18}F]fluoro-PEG-azides and ^{18}F-labeled alkynes in RCY of 85 – 94 %. As a proof-of-concept, they carried out cycloadditions with the ^{18}F-labeled prosthetic groups and the corresponding alkynes respectively azides in high RCY of 71 – 99 %. Several other groups continued this work by using the ^{18}F-labeled PEGylated prosthetic groups for labeling cRGD derivatives [54] and other peptides [55], nanoparticles [56,57] or folates. [58]

To increase the lipophilicity and metabolic stability of radiotracers, [^{18}F]fluoro-aryl-based prosthetic groups have been developed and investigated. In 2007, Ramenda *et al*. [59] published for the first time a 4-[^{18}F]fluoro-*N*-methyl-*N*-(prop-2-ynyl)-benzenesulfonamide (p-[^{18}F]F-SA), which was obtained in RCY of 32 ± 5 %. Subsequently, this prosthetic group was used for radiolabeling an azidofunctionalized neurotensin giving a RCY of 66 %. Furthermore, the same group used the [^{18}F]fluoroaryl prosthetic group for the labeling of human serum albumin (HSA) [60] and other proteins, phosphopeptides and

L-RNA [61] in good RCY. A pyridine-based ^{18}F-prosthetic group was first introduced by Inkster *et al*. [62] in 2008 by reacting [^{18}F]FPy5yne with a model peptide in RCY of 18.7
% and an overall reaction time of 160 min. They started from either 2-nitro- or 2-trimethylammonium pyridine to synthesize [^{18}F]FPy5yne with a RCY of 42 %. Furthermore, [^{18}F]fluoro-pyridine derivatives have been used to radiolabel cRGDs [63] and the *D*-amino acid analog of WT-pHLIP. [64]

In 2009, Vaidyanathan *et al.* [65] presented a prosthetic group based on a 4-[^{18}F]fluorobenzoate. Propargyl-4-[^{18}F]fluorobenzoate ([^{18}F]PFB), which could be obtained in RCY of 58 ± 31 % within 15 min. To investigate the labeling properties of this new prosthetic group, numerous compounds have been ^{18}F-labeled using [^{18}F]PFB with RCY from 37 % to 88 % and overall reaction times of about 1 h. Another approach was published by Li *et al.* in 2012 [66], who synthesized 4-[^{18}F]fluoro-3-nitro-*N*-2-propyn-1yl-benzamide ([^{18}F]FNPB) for ^{18}F-labeling of cRGDfK and a D4 peptide, which was identified as an EGFR targeting ligand. This approach was followed by the synthesis of 1-(azidomethyl)-4-[^{18}F]fluorobenzene by Thonon *et al..* [67] They did a multi-step radiosynthesis (4 steps), where the fluorine-18 was introduced in the first step. The desired radiolabeled product could be obtained in a RCY of 34 % within 75 min and was used itself to label a 4-ethynyl-*L*-phenylalanine-containing peptide. The same prosthetic group was also employed by Mercier *et al.* [68] and Flagothier *et al*. [69] for ^{18}F-labeling of *si*RNA. Other structural analog prosthetic groups have also been developed by Mercier *et al.* [68] and Chun *et al..* [70]

To improve the *in vivo* behavior of peptides in respect to blood clearance and stability, Maschauer and Prante developed [^{18}F]fluoro-gluco-derivatives for CuAAC-radiolabeling of Fmoc-*L*-propargylglycine with a RCY of 60 %. [71] They showed, that the ^{18}F-click labeling reaction was more convenient by using the N-anomeric derivative of the azides respectively alkynes, giving very high RCY of 71 ± 10 %. One year later, they published the first *in vivo* evaluation of a ^{18}F-labeled RGD peptide labeled with [^{18}F]FDG-N-Az in U87MG-tumor bearing mice showing an improved blood clearance and stability. [68,69] Likewise, Fischer *et al.* demonstrated in 2012, that a [^{18}F]fluorodeoxyglycosyl folate could be obtained in RCY of 5 – 25 % and subsequent biodistribution and PET-imaging studies showed a high and specific uptake of the radiotracer in FR-positive tumors [74]. The variety of new ^{18F}-labeling strategies using ^{18}F-Fluoroglycosylation is the focus of a review article as a part of this special issue provides by Maschauer and Prante. [99]

As another promising approach, Li *et al.* presented in 2013 an alkyne-functionalized aryltri[^{18}F]fluoroborate for radiolabeling azido-bombesin and azido-RGD. The major advantage of this

method is the two-step, one-pot procedure providing a water-soluble and non-coordinating aryltri[^{18}F]fluoroborate anion, which provided specific activities up to 555 GBq/µmol. [75-77]

Two new piperazine-based prosthetic groups, 1-(but-3-ynyl)-4-(3-[^{18}F]fluoropropyl)piperazine ([^{18}F]BFP) and 1-(3-azidopropyl)-4-(3-[^{18}F]fluoropropyl)piperazine ([^{18}F]AFP), have recently been developed by Pretze *et al.*. [78] Spiro salts were used as precursors, facilitating purification by using solid phase extractions (RP-18 or SiO_2-cartridges). Both prosthetic groups could be obtained in RCY of about 30 % using an automated synthesis module. To avoid Glaser coupling, which has been observed by using [^{18}F]BFP for radiolabeling of peptides, [^{18}F]AFP was used instead. An important observation was the fact, that the applied peptide formed very strong complexes with the copper catalyst, which required the use of bispidine as a strong chelating agent to remove cytotoxic copper species.

One of the latest developments describes the synthesis of an ^{18}F-labeled alanine derivative as a new prosthetic click group, reported by Schieferstein *et al.*. [6] In this case, an amino acid-based prosthetic group has been developed to improve the pharmacokinetic profile of ^{18}F-click-labeled biomolecules. The prosthetic group was obtained in good RCY of 28 ± 5 % from a two-step reaction as described in figure 2. The final ^{18}F-labeled prosthetic group was subsequently reacted with an azido-RGD as model system in RCY of 75 % within 20 min.

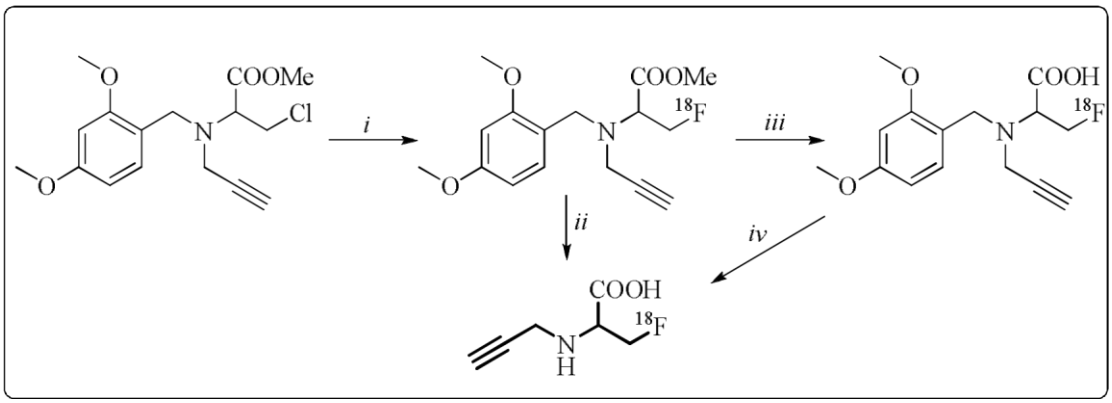

FIGURE 2: Radiosynthesis of a new amino-acid based ^{18}F-prosthetic group (*N*-propargyl-2-amino-3-[^{18}F]fluoro-propionic acid, "[^{18}F]serine") for ^{18}F-CuAAC-labeling of complex biomolecules. *i*) $[K2.2.2]^+/^{18}F^-$, DMSO, 140 °C, 10 min; *ii*) hydrochloric acid (3.3M), 100 °C, 15 min; (for analytical purposes (sequential deprotection): *iii*) sodium hydroxide (3.3 M), 60 °C, 5 min; *iv*) hydrochloric acid (3.3M), 100 °C, 15 min.

Considering above-mentioned prosthetic groups for radiolabeling with fluorine-18, table 1 summarizes important properties of those components. It has been shown, that the integration of an [^{18}F]fluoropropyl, [^{18}F]fluoro-ethyl or [^{18}F]fluoro-aryl moiety can provide an improved metabolic profile and that the glycosylation or PEGylation can further improve the *in vivo* behavior. Furthermore, for *in vivo* application a total removal of the copper catalyst is essential. This could be very challenging in the case, that peptides or proteins are able to complex copper species from the catalytic system.

TABLE 1: Summary of the prosthetic groups, reaction conditions and reaction partners applied for copper-catalyzed click ^{18}Ffluorination. (n.)d.c. = (not) decay corrected; Asc = ascorbate; DIPEA = diisopropylethylamin; TBTA = tris[(1-benzyl-1*H*-1,2,3triazol-4-yl)methyl]amine; n.d. = no data

^{18}F-prosthetic group	steps/ reaction time[1]	RCY[2]	reacting agent	catalytic system	over all reaction time[1] (CCA)	RCY[2] CCA	lit.
[^{18}F]fluoroalkynes	1 step, 10 min	36 – 81 %	N-(3-azidopropionyl) peptides	CuI/NaAsc/DIPEA	30 min	54 – 99 %	[39]
4-[^{18}F]fluoro-1-butyne	1 step, 15 min (estimated)	n.d.	glucopyranosyl azide	Cu(I)/Asc/ 2,6-lutidine	75 – 80 min	30 %	[41]
4-[^{18}F]Fluoro-1-butyne	1 step, 15 min	45 ± 3 %	2,3,4,6-tetra-O-acetyl-		30 min	27 ± 6 %	[42]
5-[^{18}F]fluoro-1-pentyne	1 step, 15 min	59 ± 6 %	b-D-glucopyranosyl azide			52 ± 5 %	
	1 step, 22 min	86 ± 2 %	$\gamma_V N_6$ specific peptide A20FMDV2 azide	CuI/Asc	66 min	8.7 ± 2.3 %	[79]
6-[^{18}F]fluoro-1-hexyne	1 step, 12 min	70 – 85 %	œ-(4-azido-butyl)-folic acid amide	CuI	1.5 h	25 – 35 %	[40]
[^{18}F]fluoroethyl azide ([^{18}F]FEA)	1 step, 15 min	55 %	terminal alkynes	excess of Cu^{2+}/Asc or copper powder	1 h	61 – 98 % respectively 15 – 98 % with copper powder	[43] [80]
		n.d.	Caspase 3/7 Selective Isatin	$CuSO_4$/Asc	n.d.	65 ± 6 %	[81]
		n.d.	RGD peptides	Cu^{2+}/Asc		47 ± 8 %	[50]
		n.d.	3-cyanoquinoline core		3 h	37 ± 3.6 %	[82]
		n.d.	apoptosis marker ICMT11	$CuSO_4$/Asc/BPDS	n.d.	1 – 3.4 % n.d.c.	[46]
		n.d.	5-ethynyl-2´deoxyuridine	CuI/ascorbic acid/DIPEA	n.d.	75 ± 10 %	[44]
		n.d.	[Tyr^3]octreotate analogues	$CuSO_4$/Asc/BPDS	30 min (estimated)	40 – 64 %	[47]
		n.d.	ICMT-11 (automated synthesis)		90 min	3 ± 2.6 % n.d.c.	[83]
		n.d.	nucleosides	$CuSO_4$/Asc	n.d.	8 – 12 % n.d.c.	[49]
		n.d.	4-(prop-2-ynyloxy)benzaldehyde		35 min	90 %	[84]
		n.d.	haloethylsulfoxides	CuI/Asc/DIPEA	n.d.	28.5 ± 2.5 %	[45]
		50 % n.d.c.	nitroaromatic	$CuSO_4$/Asc	1 h		[85]
		71 ± 4 %	RGDfK		60 min	60 ± 2 %	[51]
		55 %	alkyne-func. 6-halopurines	one-pot BPDS-copper(I) ($CuSO_4$/Asc) substrates	1 h	55 – 75 %	[48]
		n.d.	tert-butyl ester of NBoc-(S)-propargyl glycine	$CuSO_4$/Asc	2.5 h	58 ± 4 %	[86]
	Precursor: 2 steps [^{18}F]FEA: 15 min.	n.d.	3-butynyl triphenyl phosphonium bromide	$CuSO_4$, Asc	1 h	n.d.	[87]
	1 step, 5-10 min	68 – 75 %	Alkynes of benzene rings		30 min	25 – 87 %	[88]

[^{18}F]FEA from a polyflourinated sulfonate precursor	n.d.	n.d.	FtRGD		70 – 75 min	10 – 30 % n.d.c.	[52]
[^{18}F]-Fluoro-PEGAlkyne	1 step, 20 min	85 – 94 %	various azides	$CuSO_4$/Asc	10 – 30 min	71 – 99 %	[53]
	1 step, 15 min	65 ± 1.9 %	$E(RGDyK)_2$ azide	$CuSO_4$/Asc	110 min (estimated)	52 ± 8.3 %	[54]
		57 %	Nanoparticle azide	$CuSO_4$/Asc/BPDS	1 h (estimated)	58 %	[56]
[^{18}F]fluoro-PEG_3-azide	1 step, 40 min	62 ± 4 %	N-alkynylated peptide		2 h (estimated)	31± 6 %	[55]
		n.d.	ZnO nanoparticle alkynes		n.d.	> 95 %	[57]
[^{18}F]fluoro-PEG-azide	precursor: 2 steps labeling: 1 step	labeling: 58 %	œ-(11-azido-3,6,9trioxaundecanyl)folic acid amide	CuAcetate, Asc	2.5 h	8.5 %	[58]
4-[^{18}F]fluoro-Nmethyl-N-(prop-2ynyl)-benzenesulfonamide (p[^{18}F]F-SA)	precursor: 3 steps, - labeling: 1 step, 80 min	32 ± 5 %	azide functionalized neurotensin		n.d.	66 %	[59]
			azide-functionalized human serum albumin (HSA)	Cu(I)-TBTA	100 min	55 – 60 %	[60]
		n.d.	azide-functionalized phosphopeptide, protein (HAS), oligonucleotide (L-RNA)	$CuSO_4$/Asc	2 h	77 % / 55-60 % / 25 %	[61]
[^{18}F]FPy5yne	1 step, 15 min	42 %	N_3–(CH_2)4–CO–YKRI–OH (BG142)	tetrakis (acetonitrilo) copper(I) hexa fluorophos phates/ TBTA	160 min	18.7 %	[62]
			azide-functionalized DNA	CuBr/TBTA and 2,6lutidine	276 min	24.6 ± 0.5 %	
2-[^{18}F]fluoro-3-pent-4-yn-1-yloxypyridine ([^{18}F]FPyKYNE)	20 – 25 min	20 – 35 %	azide-functionalized RGD peptide	$CuSO_4$/Asc	125 min	12 – 18 %	[63]
6-[^{18}F]fluoro-2etynylpyridine	1 step, 10 min	27.5 ± 6.6 %	D-amino acid analogue of WT-pHLIP azide	Cu-Acetate/Asc	85 min	5 – 20 %	[64]
propargyl 4-[^{18}F]fluorobenzoate ([^{18}F]PFB)	precursor: 2 steps, labeling: 1 steps, 15 min	58 ± 31 %	benzyl azide, two lysine derivatives, transglutaminasereactive peptide	$CuSO_4$/Asc	1 h (estimated)	88 ± 4 %, 79 ± 33 % and 75 ± 5 % 37 ± 31 %	[65]
4-[^{18}F]fluoro-3-nitro-N-2propyn-1-yl-benzamide ([^{18}F]FNPB)	1 step, 40 min	58 %	azido-peptides cRGDfK and D4 peptide		1 h	87 – 93 %	[66]
1-(azidomethyl)-4-[^{18}F]fluorobenzene	4 steps, 75 min	34 %	4-ethynyl-*L*phenylalaninepeptide	CuI/NaAsc/ DIEA	90 min	90 %	[67]
	4 steps, 75 min	41 %	siRNA alkyne	$CuSO_4$/Asc/ TBTA	120 min	15 ± 5 %	[68]
	1 step, 45 min	84 %	siRNA-Linker (two new alkynebearing linkers)	$CuSO_4$/Asc	120 min	12 %	[69]
1-azido-4-(3-[^{18}F]fluoropropoxy)benzene	4 steps, 75 min	35 %	siRNA alkyne	$CuSO_4$/Asc	120 min	15 ± 5 %	[68]
(azidomethyl)-[^{18}F] fluorobenzene	1 step, 188 s	around 40 %	-	-	-	[70]	94 –

4-[F]fluorophenylazide		15 % around	-	-	-		[18]
3,4,6-tri-O-acetyl-2deoxy-2-[^{18}F]fluoroglucopyranosyl azide	1 step, 30 min	71 ± 10 %	Fmoc-Lpropargylglycine	$CuSO_4$/Asc	1.5 h (estimated)	60 %	[71]
	2 step, 7.5 min	n.d.	alkyne-functionalized peptides (RDG, neurotensin peptoid)	$CuSO_4$/Asc	75 min	17 – 20 % n.d.c.	[72]
		52 %	folate alkyne	Cu-Acetate/Asc	3 h	5 – 25 %	[74]
	1 step, 10 min	84 %	RGD-peptide alkyne	$CuSO_4$/Asc	16 – 24 % 1 step		[73]
		1.3 – 4.7 %	alkyne-bearing protein	CuBr/TTMA	4.1 % 70 – 75 min 80 – 100 min		[89]
		n.d.	ET_AR ligand alkyne	$CuSO_4$/Asc	70 min	20 – 25 % n.d.c.	[90]
		n.d.	cyanoquinoline (EGFR) alkyne	$CuSO_4$/Asc	90 min	8.6 ± 2.3 % n.d.c.	[91]
[^{18}F]$ArBF_3^-$	1 step, 20 min	n.d.	alkyne – functionalized RGD	Cu^I/Asc	1 h	n.d.	[75]
			alkyne –functionalized bombesin (BBN)		1 h	20 ± 10 % n.d.c.	[76]
	2 steps,	n.d.	alkyne –functionalized RGD-boronate		30 min	15 – 30 %	[92]
piperazine-based [^{18}F]AFP [^{18}F]BFP	AFP: 4 steps, 54 h BFP: 4 steps, 72 h [^{18}F]AFP: 1 step, 40 min [^{18}F]BFP: 1 step, 40 min	[^{18}F]AFP: 29 ± 5 % [^{18}F]BFP: 31 ± 9 %	N-Fmoc-e-azidoLnorleucine (amino acid), SNEW peptide	$CuSO_4$, Asc	2 h	amino acid: 59 – 79 % SNEW peptide: 17 – 25 %	[78]
[^{18}F]fluoro-serine	2 steps, 125 min	28 ± 5 %	cRDG-azide	$CuSO_4$, Asc	145 min	75 %	[6]

[1]calculated as sum from all steps, for the ^{18}F-prosthetic group respectively for the overall reaction yielding the click product, starting from fluorine-18

[2]radio chemical yields for the ^{18}F-prosthetic group starting from fluorine-18 respectively for the click reaction, decay corrected, as long as not noted elsewise

Copper-free ^{18}F-click cycloadditions

Even though a large number of novel radiotracers using click chemistry have been developed, none of them has entered clinical routine to date, apart from [^{18}F]fluoro-RGD-K5, which is already used in clinical trials in de US. This can be explained by the need of cytotoxic copper during radiotracer syntheses by using copper-catalyzed 1,3-dipolar Huisgen cycloadditions. [93] Thus, there is still a demand for facile (metal-free) and robust ^{18}F-labeling reactions for the syntheses of radiotracers for imaging of malignancies *in vivo*. This lead to the development of catalyst-free click-labeling approaches, which spare copper species during labeling steps and even enable *in vivo* pre-targeting concept. Recent developments deal with biocompatible strain-promoted copper-free versions of the

alkyne-azide cycloaddition (SPAAC), where the focus has been set on derivatives of cyclooctynes and dibenzocyclooctynes. First approaches focus on the reaction of ^{18}F-labeled cyclooctynes with azidebearing biomolecules. On the other hand, in further approaches cyclooctyne-carrying bioactive compounds are used, which can be labeled with different ^{18}F-labeled azides. In the beginning, only a few studies have been reported due to the complex and low yielding syntheses of strained cyclooctynes. [10,12,14] However, nowadays lots of cyclooctyne derivatives are commercially available, which facilitates the precursor syntheses and opens a wide range of applications.

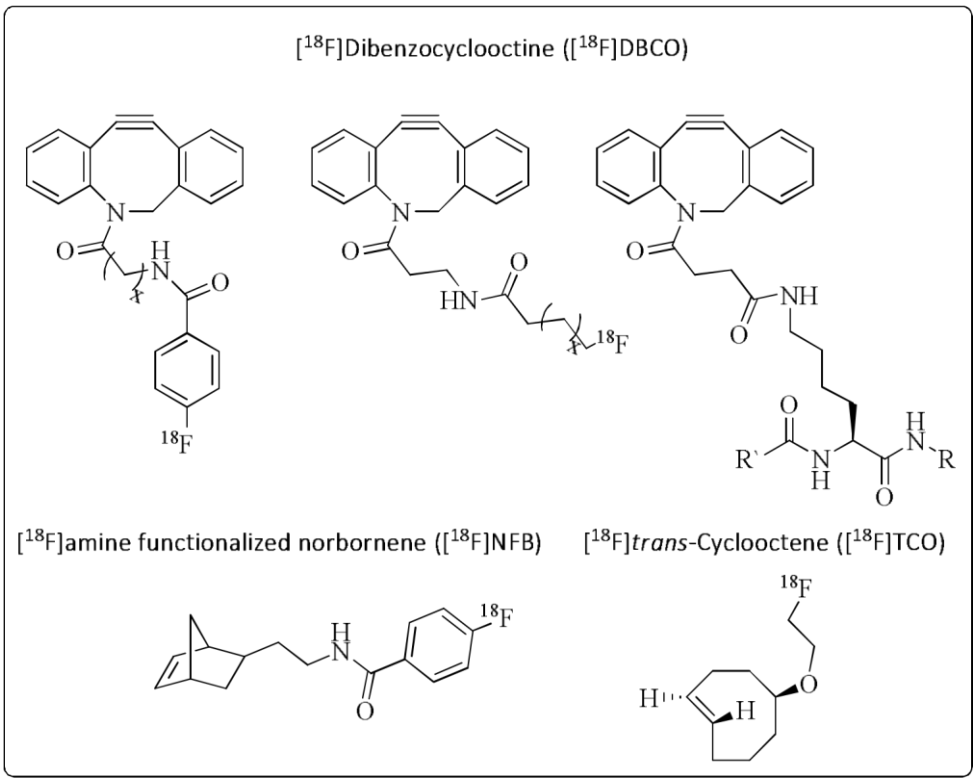

FIGURE 3: Lead structures of the most important ^{18}F-prosthetic groups applied for copper-free click ^{18}F-fluorination.

In 2011 Bouvet *et al.* [7] published the first example of a SPAAC with ^{18}F-labeled *aza*-dibenzocyclooctyne, [^{18}F]FB-DBCO, and a plethora of azides. The ^{18}F-labeled building-block was synthesized via acylation of commercially available *N*-(3-aminopropionyl)-5,6-dihydro-11,12-didehydrodibenzo[*b,f*]azocine with *N*-succinimidyl-4-[^{18}F]fluorobenzoate ([^{18}F]SFB), which can be easily prepared in an automated synthesis module. [94] The ^{18}F-labeled cyclooctyne could be obtained in a RCY of 85 % and a purity > 95 % within 60 min. The evaluation of this building-block in healthy Balb/C mice showed 60 % of intact compound at 60 min p.i. and had a blood clearance half-life of 53 s. Besides, the compound was stable in methanol and phosphate buffer over 60 min. Subsequently, [^{18}F]FB-DBCO was reacted with various azides as proof-of-principle showing different structural complexities. In all reactions, the formation of two regioisomers (1,4- and 1,5-triazole) has been observed and in some cases a separation of the regioisomers by HPLC was impossible. All ^{18}F-labeled radiotracers were obtained in good to excellent RCY of 69 – 98 % within an overall reaction time of

about 2 h. However, the reaction rates in these cases were much slower compared to other examples of bio-orthogonal reactions, limiting this new approach for *in vivo* pre-targeting applications.

A cyclooctyne derivative has been conjugated to bombesin (*aza*-DBCO-BN, 9 steps) with an overall yield of 17 % by Campbell *et al.*. [8] The *aza*-DBCO-BN was reacted with various [^{18}F]fluoro-azides giving RCY of 19 – 37 % within 30 min. In 2011, Arumugam *et al.* [9] investigated the direct ^{18}F-labeling of azadibenzocyclooctyne (DBCO) yielding the ^{18}F-labeled prosthetic group (RCY = 36 %). The radiolabeling was followed by a click reaction with an *azido*-octreotide leading to the ^{18}F-labeled octreotide in a RCY of 95 % within a total reaction time of 1.5 h. In contrast, other working groups used ^{18}F-cyclooctynes for labeling RDG-derivatives [11] as well as further integrin-specific peptides.

[10,13]

Another possibility to perform copper-free click reactions is given by the inverse electron demand Diels Alder cycloaddition between a cyclooctene and a tetrazine under the release of nitrogen. The socalled tetrazine-*trans*-cyclooctene ligation (TTCO ligation) was first published by Li *et al.* in 2010. [14] Concerning the instability of the tetrazines, it is more practical to functionalize the biomolecule with a tetrazine followed by the reaction with an ^{18}F-labeled cyclooctene. The latter are much more suitable for direct ^{18}F-labeling than tetrazines. For this purpose a nosylate precursor was used for ^{18}F-labeling of the cyclooctene providing RCY of 71 % within 15 min. To investigate the suitability of the ^{18}Fprosthetic group in click reactions, the [^{18}F]fluoro-cyclooctene was reacted with a 3,6-di(2-pyridyl)-*S*tetrazine in an excellent RCY of 98 % within 10 s, showing its outstanding feasibility for *in vivo* pretargeting approaches. These fast reaction rates made this approach very attractive, that even ^{11}Clabeling reaction were explored using the inverse electron demand Diels Alder cycloaddition between a cyclooctene and a tetrazine. [95] In 2011, a ^{18}F-labeled cyclooctene was linked to a tetrazine-RGD derivative by Selvaraj *et al.* [15] with a RCY of 90 % within 5 min at room temperature. The resulting ^{18}F-labeled tracer was tested in *in vivo* experiments showing a high tumor accumulation, which could selectively be blocked. In 2012, the group of Devaraj *et al.* [96] published for the first time the *in vivo* click reaction of *trans*-[^{18}F]fluoro-cyclooctene and a polymer-modified tetrazine (PMT). The radiolabeled peptide [^{18}F]F-PMT10 could be obtained in a RCY of 89.2 %. Whole body animal PET-scans were carried out 3 h p.i., showing renal clearance and a widespread tissue distribution as can be seen in figure 2. Previously, the same group described the synthesis of an ^{18}F-labeled cyclooctene with a RCY of 46.1 ± 12.2 %. Subsequently, this prosthetic group was clicked with a tetrazine-modified exendin-4 in RCY of 46.7 ± 17.3 %. [16]

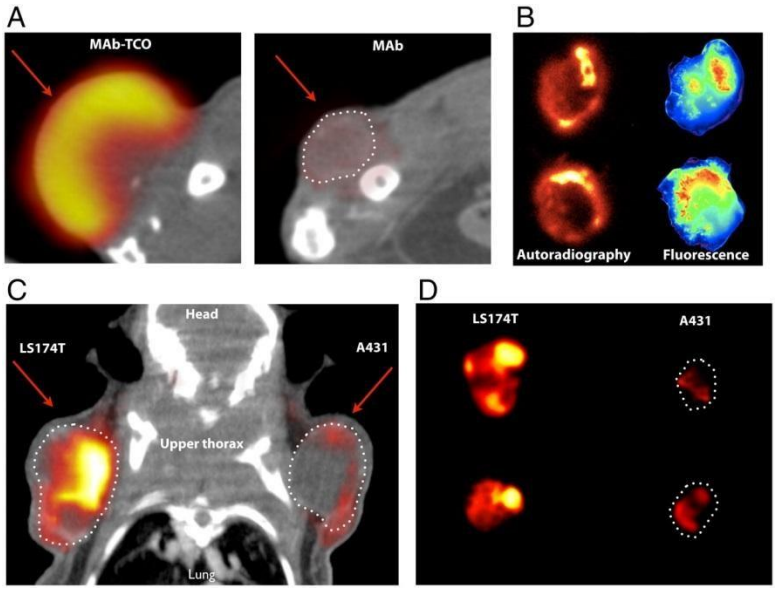

FIGURE 4: PET and autoradiography using ^{18}F-tetrazine agents. (A) PET/CT fusion of LS174T tumor xenograft labeled using either *trans*-cyclooctene (TCO) monoclonal antibodies (mAb TCO) or control unlabeled antibodies (mAb) followed by [^{18}F]FPMT10 (polymer-modified tetrazine). Arrows indicate location of the tumor xenograft. The bladder was omitted for clarity. (B) Imaging using autoradiography (left side) and fluorescence slices after targeting with fluorescence TCO monoclonal antibody and [^{18}F]F-PMT10. (C) PET/CT fusion of mouse bearing A431 and LS174T tumors after targeting with anti-A33 TCO monoclonal antibodies followed by ^{18}F-PMT10. Arrows indicate location of tumors and the liver was omitted for clarity. (D) Autoradiography of representative 1 mm LS174T and A431 tumor slices after multistep targeting. (reprinted with permission from [96]; Copyright 2012 National Academy of Sciences of the United States of America)

A similar strategy was published by Knight *et al.* in 2013, where an ^{18}F-labeled amino-functionalized norbornene was reacted with a tetrazine-modified peptide. [18] The ^{18}F-labeled norbornene was obtained using N-succinimicyl-4-[^{18}F]fluorobenzoate ([^{18}F]SFB) in RCY of 60 ± 17 % within 52 min. As a proof-of-concept, two different tetrazines, an asymmetric dipyridyl tetrazine and a tetrazine-modified bombesin peptide were labeled with ^{18}F-labeled norbornene derivative ([^{18}F]NFB)in 46 – 97 % RCY within 82 min.

Considering the copper-free click labeling of bioactive compounds with fluorine-18, both, the strainpromoted alkyne-azide cycloaddition (SPAAC), as well as the tetrazine-*trans*-cyclooctyne ligation (TTCO ligation) show promising results. Regarding *in vivo* pre-targeting approaches, only the TTCO ligation showed favorable results and reaction rates, which are suitable for this application. [96] Table 2 summarizes reaction conditions, radiochemical yields and reaction partners of those components.

TABLE 2: Summary of the prosthetic groups, reaction conditions and reaction partners applied for copper free click fluorination. DA = Diels Alder; DBCO = *aza*-dibenzocyclooctyne; TCO = *trans*-cyclooctyne;

^{18}F-prosthetic group	steps/ reaction time[1]	RCY$_2$	reacting agent	reaction type/ catalytic system	over all reaction time[1] (CCA)	RCY$_2$ CCA	lit.
[^{18}F]fluoro-COT	1 step, 15 min	71 %	3,6-diaryl-stetrazine	inverse electrondemand DA cycloaddition	30 min (without HPLC)	> 98 %	[14]
[^{18}F]FB-DBCO	1 step, 60 min	85 %	various azides	strain-promoted click 1,3-dipolar cycloaddition	2 h	69 – 98 %	[7]

TCO-derivative: Aza-DBCO-BN (Bombesin)	9 steps, -	17 %	three different [^{18}F]fluoro-azides	strain-promoted click 1,3-dipolar cycloaddition	30 min (without HPLC)	19 – 37 % (depending on azide)	[8]
[^{18}F]fluoro-DBCO	1 step, 1 h	21 %	Tyr^3-octreotide-N_3 (TATE)	strain-promoted click 1,3-dipolar cycloaddition	1.5 h	95 %	[9]
[^{18}F]fluoro-TCO	[14]	[14]	tetrazine-RGD	inverse electrondemand DA cycloaddition	30 min	90 %	[15]
[^{18}F]fluorobifunctional azadibenzocyclooctyne	1 step, 30 min	24.5 %	alkyl azide	strain-promoted click 1,3-dipolar cycloaddition	202 ± 34 min	74 ± 4.8 %	[10]
[^{18}F]fluoro-PEG_4 azide	1 step, 45 min	63 %	cRGD-DBCO	strain-promoted alkyne azide cycloaddition (SPAAC)	80 min	92 %	[11]
[^{18}F]fluorocyclooctyne	6 – 11 steps, 30 – 80 h (depending on the derivative)	20 – 57 % (depending on the derivative)	2- [^{18}F] fluoro-ethylazide	strain-promoted click 1,3-dipolar cycloaddition	30 min.	9.6 – 97 % (depending on COT and solvent)	[12] [97]
trans- [^{18}F]fluoro-cyclooctene ([^{18}F]fluoro-TCO)	1 step, 102 min	46.1 ± 12.2 %	tetrazine modified exendin-4	inverse electrondemand DA cycloaddition	3 h	46.7 ± 17.3 %	[16]
trans- [^{18}F]fluoro-cyclooctene ([^{18}F]fluoro-TCO)			polymer modified tetrazine	inverse electrondemand DA cycloaddition		89.2 % *in vivo*	[96]
[^{18}F]fluoro-aminefunctionalised norbornene	1 step, 52 min	60 ± 17 %	tetrazine (peptide-/bombesin-derivatives)	inverse electrondemand DA cycloaddition	82 min (without preparation of [^{18}F]SFB)	46 – 97 % (depending on the tetrazine)	[18]
[^{18}F]FBA-C_6-DBCO	[10]	[10]	ɲ|ɴ6-specific peptide	strain-promoted click 1,3-dipolar cycloaddition	click: 40 ± 4 min	11.9 ± 3.2 %	[13]

[1]calculated as sum from all steps, for the ^{18}F-prosthetic group respectively for the overall reaction leading to the click product, starting from fluorine-18

[2]radio chemical yields for the ^{18}F-prosthetic group starting from fluorine-18 respectively for the click reaction, decay corrected, as long as not noted elsewise

New developments in ^{18}F-click cycloadditions

The latest developments in metal-free ^{18}F-click cycloadditions have been reported by Zlatopolskiy et al. (Table 3). [19-21] In a first approach, the ^{18}F-labeled building block C-(4-[^{18}F]fluorophenyl)-N-phenyl nitrone was developed to form ^{18}F-isoxazolidines via high-yielding [3+2]cycloadditions with various maleimides [19]. C-(4-[^{18}F]fluorophenyl)-N-phenyl nitrone was obtained from the reaction of 4[^{18}F]fluorobenzaldehyde and N-phenylhydroxylamine in high RCY of 74 % with 10 min. In the subsequent click cycloaddition step, differently substituted maleimides as model dipolarophiles were used to form the corresponding isoxazolidines as endo/exo isomers in high yields of up to > 90 % within 10 min. An one-pot strategy with in situ generation of C-(4-[^{18}F]fluorophenyl)-N-phenyl nitrone provided the desired ^{18}F-isoxazolidines only in moderate yields of 25 % and only after heating to 110

°C. Under optimized conditions, ^{18}F-isoxazolidines were obtained from fast ^{18}F-click [3+2]cycloadditions.

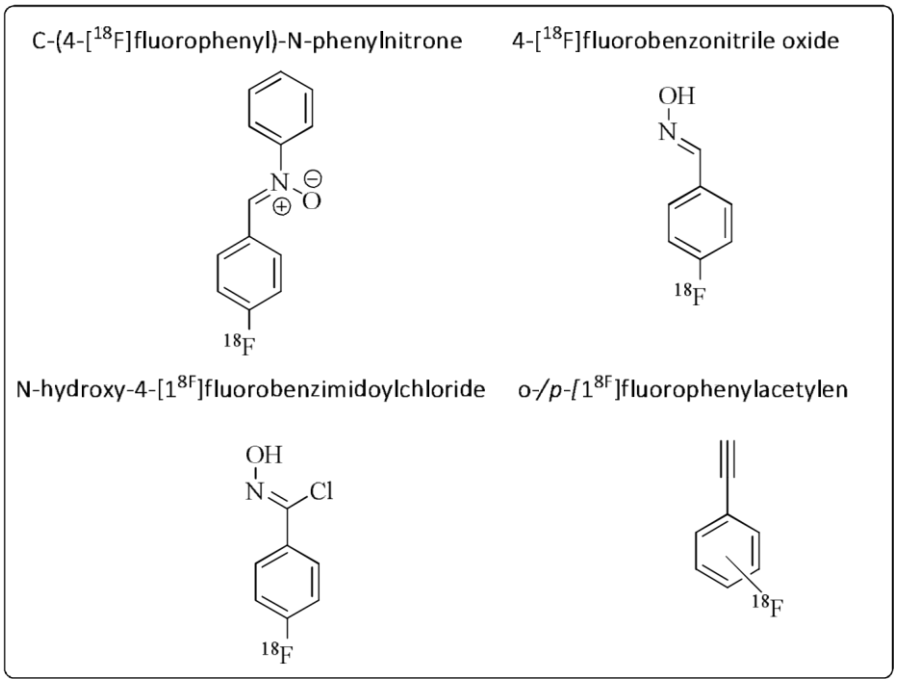

FIGURE 5: Lead structures of new ^{18}F-prosthetic groups applied for click ^{18}F-fluorination.

In further studies, the same group used 4-[^{18}F]fluorobenzonitrile oxide instead of C-(4[^{18}F]fluorophenyl)-N-phenyl nitrone as 1,3-dipol for milder reaction conditions (Table 3). [20] 4[^{18}F]fluorobenzonitrile oxide was obtained in 92 % RCY within 10 min from the reaction of 4[^{18}F]fluorobenzaldehyde (RCY: 30 – 50 %, 50 min, [98]) with hydroxylamine and subsequent treatment with phenyl iodine bis(trifluoroacetate).

TABLE 3: New developments in ^{18}F-click [3+2]cycloadditions. Showing the 1,3-dipolar ^{18}F-prosthetic groups, reaction type and conditions. FB-CHO = 4-fluorobenzaldehyde; CCA = click cycloaddition, PHA = *N*-phenylhydroxylamine; AscONa = sodium ascorbate'; BSA = bovine serum albumin; n.d. = no data

^{18}F-prosthetic group	steps/ reaction time	RCY	reacting agent	reaction type/ catalytic system	overall reaction time (CCA)	RCY CCA	lit.
C-(4-[^{18}F]fluorophenyl)-Nphenylnitrone	2 steps / 20 min, (labeling of [^{18}F]FB-CHO: 1 step, 50 min)	22 – 37 %[1] ([^{18}F]FB-CHO: 30-50 %) (^{18}F-nitrone: 74 %)	various maleimides	1,3-dipolar [3+2]cycloaddition, no catalyst	80 min (10 min)	87 – 91 %	[19]
4-[^{18}F]fluoro-benzonitrile oxide	3 steps / 20 min (labeling of [^{18}F]FB-CHO: 30-50 %)	28 – 46 %[1] (^{18}F-nitro: 74 %)	various dipolarophiles	1,3-dipolar [3+2]cycloaddition, no catalyst	80 min (10 min)	36 – 99 %	[20]

	[^{18}F]FB-CHO: 1 step, 50 min)	92 %)	cyclononyne-indomethazins (COX-2 inhibitor)			81 %	
			maleimideindomethazins (COX-2 inhibitor)			55 %	
			propyneindomethazins (COX-2 inhibitor)	35 %			
N-hydroxy-4[^{18}F]fluoroben z-imidoyl	4 steps / 20 min (labeling of [^{18}F]FB-	27 – 45 %[1] ([^{18}F]FB-CHO: 30-50%) (^{18}F-nitro oxide:	cyclononyne-ɴAla-Phe-OMe (dipeptide)	%[2] (10 min)	85 min	88	
				chloride norbornene-ɴ-Ala-	CHO: 1 step,	$^{92}_{18}$%)	82 %[2]
		99%)	(dipeptide)	50 min) benzimidoyl Cl: (	F-	Phe-OMe	
C-(4-[^{18}F]fluorophenyl)-Nphenylnitrone	2 steps / 20 min, (labeling of [^{18}F]FB-CHO: 1 step, 50 min)	22 – 37 %[1] ([^{18}F]FB-CHO: 30-50%) (^{18}F-nitrone: 74%)	terminal alkynes methyl propiolate	*radio*-Kinugasa, $CuSO_4$,AscONa (*L*-histidine)	80 min (10 min)	89 % (*trans/cis* = 2:3)	[21]
			terminal alkyne propargyl alcohol	*radio*-Kinugasa, CuI (Cu^I-stabilizing ligands or pyridine)	100 min (30 min)	82 % (*trans/cis* = 1:5) 60 % (*trans/cis* = 1:5)	
			terminal alkyne 1-propargyl uracyl (nucleobase = 4:1) chimera)			65 % (*trans/cis*	
			propiolyl-ɴ-Ala-Phe-OMe ,AscONa	*radio*-Kinugasa, $CuSO_4$ (10 min)	80 min (dipeptide)	(*L*-histidine) = 1:3) 85 %	
			propiolated protein (BSA)			32 %	
o- / *p*- phenyl acetylene	n.d.	n.d.	3,6-dihydro-2*H*- oxide	*radio*-Kinugasa, CuI (10 min)	52 %	[^{18}F]fluoro- 1,4-oxazine-4- (1,10-phenanthroline)	(*ortho*) 41 % (*para*)

[1] calculated as sum from all steps. [2] best RCY, obtained only with high precursor amounts.

After the click [3+2]cycloaddition to various ^{18}F-labeled model 2-isoxazolines and isoxazoles was successfully tested, the novel method was applied to three different COX-2 inhibitors (indomethacin conjugates) carrying dipolarophilic moieties of cyclononyne, maleimide and propyne. The resulting products were obtained in moderate to excellent RCY of 81 %, 55 % and 35 %, respectively. Noteworthy, that for the propyne derivative the milder oxidant [bis(acetoxy)iodo]benzene was used to avoid decomposition. Finally, the method was successfully adapted for ^{18}F-labeling of two model

dipeptide-conjugates, cyclononyne- and norbornene-N-Ala-Phe-OMe. However, the original cycloaddition using 4-[^{18}F]fluorobenzonitrile oxide did only provide traces of the desired products. Consequently, 4-[^{18}F]fluorobenzonitrile oxide was further treated with chloramine T (CAT) in situ forming the more stable building block N-hydroxy-4-[^{18}F]fluorobenzimidoyl chloride. The use of high precursor (peptides) amounts, the latter enabled excellent RCY of the ^{18}F-labeled dipeptides of up to 88 % within 10 min at room temperature [20]. Under optimized conditions low precursor amounts of 5 nmol (cyclononyne) and 50 nmol (norbornene-N-Ala-Phe-OMe) still allowed RCY of 56 % and 47 %, respectively.

In a very recent report, Zlatopolskiy and co-workers applied their ^{18}F-labeled nitrone, C-(4[^{18}F]fluorophenyl)-N-phenyl nitrone, for the first formation of ^{18}F-labeled N-lactames via the CuIcatalyzed Kinugasa reaction (Table 3). [21] The optimized reactions went smooth under very mild conditions to give the ^{18}F-labeled model N-lactames in high RCY and various isomeric mixtures of the trans- and cis-product. In dependency on the reactivity of the terminal alkynes, the reaction parameters needed (individual) optimization regarding catalyst system, solvent, temperature and CuIstabilizing ligands. As a biologically relevant molecule the ^{18}F-labeled nucleobase chimera was synthesized as potential PET-imaging agent for bacterial infections.

Moreover, the dipeptide N-Ala-Phe-OMe was propiolated and used in this radio-Kinugasa reaction to give excellent RCY of 85 % of the ^{18}F-labeled dipeptide under very mild conditions (aqueous solution, room temperature). [21] Similarly, this new method was successfully transferred to the ^{18}F-labeling of proteins. Bovine serum albumin (BSA) was conjugated with 3-propiolamidopropyl chloroformate. This propiolated BSA was successfully radiolabeled with fluorine-18 in the radio-Kinugasa reaction.

Conclusions

The field of click cycloadditions had and still has a major impact in ^{18}F-labeling chemistry. The very mild reaction conditions mostly applicable and the excellent efficiency of all types of these reactions are particularly suitable for ^{18}F-labeling. Especially, complex and sensitive biomolecules benefit from this methodology. No protection group chemistry is needed and the ^{18}F-click cycloaddition step provides the final radiotracer.

Besides several new ^{18}F-labeled radiotracers are available via click cycloadditions, the metal-free versions even enabled pre-targeting concepts by *in vivo* click. The latest development of a

radioKinugasa reaction towards the first ^{18}F-ɴ-lactames demonstrates the highly active field and the broad applicability of ^{18}F-click cycloadditions.

References

[1] M. E. Phelps, “Positron emission tomography provides molecular imaging of biological processes,” *Proceedings of the National Academie of Sciences U. S. A.*, vol. 97, no. 16, pp. 9226–33, 2000.

[2] J. S. Fowler and A. P. Wolf, "The Synthesis of Carbon-11, Fluorine-18 and Nitrogen-13 Labeled radiotracers for Biomedical Applications," Bnl—31222 de82 013799.

[3] H. H. Coenen, K. Franken, and P. Kling, “Direct Electrophilic Radiofluorination of Phenylalanine, Tyrosine and Dopa,” *Applied Radiation and Isotopes*, vol. 39, no. 12, pp. 1243–1250, 1988.

[4] C. Eckelman and J. Jo, “One-Step Synthesis of ^{18}F-labeled [^{18}F]-N-succinimidyl 4-(fluoromethyl)benzoate for Protein Labeling,” *Applied Radiation and Iostopes*, vol. 45, no. 12, pp. 1155-1163, 1994.

[5] R. Huisgen,“1.3-Dipolare Cycloadditionen,” *Angewandte Chemie*, no. 13, pp. 604-637, 1963.

[6] H. Schieferstein and T. L. Ross, “A Polar ^{18}F-Labeled Amino Acid Derivative for Click-Labeling of Biomolecules,” *European Journal of Organic Chemistry*, vol. 2013, no. 17, pp. 3546-50, 2014.

[7] V. Bouvet, M. Wuest, and F. Wuest, “Copper-free click chemistry with the short-lived positron emitter fluorine-18,” *Organic & Biomolecular Chemistry*, vol. 9, no. 21, pp. 7393–9, 2011.

[8] L. S. Campbell-Verduyn, L. Mirfeizi, A. K. Schoonen, R. a Dierckx, P. H. Elsinga, and B. L. Feringa, “Strain-promoted copper-free ‘click’ chemistry for ^{18}F-radiolabeling of bombesin,” *Angewandte Chemie International Edition*, vol. 50, no. 47, pp. 11117–20, 2011.

[9] S. Arumugam, J. Chin, R. Schirrmacher, V. V Popik, and A. P. Kostikov, “[^{18}F]azadibenzocyclooctyne ([^{18}F]ADIBO): a biocompatible radioactive labeling synthon for peptides using catalyst free [3+2] cycloaddition,” *Bioorganic & Medicinal Chemistry Letters*, vol. 21, no. 23, pp. 6987–91, 2011.

[10] R. D. Carpenter, S. H. Hausner, and J. L. Sutcliffe, “Copper-Free Click for PET: Rapid 1,3-Dipolar Cycloadditions with a Fluorine-18 Cyclooctyne,” *ACS Medicinal Chemistry Letters*, vol. 2, no. 12, pp. 885–889, 2011.

[11] K. Sachin, V. H. Jadhav, E.-M. Kim, H. L. Kim, S. B. Lee, H.-J. Jeong, S. T. Lim, M.-H. Sohn, and D. W. Kim, “F-18-labeling protocol of peptides based on chemically orthogonal strain-promoted cycloaddition under physiologically friendly reaction conditions,” *Bioconjugate Chemistry*, vol. 23, no. 8, pp. 1680–6, 2012.

[12] H. L. Evans, R. L. Slade, L. Carroll, G. Smith, Q.-D. Nguyen, L. Iddon, N. Kamaly, H. Stöckmann, F. J. Leeper, E. O. Aboagye, and A. C. Spivey, “Copper-free click-a promising tool for pre-targeted PET imaging,” *Chemical Communications*, vol. 48, no. 7, pp. 991–3, 2012.

[13] S. H. Hausner, R. D. Carpenter, N. Bauer, and J. L. Sutcliffe, “Evaluation of an integrin ɲ|ɴ6specific peptide labeled with [^{18}F]fluorine by copper-free, strain-promoted click chemistry,” *Nuclear Medicine and Biolology*, vol. 40, no. 2, pp. 233–9, 2013.

[14] Z. Li, H. Cai, M. Hassink, M. L. Blackman, R. C. D. Brown, P. S. Conti, and J. M. Fox, “Tetrazinetrans-cyclooctene ligation for the rapid construction of 18F-labeled probes,” *Chemical Communications*, vol. 46, no. 42, pp. 8043–5, 2010.

[15] R. Selvaraj, S. Liu, M. Hassink, C.-W. Huang, L.-P. Yap, R. Park, J. M. Fox, Z. Li, and P. S. Conti, “Tetrazine-trans-cyclooctene ligation for the rapid construction of integrin ɲ|ɴJ targeted PET tracer based on a cyclic RGD peptide,” *Bioorganic & Medicinal Chemistry Letters*, vol. 21, no. 17, pp. 5011–4, 2011.

[16] E. J. Keliher, T. Reiner, G. M. Thurber, R. Upadhyay, and R. Weissleder, “Efficient 18F-Labeling of Synthetic Exendin-4 Analogues for Imaging Beta Cells,” *ChemistryOpen*, vol. 1, no. 4, pp. 177–183, 2012.

[17] N. Devaraj, “Advancing Tetrazine Bioorthogonal Reactions through the Development of New Synthetic Tools,” *Synlett*, vol. 23, no. 15, pp. 2147–2152, 2012.

[18] J. C. Knight, S. Richter, M. Wuest, J. D. Way, and F. Wuest, “Synthesis and evaluation of an ^{18}Flabelled norbornene derivative for copper-free click chemistry reactions,” *Organic & Biomolecular Chemistry*, vol. 11, no. 23, pp. 3817–25, 2013.

[19] B. D. Zlatopolskiy, R. Kandler, F. M. Mottaghy, and B. Neumaier, “C-(4-[^{18}F]fluorophenyl)-Nphenyl nitrone: A novel ^{18}F-labeled building block for metal free [3+2]cycloaddition,” *Applied Radiation and Isotopes*, vol. 70, no. 1, pp. 184–92, 2012.

[20] B. D. Zlatopolskiy, R. Kandler, D. Kobus, F. M. Mottaghy, and B. Neumaier, “Beyond azidealkyne click reaction: easy access to ^{18}F-labelled compounds via nitrile oxide cycloadditions,” *Chemical Communications*, vol. 48, no. 57, pp. 7134–6, 2012.

[21] B. D. Zlatopolskiy, P. Krapf, R. Richarz, H. Frauendorf, F. M. Mottaghy, and B. Neumaier, “Synthesis of 18F-Labelled ɴ-Lactams by Using the Kinugasa Reaction,” *Chemistry - A European Journal*, vol.20, pp. 4697-4703, 2014.

[22] V. V Rostovtsev, L. G. Green, V. V Fokin, and K. B. Sharpless, “A Stepwise Huisgen Cycloaddition Process□: Copper(I) -Catalyzed Regioselective "Ligation" of Azides and Terminal Alkynes,”*Angewandte Chemie*, vol.114, no. 14, pp. 2708–2711, 2002.

[23] C. W. Tornøe, C. Christensen, and M. Meldal, “Peptidotriazoles on Solid Phase□: [1 , 2 , 3] Triazoles by Regiospecific Copper(I)-Catalyzed 1 , 3-Dipolar Cycloadditions of Terminal Alkynes to Azides,” *Journal of Organic Chemistry*, no. I, pp. 3057–3064, 2002.

[24] M. Gil, M. Arévalo, and Ó. López, “Click Chemistry - What’s in a Name? Triazole Synthesis and Beyond,” *Synthesis*, vol. 2007, no. 11, pp. 1589–1620, 2007.

[25] K. D. Hänni and D. a Leigh, “The application of CuAAC ‘click’ chemistry to catenane and rotaxane synthesis.,” *Chemical Society Reviews*, vol. 39, no. 4, pp. 1240–51, 2010.

[26] Y. Hua and A. H. Flood, “Click chemistry generates privileged CH hydrogen-bonding triazoles: the latest addition to anion supramolecular chemistry,” *Chemical Society Reviews*, vol. 39, no. 4, p. 1262, 2010.

[27] C. O. Kappe and E. Van der Eycken, “Click chemistry under non-classical reaction conditions,” *Chemical Society Reviews*, vol. 39, no. 4, pp. 1280–90, 2010.

[28] J. E. Hein and V. V Fokin, “Copper-catalyzed azide-alkyne cycloaddition (CuAAC) and beyond: new reactivity of copper(I) acetylides,” *Chemical Society Reviews*, vol. 39, no. 4, pp. 1302–15, 2010.

[29] S. K. Mamidyala and M. G. Finn, “In situ click chemistry: probing the binding landscapes of biological molecules,” *Chemical Society Reviews*, vol. 39, no. 4, pp. 1252–61, 2010.

[30] R. a. Decréau, J. P. Collman, and A. Hosseini, “Electrochemical applications. How click chemistry brought biomimetic models to the next level: electrocatalysis under controlled rate of electron transfer,” *Chemical Society Reviews*, vol. 39, no. 4, p. 1291, 2010.

[31] A. H. El-Sagheer and T. Brown, “Click chemistry with DNA,” *Chemical Society Reviews*, vol. 39, no. 4, pp. 1388–405, 2010.

[32] W. H. Binder and R. Sachsenhofer, “‘Click Chemistry in Polymer and Materials Science,” *Macromolecular Rapid Communications*, vol. 28, no. 1, pp. 15–54, 2007.

[33] P. L. Golas and K. Matyjaszewski, “Marrying click chemistry with polymerization: expanding the scope of polymeric materials,” *Chemical Society Reviews*, vol. 39, no. 4, pp. 1338–54, 2010.

[34] M. Pretze, D. Pietzsch, and C. Mamat, “Recent trends in bioorthogonal click-radiolabeling reactions using fluorine-18,” *Molecules*, vol. 18, no. 7, pp. 8618–65, 2013.

[35] R. Schirrmacher, C. Wängler, and E. Schirrmacher, “Recent Developments and Trends in Applications ^{18}F-Radiochemistry□: Syntheses and Applications,” *Mini-Reviews in Organic Chemistry*, vol.4, no.4, pp. 317–329, 2007.

[36] M. Glaser and E. G. Robins, “‘Click labelling’ in PET radiochemistry,” *Journal of Labelled Compounds and Radiopharmaceuticals*, vol. 52, no. 10, pp. 407–414, 2009.

[37] T. L. Ross, "The Click Chemistry Approach Applied to Fluorine-18", *Current Radiopharmaceuticals*, vol.3, pp.202-223, 2010

[38] A. Michael, “Über die Einwirkung von Diazobenzolimid auf Acetylendicarbonsäuremethylester”, *Advanced Synthesis &* Catalysis, vol. 48, no. 1, pp. 94–95, 1893.

[39] J. Marik and J. L. Sutcliffe, “Click for PET: rapid preparation of [^{18}F]fluoropeptides using CuI catalyzed 1,3-dipolar cycloaddition,” *Tetrahedron Letters*, vol. 47, no. 37, pp. 6681–6684, 2006.

[40] T. L. Ross, M. Honer, P. Y. H. Lam, T. L. Mindt, V. Groehn, R. Schibli, P. A. Schubiger, and S. M. Ametamey, “Fluorine-18 click radiosynthesis and preclinical evaluation of a new ^{18}F-labeled folic acid derivative,” *Bioconjugate Chemistry*, vol. 19, no. 12, pp. 2462–2470, 2008.

[41] D. H. Kim, Y. S. Choe, K.-H. Jung, K.-H. Lee, J. Y. Choi, Y. Choi, and B.-T. Kim, “A ^{18}F-labeled glucose analog: synthesis using a click labeling method and in vitro evaluation,” *Archives of Pharmacal Research*, vol. 31, no. 5, pp. 587–593, 2008.

[42] D. H. Kim, Y. S. Choe, and B.-T. Kim, “Evaluation of 4-[^{18}F]fluoro-1-butyne as a radiolabeled synthon for click chemistry with azido compounds.,” *Applied Radiation and Isotopes*, vol. 68, no. 2, pp. 329–33, 2010.

[43] M. Glaser and A. Erik, “‘Click Labeling’ with 2- [^{18}F] Fluoroethylazide for Positron Emission Tomography,” *Bioconjugate Chemistry*, vol. 18, pp. 989–993, 2007.

[44] U. Ackermann, G. O’Keefe, S.-T. Lee, a. Rigopoulos, G. Cartwright, J. I. Sachinidis, a. M. Scott, and H. J. Tochon-Danguy, “Synthesis of a [^{18}F]fluoroethyltriazolylthymidine radiotracer from [18F]2-fluoroethyl azide and 5-ethynyl-2□-deoxyuridine,” *Journal of Labelled Compounds and Radiopharmaceuticals*, vol. 54, no. 5, pp. 260–266, 2011.

[45] E. Laurens, S. D. Yeoh, A. Rigopoulos, D. Cao, G. a Cartwright, G. J. O’Keefe, H. J. TochonDanguy, J. M. White, A. M. Scott, and U. Ackermann, “Radiolabelling and evaluation of novel haloethylsulfoxides as PET imaging agents for tumor hypoxia,” *Nuclear Medicine and Biology*, vol. 39, no. 6, pp. 871–82, 2012.

[46] M. Glaser, J. Goggi, G. Smith, M. Morrison, S. K. Luthra, E. Robins, and E. O. Aboagye, “Improved radiosynthesis of the apoptosis marker ^{18}F-ICMT11 including biological evaluation,” *Bioorganic & Medicinal Chemistry Letters*, vol. 21, no. 23, pp. 6945–9, 2011.

[47] L. Iddon, J. Leyton, B. Indrevoll, M. Glaser, E. G. Robins, A. J. T. George, A. Cuthbertson, S. K. Luthra, and E. O. Aboagye, “Synthesis and in vitro evaluation of [^{18}F]fluoroethyl triazole

labelled [Tyr3]octreotate analogues using click chemistry," *Bioorganic & Medicinal Chemistry Letters*, vol. 21, no. 10, pp. 3122–7, 2011.

[48] E. Galante, B. W. Schoultz, M. Koepp, and E. Arstad, "Chelator-accelerated one-pot 'click' labeling of small molecule tracers with 2-[^{18}F]fluoroethyl azide," *Molecules*, vol. 18, no. 5, pp. 5335–47, 2013.

[49] G. Smith, R. Sala, L. Carroll, K. Behan, M. Glaser, E. Robins, Q.-D. Nguyen, and E. O. Aboagye, "Synthesis and evaluation of nucleoside radiotracers for imaging proliferation," *Nuclear Medicine and Biology*, vol. 39, no. 5, pp. 652–65, 2012.

[50] M. Glaser, M. Solbakken, D. R. Turton, R. Pettitt, J. Barnett, J. Arukwe, H. Karlsen, A. Cuthbertson, S. K. Luthra, and E. Arstad, "Methods for ^{18}F-labeling of RGD peptides: comparison of aminooxy [^{18}F]fluorobenzaldehyde condensation with 'click labeling' using 2[^{18}F]fluoroethylazide, and S-alkylation with [^{18}F]fluoropropanethiol," *Amino Acids*, vol. 37, no. 4, pp. 717–24, 2009.

[51] J. Li, L. Shi, L. Jia, D. Jiang, W. Zhou, W. Hu, Y. Qi, and L. Zhang, "Radiolabeling of RGD peptide and preliminary biological evaluation in mice bearing U87MG tumors," *Bioorganic & Medicinal Chemistry*, vol. 20, no. 12, pp. 3850–5, 2012.

[52] R. Bejot, J. Goggi, S. S. Moonshi, and E. G. Robins, "A practical synthesis of [^{18}F]FtRGD: an angiogenesis biomarker for PET," *Journal of Labelled Compounds and Radiopharmaceuticals*, vol. 56, no. 2, pp. 42–9, 2013.

[53] U. Sirion, H. J. Kim, J. H. Lee, J. W. Seo, B. S. Lee, S. J. Lee, S. J. Oh, and D. Y. Chi, "An efficient F18 labeling method for PET study: Huisgen 1,3-dipolar cycloaddition of bioactive substances and F-18-labeled compounds," *Tetrahedron Letters*, vol. 48, no. 23, pp. 3953–3957, 2007.

[54] Z.-B. Li, Z. Wu, K. Chen, F. T. Chin, and X. Chen, "Click chemistry for ^{18}F-labeling of RGD peptides and microPET imaging of tumor integrin alphavbeta3 expression," *Bioconjugate Chemistry*, vol. 18, no. 6, pp. 1987–94, 2007.

[55] H. S. Gill and J. Marik, "Preparation of ^{18}F-labeled peptides using the copper(I)-catalyzed azidealkyne 1,3-dipolar cycloaddition.," *Nature Protocols*, vol. 6, no. 11, pp. 1718–25, 2011.

[56] N. K. Devaraj, E. J. Keliher, G. M. Thurber, M. Nahrendorf, and R. Weissleder, "^{18}F-labeled nanoparticles for in vivo PET-CT imaging," *Bioconjugate Chemistry*, vol. 20, no. 2, pp. 397–401, 2009.

[57] C.-M. Lee, H.-J. Jeong, D. W. Kim, M.-H. Sohn, and S. T. Lim, "The effect of fluorination of zinc oxide nanoparticles on evaluation of their biodistribution after oral administration," *Nanotechnology*, vol. 23, no. 20, p. 205102, 2012.

[58] H. Schieferstein, T. Betzel, C. R. Fischer, and T. L. Ross, "^{18}F-click labeling and preclinical evaluation of a new ^{18}F-folate for PET imaging," *European Journal of Nuclear Medicine and Molecular* Imaging, vol. 68, no.3, pp. 1–10, 2013.

[59] T. Rameda, R. Bergmann, and F. Wüst, "Synthesis of ^{18}F-labeled Neurotensin(8-13) via CopperMediated 1,3-Dipolar [3+2]Cycloaddition Reaction," *Letters in Drug Design & Discovery*, vol. 4, pp. 279–285, 2007.

[60] T. Ramenda, T. Kniess, R. Bergmann, J. Steinbach, and F. Wuest, "Radiolabelling of proteins with fluorine-18 via click chemistry," *Chemical Communications*, no. 48, pp. 7521–3, 2009.

[61] T. Ramenda, J. Steinbach, and F. Wuest, "4-[^{18}F]Fluoro-N-methyl-N-(propyl-2-yn-1yl)benzenesulfonamide ([^{18}F]F-SA): a versatile building block for labeling of peptides, proteins and oligonucleotides with fluorine-18 via Cu(I)-mediated click chemistry," *Amino Acids*, vol. 44, no. 4, pp. 1167–80, 2013.

[62] J. a. H. Inkster, B. Guérin, T. J. Ruth, and M. J. Adam, "Radiosynthesis and bioconjugation of [^{18}F]FPy5yne, a prosthetic group for the ^{18}F-labeling of bioactive peptides," *Journal of Labelled Compounds and Radiopharmaceuticals*, vol. 51, no. 14, pp. 444–452, 2008.

[63] A. C. Valdivia, M. Estrada, T. Hadizad, D. J. Stewart, R. S. Beanlands, and J. N. DaSilva, "A fast, simple, and reproducible automated synthesis of [^{18}F]FPyKYNE-c(RGDyK) for $\alpha_v\beta_3$ receptor positron emission tomography imaging," *Journal of Labelled Compounds and Radiopharmaceuticals*, vol. 55, no. 2, pp. 57–60, 2012.

[64] P. Daumar, C. a Wanger-Baumann, N. Pillarsetty, L. Fabrizio, S. D. Carlin, O. a Andreev, Y. K. Reshetnyak, and J. S. Lewis, "Efficient ^{18}F-labeling of large 37-amino-acid pHLIP peptide analogues and their biological evaluation.," *Bioconjugate Chemistry*, vol. 23, no. 8, pp. 1557–66, 2012.

[65] G. Vaidyanathan, B. J. White, and M. R. Zalutsky, "Propargyl 4-[^{18}F]fluorobenzoate: A Putatively More Stable Prosthetic group for the Fluorine-18 Labeling of Biomolecules via Click Chemistry," *Current Radiopharmaceuticals*, vol. 2, no. 1, pp. 63–74, 2009.

[66] Y. Li, Y. Liu, L. Zhang, and Y. Xu, "One-step radiosynthesis of 4-[^{18}F]flouro-3-nitro-N-2-propyn-1yl-benzamide ([^{18}F]FNPB): a new stable aromatic porosthetic group for efficient labeling of peptides with fluorine-18," *Journal of Labelled Compounds and Radiopharmaceuticals*, vol. 55, no. 6, pp. 229–234, 2012.

[67] D. Thonon, C. Kech, J. Paris, C. Lemaire, and A. Luxen, "New strategy for the preparation of clickable peptides and labeling with 1-(azidomethyl)-4-[^{18}F]-fluorobenzene for PET," *Bioconjugate Chemistry*, vol. 20, no. 4, pp. 817–23, 2009.

[68] F. Mercier, J. Paris, G. Kaisin, D. Thonon, J. Flagothier, N. Teller, C. Lemaire, and A. Luxen, "General method for labeling siRNA by click chemistry with fluorine-18 for the purpose of PET imaging," *Bioconjugate Chemistry*, vol. 22, no. 1, pp. 108–14, 2011.

[69] J. Flagothier, G. Kaisin, F. Mercier, D. Thonon, N. Teller, J. Wouters, and A. Luxen, "Synthesis of two new alkyne-bearing linkers used for the preparation of siRNA for labeling by click chemistry with fluorine-18," *Applied Radiation and Isotopes*, vol. 70, no. 8, pp. 1549–57, 2012.

[70] J.-H. Chun and V. W. Pike, "Single-Step Radiosynthesis of '^{18}F-Labeled Click Synthons' from Azide-Functionalized Diaryliodonium Salts," *European Journal of Organic Chemistry*, vol. 2012, no. 24, pp. 4541–4547, 2012.

[71] S. Maschauer and O. Prante, "A series of 2-O-trifluoromethylsulfonyl-D-mannopyranosides as precursors for concomitant ^{18}F-labeling and glycosylation by click chemistry," *Carbohydrate Research*, vol. 344, no. 6, pp. 753–61, 2009.

[72] S. Maschauer, J. Einsiedel, R. Haubner, C. Hocke, M. Ocker, H. Hübner, T. Kuwert, P. Gmeiner, and O. Prante, "Labeling and glycosylation of peptides using click chemistry: a general approach to 18F-glycopeptides as effective imaging probes for positron emission tomography," *Angewandte Chemie International Edition*, vol. 49, no. 5, pp. 976–9, 2010.

[73] S. Maschauer, R. Haubner, T. Kuwert, and O. Prante, "^{18}F-Glyco-RGD Peptides for PET Imaging of Integrin Expression: Efficient Radiosynthesis by Click Chemistry and Modulation of Biodistribution by Glycosylation," *Molecular Pharmacology*, vol. 11, no. 2, pp. 505-15, 2013.

[74] C. R. Fischer, C. Müller, J. Reber, A. Müller, S. D. Krämer, S. M. Ametamey, and R. Schibli, "[^{18}F]fluoro-deoxy-glucose folate: a novel PET radiotracer with improved in vivo properties for folate receptor targeting," *Bioconjugate Chemistry*, vol. 23, no. 4, pp. 805–13, 2012.

[75] Y. Li, J. Guo, S. Tang, L. Lang, X. Chen, and D. M. Perrin, "One-step and one-pot-two-step radiosynthesis of functional imaging," *Journal of Labelled Compounds and Radiopharmaceuticals*, vol. 3, no. 1, pp. 44–56, 2013.

[76] Y. Li, Z. Liu, C. W. Harwig, M. Pourghiasian, J. Lau, K. Lin, P. Schaffer, F. Benard, and D. M. Perrin, "^{18}F-click labeling of a bombesin antagonist with an expressing the GRP-receptor," *American Journal of Nuclear Medicine and Molecular Imaging*, vol. 3, no. 1, pp. 57–70, 2013.

[77] Z. Liu, Y. Li, J. Lozada, P. Schaffer, M. J. Adam, T. J. Ruth, and D. M. Perrin, "Stoichiometric leverage: rapid ^{18}F-aryltrifluoroborate radiosynthesis at high specific activity for click conjugation," *Angewandte Chemie International Edition*, vol. 52, no. 8, pp. 2303–7, 2013.

[78] M. Pretze and C. Mamat, "Automated preparation of [^{18}F]AFP and [^{18}F]BFP: Two novel bifunctional ^{18}F-labeling building blocks for Huisgen-click," *Journal of Fluorine Chemistry*, vol. 150, pp. 25–35, 2013.

[79] S. H. Hausner, J. Marik, M. K. J. Gagnon, and J. L. Sutcliffe, "In vivo positron emission tomography (PET) imaging with an alphavbeta6 specific peptide radiolabeled using ^{18}F-'click' chemistry: evaluation and comparison with the corresponding 4-[^{18}F]fluorobenzoyl- and 2[^{18}F]fluoropropionyl-peptides," *Journal of Medicinal Chemistry*, vol. 51, no. 19, pp. 5901–4, 2008.

[80] D. Kobus, Y. Giesen, R. Ullrich, H. Backes, and B. Neumaier, "A fully automated two-step synthesis of an ^{18}F-labelled tyrosine kinase inhibitor for EGFR kinase activity imaging in tumors," *Applied Radiation and Isotopes*, vol. 67, no. 11, pp. 1977–84, 2009.

[81] G. Smith, M. Glaser, M. Perumal, Q. Nguyen, B. Shan, E. Årstad, and E. O. Aboagye, "Design , Synthesis , and Biological Characterization of a Caspase 3 / 7 Selective Isatin Labeled with 2-[^{18}F]fluoroethylazide," *Journal of Medicinal Chemistry*, no. Scheme 1, pp. 8057–8067, 2008.

[82] F. Pisaneschi, Q.-D. Nguyen, E. Shamsaei, M. Glaser, E. Robins, M. Kaliszczak, G. Smith, A. C. Spivey, and E. O. Aboagye, "Development of a new epidermal growth factor receptor positron emission tomography imaging agent based on the 3-cyanoquinoline core: synthesis and biological evaluation," *Bioorganic & Medicinal Chemistry*, vol. 18, no. 18, pp. 6634–45, 2010.

[83] R. Fortt, G. Smith, R. O. Awais, S. K. Luthra, and E. O. Aboagye, "Automated GMP synthesis of [^{18}F]ICMT-11 for in vivo imaging of caspase-3 activity," *Nuclear Medicine and Biology*, vol. 39, no. 7, pp. 1000–5, 2012.

[84] D. Zhou, W. Chu, C. S. Dence, R. H. Mach, and M. J. Welch, "Highly efficient click labeling using 2-[^{18}F]fluoroethyl azide and synthesis of an ^{18}F-N-hydroxysuccinimide ester as conjugation agent," *Nuclear Medicine and Biology*, vol. 39, no. 8, pp. 1175–81, 2012.

[85] R. Bejot, L. Carroll, K. Bhakoo, J. Declerck, and V. Gouverneur, "A fluorous and click approach for screening potential PET probes: Evaluation of potential hypoxia biomarkers," *Bioorganic & Medicinal Chemistry*, vol. 20, no. 1, pp. 324–9, 2012.

[86] K. K. S. Sai, C. Huang, L. Yuan, D. Zhou, D. Piwnica-Worms, J. R. Garbow, J. a Engelbach, R. H. Mach, K. M. Rich, and J. McConathy, "^{18}F-AFETP, ^{18}F-FET, and ^{18}F-FDG imaging of mouse DBT gliomas," *Journal of Nuclear Medicine*, vol. 54, no. 7, pp. 1120–6, 2013.

[87] A. Haslop, A. Gee, C. Plisson, and N. Long, "Fully automated radiosynthesis of [1-(2-[^{18} F]fluoroethyl),^{1}H[1,2,3]triazole 4-ethylene] triphenylphosphonium bromide as a potential positron emission tomography tracer for imaging apoptosis," *Journalof Labelled Compounds and Radiopharmaceuticals*, vol. 56, no. 6, pp. 313–6, 2013.

[88] L. Jia, Z. Cheng, L. Shi, J. Li, C. Wang, D. Jiang, W. Zhou, H. Meng, Y. Qi, D. Cheng, and L. Zhang, "Fluorine-18 labeling by click chemistry: multiple probes in one pot," *Applied Radiation and Isotopes*, vol. 75, pp. 64–70, 2013.

[89] O. Boutureira, F. D'Hooge, M. Fernández-González, G. J. L. Bernardes, M. Sánchez-Navarro, J. R. Koeppe, and B. G. Davis, "Fluoroglycoproteins: ready chemical site-selective incorporation of fluorosugars into proteins," *Chemical Communications*, vol. 46, no. 43, pp. 8142–4, 2010.

[90] S. Maschauer, K. Michel, P. Tripal, K. Büther, T. Kuwert, O. Schober, K. Kopka, B. Riemann, and O. Prante, "Synthesis and in vivo evaluation of an ^{18}F-labeled glycoconjugate of PD156707 for imaging ETA receptor expression in thyroid carcinoma by positron emission tomography," *Americam Journal of Nuclear Medicine and Molecular Imaging*, vol. 3, no. 5, pp. 425–36, 2013. [91] F. Pisaneschi, R. L. Slade, L. Iddon, G. P. C. George, Q.-D. Nguyen, A. C. Spivey, and E. O. Aboagye, "Synthesis of a new fluorine-18 glycosylated 'click' cyanoquinoline for the imaging of epidermal growth factor receptor," *Journal of Labelled Compounds and Radiopharmaceuticals*, vol. 57, no. 2, pp. 92–6, 2014.

[92] Z. Liu, Y. Li, J. Lozada, P. Schaffer, M. J. Adam, T. J. Ruth, and D. M. Perrin, "Stoichiometric Leverage: Rapid ^{18}F-Aryltrifluoroborate Radiosynthesis at High Specific Activity for Click Conjugation," *Angewandte Chemie*, vol. 125, no. 8, pp. 2359–2363, 2013.

[93] G. J. Brewer, "Copper toxicity in the general population," *Clinical Neurophysiology*, vol. 121, no. 4, pp. 459–60, 2010.

[94] P. Mäding, F. Füchtner, and F. Wüst, "Module-assisted synthesis of the bifunctional labelling agent N-succinimidyl 4-[^{18}F]fluorobenzoate ([^{18}F]SFB)," *Applied Radiation and Isotopes*, vol. 63, no. 3, pp. 329–32, 2005.

[95] M. M. Herth, V. L. Andersen, S. Lehel, J. Madsen, G. M. Knudsen, and J. L. Kristensen, "Development of a 11C-labeled tetrazine for rapid tetrazine-trans-cyclooctene ligation," *Chemical Communications*, vol. 49, no. 36, pp. 3805–7, 2013.

[96] N. K. Devaraj, G. M. Thurber, E. J. Keliher, B. Marinelli, and R. Weissleder, "Reactive polymer enables efficient in vivo bioorthogonal chemistry," *Proceedings of the National Academy of Sciences*, vol. 109, no. 13, 2012.

[97] M. Fani, X. Wang, G. Nicolas, C. Medina, I. Raynal, M. Port, and H. R. Maecke, "Development of new folate-based PET radiotracers: preclinical evaluation of ^{68}Ga-DOTA-folate conjugates," *European Journal of Nuclear Medicine and Molecular Imaging*, vol. 38, no. 1, pp. 108–19, 2011.

[98] M. S. Haka, M. R. Kilbourn, G. L. Leonard Watkins, and S. A. Toorongian, "Aryltrimethylammonium trifluoromethanesulfonates as precursors to aryl [^{18}F] fluorides: improved synthesis of [^{18}F] GBR-13119," *Journal of Labelled Compounds and Radiopharmaceuticals*, vol. 27, pp. 823–833, 1989.

[99] S. Maschauer, and O. Prante, "Sweetening Pharmaceutical Radiochemistry by ^{18}F-Fluoroglycosylation: A short Review", Biomed Research International, pp. 1-16, 2014

2. Aims and objectives

2. Aims and objectives

The most accurate and early diagnosis of tumors is essential for a promising approach to individualized therapy in cancer. Moreover, due to the lack of efficient treatment options for the widespread disease cancer, addressing certain cancer-specific structures for diagnosis and therapy is of outstanding importance. The positron emission tomography (PET) has emerged as a very powerful imaging tool for visualization of biochemical and physiological processes in the human body. Thus, PET can be used to translate novel imaging radiotracer from *bench to bedside* and to improve tumor diagnosis.

For the imaging of various tumor types a broad variety of targets can be addressed. Therefore, an appropriate radiolabeling method for a multitude of different individual targeting vectors needs to be available. The herein work presented should focuss on novel ^{18}F- and ^{68}Ga-radiolabeling methods for various target/targeting vector systems (e.g. melanocortin-1 receptor/peptides, fibroblast activation protein/microbodies, folate receptor/folates). Alongside the synthesis of novel radiolabeling precursors and the systematic evaluation and optimization of the radiolabeling reaction, the investigation of structure-affinity relationships in terms of preclinical studies are described.

The folate receptor (FR) is known as a well established oncological target for tumor imaging as well as targeted chemotherapy due to its (over)epression on various human carcinomas. Most of the ^{18}Flabeled folate derivatives for PET imaging suffer from either inefficient radiosyntheses or inappropriate *in vivo* characteristics. Copper-catalyzed cycloaddition (CuAAC) reactions using ^{18}Fprosthetic groups have found to be very suitable for the radiolabeling of folate derivatives due to biorthogonal and mild click conditions. For the application of [^{18}F]fluoro-click-folates in clinics, the complete removal of cyctotoxic copper after the click reaction might be a crucial challenge.

1. The aim of this work was to develop a copper-free labeling strategy for the radiolabeling of sensitive biomolecules with fluorine-18 for PET imaging. After optimization of the radiolabeling conditions for the novel dibenzocyclooctyne(DBCO)-based ^{18}F-prosthetic group, the general feasibility of this strain-promoted azide-alkyne cycloaddition (SPPAC) approach should be validated by click reactions with various biomolecule-azides. Because of the outstanding relevance of folate derivatives as tumor imaging radiotracers, [^{18}F]fluoro-DBCOfolate should be further evaluated *in vivo* concerning tumor uptake and abdominal background.

2. To further improve the pharmacokinetic profile of the folate derivative, a recently reported alanine-based ^{18}F-prosthetic group should also be used for radiolabeling. Moreover, both labeling strategies (CuAAC and SPAAC) should be compared in terms of reaction conditions, radiochemical yields, influence on the overall lipophilicity of the radiotracer and consequently its *in vivo* biodistribution and accumulation pattern.

3. According to the approach to use the well established tumor imaging radiotracer [^{18}F]fluorodeoxy-glucose ([^{18}F]FDG) as a prosthetic group, we aimed to create a 2in1 approach for the novel alanine-based prosthetic group [^{18}F]fluoro-alakyne. Since highly proliferating tumor cells show an increased protein synthesis rate, radiolabeled amino acids have been extensively investigated as tumor imaging tools. The *in vivo* behavior of [^{18}F]fluoro-alakyne should be evaluated via µPET imaging concerning tumor visibility and tumor-to-background contrast.

Monoclonal antibodies and proteins often show high tumor selectivity and specificity, but are very sensitive in biological systems and to chemical influences. To further improve the thermal and proteolytic stability of peptides, cysteine-knot microbodies have been developed within the last years. They mostly show very fast pharmacokinetics combined with biological, metabolical and chemical stability. These highly selective and cancer-specific molecules cannot only be used to localize tumors, but also for the selection of patients for a cancer therapy with specific ligands binding to the detected tumor associated proteins. Classical anti-cancer therapy normally suffers from poor selectivity and toxic side effects to healthy tissue. The conjugation of the toxin to specific ligands would not harm healthy cells and optimize the therapy results for the patient.

4. A second part of this work aimed at the development of an appropriate strategy for the radiolabeling of larger molecules such as microbodies with both fluorine-18 and gallium-68. Both, the use of different ^{18}F-prosthetic groups and the attachment of a chelator to the microbody followed by ^{68}Ga-labeling should be evaluated.

5. The most suitable radiolabeling method should then be applied to a novel microbody with specificity to fibroblast activation protein (FAP), which was identified and produced by the BioNTech group. Preclinical evaluation of the radiolabeled microbody will focuss on *in vitro* cell studies concerning internalization and specificity to huFAP-positive cells.

6. Multivalent radiotracers are thought to provide increased internalization due to enhanced retention of the radiotracer at the target site. Therefore, the effect of the formation of a microbody-tetramer on the internalization and specificity of the microbody should be investigated.

3. Results and discussion

3. Results and discussion

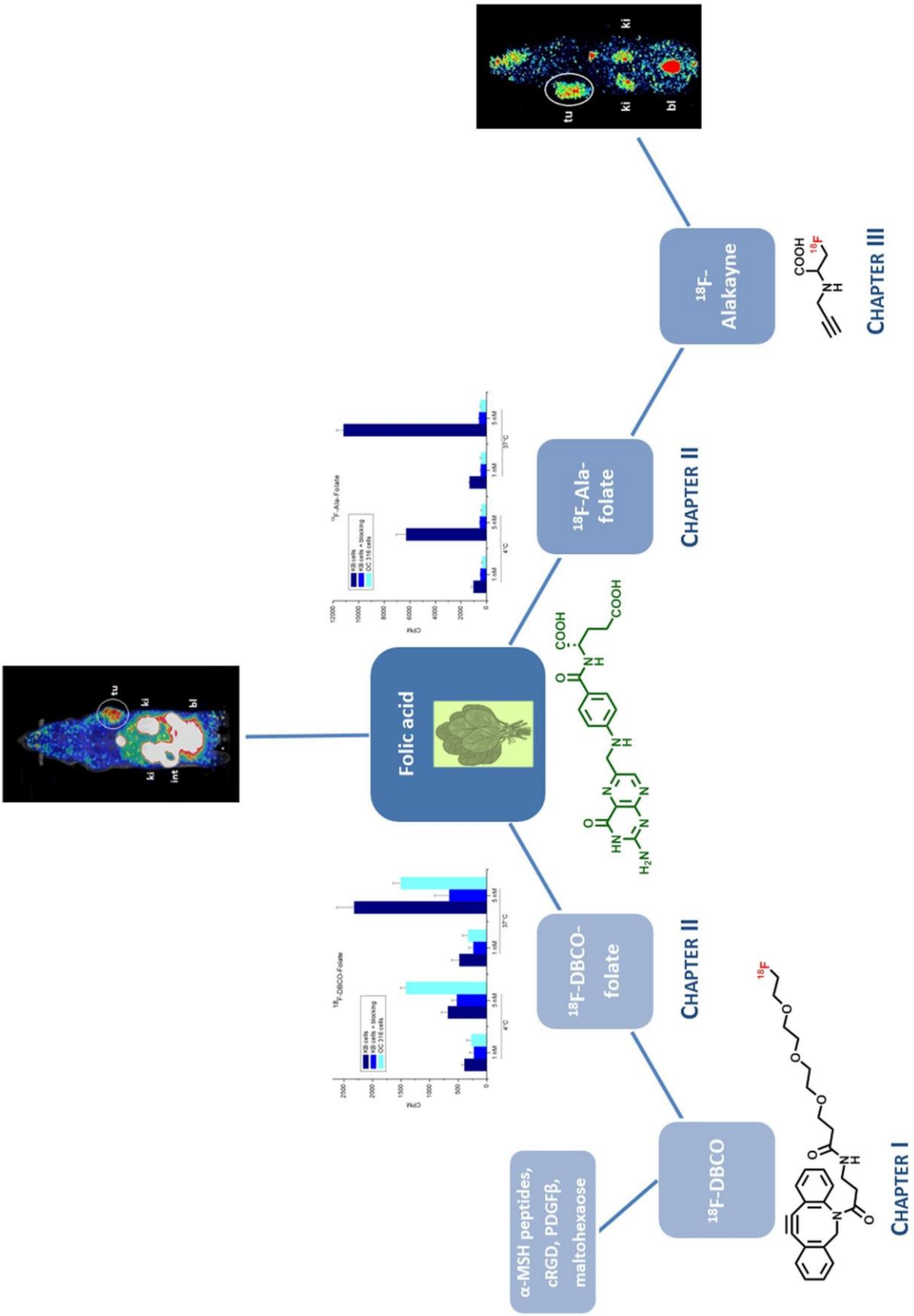

Figure 1: Illustration of the cumulated work with fluorine-18.

Figure 1 illustrates the different approaches for the radiolabeling of a folate derivative with fluorine-18 via two different ^{18}F-prosthetic groups for the imaging of FR-positive tumors using PET. CHAPTER I

contains the development and evaluation of a novel (aza)dibenzocyclooctyne(DBCO)-based ^{18}Fprosthetic group including exemplary copper-free click reactions with different biomolecule-azides (RGD, MSH-peptides, folic acid). Further *in vitro* and *in vivo* evaluation of the [^{18}F]fluoro-DBCO-folate using FR-positive KB cells and xenografts are part of CHAPTER II. To improve the *in vivo* behaviour of the folate derivative a recently published alanine-based prosthetic group ([^{18}F]fluoro-alakyne) was used for the radiolabeling. The results of the cell and animal µPET studies with this much more hydrophlic folate derivative can also been found in CHAPTER II. To create a 2in1 approach, the [^{18}F]fluoro-alakyne has also been investigated as a tumor imaging candidate itself. The results of the *in vitro* cell and *in vivo* small animal µPET studies can be found in CHAPTER III.

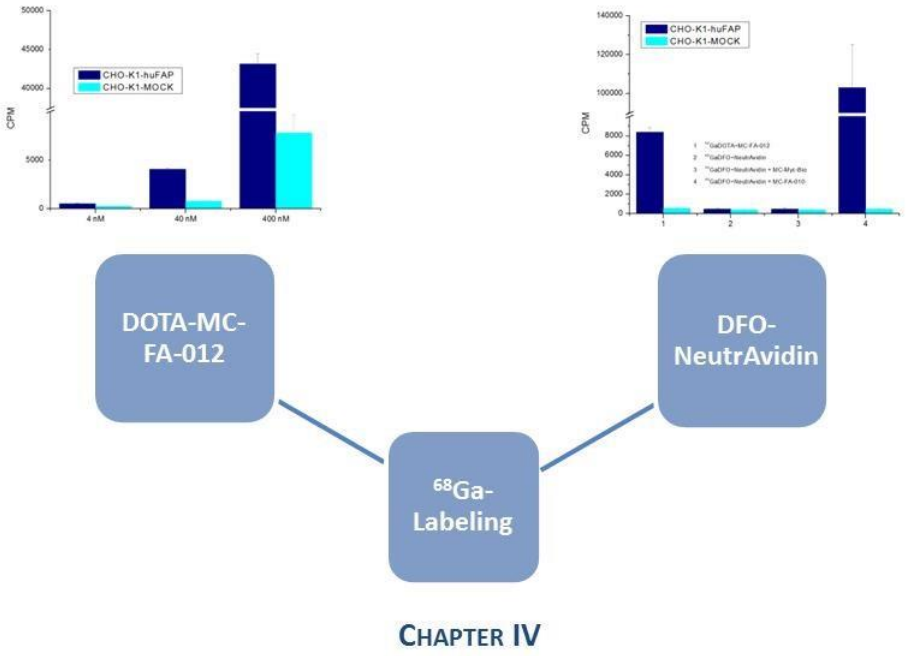

Figure 2: Illustration of the cumulated work with gallium-68.

CHAPTER IV summarizes the *in vitro* evaluation of a FAP-specific microbody labeled with gallium-68 (figure 2). Additionally the influence of the formation of a microbody-tetramer on the amount of internalized microbody was investigated (multivalency approach).

The following chapter comprises the major results and conclusions, which are based on the findings described in the *Publications and Ongoing studies*.

Fluorine-18 provides ideal nuclear physical characteristics for the application in positron emission tomography (PET). The challenge now consists in finding an appropriate ^{18}F-radiolabeling strategy especially for sensitive biomolecules. Direct ^{18}F-labeling requires very harsh conditions such as high

temperatures and strong bases and is therefore often not the method of choice for the radiofluorination of biomolecules. Consequently ^{18}F-prosthetic groups have been used instead for decades, because they can be attached under very mild conditions. Especially the copper-catalyzed variant of the Huisgen 1,3-dipolar cycloaddition enables the formation of a triazole from an azide and a terminal alkyne under very mild and biorthogonal conditions. One great disadvantage of this approach is the need of cytotoxic copper as a catalyst during radiosynthesis. This requires an extensive work-up guaranteeing a complete removal of copper for *in vivo* application.

The aim of this work was to develop and evaluate a copper-free labeling strategy based on (aza)dibenzocyclooctyne (DBCO) for the radiolabeling of biomolecules with fluorine-18. To reduce the lipophilicity of the prosthetic group a triethylene glycol spacer was introduced to the (aza)dibenzocyclooctyne as depicted in scheme 1. Both precursor molecules 1 and 2 were synthesized in moderate overall yields of 28 % and 56 % respectively over four steps.

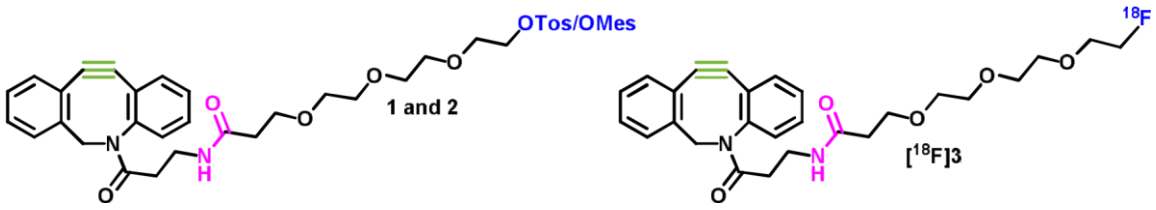

Scheme 1: Chemical structure of novel precursor molecules 1 (OTos) and 2 (OMes) and of the novel prosthetic group [^{18}F]fluoro-DBCO ([^{18}F]3).

The ^{18}F-radiolabeling reaction was screened and optimized using two different leaving groups, different bases and base amounts, reaction temperatures and precursor amounts. The highest radiochemical yields (ш 90 %) were achieved with the tosylated precursor 1 using tetraethylammonium bicarbonate in acetonitrile for 10 min at 100 °C (scheme 1). The most crucial part of the radiosynthesis was the evaluation of the appropriate base amount. If the amount was below 17 µmol no ^{18}F-labeling was observed. On the other hand, an increasing decomposition of the precursor molecule was observed by enhancing the base amount too much.

In the following, several molecules have been tested in copper-free click reactions with the novel ^{18}Fprosthetic group to test its viability. Very high yields were achieved for azide-functionalized RGD, a folate derivative, two ɲ-MSH derivatives (linear and cyclic), a PDGF-ɴ peptide and maltohexaose as depicted in figure 3.

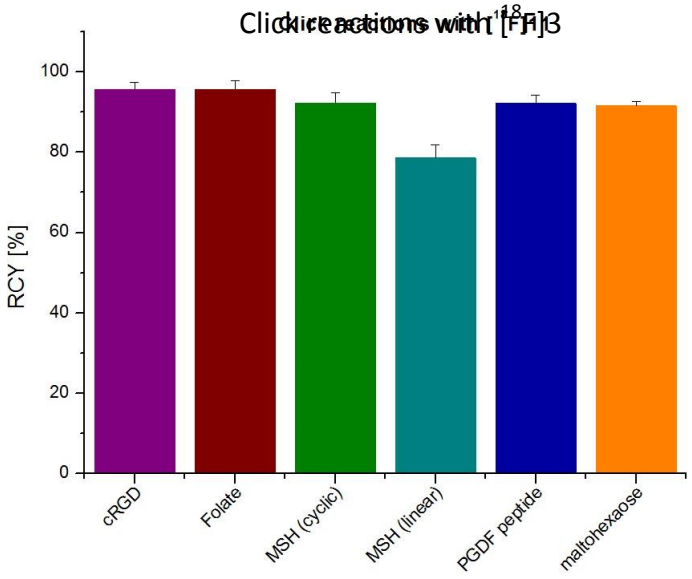

Figure 3: Radiolabeling of various azides with [^{18}F]3. RCY after 20 min displayed in a bar chart. Errors are given as standard deviation representing n = 3.

The MC1R is known to be overexpressed on malignant melanoma and therefore displays an ideal target for the early diagnosis of skin cancer. The ɲ-MSH (ɲ-melanocyte-stimulation hormone) shows affinities to the MC1R in the nanomolar range. Despite there are already a few ɲ-MSH derivatives radiolabeled with PET nuclides showing promising *in vivo* characteristics, there is still a high demand on developing especially cyclic peptides with high affinities to the MC1R. Cyclization of the peptides prevents proteolytic degradation and therefore enhances the tumor uptake and retention.

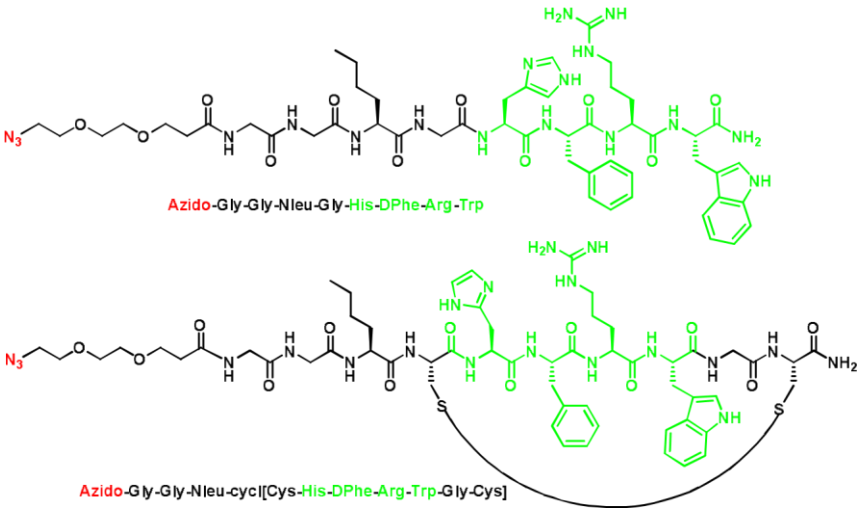

Scheme 2: Schematic illustration of a linear and a cyclic ɲ-MSH peptide with specificity to the MC1R.

The azido-functionalized ɲ-MSH peptides with specificities to the MC1R (melanocortin-1 receptor) shown in scheme 2 were synthesized using solid phase peptide synthesis. Higher RCYs were achieved for the cyclic peptide, which might be due to the better accessibility of the azide-function. The linear peptide can form super lattices in which the azide is located in the inside. To further increase the proteolytic and thermal stability an azide-functionalized microbody (MC-ME-030) with high affinities

to the MC1R was designed by the BIONTech group. Unfortunately, neither the conventional coppercatalyzed click cycloaddition ([^{18}F]fluoro-TEG-alkyne) nor the novel copper-free variant ([^{18}F]fluoroDBCO) resulted in satisfying RCY. Only with the [^{18}F]fluoro-DBCO a conversion was observed at all ;ч 20 %), but only with very high amounts of microbody (3 mg for each labeling reaction) and at increased reaction temperatures (70 °C). Based on these results, a derivatization of microbodies with a chelator followed by radiolabeling with gallium-68 will be preferred for all following studies (CHAPTER IV). However, the general feasibility of this novel copper-free ^{18}F-labeling strategy was furthermore proven by click reactions with maltohexaose and a PDGF-N peptide. Radiolabeled maltohexaose can be used to differentiate between bacterial infections and aseptic inflammations using PET. [^{68}Ga]GaDOTA-maltohexaose ([^{68}Ga]Ga-DMALTO) already showed specific uptake by cultured *E. coli.*, but only a low and unspecific uptake by macrophages. [1] In this study it was possible to distinguish between *E. coli* infection and sterile LPS-induced inflammation *in vivo*. We now applied the novel copper-free labeling strategy to a maltohexaose-azide to provide [^{18}F]fluoro-maltohexaose in high yields (ш 90 %) under mild conditions (40 °C, PBS buffer).

Based on the high potential of this novel DBCO-based ^{18}F-prosthetic group, further investigations to create an iodonium salt precursor were carried out. This “minimalistic approach” reduces the synthesis time dramatically, because no time consuming azeotropic drying is necessary. Furthermore the radiolabeling reaction can be performed in protic solvents and no additional bases are needed. [2, 3] The use of diaryliodonium salts enables the regioselective nucleophilic radiofluorination of arenes with n.c.a. [^{18}F]fluoride. Direct elution of [^{18}F]fluoride from the anion exchange resin is possible with alcoholic solution of these iodonium precursors.

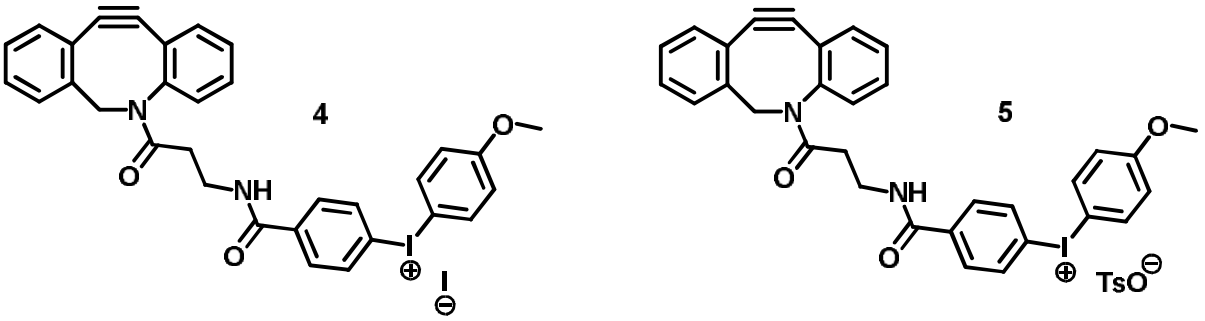

Scheme 3: Chemical structure of two novel DBCO-iodonium salt precursors 4 and 5.

First, the iodonium salt carrying a carboxylic acid function was synthesized and then coupled to the DBCO moiety via amide bond formation. Unfortunately, the overall yields were very low which might be due to the instability of the iodonium salt. [4] Especially the purification steps (precipitation of the product) turned out to be very challenging in terms of product loss. First radiolabeling reactions resulted in quantitative elution of [^{18}F]fluoride using 4 respectively 5 (scheme 3) in methanol, but only low RCY of around 20 % were achieved. Further evaluations concerning the use of different counter

ions and leaving groups as well as reaction temperatures and solvents did not result in better and reproducible radiochemical yields. [5] Therefore, this novel precursor strategy was found to be not superior over the well-established nucleophilic substitution of a tosyl group in this case.

To enable the formation of a multivalent radiotracer, a dimeric DBCO-based ^{18}F-prosthetic group should be developed enabling the coupling of two targeting vectors. This would enhance the probability of interaction and prolongs the retention time at the target side. [6]

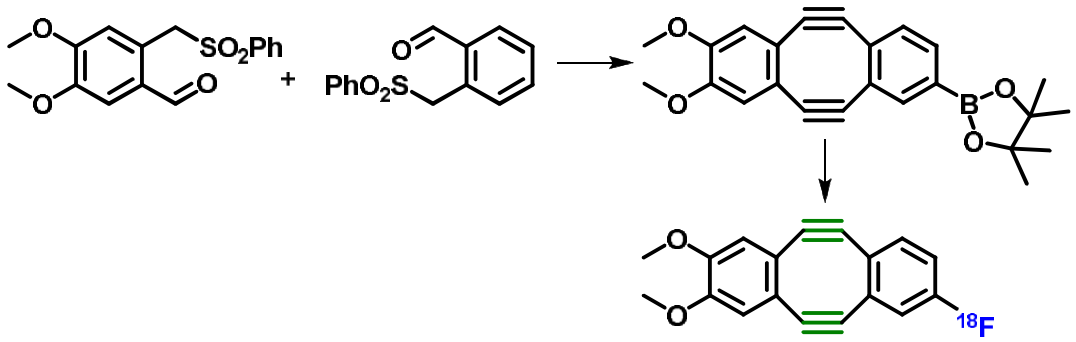

Scheme 4: Synthesis route of dimeric DBCO-based ^{18}F-prosthetic group.

The synthesis route started with 3,4-dimethoxytoluene and 4-bromo-2-methylbenzoic acid and involved altogether ten reaction steps. The ring closure step (scheme 4) turned out to be the most challenging one especially in terms of separation of the three reaction products. Furthermore the results presented in CHAPTER II suggested that the unpolar DBCO-moiety has a negative influence on the overall lipophilicity of the radiotracer. This resulted in unfavorable accumulation in FR-negative tissue and low tumor uptake for an [^{18}F]fluoro-DBCO-folate derivative. Therefore, no significant improvement is expected for a multimeric folate derivative using a dimeric ^{18}F-labeled DBCOderivative.

As already mentioned in the introduction, the folate receptor (FR) is (over)expressed on malignant cells, wherefore it is known as an oncological target for imaging and therapy for decades. Several ^{18}Ffolates have already been developed and evaluated using either direct labeling strategies or ^{18}Fprosthetic groups. The direct labeling strategy in general requires distinctive protecting groups and therefore complicates the precursor synthesis. Furthermore, the direct radiolabeling reactions often lead to low RCYs. In contrast, the click approach enables the attachment of ^{18}F-prosthetic groups under very mild and biorthogonal conditions. Most of the established prosthetic groups unfortunately have a negative influence on the lipophilicity and therefore impair the pharmacokinetic profile of the radiotracer. Therefore, directly labeled folate derivatives always provided better *in vivo* characteristics. The major challenge consists in finding the right balance between reducing the abdominal background and providing the [^{18}F]fluoro-folate in high RCYs within an appropriate synthesis time.

Copper-catalyzed click reactions in general suffer from the problem to ensure complete removal of the cytotoxic copper after radiolabeling reaction. This might be a challenge when applying [^{18}F]fluoroclick-folates for human use. The aim of this work was the evaluation of an [^{18}F]fluoro-DBCO-folate 6 (scheme 5) *in vitro* and *in vivo* to learn more about the influence of this novel copper-free labeling approach (CHAPTER I) on the pharmacokinetic profile of the folate derivative.

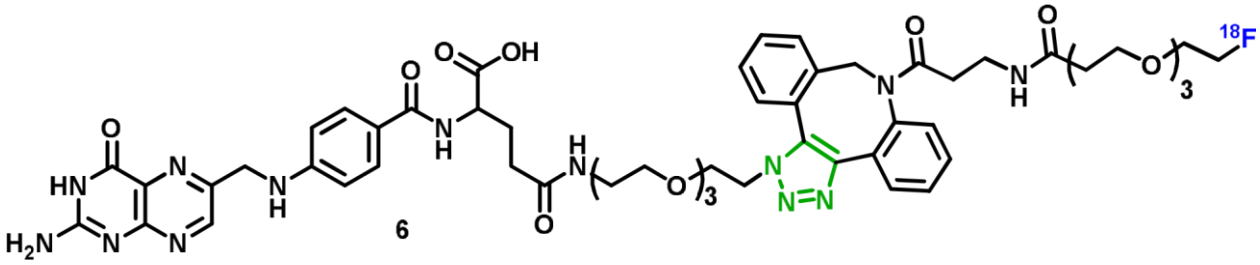

Scheme 5: Chemical structure of the novel [^{18}F]fluoro-DBCO-folate 6.

The copper-free click reaction of azide-functionalized folate derivative and [^{18}F]fluoro-DBCO provided the novel radiotracer in moderate overall yields and, unfortunately, only a low specific activity. Determination of the lipophilicity (logD value of 0.69 ± 0.08) gave us the first hint that the influence of the large unpolar prosthetic group might be too dominant. The high lipophilicity of [^{18}F]fluoro-DBCOfolate indicates a predominant hepatobiliary excretion pathway enhancing the abdominal background. Despite high affinity to the FR was confirmed by *in vitro* displacement assays with [^{3}H]folic acid, only a low specificity was observed during internalization studies with human KB cells (FR positive) and OC316 cells (FR negative). Biodistribution studies with KB-tumor bearing mice showed only low uptake in the tumor (0.48 ± 0.14 %ID/g tissue) and other FR-positive tissues (kidneys: 3.96 ± 0.38 %ID/g tissue) but high accumulation in the abdominal region. Consequently, the tumor was not visible in the small animal µPET images as maximum intensity projections (MIP). Summarizing it can be said, that the novel copper-free labeling strategy using [^{18}F]fluoro-DBCO as a prosthetic group has proven its viability in terms of mild reaction conditions and promising RCYs by evaluating different biomoleculeazides. However, first *in vitro* and *in vivo* evaluations suggest the application of this labeling strategy rather for larger biomolecules such as peptides, proteins or nanoparticles. For such larger structures the influence of the prosthetic group is negligible.

Based on these results, a recently published hydrophilic prosthetic group ([^{18}F]fluoro-alakyne) was used for the radiolabeling of the folate derivative to increase its hydrophilicity and improve the *in vivo* behavior.

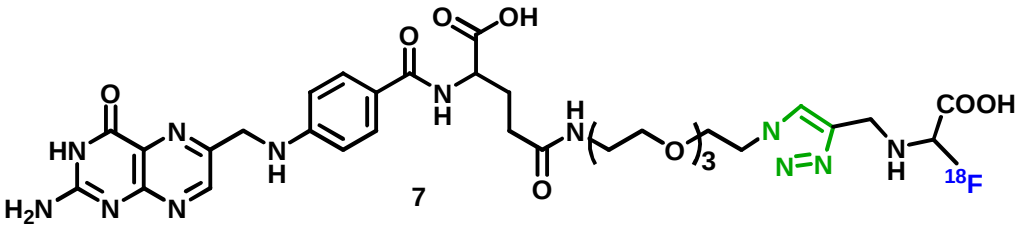

Scheme 6: Chemical structure of the novel [^{18}F]fluoro-ala-folate 7.

Indeed, for using the [^{18}F]fluoro-alakyne as a prosthetic group a copper catalyst needed to be applied for the click reaction. The small and hydrophilic alanine derivative had a much lower influence on the lipophilicity of the folate derivative compared to the [^{18}F]fluoro-DBCO. The lower logD value of -1.43 ± 0.08 resulted in a reduced unspecific binding in cell internalization studies and a slightly higher affinity to the FR. Despite a still high accumulation of [^{18}F]fluoro-ala-folate 7 (scheme 6) in the intestines, the tumor was clearly visible in the µPET image (figure 4, D).

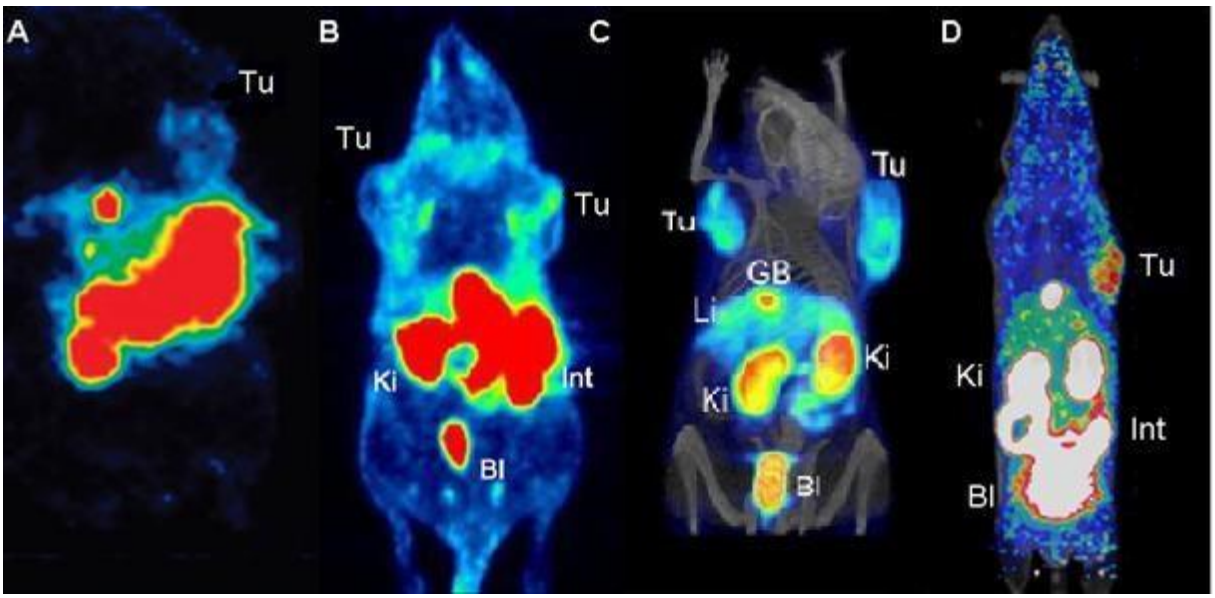

Figure 4: A) horizontal whole body PET image of [^{18}F]fluoro-click-folate; [7] B) MIP of [^{18}F]fluoro-OEG-click-folate; [8] C) 3D PET/CT image of [^{18}F]FDG-folate; [9] D) MIP of [^{18}F]fluoro-ala-folate.

Figure 4 provides an overview of PET images for all published [^{18}F]fluoro-folates radiolabeled based on click reactions. The first [^{18}F]fluoro-click-folate published in 2008 by Ross *et al.* (A) showed distinctive hepatobiliary excretion due to its high lipophilicity. [7] Increasing the polarity by introducing an oligoethylene glycol moiety to the prosthetic group resulted in reduced abdominal background (B). [8] The greatest advantage within the last years has been made by Fischer *et al.* by using [^{18}F]FDG as a highly polar prosthetic group. A clearly enhanced tumor uptake was achieved while further reducing the general background (C). [9, 10] The [^{18}F]fluoro-ala-folate can be ranged between the [^{18}F]fluoroOEG-click-folate and the [^{18}F]FDG-folate. Due to incomplete separation of the precursor molecule the [^{18}F]fluoro-ala-folate carries a high load of non-radioactive mass, which reduces the

specific activity. This explains the overall quite low accumulation in FR-positive tissue (tumor: 1.68 ± 0.13 %ID/g tissue) and kidneys: 14.38 ± 3.39 %ID/g tissue). The tumor-to-blood (10.11), tumor-to-liver (0.98) and tumorto-kidney-ratios (0.12) are also comparable to the ones observed for the [^{18}F]fluoro-OEG-click-folate as well as the [^{18}F]FDG-folate. Summarizing it can be said, that the novel [^{18}F]fluoro-ala-folate showed good and FR-tumor specific uptake, wherefore it can be seen as a promising candidate for PET imaging of FR-positive tumors. Further work will focus on the development of an improved precursor molecule with a 1-napthalensulfonyl leaving group (scheme 7). This modified precursor 8 will enable a complete separation of [^{18}F]fluoro-alakyne from the precursor molecule and therefore enhances the specific activity of the final radiotracer.

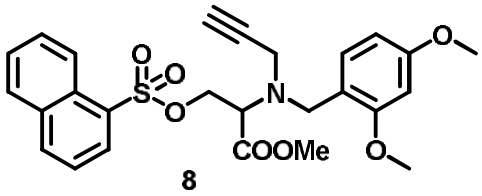

8

Scheme 7: Chemical structure of a novel precursor molecule 8.

In general the use of prosthetic groups prolongs the radiosynthesis time up to sometimes 3 h. Therefore, we had the idea to develop a 2in1 approach, where the ^{18}F-prosthetic group cannot only be used as a radiolabeling agent but also as a tumor imaging radiotracer itself. This approach would broaden the application range of the [^{18}F]fluoro-alakyne synthesis extensively. While the click reaction with a targeting vector (e.g. folic acid) is performed, a certain amount of the prosthetic group can already be used to perform PET imaging. This procedure would enable the imaging of one patient with two different radiotracers within one day, since the [^{18}F]fluoro-alakyne is preliminary and fast excreted through the renal pathway. Through this approach a broader variety of tumors can be addressed. The high potential of [^{18}F]fluoro-alakyne as a polar prosthetic group has already been pointed out in CHAPTER II.

Since amino acids play an important role during protein synthesis, cancer cells have a higher demand on these nutrients. Complementary to [^{18}F]FDG, radiolabeled amino acids have been successfully used for tumor imaging for decades, because they can be used to differentiate between tumor lesions and inflammation. In terms of oncology, brain tumor imaging is the most established application of radiolabeled amino acid derivatives as already described in the *Introduction*. For brain tumor imaging especially [^{18}F]FET ([^{18}F]fluoroethyltyrosine) and [^{18}F]FDOPA are well established radiotracers. In addition to the tracers targeting system L, a few ^{18}F-labeled amino acids for other amino acid transporters such as system A or the glutamate transporter have been developed within the last years. Special attention needs to be paid on the characterization of the transport mechanism of ^{18}Fradiolabeled amino acids. [11]

The results of the *in vitro* and *in vivo* evaluation of [^{18}F]fluoro-alakyne as a radiotracer for the imaging of non-small cell lung cancer using PET are summarized in CHAPTER III. Competition and transstimulation assays have been performed to characterize the responsible transporter system. Unfortunately no intracellular retention of [^{18}F]fluoro-alakyne was observed for the trans-stimulation with PBS and medium, which suggests an 1:1-exchange transport and no trapping in the tumor cells by incorporation in proteins. However, a clear visibility of the tumor was achieved in µPET imaging studies although the tumor uptake (0.28 ± 0.06 %ID/g tissue) was low. Since [^{18}F]fluoro-alakyne showed no unspecific binding at all and an exclusively renal excretion pattern, a very favorable tumorto-back-ground-contrast was achieved.

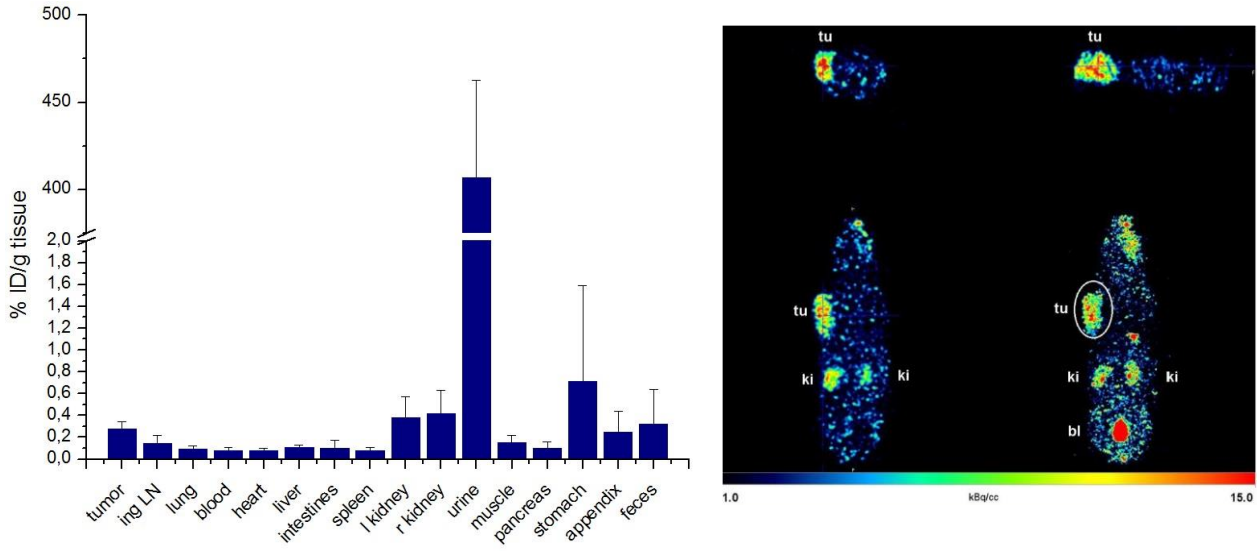

Figure 5: Results of biodistribution and PET imaging studies of [^{18}F]fluoro-alakyne.

These results confirm the high potential of this novel alanine-based radiotracer for tumor imaging. Further investigations concerning the range of application for other tumor types and the differentiation between tumor lesions and inflammatory processes are mandatory.

Since fluorine-18 needs to be attached covalently to the molecule, a quite high amount of precursor molecule (µmol range) is necessary. Especially in terms of larger structures with a high molecular weight (e.g. microbodies) this means, that even a few mg need to be used for each direct radiolabeling step. The same counts for the covalently click reaction of ^{18}F-prosthetic groups with biomoleculeazides. In the case of easy and low cost available precursor molecules this is not problematic. But in terms of rarely available and cost-intensive microbodies or antibodies the complexation of gallium-68 might be an interesting and cost-efficient alternative. Therefore, the microbody needs to be derivatized with a chelator, but for the radiolabeling reaction itself only a few nmol are necessary.

It was not possible to label azide-functionalized microbodies neither via copper-catalyzed click reaction ([^{18}F]fluoro-TEG-alkyne) nor via the novel copper-free variant ([^{18}F]fluoro-DBCO) with fluorine-18 in

satisfying radiochemical yields. Therefore, a fibroblast activation protein (FAP) specific microbody was derivatized with a DOTA chelator and radiolabeled with gallium-68. FAP is known as an oncological target for therapy and diagnosis due to its upregulation in reactive stromal fibroblast of human epithelial cancers. The results of this investigation are summarized in CHAPTER IV. [^{68}Ga]GaDOTA-MC-FA-012 was achieved in almost quantitative radiochemical yields and provided fast and specific uptake in FAP-positive cells (figure 6).

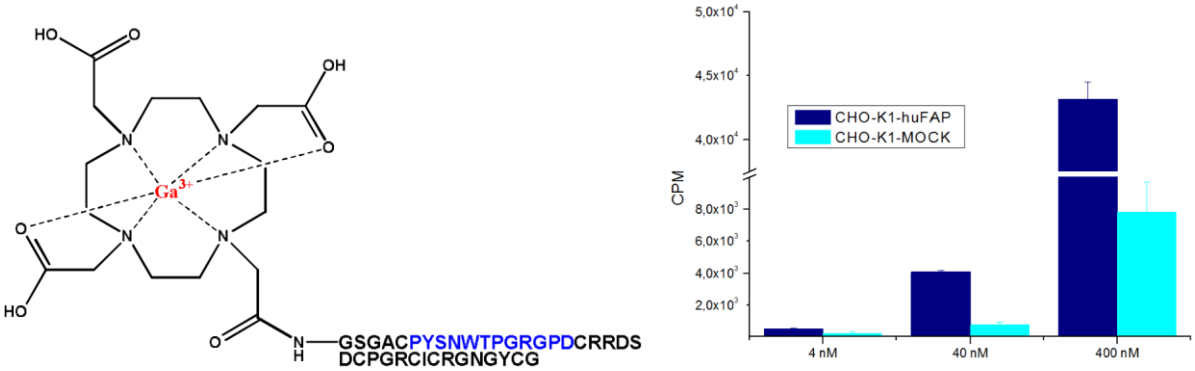

Figure 6: Chemical structure of [^{68}Ga]Ga-DOTA-MC-FA-012 (left) and results of internalization study in huFAP positive CHOK1-huFAP and huFAP negative CHO-K1-MOCK cells (right).

Based on these findings, a multivalent approach was investigated to enhance the intracellular uptake and specificity of the microbody. The higher accumulation of multivalent radiotracer is principally based on two mechanisms: (1) rolling and (2) rebinding (figure 7). If one cell-surface interaction dissociates there is another targeting vector nearby. In case of larger spacer molecules between two targeting vectors, even simultaneous binding at two target sides is possible. A few studies already proved the general benefit of this approach in terms of higher tracer accumulation and therefore reducible injection amount for therapeutic application. [12-14]

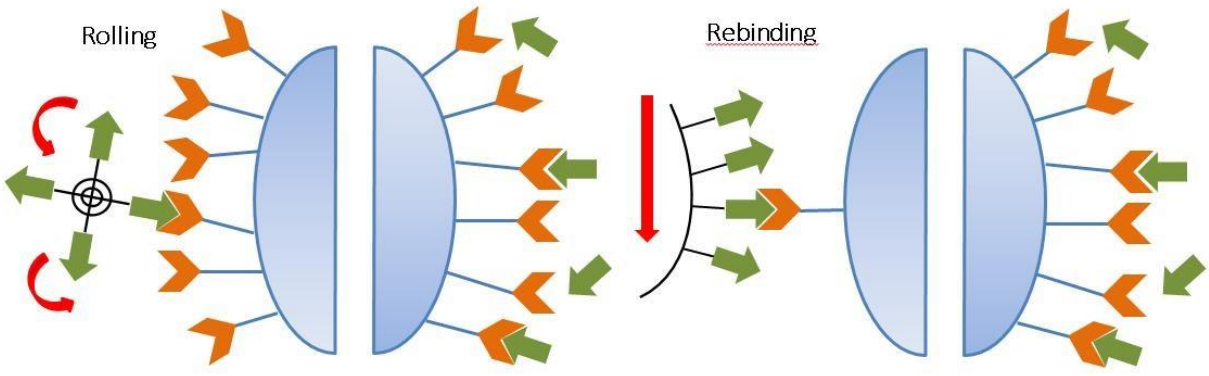

Figure 7: Rolling and rebinding of a multivalent radiotracer.

In case of the FAP-specific microbody, ^{68}Ga-labeled DFO-neutrAvidin was used to form a tetramer with MC-FA-10-biotin (figure 8). A 14-times higher accumulation was observed in huFAP-positive cells for the MC-FA-10-tetramer compared to the monomer. Furthermore, the unspecific accumulation in huFAP-negative cells was below 1 % compared to the amount accumulated in the positive cells, which

indicates a higher specificity of the tetramer. In conclusion, this novel FAP-specific microbody is a very promising candidate for further *in vivo* evaluation as diagnostic tool.

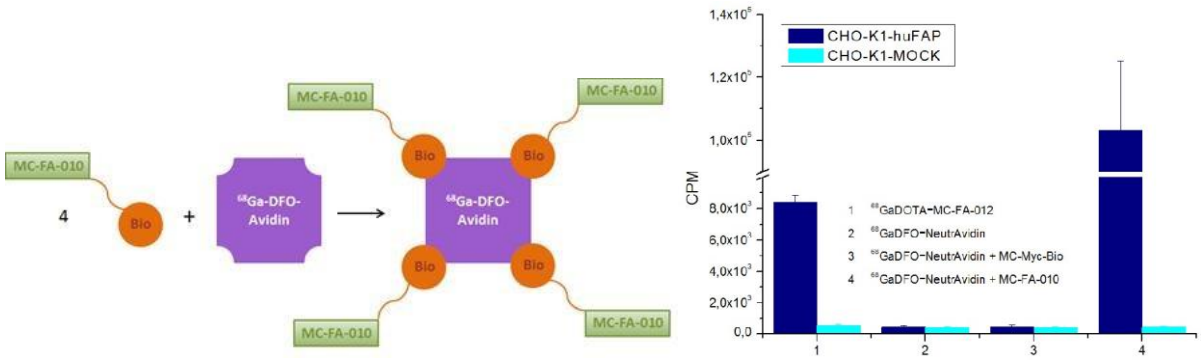

Figure 8: Schematic illustration of avidin-biotin interaction (left) and internalization of ^{68}Ga-labeled MC-FA derivatives.

3.1. References

[1] S. Schneefeld, S. Eilert, J. Thackerary, X. Wang, N. Murthy, G.-J. Meyer, J. Bankstahl, F. Bengel, and T. L. Ross,"Preliminary evaluation of ^{68}Ga-DOTA-maltohexaose as a specific PETradiotracer for bacterial infections," *Journal of Nuclear Medicine*, no. 57, p. 382, 2016.

[2] T. L. Ross, J. Ermert, C. Hocke, and H. H. Coenen, "Nucleophilic ^{18}F-fluorination of heteroaromatic iodonium salts with no-carrier-added [^{18}F]fluoride," *Journal of the American Chemical Society*, vol. 129, no. 25, pp. 8018–8025, 2007.

[3] R. Richarz, P. Krapf, F. Zarrad, E. A. Urusova, B. Neumainer, and B. D. Zlatopolskiy, "Neither azeotropic drying, nor base nor other additives: a minimalistic approach to ^{18}F-labeling," *Organic & Biomolecular Chemistry*, vol. 12, no. 40, pp. 8094–8099, 2014.

[4] T. Grus, "Synthese und Evaluierung DBCO-basierter ^{18}F-prosthetischer Gruppen für die kupferfreie ^{18}F-Markierung," *Bachelorarbeit*, Johannes Gutenberg-Universität Mainz, 2015.

[5] M. Sieberger, "Entwicklung Dibenzocyclooctin (DBCO)-basierter prosthetischer Gruppen für die kuperfreie ^{18}F-Markierung von Biomolekül-Aziden," *Bachelorarbeit*, Johannes GutenbergUniversität Mainz, 2015.

[6] P. I. Kitov, and D. R. Bundle, "On the nature of the multivalency effect: a thermodynamic model," *Journal of the American Chemical Society*, vol. 125, no. 52, pp. 16271–16284, 2003.

[7] T. L. Ross, M. Honer, P. Y. Lam, T. L. Mindt, V. Groehn, R. Schibli, P. A. Schubiger, and S. M. Ametamey, "Fluorine-18 Click Radiosynthesis and Preclinical Evaluation of a New ^{18}F-Labeled Folic Acid Derivative," *Bioconjugate Chemistry*, vol. 19, no. 12, pp. 2462–2470, 2008.

[8] H. Schieferstein, T. Betzel, C. R. Fischer, and T. L. Ross, "^{18}F-click labeling and preclinical evaluation of a new -folate for PET imaging," *EJNMMI research*, vol. 3, no. 1, p. 68, 2013.

[9] S. D. Boss, T. Betzel, C. Müller, C. R. Fischer, S. Haller, J. Reber, V. Goehn, R. Schibli, and S. M. Ametamey, "Comparative Studies of Three Pairs of ɲ- and œ-Conjugated Folic Acid Derivatives Labeled with Fluorine-18," *Bioconjugate Chemistry*, vol. 27, no. 1, pp. 74–86, 2016.

[10] C. R. Fischer, C. Müller, J. Rebert, A. Müller, S. D. Krämer, S. M. Ametamey, and R. Schibli, "[^{18}F]Fluoro-Deoxy-Glucose Folate: A Novel PET Radiotracer with Improved in Vivo Properties for Folate Receptor Targeting," *Bioconjugate Chemistry*, vol. 23, no. 4, pp. 805–813, 2012.

[11] C. Huang, and J. McConathy, "Fluorine-18 Labeled Amino Acids for Oncologic Imaging with Positron Emission Tomography," *Current Topics in Medicinal Chemistry*, vol. 13, no. 8, pp. 871–891, 2013.

[12] X. Montet, M. Funovics, K. Montet-Abou, R. Weissleder, and L. Josephson, "Multivalent effects of RGD peptides obtained by nanoparticle display," *Journal of Medicinal Chemistry*, vol. 49, no. 20, pp. 6087–6093, 2006.

[13] C. B. Carlson, P. Mowery, R. M. Owen, E. C. Dykhuizen, and L. L. Kiessling, "Selective tumor cell targeting using low-affinity, multivalent interactions," *ACS Chemical Biology*, vol. 2, no. 2, pp. 119–127, 2007.

[14] G. V. Dubacheva, T. Curk, B. M. Mognetti, R. Auzély-Velty, D. Frenkel, and R. P. Richter, "Superselective targeting using multivalent polymers," *Journal of the American Chemical Society*, vol. 136, no. 5, pp. 1722–1725, 2014.

3.2. List of illustrations

4. Summary

4. Summary

Different target/targeting vector systems require variable radiolabeling strategies to enable routine clinical tumor diagnosis via PET. The herein presented work focused on the development and evaluation of novel methods for the radiolabeling of various targeting vectors (e.g. peptides, microbodies, folates) with fluorine-18 and gallium-68. Copper-catalyzed and copper-free click reactions were applied for the attachment of ^{18}F-prosthetic groups to biomolecule-azides. This included the synthesis of novel precursor molecules (e.g. DBCO, alakyne, peptides, folate-azide) as well as the evaluation and optimization of the radiolabeling reaction (CuAAC, SPAAC). Furthermore, chelators were attached to microbodies enabling generator-based radiolabeling with gallium-68. The novel radiotracers can be used for tumor imaging using PET by addressing selectively specific target sites (e.g. melanocortin-1 receptor, fibroblast activation protein, folate receptor). Preclinical studies concerning the structure-affinity relationships have been performed with four novel radiotracers ([^{18}F]fluoro-DBCO-folate, [^{18}F]fluoro-ala-folate, [^{18}F]fluoro-alakyne and [^{68}Ga]Ga-DOTA-MC-FA-012). Therefore *in vitro* cell studies, *ex vivo* biodistribution and *in vivo* µPET scans using xenograft animal models have been performed.

1. From copper-catalyzed to copper-free click cycloadditions

Numerous [^{18}F]fluoro-folates for PET imaging and folate-based drug delivery systems have already proven the great potential of the folate receptor targeting concept for diagnosis and therapy. However, there is still a lack of a reliable and high yielding radiosynthesis for the application of ^{18}Flabeled folate derivatives for routine clinical use. Besides good radiochemical yields, especially the minimization of the influence of the radiolabeling strategy on the pharmacokinetic properties of the folate derivatives has been a research focus during the last years. The first improvement has been made by applying the click chemistry approach to the radiolabeling of folate derivatives. This reaction proceeds under very mild and bioorthogonal conditions sparing any protection groups on the part of the biomolecule. Only the need of a copper catalyst during radiosynthesis can be seen as a drawback of this method. Therefore, a copper-free variant of the azide-alkyne cycloaddition using a (aza)dibenzocyclooctyne (DBCO)-based prosthetic group has been development and evaluated using different biomolecule-azides within this work.

For the first time, the copper-free click labeling strategy was applied to a folate derivative by using the novel [^{18}F]fluoro-DBCO. *In vitro*, *ex vivo* and *in vivo* preclinical studies showed that the increased

lipophilicity referable to the large hydrophobic prosthetic group has a negative influence on the tumor uptake. Nevertheless, the general feasibility of this novel copper-free labeling strategy in terms of mild

click reaction conditions and high radiochemical yields has been proven with various biomoleculeazides (cRGD, ɲ-MSH peptides, maltohexaose, PDGF-ʁ peptide). Concluding, the novel [^{18}F]fluoroDBCO was found to be more suitable for larger structures such as antibodies or nanoparticles, where its influence on the lipophilicity is negliable.

2. From [^{18}F]fluoro-DBCO to [^{18}F]fluoro-alakyne

Based on the *in vitro* and *in vivo* evaluation of [^{18}F]fluoro-DBCO-folate, the recently reported [^{18}F]fluoro-alakyne was found to be much more suitable for the radiolabeling of small lipophilic structures such as folic acid. This amino acid-based ^{18}F-prosthetic group, indeed, required the application of a copper catalyst during radiosynthesis, but exhibits a much more favorable lipophilicity and small molecular size. *Ex vivo* biodistribution and *in vivo* µPET studies showed a moderate tumor uptake, but an enhanced tumor-to-background contrast due to reduced abdominal background limited to the intestines, the kidneys and the bladder of the more hydrophilic [^{18}F]fluoro-ala-folate. The tumor and other FR-positive tissues were clearly visible. Comparing both radiolabeling strategies (CuAAC and SPAAC), slithly higher radiochemical yields were achieved for the [^{18}F]fluoro-ala-folate, but within a longer synthesis time. The different ^{18}F-prosthetic groups had, as expected, no influence on the affinity of the folate derivative to the FR. A higher unspecific binding was observed during cell studies for the [^{18}F]fluoro-DBCO-folate due to its increased lipophilicity and in the µPET scan the tumor was not visible due to high abdominal background. Concluding, both ^{18}F-prosthetic groups are in general suitable for the labeling of biomoluecule-azides, but for small molecules the use of [^{18}F]fluoroalakyne would be the method of choice.

3. [^{18}F]fluoro-alakyne: 2in1 approach

To enhance the application range of the novel [^{18}F]fluoro-alakyne, not only as a prosthetic group, this alanine-based molecule was evaluated as a tumor imaging candidate itself. Up to date most of the ^{18}Flabeled amino acid-based radiotracers suffer from undesirable abdominal accumulation limiting their application to the diagnosis of brain tumors. *Ex vivo* biodistribution and *in vivo* µPET studies with NCIH1975 (non-small cell lung cancer) tumor bearing mice showed almost no unspecific accumulation

and an exclusively renal excretion pathway. Despite the tumor uptake was very low, a favorable tumor-to-background contrast was achieved. Further evaluation concerning the application range of this novel radiotracer for other cancer types and the differentiation between tumors and inflammation are planned. These investigations show that the [^{18}F]fluoro-alakyne can both be used as a polar ^{18}F-prosthetic group and a highly potential tumor imaging radiotracer at the same time. This 2in1 approach broadens the application range of [^{18}F]fluoro-alakyne for various different tumor types and therefore improves the benefit for the patient.

4. From ^{18}F-labeled small molecules to ^{18}F-labeled microbodies

Despite ^{18}F-labeled small molecules mostly show favorable pharmacokinetics and provide a high contrast in tumor imaging, biomacromolecules such as monoclonal antibodies or proteins often provide higher tumor selectivity and specificity. Unfortunately, peptides and fragmented antibodies are very sensitive in biological systems and to chemical influences. Instead, cysteine-knot microbodies show a higher thermal and proteolytic stability combined with high cancer specificity enabling clear localization of tumors. The BioNTech group has identified and produced novel microbodies for various different targets (e.g. melanoma, fibroblast activation protein). The aim of the herein presented work was the development of an appropriate radiolabeling strategy to make these novel targeting vectors available for tumor diagnosis using PET. First, the well established copper-catalyzed click cycloaddition (CuAAC) using [^{18}F]fluoro-TEG-alkyne was tested. Unfortunately, no click reaction was observed and it was assumed that the copper catalyst might be trapped withing the large peptide-based structure. Therefore, a copper-free radiolabeling method using the novel [^{18}F]fluoro-DBCO was used instead. This approach provided the desired ^{18}F-labeled microbody, but in unsatisfying radiochemical yields (< 20 %) and only with a high precursor amount of around 3 mg for each radiolabeling reaction. Since the production of microbodies is very cost-intensive, this strategy was found to be not the method of choice for these targeting vectors.

5. From ^{18}F-labeled microbodies to ^{68}Ga-analogs

Although fluorine-18 shows superior nuclear physical characteristics to gallium-68 for application in PET, there are some applications where gallium-68 is more suitable. Since cyclotrons are not available at every clinic and radioactive transportation is quite cost-intensive, the use of a germanium68/gallium-68-generator is a good alternative especially for routine clinical use. When radiotracers are available via *kit-type* labeling not even radiochemist are necessary for the production of the radiopharmaceuticals for tumor diagnosis. The radiolabeling then can be performed by the clinical staff.

Furthermore, in the case of larger structures such as microbodies, the high precursor amount, which is necessary for the covalent attachment of fluorine-18, makes this labeling method not costefficient. Derivatization with a chelator for the radiolabeling with e.g. gallium-68 also requires a certain amount of microbody, but for each radiolabeling synthesis itself only a few nmol are needed, which lowers the overall costs for the imaging.

The fibroblast activation protein (FAP) is upregulated in reactive stromal fibroblasts of epithelial cancers and therefore displays an ideal oncological target for diagnosis and therapy. Within the last years, many monoclonal antibodies for therapeutic application have been developed, but there is still a lack of FAP specific radiotracers for diagnosis. Therefore, the novel microbody MC-FA-012 has been

identified and produced by the BioNTech group to image FAP-positive tumors. [^{68}Ga]Ga-DOTA-MC-FA012 showed specific internalization in FAP-positive cells, which proves the high potential of this novel microbody as tumor imaging candidate.

6. From monomer to tetramer – multivalency approach

In general, multivalent radiotracers are thought to provide enhanced tumor internalization due to increased retention of the targeting vector at the target site. The ^{68}Ga-labeled neutrAvidin-biotin tetramer of the novel microbody MC-FA-010 showed higher internalization and increased specificity in FAP-positive cells compared to the monomer. This means that less amount of the radioactive labeled compound needs to be applied to the human body reducing the radiation exposure for the patient.

Concluding, this work describes the whole process of novel radiotracer development, starting from target identification and targeting vector selection, followed by choosing an appropriate radiolabeling method and optimizing the radiolabeling reaction. Thereby small molecules (folate- and alaninederivative) as well as microbodies have been evaluated in preclinical studies. This work demonstrates clearly the high influence of the radiolabeling strategy (copper-free or copper-catalyzed click) on the overall lipophilicity of the radiotracer. This influences strongly the biodistribution and excretion pathway of the radiopharmaceutical and therefore has a significant influence on the tumor uptake. Furthermore, the multivalency approach has been found to be a very suitable tool to enhance

tumor accumulation and specificity of a certain radiotracer without major changes of the targeting vector itself.

5. Publications and ongoing studies

5. Publications and ongoing studies

"A ^{18}F-labeled dibenzocycloocytne (DBCO) derivative for copper-free click labeling of biomolecules"

Kathrin Kettenbach, Tobias L. Ross

Medicinal Chemical Communications (MedChemComm), 2016, 7, 654-657

"*In vitro* and *in vivo* comparison study of a folate derivative labelled with fluorine-18 via copperfree and copper-catalyzed click cycloaddition"

Kathrin Kettenbach, Hanno Schieferstein, Stefanie Pektor, Raphael Eckert, Laura M. Reffert, Georg Otto, Matthias Miederer, Frank Rösch, Tobias L. Ross

Submitted to Bioorganic and Medicinal Chemistry

„^{18}F-Alakyne: not only a protethetic group, but also a very promising tumor imaging candidate"

Kathrin Kettenbach, Hanno Schieferstein, Nicole Bausbacher, Barbara Biesalski, Wolfgang Müller-Klieser, Frank Rösch, Tobias L. Ross in

preparation for submission

„Radiolabeling and Evaluation of a FAP specific Microbody®"

Kathrin Kettenbach, Benedikt Sandhöfer, Joycleyn Wüstehube-Lausch, Matin Daneschdar, Ugur Sahin, Frank Rösch, Tobias L. Ross in

preparation for submission

A ^{18}F-labeled Dibencocyclooctyne (DBCO) derivative for Copperfree Click Labeling of Biomolecules

Kathrin Kettenbach[1], Tobias L. Ross[1,2]

[1] Institute of Nuclear Chemistry, Johannes Gutenberg University Mainz, 55128 Mainz, Germany

[2] Radiopharmaceutical Chemistry, Department of Nuclear Medicine, Hannover Medical School, 30625 Hannover, Germany

The new prosthetic group ^{18}F-TEG-DBCO (dibenzocyclooctyne) can be prepared within a total reaction time of 60 min including purification with an overall yield (n.d.c.) of (34±5) %. Copperfree click cycloadditions with an azido-cRGD, a folate-azide and two ɲ-MSH analogue azidopeptides resulted in very high RCYs and fast reaction kinetics.

For non-invasive *in vivo* imaging of processes and pharmacokinetics of radiolabeled biomolecules, the positron emission tomography (PET) is one of the most powerful methods. [1] For PET applications, fluorine-18 has ideal nuclear characteristics and is the most commonly applied radionuclide in PET. The relatively long half-life of 110 minutes enables multi-step radiosyntheses and the rather low ɴ+energy ensures a very high spatial resolution in tomography. [2] The challenge for nuclear chemists consists in finding appropriate ^{18}F-labeling strategies, especially for sensitive biomolecules. Most of them are sensitive to the commonly used harsh conditions in direct ^{18}F-labeling reactions such as high temperatures and strong basic conditions. [3,4] As a result, the development of indirect labeling strategies via ^{18}F-prosthetic groups, which can subsequently be attached to biomolecules under mild reaction conditions, is needed. [5-7] Besides, the radiolabeling reaction should allow a bioorthogonal ^{18}F- labeling to treat the multitude of functional groups in bioactive compounds with respect. The most prominent example of such reactions, which fulfills all the mentioned criteria, is given by the copper(I)-catalyzed azide-alkyne cycloaddition (CuAAC) first published by Sharpless *et al.* in 2001. [8] This variant of the Huisgen 1,3-dipolar cycloaddition of terminal alkynes and azides enables ^{18}Flabeling with high specificity and excellent yields under mild conditions. [9,10] In the last decade, a widespread spectrum of PET tracers has been synthesized using the CuAAC method for ^{18}F-labeling of bioactive compounds. [11] One of the latest developments is based on an amino acid, which is thought to minimize the influence on the pharmacokinetic properties of the intended radiotracer. As amino acid derived ^{18}F-prosthetic group, it is particularly suitable for peptides and proteins. [12] However, with all the advantages of the copper(I)-catalyzed cycloaddition goes along one major disadvantage. The need of cytotoxic copper species as catalyst in the click reaction causes an extensive work-up guaranteeing a complete removal of the copper for in vivo applications. This fact led to the necessity of alternative fast and copper-free click reaction strategies. By using strained alkynes instead of terminal alkynes, copper is no longer needed to catalyze the click reaction. These so-called strainpromoted click reactions were first reported by Baskin et al. [13] and can be carried out between cyclooctyne derivatives and azides or tetrazines as 3+2 cycloaddition. [11] The use of azadibenzocycloocytnes for copper-free click reactions was first reported by Kuzmin et al. in 2010. [14] Recently, Arumugam et al. published the development of an ^{18}F-labeled azadibenzocyclooctyne for ^{18}F-labeling of peptides via a strain-promoted click reaction without the use of a copper species, showing the high potential of this concept for ^{18}F-labeling of biomolecules. [15] Our aim was to develop a new ^{18}F-prosthetic group based

on (aza)dibenzocyclooctyne (DBCO) for radiolabeling of biomolecules such as peptides and microproteins. For reduced lipophilicity, we introduced a triethylene glycol spacer to the azadibenzocyclooctyne. Two different leaving groups, different bases, base concentrations and precursor amounts during radiolabeling were evaluated for optimized ^{18}Flabeling. Consequently, two DBCO-based precursors and the non-radioactive reference compound were synthesized and the ^{18}F-labeling reaction was optimized. Finally, we performed a proof-ofprinciple click reaction with the new ^{18}F-labeled prosthetic group and an azido-functionalized cyclic Arg-Gly-Asp (cRGD) peptide as a model system. This peptide is used as the gold-standard vector in targeting the $\alpha_V\beta_3$ integrin. [16,17] Furthermore, we carried out further copper-free click reactions using a folate-azide for targeting the folate receptor and two α-MSH analogue azido-functionalized peptides with high specificities to the melanocortin receptor 1 (MC1R).

The syntheses of reference compound 11 and the ^{18}F-labeling precursors 9 and 10 are depicted in scheme 1. The synthesis started from commercially available triethylene glycol 2. In the first step, 2 was reacted with tert-butylacrylate 1 to create a carboxylic acid function enabling desired amide coupling. [18] Compound 3 was then reacted with either p-toluenensulfonyl chloride [19] or methansulfonyl chloride [20] to transfer the hydroxyl function into suitable leaving groups for the nucleophilic radiofluorination reaction. Subsequently, protected intermediates 4 and 6 were deprotected by trifluoroacetic acid in dichloromethane at room temperature to yield 5 and 7. [21] Both linker groups were coupled via an amide bond to the dibenzocyclooctyne (DBCO)-amine 8, using HBTU (N,N,N´,N´-tetramethyl-O-(1H-benzotriazol-1-yl)uranium -hexafluorophosphate) as coupling reagent and N,N-diisopropylethylamine (DIPEA) as base. The coupling was performed at room temperature for 12h to yield the desired precursors for the ^{18}F-fluorination reaction in overall yields of 28 % (for precursor 9) and 56 % (for precursor 10) over four steps. Due to the quite high costs for DBCO-amine 8, we aimed to insert this component in the last synthesis step. In relation to the amounts of 8, the yields were good to very high, leading to 56 % respectively 87 %. The reference compound was synthesized through ^{19}F-fluorination of 9 using tetrabutylammonium fluoride (TBAF) at 120 °C for 2h to yield 11 in excellent yields of 82 %.

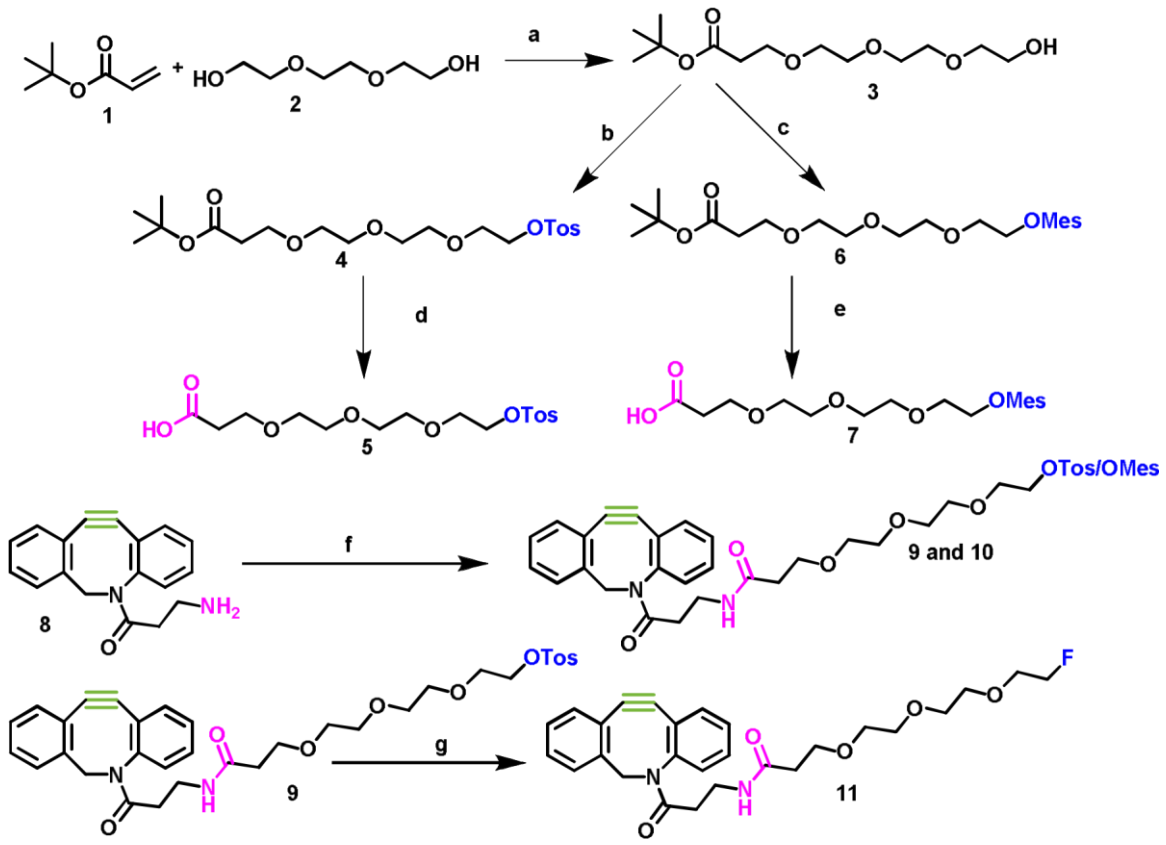

Scheme 1: Synthesis of alkyne-functionalized reference compound 11 and labeling precursors 9 and 10. Regents and conditions: a) sodium, THF, 24h, rt; b) TEA, p-toluenesulfonyl chloride, DCM, 1h, 0 °C – rt; c) TEA, methansulfonyl chloride, 1h, 0 °C – rt; d) TFA, DCM, 4h, rt; e) TFA, DCM, 4h, rt; f) TEG-carboxylic acid, N,N,N´,N´-tetramethyl-O-(1H-benzotriazol-1yl)uranium-hexafluorophosphate (HBTU), N,N-diisopropylethylamine (DIPEA), DMF, 24h, rt; g) tetrabutylammonium fluoride, THF, 2h, 80 °C.

The radiofluorination of precursor 9 is depicted in scheme 2. The radiolabeling of precursor 9 and 10 was optimized using different parameters such as various bases, base concentrations, reaction time and different amounts of precursors. Initially, the use of two different bases, tetrabutylammonium hydroxide (TBA-OH) and tetraethylammonium bicarbonate (Et_4NHCO_3) in acetonitrile were screened. The use of TBA-OH caused decomposition of the precursors and a RCY of only 30 % was achievable. The use of precursor 9 (7.5 mg, 12 µmol) in acetonitrile and tetraethylammonium bicarbonate gave the highest RCY of ш90 % within 10 minutes. For further evaluation of precursor 9 and 10, tetraethylammonium bicarbonate was used as base. With a base amount below 17 µmol, no ^{18}Flabeling was observed, while increasing the base amount higher than 17 µmol resulted in reduced yields. Besides, the amount of precursor played an important role. Reaction kinetics were monitored for 2.5, 5.0 and 7.5 mg (4, 8 and 12 µmol) of precursor 9. By increasing the amount of precursor (12 µmol) RCYs of ш90 % after 10 min were observed. No signifincant differences in RCYs were observed in dependence on the different leaving groups.

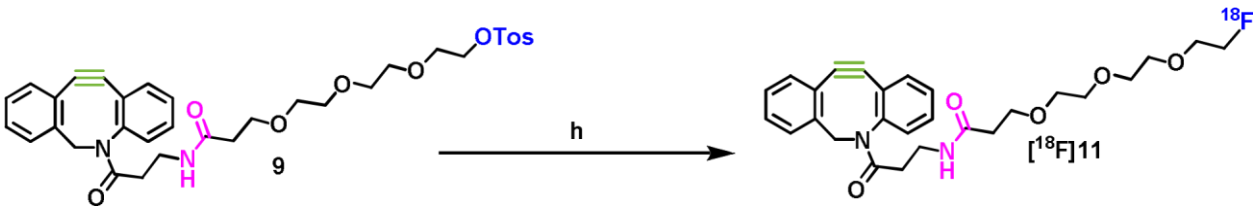

Scheme 2: Synthesis of ^{18}F-prosthetic group [^{18}F]11. Reagents and conditions: h) n.c.a. [^{18}F]fluoride, Et_4NHCO_3, MeCN, 100 °C, 10 min, RCY 91 %.

Isolation of the final ^{18}F-labeled prosthetic group was performed by fixation of the product fraction obtained from semi-preparative HPLC on a C18 reversed phase cartridge, followed by elution of the ^{18}F-prosthetic group from the resin with acetonitrile (1 mL). Exemplary radio-HPLC chromatogram of the crude mixture after radiolabeling of [^{18}F]11 is shown in the electronic supplementary information (ESI). The solvent was removed under reduced pressure and the ^{18}F-prosthetic group was resolved in the desired solvent to perform the subsequent click reaction. The new ^{18}F-prosthetic group was synthesized and isolated within only 60 min. in an excellent overall yield (n.d.c.) of 34±5 %, ready for copper-free click reactions with azido-functionalized biomolecules. For the lipophilicity of the ^{18}Fprosthetic group a logD value of 1.20 ± 0.07 was calculated using the octanol-water distribution coefficient.

To test the viability of [^{18}F]11, it was used in a copper-free cycloaddition with azido-functionalized cRGD peptide 12 (1 mg, 1.1 µmol), as shown in scheme 3, as a model system.

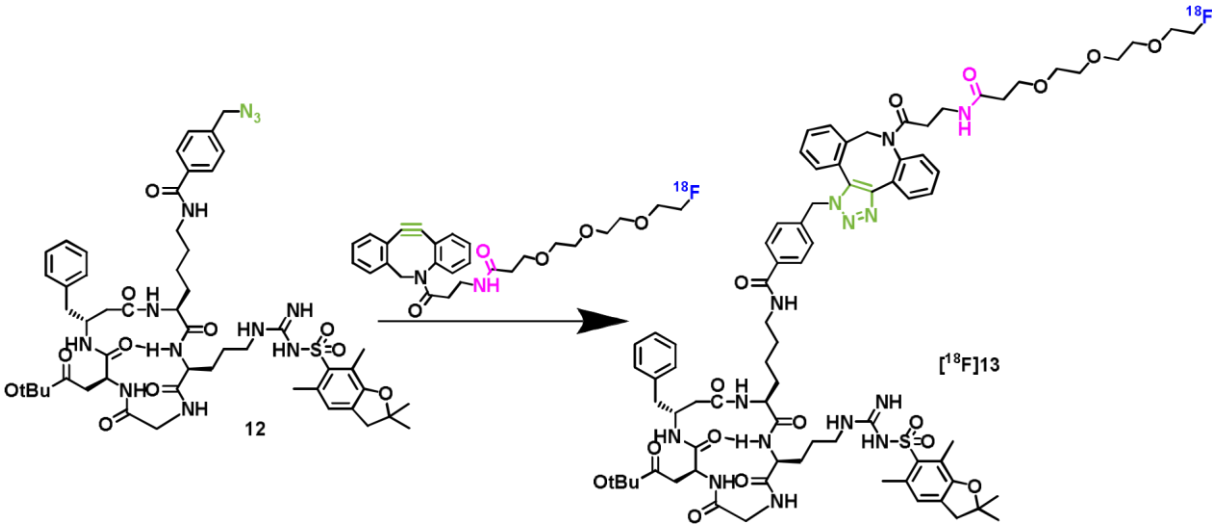

Scheme 3: SPAAC of protected azido-functionalized cRGD 18 and the new prosthetic group [^{18}F]11. Click reaction conditions: PBS buffer/acetonitrile (1:1), 25 °C or 40 °C, 5 min, RCY 93 %.

The copper free ^{18}F-click reaction gave the desired peptide [^{18}F]13 in excellent RCY of 93 % within 5 min, which shows the particularly high potential of the new prosthetic group for ^{18}F-labeling of sensitive biomolecules under very mild conditions (25 °C, phosphate-buffered saline (PBS, pH 7.4), 5 min). An exemplary radio-HPLC chromatogram of [^{18}F]13 in comparison to the ^{18}F-prosthetic group [^{18}F]11 is shown in the ESI.

Furthermore, an azido-functionalized folate derivative as well-known tumor targeting vector was ^{18}Flabeled in a copper free click reaction using the new ^{18}F-prostehtic group. Remarkably, quantitative ^{18}F-click labeling was observed after a few minutes at room temperature and a good (low) logD value of 0.6 ± 0.07 was determined for the final [^{18}F]fluoro-folate. The ^{18}F-labeled folate can be separated from unreacted folate-azide by HPLC and C18 SPE. The stability of the [^{18}F]fluoro-folate was analyzed in human serum at 37 °C. After 1.0h and 1.5h, ш95 % intact [^{18}F]fluoro-folate was observed. To our best knowledge this is the first report of a new [^{18}F]fluoro-folate labeled via a copper-free click approach.

Two different azido-functionalized ɲ-MSH analogue peptides, N_3-TEG-Gly-Gly-Nleu-Gly-His-DPhe-ArgTrp-NH_2 and N_3-TEG-Gly-Gly-Nleu-[Cys-His-DPhe-Arg-Trp-Gly-Cys]-NH_2, with high specificities to the MC1R (melanocortin receptor 1) were prepared by using solid phase peptide synthesis (SPPS). [22] Both peptides were radiolabeled with the ^{18}F-prostehtic group in a copper-free click cycloaddition. For the linear peptide, RCY of up to 79 % after 20 min were observed for 0.4 µmol peptide at 40 °C. For the cyclic ɲ-MSH analogue the click reaction proceeded with excellent RCY of 92 % even with a lower amount of only 0.2 µmol peptide at 40 °C.

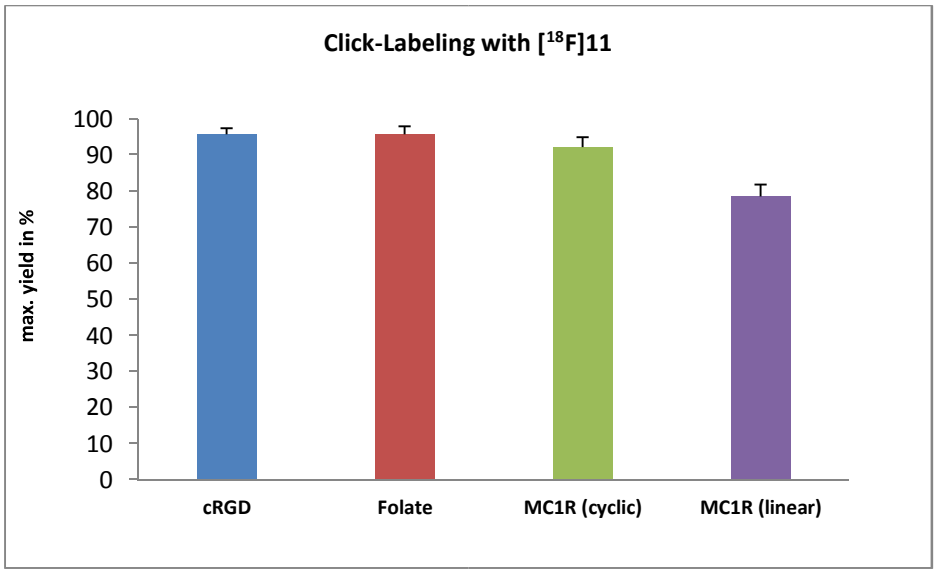

Scheme 4: Radiolabeling of various azides with [^{18}F]11. RCY after 20 min displayed in a bar chart. Errors are given as standard deviation representing n = 3.

Summarized conditions, RCY and kinetics for the four biomolecule-azides, which were tested in copper-free click reactions with the new ^{18}F-prosthetic group are shown in the ESI. The RCY are also displayed as a bar chart in scheme 4.

Especially for the radiolabeling of sensitive biomolecules, the use of ^{18}F-prosthetic groups is of particular interest, where the use of harsh conditions for direct ^{18}F-labeling reactions is excluded. Due

to the toxicity of copper, the attachment of the ^{18}F-prosthetic groups via copper(I)-catalyzed cycloaddition is no longer the first choice. The use of strained alkynes for copper-free cycloaddition enables selective radiolabeling of azido-functionalized biomolecules under very mild conditions.

The herein reported synthesis strategy of a ^{18}F-labeled DBCO-based prosthetic group enables copperfree ^{18}F-click labeling of various biomolecule-azides under very mild conditions and with outstanding efficacy. The organic syntheses provided the two precursors in good to high yields over four steps. The organic syntheses are robust and very reliable, and referred to DBCO-amine, the strategy and yields were optimized for economic reasons. High to excellent results were obtained for the ^{18}F-labeling of the two different precursors, which are available and ready-to-use for subsequent ^{18}F-click reactions within only 60 min and in high yields of 34 % (n.d.c.).

The new ^{18}F-prosthetic group performs outstandingly in copper-free click reactions with different biomolecule-azides, which are known as excellent tumor targeting vectors of common interest. [23,24,25,16,17] All click reactions proceeded with excellent to even quantitative yields under very mild conditions (water or PBS, RT or 40 °C) with very fast reaction kinetics. The tested biomoleculeazides (RGD, linear MSH-peptides and folic acid) were not achievable in such good yields with conventional copper(I)-catalyzed click cycloaddition. [11]

In cases of non-quantitative ^{18}F-click labeling, the ^{18}F-labeled products were easily separated by radioHPLC from the unreacted ^{18}F-prostehtic group. For the ^{18}F-labeled folate derivative a low logD value of

0.6 ± 0.07 was determined. High stability was observed in human serum at 37 °C over a period of 1.5h. Further in vitro and in vivo evaluation of the new [^{18}F]fluoro-folate using human KB cells and PET imaging are ongoing. Similarly, investigations and evaluation using the other new ^{18}F-tracers derived from copper-free ^{18}F-click labeling in in vivo PET imaging are planned.

REFERENCES

[1] N. Johnsson, and K. Johnsson, “Chemical Tools for Biomolecular Imaging,” *ACS Chemical* Biology, vol. 2, no.1, pp. 31-8, 2007.

[2] J. Ermert, and H.H. Coenen, “Methods for ^{11}C-labeling and ^{18}F-labeling of amino acids and derivatives for positon emission tomography imaging,” *Journal of Labelled Compounds and Radiopharmaceuticals*, vol. 56, no. 3-4, pp. 225-36, 2013.

[3] H. H. Coenen, R.H. Elsinga, R. Iwata, M. R. Kilbourn, M. R. a Pillai, G. R. Rajan, H. N. Wagner, and J. J. Zaknun, “Fluorine-18 radiopharmaceuticals beyond [^{18}F]FDG for use in oncology and neurosciences,” *Nuclear Medicine and Biology*, vol. 37, no.7, pp. 727-40, 2010.

[4] L. Lang, and W. C. Eckelman, "One-step synthesis of ^{18}F-labeled [^{18}F]N-succinimidyl 4(fluoromethyl)benzoate for protein labeling," *Applied Radiation and Isotopes*, vol. 45, no.12, pp. 1155-63, 1994.

[5] S. Okarvi, "Recent progress in fluorine-18 labelled peptide radiopharmaceuticals," *European Journal of Nuclear Medicine,* vol. 28, no.7, pp. 929-38, 2001.

[6] T. Poethko, M. Schottelius, G. Thumshirn, U. Hersel, M. Herz, G. Henriksen, H. Kessler, M. Schwaiger, and H. Wester, "Two-step Methodology for High-Yield Routine Radiohalogenation of Peptides: ^{18}F-Labeled RGD and Octreotide Analogs," *The Journal of Nuclear Medicine*, vol. 45, no. 5, pp. 892-902, 2004.

[7] T. Priem, C. Bouteiller, D. Camporese, X. Brune, J. Hardouin, A. Romieu, and P.-Y. Renard, "A novel sulfonated prosthetic group for ^{18}F-radiolabelling and imparting water solubility of biomolecules and cyanine fluorophores," *Organic & Biomolecular Chemistry*, vol. 11, no.3, pp. 469-79, 2013.

[8] H.C. Kolb, M.G. Finn, and K.B. Sharpless, "Click Chemistry: Diverse Chemical Function from a Few Good Reactions," *Angewandte Chemie International Edition*, vol. 40, no.11, pp. 2004 – 2021, 2001.

[9] R. Huisgen, "1,3-Dipolar Cycloadditions. Past and Future," *Angewandte Chemie International Edition,* vol. 2, no.10, pp. 565-98, 1963.

[10] J. Marik, and J. L. Sutcliffe, "Click for PET: rapid preparation of [^{18}F]fluoropeptides using Cu^{I} catalyzed 1,3-dipolar cycloaddition," *Tetrahedron Letters*, vol. 47, no. 37, pp. 66816684, 2006.

[11] K. Kettenbach, H. Schieferstein, and T.L. Ross, "^{18}F-Labeling Using Click Cycloadditions" *BioMed Research International, vol.* 2014, pp. 1-16, 2014.

[12] H. Schieferstein, and T. L. Ross, "A Polar ^{18}F-Labeled Amino Acid Derivative for Click Labeling of Biomolecules," *European Journal of Organic Chemistry,* vol. 2013, no. 17, pp. 3546-50, 2014.

[13] J.M. Baskin, J.A. Prescher, S.T. Laughlin, N.J. Agard, P.V. Chang, I.A. Miller, A. Lo, J.A. Codelli, and C.R. Bertozzi, "Copper-free click chemistry for dynamic *in vivo* imaging," *Proceedings of the National Academy of Sciences*, vol. 105, no. 43, pp. 16793-7, 2007.

[14] A. Kuzmin, A. Poloukhtine, M.A. Wolfert, and V.V. Popik, "Surface Functionalization Using Catalyst-free Azide-Alkyne Cycloaddition," *Bioconjugate Chemistry*, vol. 21, no. 11, pp. 2076-85, 2010.

[15] S. Arumugam, J. Chin, R. Schirmacher, V. V. Popik, and A. P. Kostikov, "[^{18}F]Azadibenzocyclooctyne ([^{18}F]ADIBO): A biocompatible radioactive labeling synthon for peptides using catalyst free [3+2] cycloaddition," *Bioorganic & Medicinal Chemistry Letters,* vol. 21, no. 23, pp. 6987-91, 2011.

[16] A. Almutairi, R. Rossin, M. Shokeen, A. Hagooly, A. Ananth, B. Capoccia, S- Guillaudeu, D. Abendschein, C. J. Anderson, M. J. Welch, and J. M. J. Fréchet, "Biodegradable dendritic positron-emitting nanoprobes for the noninvasive imaging of angiogenesis," *Proceedings of the National Academy of Sciences,* vol. 106, no.3, pp. 685-90, 2009.

[17] Z.-B. Li, Z. Wu, K. Chen, F. T. Chin, and X. Chen, "Click Chemistry for ^{18}F-Labeling of RGD Peptides and microPET Imaging of Tumor Integrin $\mu_v N_3$ Expression," *Bioconjugate Chemistry*, vol. 18, no.6, pp. 1987-94, 2007.

[18] O. Seitz, and H. Kunz, "HYCRON, an Allylic Anchor for High-Efficiency Solid Phase Synthesis of Protected Peptides and Glycopeptides," The *Journal of Organic Chemistry*, vol. 62, no. 4, pp. 813-26, 1997.

[19] S. A. Campos, J. D. Harling, A. H. Miah, and I. E. D. Smith, "Proteolysis targeting chimeras (protacs) directed to the modulation of the estrogen receptor," *Patent*, WO 2014108452 A1, 2014.

[20] S. Keil, C. Claus, W. Dippold, and H. Kunz, "Towards the Development of Antitumor Vaccines: A Synthetic Conjugate of a Tumor-Associated MUC1 Glycopeptide Antigen and a Tetanus Toxin Epitope," Angewandte Chemie International Edition, vol. 40, no.2, pp. 36669, 2001.

[21] Y. Hirata, S. Hosoe, M. Maemoto, M. Sugawara, A. Yanagisawa, and J. Ouchi, "Fused thiophene derivative," *Patent*, WO 2013129435 A1, 2013.

[22] M. Amblard, J. Fehrentz, J. Mertinez, and G. Subra, "Methods and protocols of modern solid phase peptide synthesis," *Molecular Biotechnology,* vol. 33, no. 3, pp. 239-54, 2006.

[23] C. P. Leamon, and P. S. Low, "Folate-mediated targeting: from diagnosis to drug and gene delivery," *Drug Discovery Today*, vol. 6, no. 1, pp. 44-51, 2001.

[24] W. Siegrist, F. Solca, S. Stutz, L. Giuffre, S. Carrel, J. Girard, and A. Eberle, "Characterization of Receptors of ɲ-Melanocyte-stimulating Hormone on Human Melanoma Cells," *Cancer Research,* vol. 49, no. 22, pp. 6352-58, 1989.

[25] F. Salazar-Onfray, M. López, A. Lundqvist, A. Aguirre, A. Escobar, A. Serrano, C. Korenblit, M. Petersson, V. Chhajlani, O. Larsson, and R. Kiessling, "Tissue distribution and differential expression of Melanocortin 1 receptor, a malignant melanoma marker," *British Journal of Cancer,* vol. 87, no.4, pp. 414-22, 2002.

Supplementary Data

A ^{18}F-labeled Dibencocyclooctyne (DBCO) derivative for Copperfree Click Labeling of Biomolecules

Kathrin Kettenbach[1], Tobias L. Ross[1,2]

[1] Institute of Nuclear Chemistry, Johannes Gutenberg University Mainz, 55128 Mainz, Germany

[2] Radiopharmaceutical Chemistry, Department of Nuclear Medicine, Hannover Medical School, 30625

Hannover, Germany

Content

I. Organic Syntheses of Dibenzocyclooctyne(DBCO)-Derivatives

I.1. General

All regents were purchased from Acros Organics, Bachem, Deutero, Fisher-Scientific, Fluka, Jena Bioscience, Lancester, Merck AG, Sigma-Aldrich, Solvay-Organics and VWR and used without further purification. Reactions were monitored using thin layer chromatography (performed in Merck silica gel 60 F254) or high-performance liquid chromatography (HPLC). ^{1}H NMR spectra and ^{19}F NMR spectra were recorded using an AC-300-Spektrometer (300-MHz-T-NMR-spectrometer AC 300, Bruker Analytik GmbH) in $DCCl_3$ or DMSO-d_6. ^{13}C NMR spectra were measured on an Avance II-400Spectrometer (400 MHz). Chemical shifts for ^{1}H NMR and ^{13}C NMR were referenced to tetramethylsilane (0.00 ppm) and ^{19}F NMR were referenced to trichloro-fluoro-methane (0.00 ppm). FD and ESI mass spectrometry were performed on a MAT 95-MS 7500 CE and a HP 4500 (Agilent Technologies and Hewlett-Packard, respectively, both Santa Clara, CA, USA).

Radiosyntheses were performed manually (starting activities < 4 GBq) using conventional heating. Analytical HPLC analysis and radio-HPLC were performed on a Dionex P680A pump, a Raytest NaI scintillation counter (Gabi) and a Dionex UVD 170U (254 nm) absorbance detector. Dionex Chromeleon software was used for UV-data analysis and Raytest Gina star software for radioactivity detection.

Ethical statement

All experiments with commercial available human serum (Sigma Aldrich, H4522, from human male AB plasma) were conducted in accordance with the local law and national and institutional guidelines and ethics. The officer for biological safety has approved the performed experiments and informed consent was obtained for any experiment with commercial available human serum.

I. 2. Synthesis of DBCO labeling precursor

Tert-butyl-3-(2-(2-(2-hydroxyethoxy)ethoxy)ethoxy)propanoate (3)

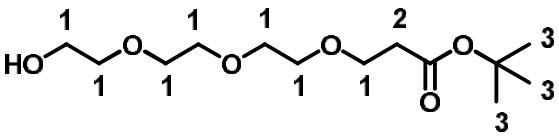

To a solution of triethylene glycol 1 (5.8 g, 38.6 mmol) in dry tetrahydrofuran (60 mL) sodium (12.8 mg, 0.56 mmol) was added and stirred for 30 min at rt. Then *tert*-butyl acrylate (2.28 g, 17.8 mmol) was added and the reaction was stirred for 24 h at rt. 400 µL 1 M hydrochloric acid were added to neutralize the reaction solution. Ethyl acetate (20 mL) was added and the organic layer was extracted 3-times (10 mL) with water and brine. The organic layers

were dried over magnesium sulfate and the solvent was removed under reduced pressure obtaining 3 as colorless oil (3.65 mg, 13.12 mmol, 74 %).

^{1}H-NMR (300 MHz, $CDCl_3$, Me_4Si): ω [ppm] = 1.42 (s, 9H, 3-H), 2.48 (2H, t, 6.5 Hz, 2-H), 3.61 – 3.71 (14H, m, 1-H).

MS (ESI positive): m/z 301.13 ([M+Na]$^+$, 73.12 %), 317.13 ([M+K]$^+$, 62.19 %), calculated for $C_{13}H_{26}O_6$: 278.34.

Tert-butyl-3-(2-(2-(2-tosyloxyethoxy)ethoxy)ethoxy)propanoate (4)

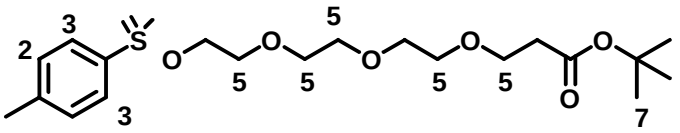

Compound 3 (1.02 g, 3.65 mmol) and **7** triethylamine (0.87 mL, 0.63 mg, 6.24 mmol) were dissolved in **1** **2** dichloromethane (20 mL) and cooled to 0 °C. Then toluenesulfonyl chloride (720 mg, 4.2 mmol) was added and the reaction mixture was stirred for 10 minutes at 0 °C. The ice bath was removed and the reaction was stirred for an additional hour at rt. The solvent was removed under reduced pressure and the product was purified by column chromatography (n-hexane:ethyl acetate/2:1, R_f = 0.24) obtaining 4 as colorless oil (1.05 g, 2.43 mmol, 67 %).

^{1}H-NMR (300 MHz, $CDCl_3$, Me_4Si): ω [ppm] = 1.44 (9H, s, 7-H), 2.44 (3H, s, 1-H), 2.49 (2H, t, 6.5 Hz, 6H), 3.59 – 3.68 (12H, m, 5-H), 4.15 (2H, t, 4.9 Hz, 4-H), 7.32 (2H, d, 8.8 Hz, 2-H), 7.78 (2H, d, 8.2 Hz, 3-H).

MS (ESI positive): m/z 455.20 ([M+Na]$^+$), 471.17 ([M+K]$^+$), calculated for $C_{34}H_{38}N_2O_8S$: 432.53. 3-(2-(2-(2-tosyloxyethoxy)ethoxy)ethoxy)propanoate (5)

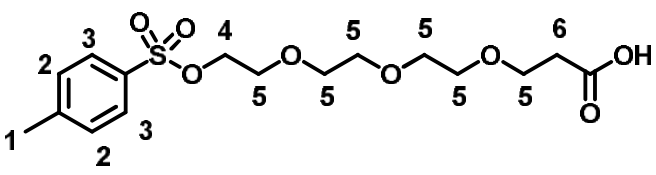

Compound 4 (100 mg, 0.32 mmol) was dissolved in dichloromethane chloride (1.3 mL) and the carboxyl acid function was deprotected with trifluoroacetic acid (1.3 mL, 1.94 g, 17 mmol) for 4 h. The solvent was removed under reduced pressure and the trifluoroacetic acid was removed by codestillation with toluene (4-times, 3 mL each), obtaining 5 as colorless oil (86 mg, 0.22 mmol, 99 %).

^{1}H-NMR (300 MHz, $CDCl_3$, Me_4Si): ω [ppm] = 2.44 (3H, s, 1-H), 2.63 (2H, t, 6.2 Hz, 6-H), 3.59 (8H, m, 5H), 3.69 (2H, t, 5 Hz, 5-H) 3.76 (2H, t, 6.1 Hz, 5-H), 4.15 (2H, t, 4.7 Hz, 4-H), 7.33 (2H, d, 8.4 Hz, 2-H), 7.78 (2H, d, 8.5 Hz, 3-H).

MS (ESI positive): m/z 399.13 ([M+Na]$^+$), 415.11 ([M+K]$^+$), calculated for $C_{16}H_{24}O_8S$: 376.12.

Tert-butyl-3-(2-(2-(2-mesyloxyethoxy)ethoxy)ethoxy)propanoate (6)

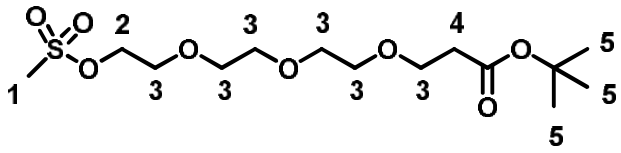

Compound 3 (500 mg, 1.8 mmol) and triethylamine (0.42mL, 0.31 mg, 3.1 mmol) were dissolved in dichloromethane (10 mL) and cooled to 0 °C. Then methanesulfonyl chloride (266 mg, 1.97 mmol) was added and the reaction mixture was stirred for 10 minutes at 0 °C. The ice bath was removed and the reaction was stirred for an additional hour at rt. The solvent was removed under reduced pressure and the product was purified by column chromatography (n-hexane:ethyl acetate/1:1, R_f = 0.2) obtaining 6 as colorless oil (567 mg, 1.6 mmol, 88 %).

^{1}H-NMR (300 MHz, $CDCl_3$, Me_4Si): ω [ppm] = 1.44 (9H, s, 5-H), 2.49 (2H, t, 6.5 Hz, 4-H), 3.07 (3H, s, 1H), 3.56 – 3.77 (12H, m, 3-H), 4.37 (2H, t, 4.6 Hz, 2-H).

MS (ESI positive): m/z 379.12 ([M+Na], 100 %), 395.11 ([M+K], 78.67 %), calculated for $C_{10}H_{20}O_8S$: 356.16.

3-(2-(2-(2-mesyloxyethoxy)ethoxy)ethoxy)propanoate (7)

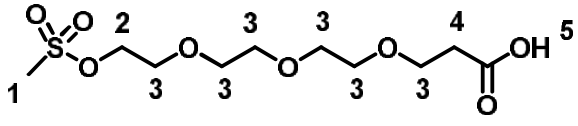

Compound 6 (100 mg, 0.27 mmol) was dissolved in dichloromethane chloride (1.3 mL) and the carboxic acid function was deprotected with trifluoroacetic acid (1.3 mL, 1.94 g, 17 mmol) for 4 h. The solvent was removed under reduced pressure and the trifluoroacetic acid was removed by codestillation with toluene (4-times, 3 mL each), obtaining 7 as colorless oil (80 mg, 0.31 mmol, 98 %).

^{1}H-NMR (300 MHz, $CDCl_3$, Me_4Si): ω [ppm] = 2.60 (2H, t, 6.2 Hz, 4-H), 3.04 (3H, s, 1-H), 3.60 – 3.73 (12H, m, 3-H), 4.34 (2H, t, 4.5 Hz, 2-H), 9.15 (1H, s, 5-H).

MS (ESI positive): m/z 301.15([M]$^+$, 40.30 %, 323.06 ([M+Na]$^+$, 100 %), 339.06 ([M+K]$^+$, 63.77 %) calculated for $C_{10}H_{20}O_8S$: 300.09.

3-(2-(2-(2-tosyloxyethoxy)ethoxy)ethoxy)-N-[3-oxo-N-(DBCO)propyl]propanamid (9)

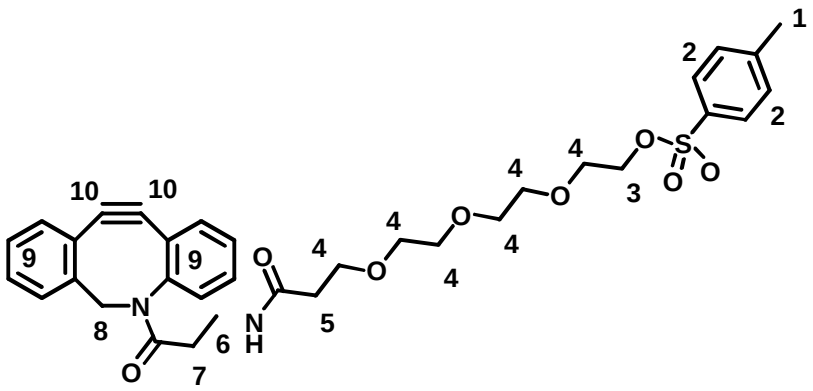

A solution of compound 5 (28 mg, 0.072 mmol), *N,N,N´,N´´*-Tetramethyl-*O*-(1-*H*-benzotriazol-1yl)uranium hexafluorophosphate (HBTU) (41 mg, 0.11 mmol) and *N,N*-Diisopropylethylamine (100 µL, 0,58 mmol) in dry dimethylformamide (1 mL) was stirred for 30 min at rt. Then Dibenzocyclooctyneamine (DBCO-amine) (20 mg, 0.072 mmol) was dissolved in dry dimethylformamide (1 mL) and added to the reaction solution. After stirring the reaction mixture at rt for 12 h, the solvent was removed under reduced pressure and the product was purified by column chromatography

(dichloromethane:methanol/30:1, R_f = 0.22) obtaining 9 as yellow oil (25 mg, 0.04 mmol, 56 %). ^{13}C-NMR (400 MHz, $CDCl_3$, Me_4Si): ω [ppm] =21.69 (1-C), 34.34 (7-C), 35.39 (6-C), 36.32 (5-C), 55.45 (8C), 66.69 – 70.68 (4-C), 107.83 (10-*C*), 114.62 – 150.85 (9-C).

MS (ESI positive): m/z 635.22 ([M]$^+$, 100 %), 657.21 ([M+Na]$^+$, 25.92 %), 673.19 ([M+K]$^+$, 3.99 %), m/z (high resolution) 657.2259 ([M+Na]$^+$, 100 %), calculated for $C_{34}H_{38}N_2O_8S$: 634.2349.

[1] H-NMR (400 MHz, $CDCl_3$, Me_4Si): ω [ppm] = 1.98 (1H, m, 7-H) und 2.58 (1H, m, 7-H), 2.38 (2H, d, 6 Hz, 5-H), 2.45 (3H, s, 1-H), 3.26 – 3.39 (2H, m, 6-H), 3.49 – 3.75 (13 H, m, 4-H und 8-H), 4.15 (2H, t, 4.7 Hz, 3-H), 5.15 (1H, dd, 8 Hz & 14.5 Hz, 8-H), 7.25 – 7.44 (9H, m, 9-H und 2-H), 7.66 (1H, d, 7.7 Hz, 9-H), 7.78 (2H, d, 9.0 Hz, 2-H).

3-(2-(2-(2-mesyloxyethoxy)ethoxy)ethoxy)-N-[3-oxo-N-(DBCO)propyl]propanamid (10)

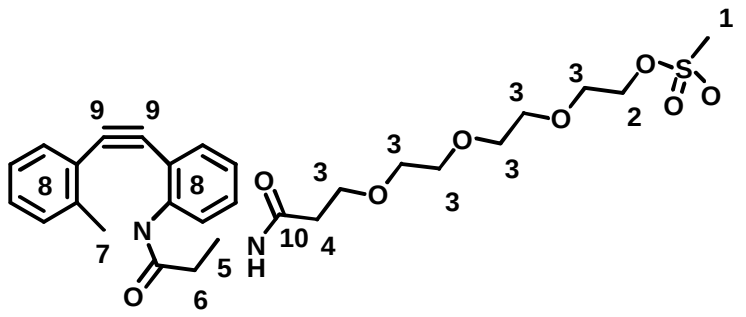

A solution of compound 7 (22 mg, 0.072 mmol), *N,N,N´,N´´*-Tetramethyl-*O*-(1-*H*-benzotriazol-1yl)uranium hexafluorophosphate (HBTU) (41 mg, 0.11 mmol) and *N,N*-Diisopropylethylamine (100 µL, 0,58 mmol) in dry dimethylformamide (1 mL) was stirred for 30 min at RT. Then Dibenzocyclooctyneamine (DBCO-amine) (20 mg, 0.072 mmol) was dissolved in dry dimethylformamide (1 mL) and added to the reaction solution. After stirring the reaction mixture at RT for 12 h, the solvent was removed under reduced pressure and the product was purified by column chromatography
(dichloromethane:methanol/20:1, R_f = 0.27) obtaining 10 as yellow oil (30 mg, 0.05 mmol, 87 %).

^{1}H-NMR (400 MHz, $CDCl_3$, Me_4Si): ω [ppm] = 1.97 – 2.02 (1H, m, 6-H) und 2.52. – 2.54 (1H, m, 6-H), 2.37 (2H, dd, 5.6 HZ & 6.6 Hz, 4-H), 3.07 (3H, s, 1-H), 3.3 (2H, m, 5-H), 3.52 – 3.64 (10 H, m, 3-H), 3.75 (3 H, m, 3-H und 7-H), 4.36 (2H, t, 4.6 Hz, 2-H), 5.13 – 5.16 (1H, d, 13.7 Hz, 7-H), 7.32 – 7.42 (7H, m, 8H), 7.67 – 7.69 (1H, d, 7.5 Hz, 8-H).

^{13}C-NMR (400 MHz, $CDCl_3$, Me_4Si): ω [ppm] = 34.54 (6-C), 35.41 (5-C), 36.56 (4-C), 37.67 (1-C), 55.55 (7-C), 66.92 – 70.62 (3-C), 107.77 (9-C), 114.68 – 150.97 (8-C), 171.92 (10-C).

MS (ESI positive): m/z 581.15 ($[M+Na]^+$, 100 %), 597.17 ($[M+K]^+$, 11.74 %); calculated for $C_{28}H_{34}N_2O_8S$: 558.2036.

I. 2. Synthesis of DBCO reference compound

3-(2-(2-(2-fluoroethoxy)ethoxy)ethoxy)-N-[3-oxo-N-(DBCO)propyl]propanamid (11)

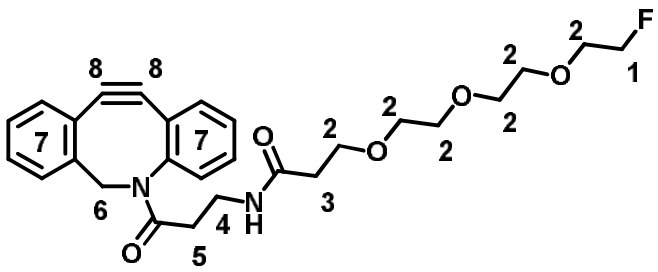

A solution of compound 9 (29.5 mg, 0,047 mmol) and tetrabutylammonium fluoride (93.5 µL, 0,093 mmol) in dry tetrahydrofuran (15 mL) was heated to reflux for 2 h. The solvent was removed under reduced pressure. The product was purified by column chromatography (dichloromethane:methanol/30:2, R_f = 0.38) obtaining 11 as a colorless oil (18.4 mg, 0.038 mmol, 82 %)

^{1}H-NMR (400 MHz, $CDCl_3$, Me_4Si): ω [ppm] = 1.95 – 2.02 (1H, m, 5-H), 2.35 (2H, dd, 5.6 Hz und 6.7 Hz, 3-H), 2.50 (1H, dd, 2.8 Hz und 4.7 Hz, 1-H), 3.24 – 3.40 (2H, m, 4-H), 3.61 – 3.72 (12H, m, 2-H), 3.77 (1H, t, 4.2 Hz, 6-H), 4.50 (1H, t, 4.1 Hz, 1-H), 4.62 (1H, t, 4.4 Hz, 1-H), 5.11 (1H, d, 14.4 Hz, 6-H), 7.29 – 7.44 (7 H, m, 7-H), 7.68 (1H, d, 7.2 Hz, 7-H)

^{13}C-NMR (400 MHz, $CDCl_3$, Me_4Si): ω [ppm] = 34.76 (5-C), 35.17 (4-C), 36.86 (3-C), 55.49 (6-C), 67.11 – 70.82 (2-C), 107.56 (8-C), 125.70 – 132.37 (7-C)

^{19}F-NMR (400 MHz, $CDCl_3$, CCl_3F): ω [ppm] = -77.20

MS (ESI positive): m/z 483.24 ($[M]^+$, 100 %), 505.22 ($[M + Na]^+$, 40.82 %), 521.20 ($[M+K]^+$, 4.59 %); m/z (high resolution) 483.2306 ($[M]^+$, 100 %); 505.2107 ($[M+Na]^+$, 100 %); calculated for $C_{27}H_{31}FN_2O_5$: 482.2217

II. ^{18}F-labeling of DBCO precursor

II.1. General radiolabeling methods

N.c.a. [^{18}F]fluoride ion was produced using the $^{18}O(p,n)^{18}F$ nuclear reaction. The aqueous ^{18}F-solution was then trapped on an anion exchange resin (Sep Pak light Waters Accell Plus QMA cartridge), which was pre-conditioned with 1 M potassium carbonate solution (10 mL) and rinsed with millipore water (10 mL). For the elution of the QMA either tetrabutylammonium hydroxide solution or tetraethylammonium bicarbonate solution was used. The reaction kinetic was screened via radio-TLC by taking aliquots after 1, 3, 5, 10, 15, 30 min after addition of the activity to the precursor. The labeling reaction was optimized due to the amount of precursor, use of different bases and base concentrations and reaction time.

II.1.1.Tetrabutylammonium hydroxide solution (TBA-OH)

Elution of the [^{18}F]fluoride ion from the QMA cartridge was performed using 900 µl of a methanolic tetrabutylammoniumhydroxide solution (TBA-OH x 30 H_2O in 2 mL methanol). The azeotropic drying was performed using a helium stream and heating to 85 °C for 20 min under reduced pressure (250 mbar). Within this time, dry acetonitrile (3 x 1 mL) was added and evaporated to yield final dry [^{18}F]fluoride-base mixture.

II.1.2. Tetraethylammonium bicarbonate solution ($Et_4N{\cdot}HCO_3$)

Elution of the ^{18}F-fluoride ion from the QMA cartridge was performed using a solution (450 µL or more), containing tetraethylammonium bicarbonate (3.4 mg, 17 µmol) dissolved in acetonitrile (405 µL) and water (45 µL). The azeotropic drying was performed using a helium stream and heating to 85 °C for 20 min under reduced pressure (250 mbar). Within this time dry acetonitrile (4 x 1 mL) was added and evaporated to yield final dry [^{18}F]fluoride-base mixture.

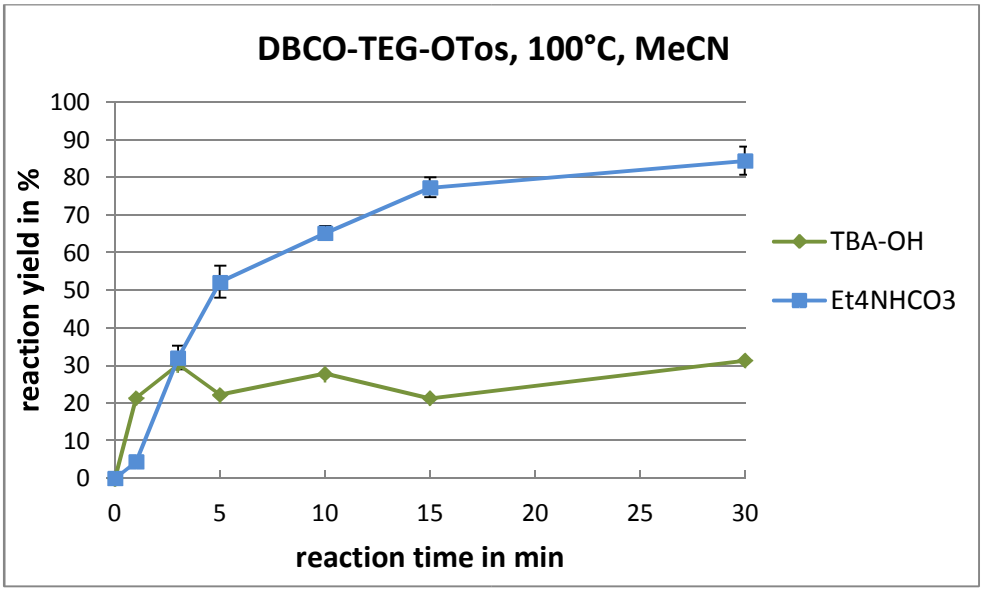

Figure 1: Radiolabeling kinetics of [^{18}F]11 at 100 °C in dependence on the use of two different bases (Tetrabutylammonium hydroxide and Tetraethylammonium bicarbonate).

II.2. Synthesis of [^{18}F]11

After azeotropic drying of the [^{18}F]fluoride ion, the [^{18}F]fluoride-base mixture was dissolved in acetonitrile (0.5 mL) and transferred into a 5-mL sealed reaction vial containing the DBCO-precursor 9 dissolved in acetonitrile (0.5 mL). The reaction mixture was heated to 100 °C for 15 min (30 min for determining the kinetics) followed by quenching the labeling reaction with water (1 mL) and injection into a semi-preperative HPLC system at a flow of 2.5 mL/min, whereas A is water and B is acetonitrile. The following method was used: 50 % A (isocratic).After purification using semi-preparativ HPLC

(figure 2), the fraction was diluted with water (10 mL) and fixed on a Sep-Pak light SPE cartridge (Sep Pak Light tC18). The fixed ^{18}F-prosthetic group was eluted with acetonitrile (1 mL) into a reaction vessel and the acetonitrile was removed using helium steam at 85 °C under reduced pressure (500 mbar) within 15 min. The dried prosthetic group was solved in the preferred reaction solvent to perform the click reaction. The ^{18}F-prosthetic group was prepared in an overall reaction time of 60 min in one step with an overall yield (n.d.c.) of (34±5) %.

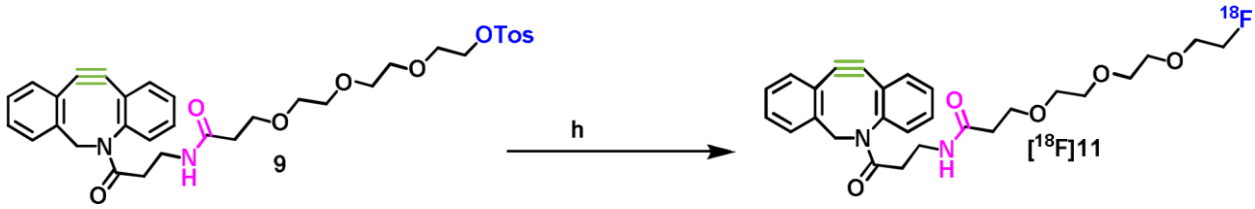

Scheme 1: Radiolabeling of prosthetic group [^{18}F]11. Regents and conditions: h.) $Et_4N{\cdot}HCO_3/^{18}F^-$, acetonitrile, 100 °C, 15 min.

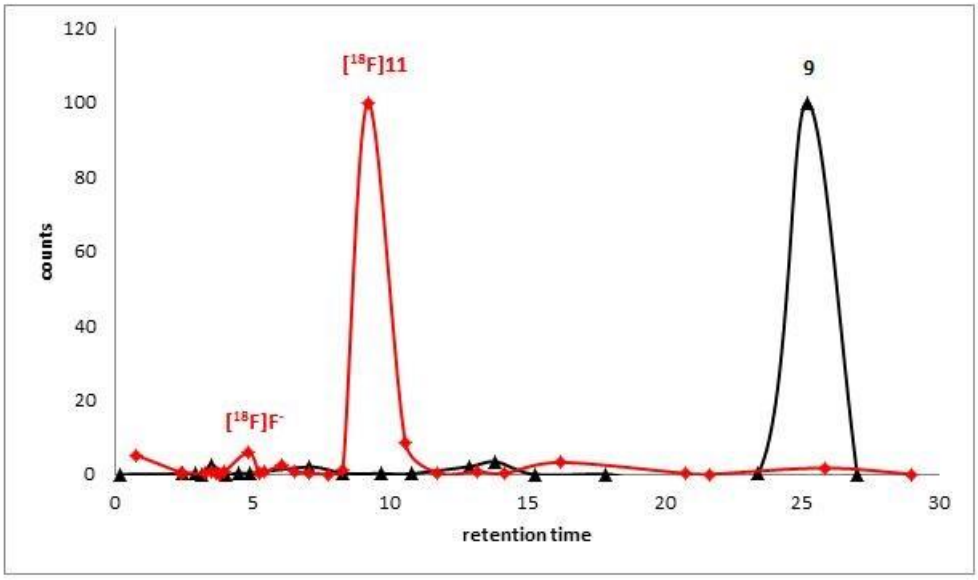

Figure 2: Analytical radio-HPLC chromatogram of the crude reaction mixture of the radiosynthesis of [^{18}F]11. Peak intensities are normalized to the maximum intensity. Analytical (radio-)HPLC was performed with a Phenomenex Luna C18 column (5 µm, 250x10 mm) with the following conditions: Flow of 0.7 mL min-1, with an isocratic eluent of water/acetonitrile (1:1) for 30 min. Red is the radioactive trace and black is the UV trace.

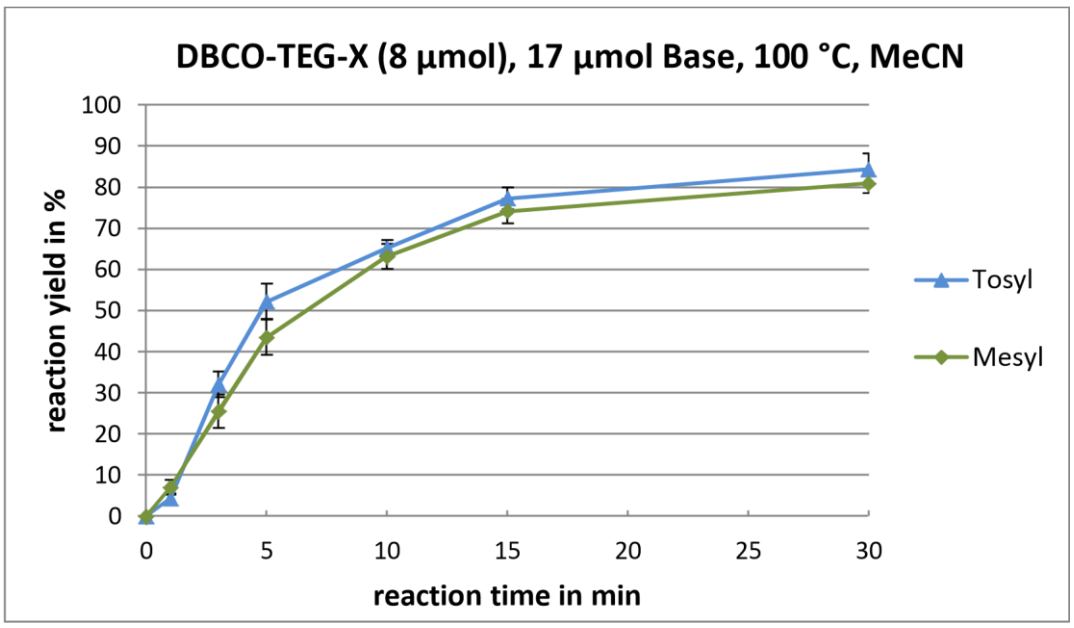

Figure 3: Radiolabeling kinetics of [^{18}F]11 at 100 °C in dependence on different leaving groups (tosyl and mesyl).

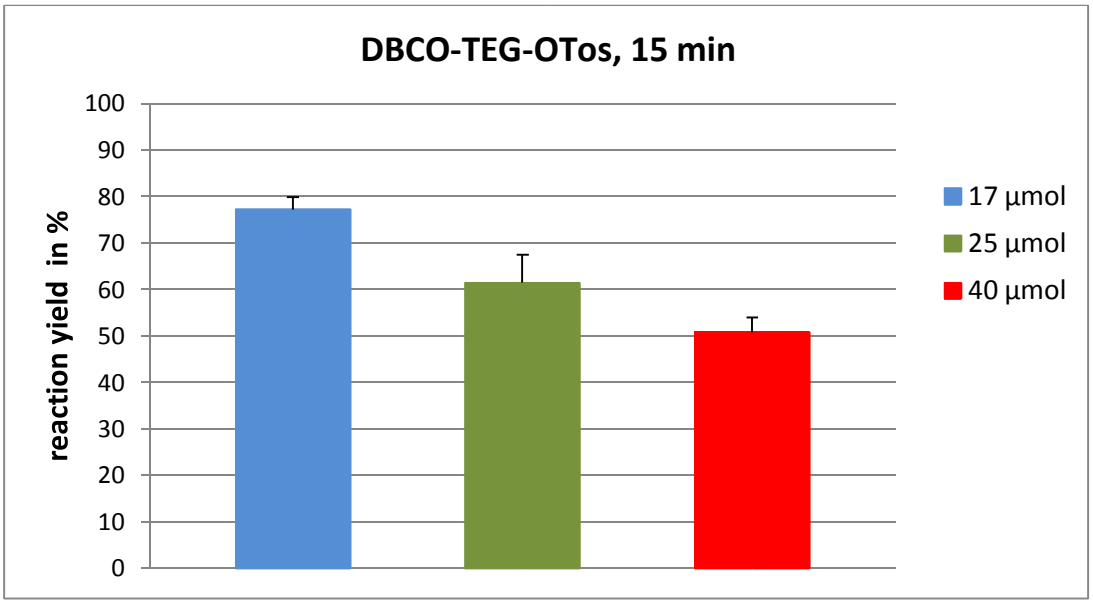

Figure 4: Radiolabeling kinetics of [^{18}F]11 at 100 °C in dependence on the amount of tetraethylammonium bicarbonate.

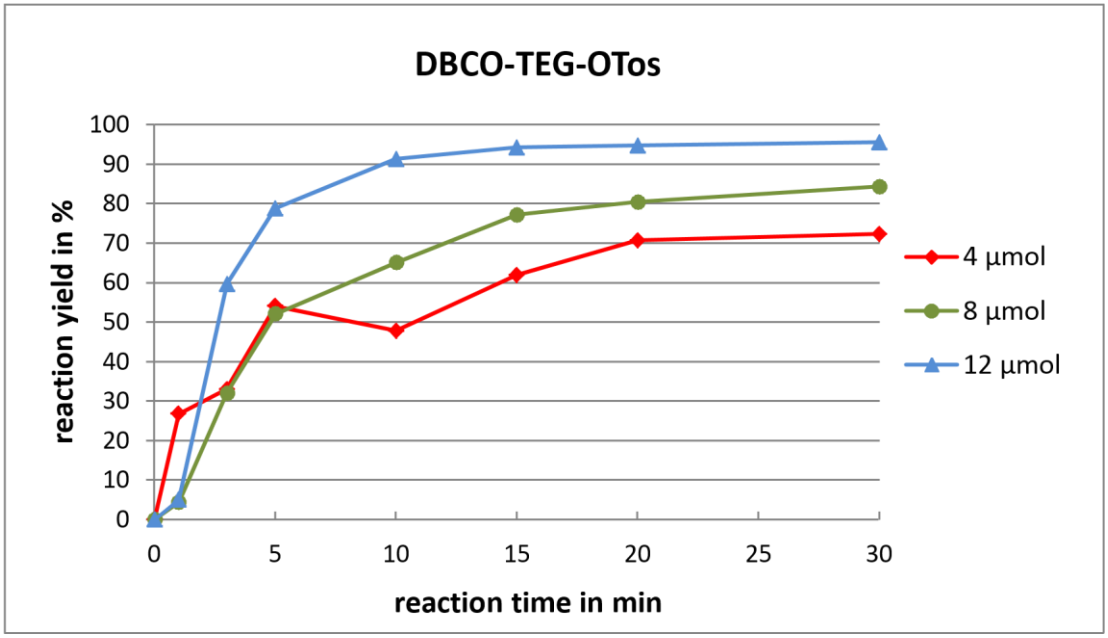

Figure 5: Radiolabeling kinetics of [^{18}F]11 at 100 °C in dependence on the amount of precursor 9.

II.3. Octanol-water partition coefficient (logD octanol/water)

To determine the lipophilicity of the radiolabeled ^{18}F-prostehtic group, approximately 0.55 mCi of the radiolabeled prosthetic group were diluted in 0.7 mL phosphate-buffered saline (PBS). An equal volume of 1-octanole was added to obtain a binary phase system. After stirring the samples at 1.500 1/min for 2 min, the two layers were separated by centrifuge (12.000 U/min for 2 min). 300-µL samples were taken from each layer and radioactivity was measured using a curimeter. Besides activity was also determined using a TLC plate.

III. Labeling of Biomolecules

III.1. Copper-free cycloaddition of [^{18}F]11 and azido-functionalized cRDG as model system

The prosthetic group [^{18}F]11 was dissolved in PBS buffer (200 µL) and acetonitrile (100 µL) and cRGD 12 (1 mg, 1.1 µmol) in 50 µL acetonitrile/water (1:1) was added. Independent from temperature (25 °C and 40 °C) RCY of ш 80 % were observed after 5 min. Decreased precursor amount leaded to slower kinetics and an overall lower RCY of only 75 %.

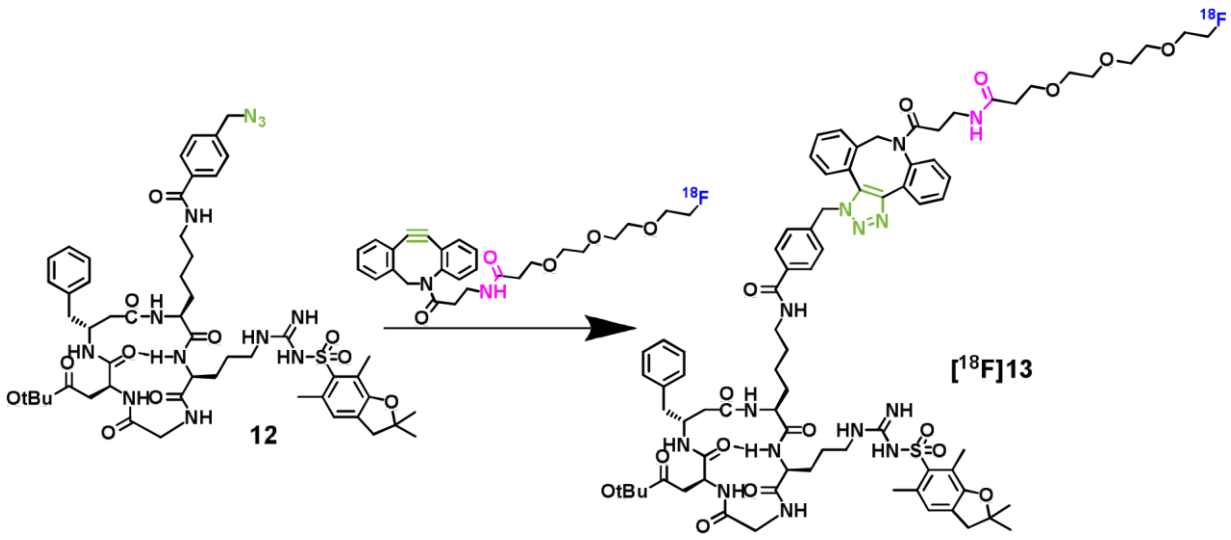

Scheme 2: SPAAC of protected azido-functionalized cRGD 12 and the new prosthetic group [^{18}F]11. Click reaction conditions: PBS buffer/acetonitrile (1:1), 25 °C or 40 °C, 30 min.

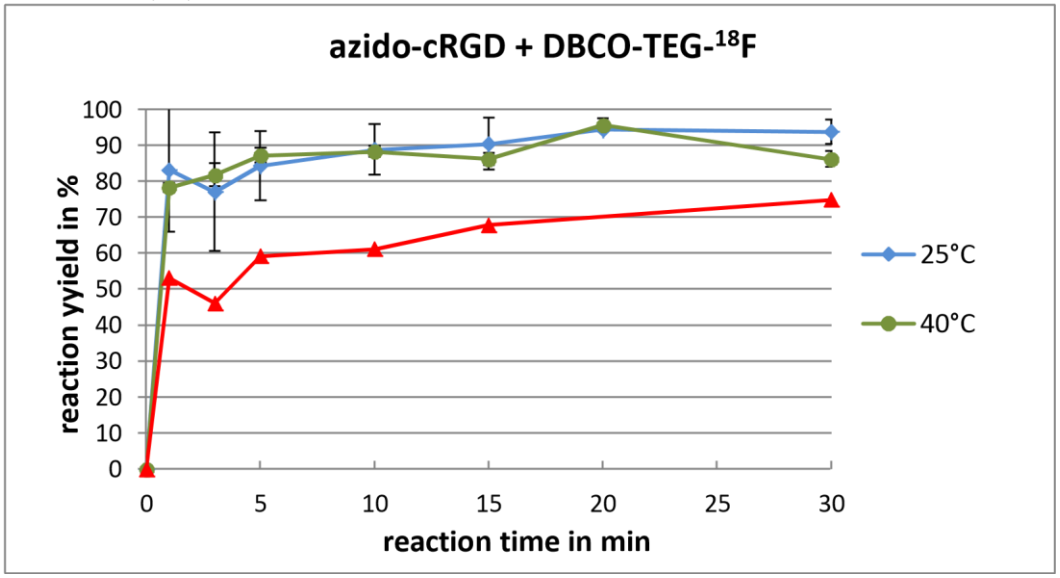

Figure 6: Radiolabeling kinetics of cRGD 12 with [^{18}F]11 in dependence on temperature and precursor amount.

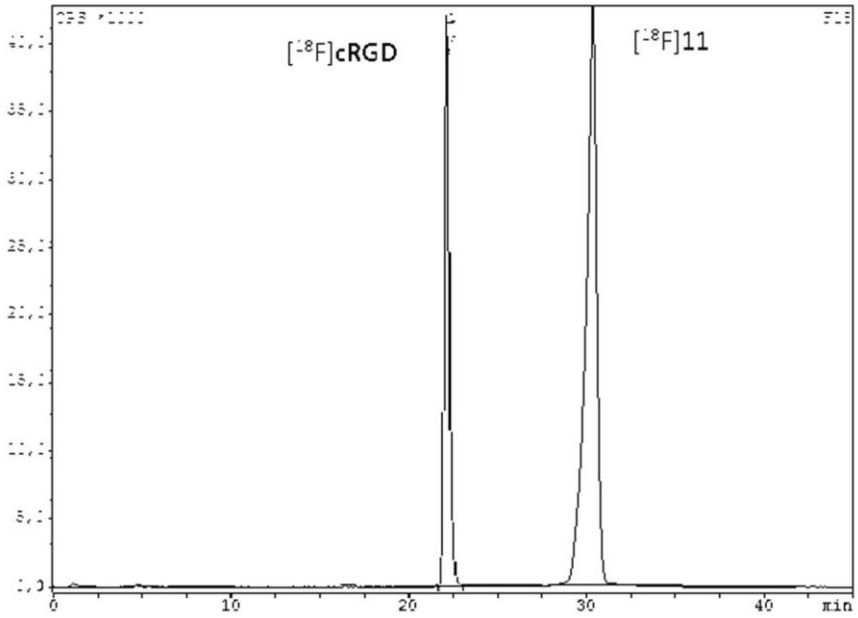

Figure 7: Analytical radio-HPLC chromatogram of the click radiosynthesis of [^{18}F]RGD. Analytical radio-HPLC was performed with a Phenomenex Luna C18 column (5 µm, 250x20 mm) using the following conditions: Flow 0.7 ml min-1, with eluent A was water with 0.1 % TFA (trifluoroacetic acid) and eluent B was acetonitrile with 0.1 % TFA. The following method was used: 0 - 40 min, 5 – 95 % eluent B (gradient).

III.2. Copper-free cycloaddition of [^{18}F]11 and azido-functionalized ɲ-MSH analogue Peptide

The prosthetic group [^{18}F]11 was dissolved in PBS buffer (200 µL) and ɲ-MSH Peptide 14 (0.5 mg, 0.4 µmol and 0.125 mg, 0.1 µmol) in 200 µL PBS was added. RCYs varied between 44 % and 79 % depending a lot on precursor amount (0.1 µmol and 0.4 µmol) and temperature (25 °C and 40 °C).

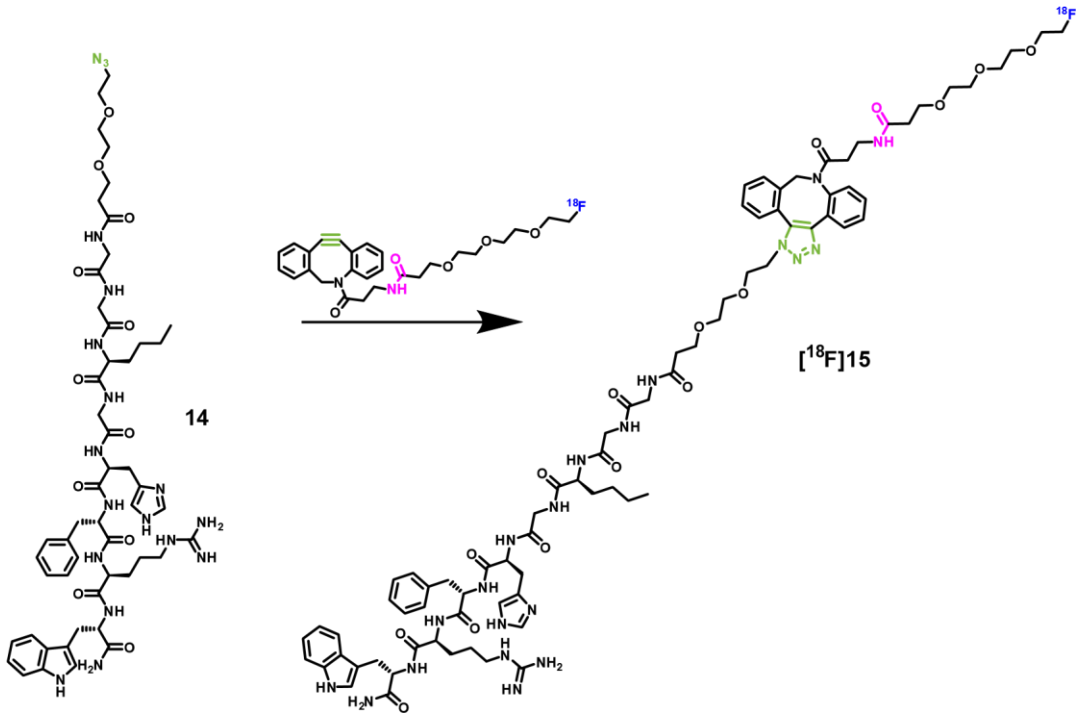

Scheme 3: SPAAC of ɲ-MSH Peptide 14 and prosthetic group [^{18}F]11. Click reaction conditions: PBS buffer 25 °C and 40 °C, 30 min.

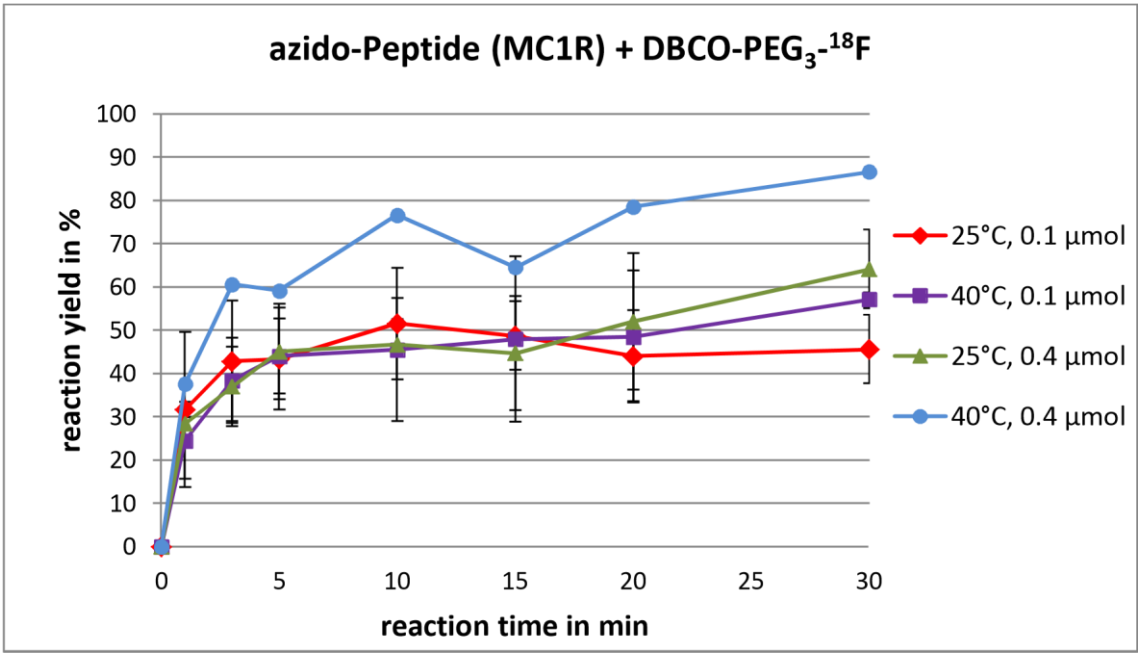

Figure 8: Radiolabeling kinetics of ɲ-MSH Peptide 14 with [^{18}F]11 in dependence on temperature and precursor amount.

III.3. Copper-free cycloaddition of [^{18}F]11 and azido-functionalized folate-derivative

The prosthetic group [^{18}F]11 was dissolved in PBS buffer (200 µL) and azide-funktionalized folatederivative 16 (0.5 mg, 1 µmol) in 200 µL PBS was added. Quantitative labeling was observed after 3 min for 25 °C and 40 °C.

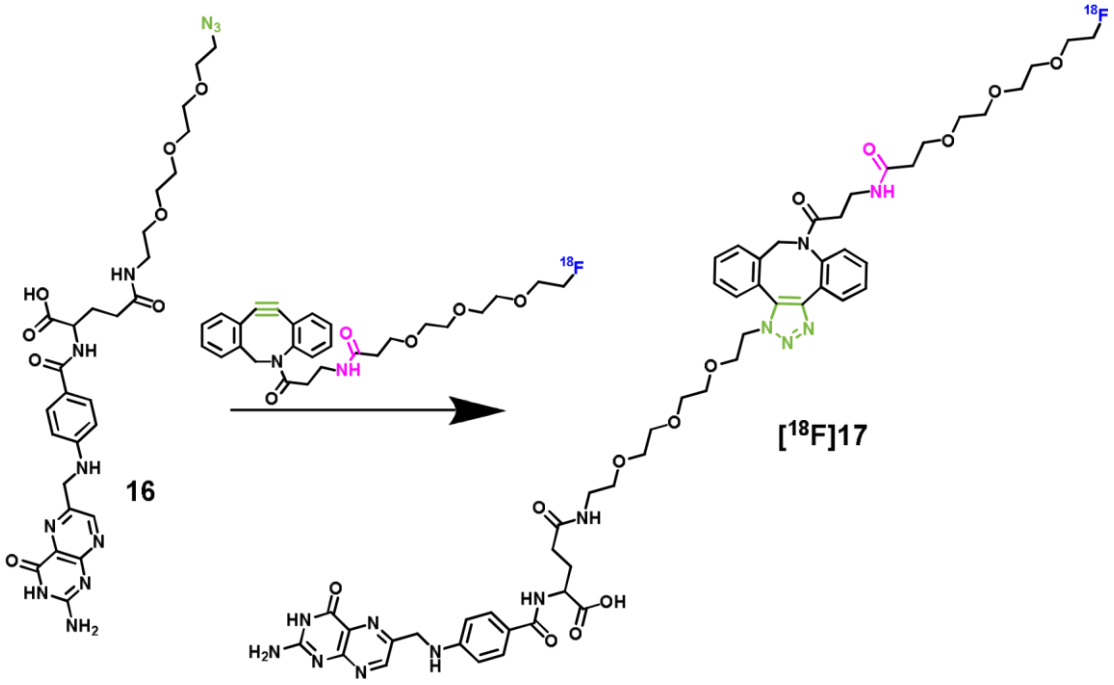

Scheme 4: SPAAC of azide-functionalized folate-derivative 16 and prosthetic group [^{18}F]11. Click reaction conditions: PBS buffer 25 °C and 40 °C, 30 min.

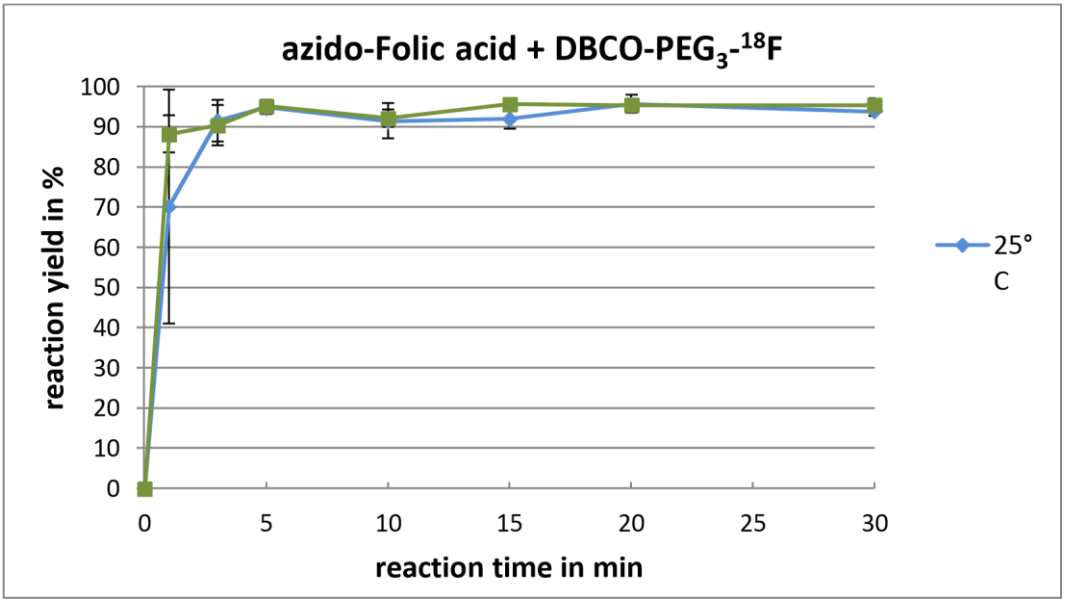

Figure 9: Radiolabeling kinetics of azido-folic acid 16 with [^{18}F]11 in dependence on temperature.

Table 1: Screening of copper-free cycloaddition reactions with various biomolecule-azides. [a] Conversion was determined by analytical radio TLC. Errors are given as standard deviation representing n = 3.

Compuond	M_W [g/mol]	Solvent	Amount	Temp.	Click time	RCY[a] [%]	cRGD
997.4		H_2O:MeCN (1:1)	1 µmol	25 °C	20 min	94.4 ± 0.6	
				40 °C		95.7 ± 1.7	
74.2	Folate-641.3	PBS	0.5 µmol	25 °C		95.7 ± 2.2	azide
							40 °C
	95.5 ± 1.3						
~~MC1R-~~	~~1112.6~~		~~0.1 µmol~~	~~25 °C~~		~~44.1 ± 10.5~~	
Peptide (linear)				40 °C		48.5 ± 15.3	
			0.4 µmol	25 °C		52.0 ± 15.9	
				40 °C		78.6 ± 2.7	
MC1R-Peptide (cyclic)	1316.6		0.2 µmol	40 °C		92.2 ± 3.2	

Ethical statement

All experiments with commercial available human serum (Sigma Aldrich, H4522, from human male AB plasma) were conducted in accordance with the local law and national and institutional guidelines and ethics. The officer for biological safety has approved the performed experiments and informed consent was obtained for any experiment with commercial available human serum.

Acknowledgments

The authors thank the Max Planck Graduate Center for supporting Kathrin Kettenbach.

IV. Analysis

IV.I. NMR data

Tert-butyl-3-(2-(2-(2-hydroxyethoxy)ethoxy)ethoxy)propanoate (3)

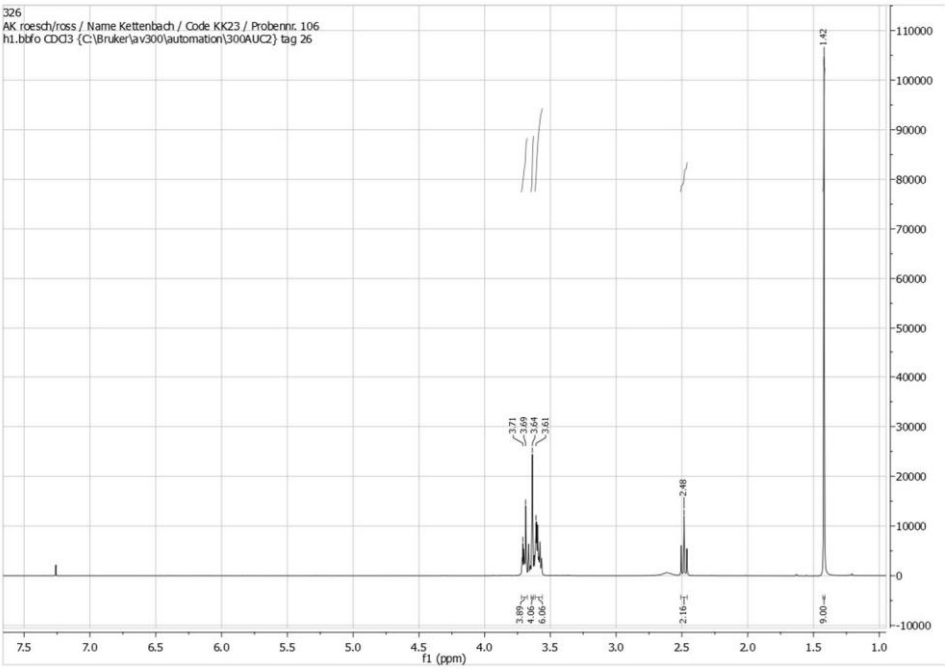

^{1}H-NMR (300 MHz, $CDCl_3$, Me_4Si): ω [ppm] = 1.42 (s, 9H, COOC*H*$_3$), 2.48 (2H, t, 6.5 Hz, C*H*$_2$COOCH$_3$), 3.61 – 3.71 (14H, m, PEG-C*H*$_2$).

Tert-butyl-3-(2-(2-(2-tosyloxyethoxy)ethoxy)ethoxy)propanoate (4)

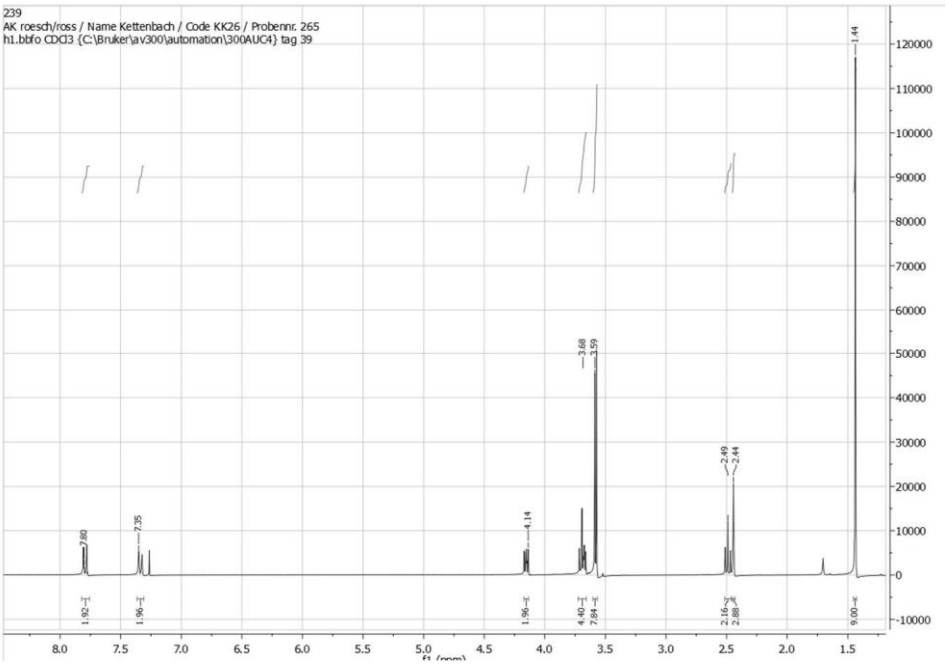

^{1}H-NMR (300 MHz, $CDCl_3$, Me_4Si): ω [ppm] = 1.44 (9H, s, COOC*H*$_3$), 2.44 (3H, s, Tosyl-C*H*$_3$), 2.49 (2H, t, 6.5 Hz, CH_3OOCC*H*$_2$), 3.59 – 3.68 (12H, m, PEG-C*H*$_2$), 4.15 (2H, t, 4.9 Hz, Tosyl-O-C*H*$_2$), 7.32 (2H, d, 8.8 Hz, Tosyl-C*H*), 7.78 (2H, d, 8.2 Hz, Tosyl-C*H*).

3-(2-(2-(2-tosyloxyethoxy)ethoxy)ethoxy)propanoate (5)

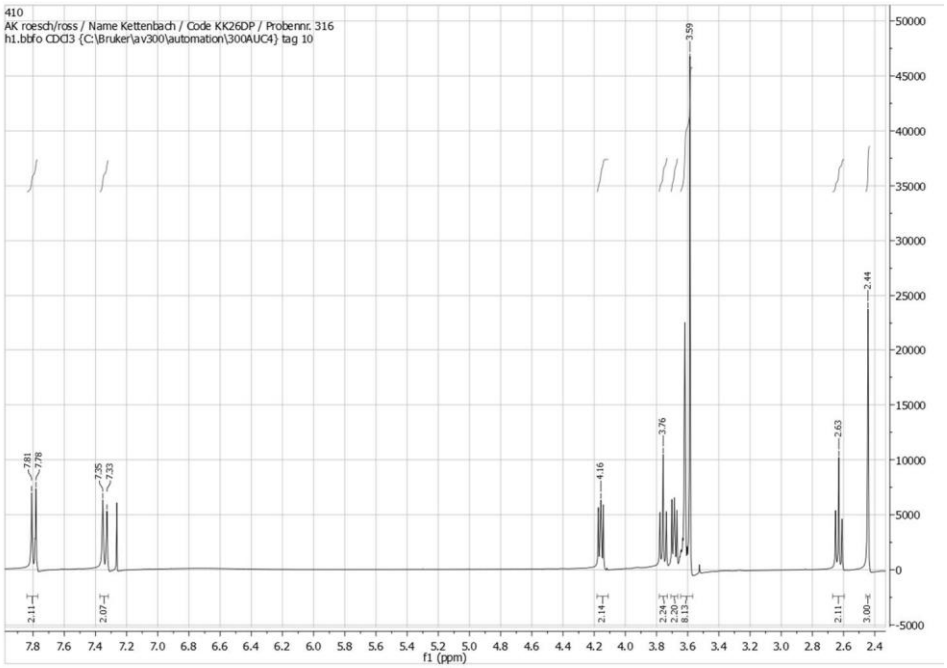

^{1}H-NMR (300 MHz, $CDCl_3$, Me_4Si): ω [ppm] = 2.44 (3H, s, Tosyl-C*H*$_3$), 2.63 (2H, t, 6.2 Hz, CH_3OOCCH_2), 3.59 (8H, m, PEG-C*H*$_2$), 3.69 (2H, t, 5 Hz, PEG-C*H*$_2$) 3.76 (2H, t, 6.1 Hz, PEG-C*H*$_2$), 4.15 (2H, t, 4.7 Hz, Tosyl-O-C*H*$_2$), 7.33 (2H, d, 8.4 Hz, Tosyl-C*H*), 7.78 (2H, d, 8.5 Hz, Tosyl-C*H*).

Tert-butyl-3-(2-(2-(2-mesyloxyethoxy)ethoxy)ethoxy)propanoate (6)

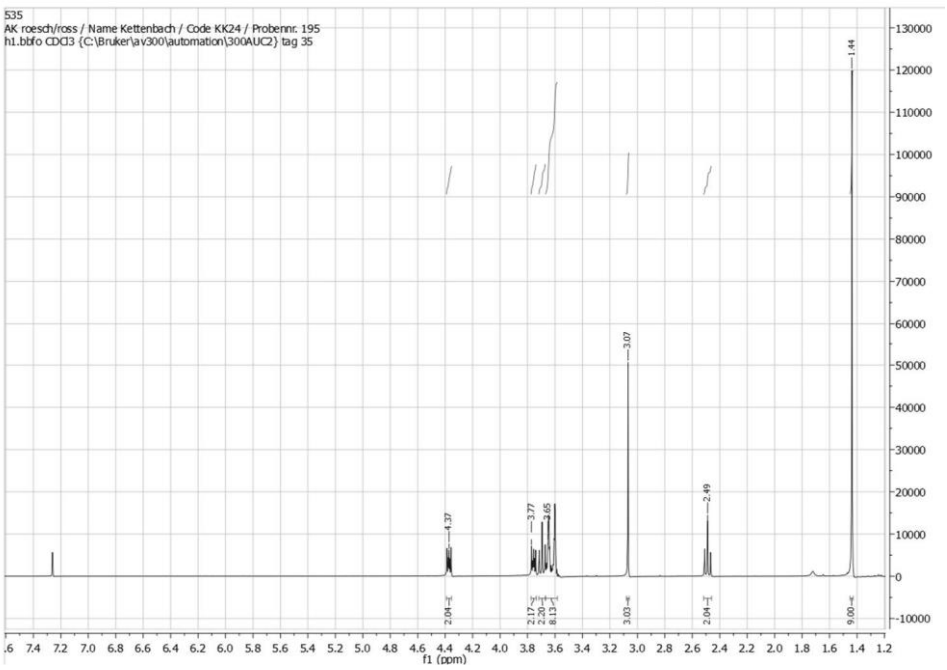

^{1}H-NMR (300 MHz, $CDCl_3$, Me_4Si): ω [ppm] = 1.44 (9H, s, COOC*H*$_3$), 2.49 (2H, t, 6.5 Hz, CH_3COOCH_2), 3.07 (3H, s, Mesyl-C*H*$_3$), 3.56 – 3.77 (12H, m, PEG-C*H*$_2$), 4.37 (2H, t, 4.6 Hz, Mesyl-C*H*$_2$).

3-(2-(2-(2-mesyloxyethoxy)ethoxy)ethoxy)propanoate (7)

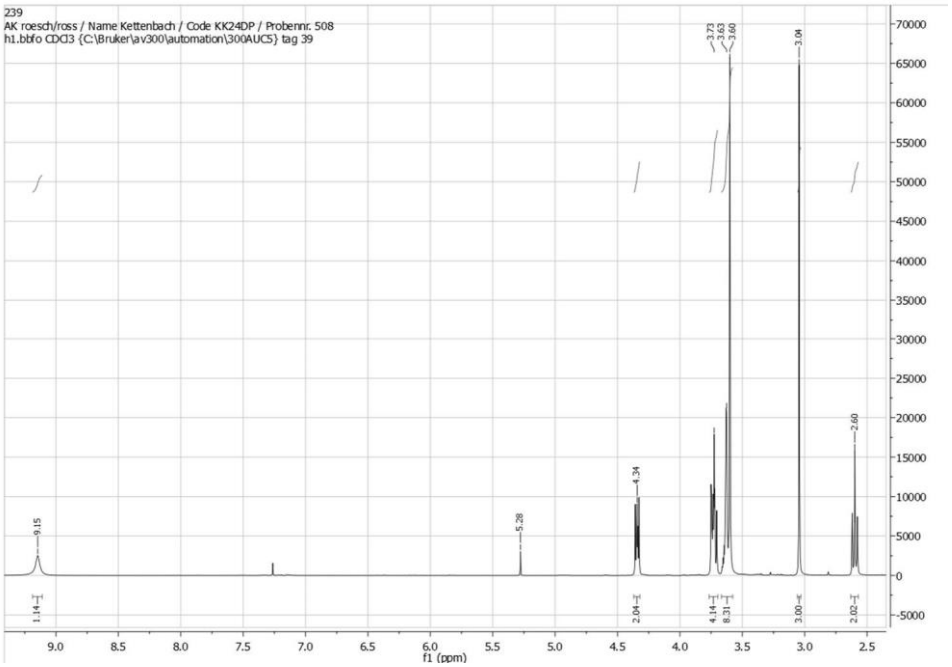

^{1}H-NMR (300 MHz, $CDCl_3$, Me_4Si): ω [ppm] = 2.60 (2H, t, 6.2 Hz, CH_3COOCH_2), 3.04 (3H, s, Mesyl-C*H*$_3$), 3.60 – 3.73 (12H, m, PEG-C*H*$_2$), 4.34 (2H, t, 4.5 Hz, Mesyl-C*H*$_2$), 9.15 (1H, s, O*H*).

3-(2-(2-(2-tosyloxyethoxy)ethoxy)ethoxy)-N-[3-oxo-N-(DBCO)propyl]propanamid (9)

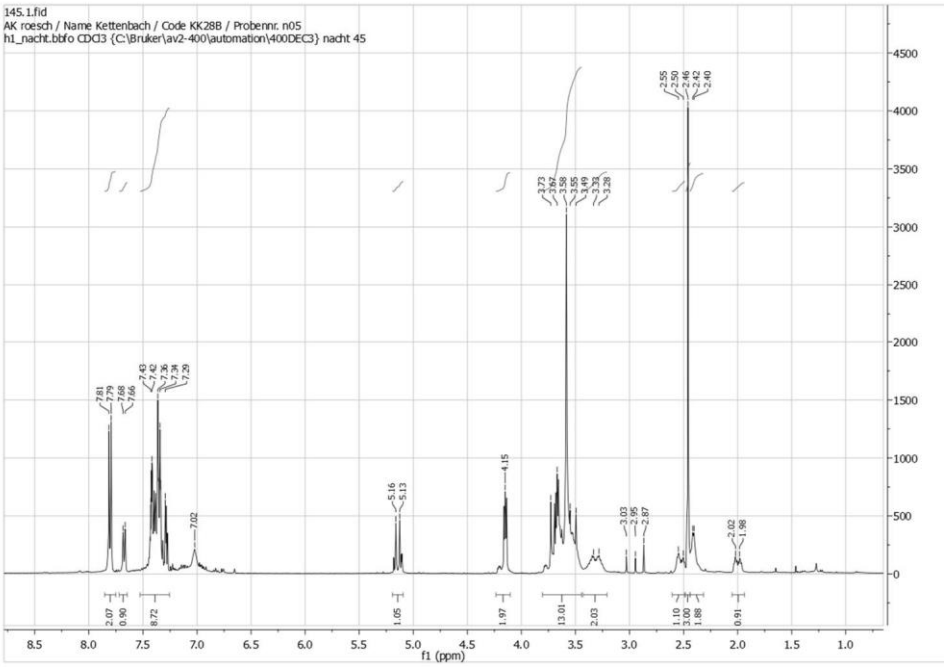

^{1} H-NMR (400 MHz, $CDCl_3$, Me_4Si): ω [ppm] = 1.98 (1H, m, N-CO-C*H*$_2$-CH_2-NH-CO) und 2.58 (1H, m, NCO-C*H*$_2$-CH_2-NH-CO), 2.38 (2H, d, 6 Hz, PEG-C*H*$_2$-CO-NH), 2.45 (3H, s, Tosyl-C*H*$_3$), 3.26 – 3.39 (2H, m, N-

CO-CH_2-CH_2-NH-CO), 3.49 – 3.75 (13 H, m, PEG-CH_2 und DBCO-CH_2), 4.15 (2H, t, 4.7 Hz, Tosyl-SO_2-OCH_2), 5.15 (1H, dd, 8 Hz & 14.5 Hz, DBCO-CH_2), 7.25 – 7.44 (9H, m, DBCO- und Tos-C*H*), 7.66 (1H, d, 7.7 Hz, DBCO-C*H*), 7.78 (2H, d, 9.0 Hz, Tos-C*H*).

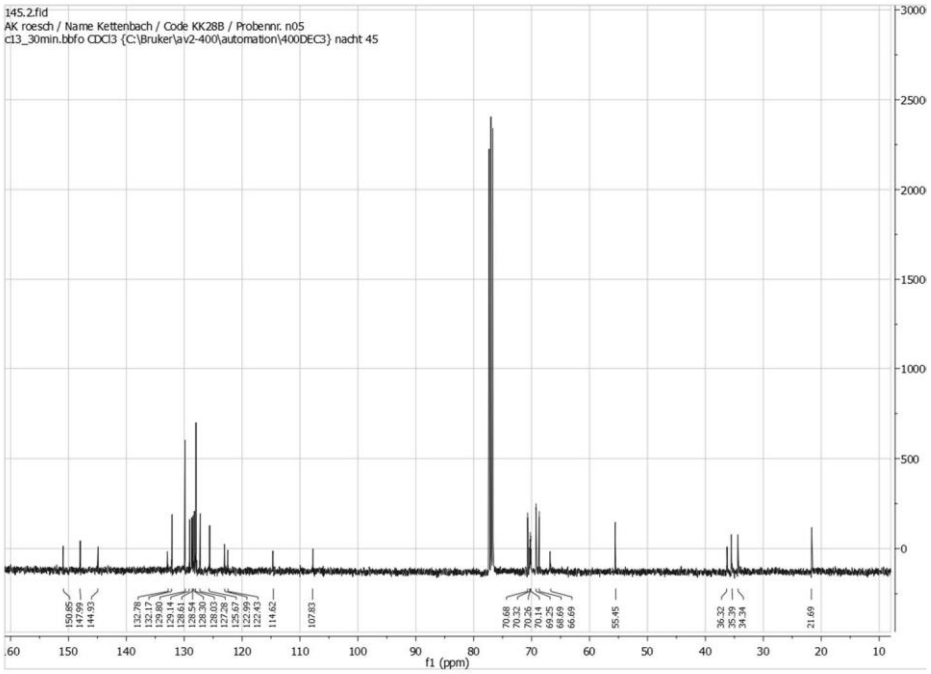

^{13}C-NMR (400 MHz, $CDCl_3$, Me_4Si): ω [ppm] =21.69 (Tosyl-*C*H_3), 34.34 (DBCO-CO-*C*H_2-CH_2-NH-CO), 35.39 (DBCO-CO-CH_2-*C*H_2-NH-CO), 36.32 (NH-CO-*C*H_2-CH_2-PEG-Tosyl), 55.45 (DBCO-*C*H_2), 66.69 – 70.68 (PEG-*C*H_2), 107.83 (Alkyne-*C*), 114.62 – 150.85 (aromatic *C*-atoms). HSQC-2D-NMR

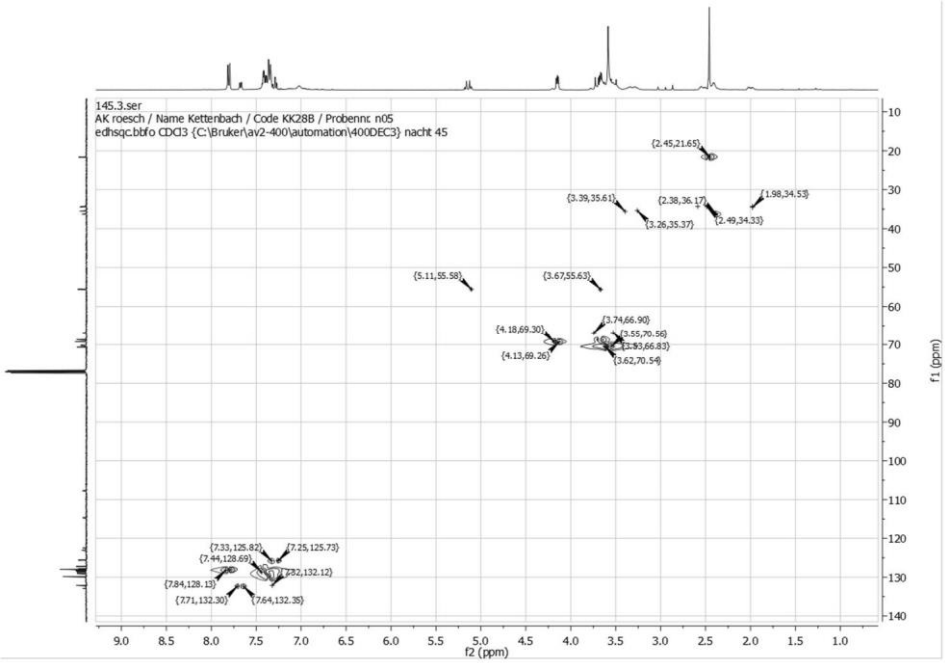

HMBC-2D-NMR

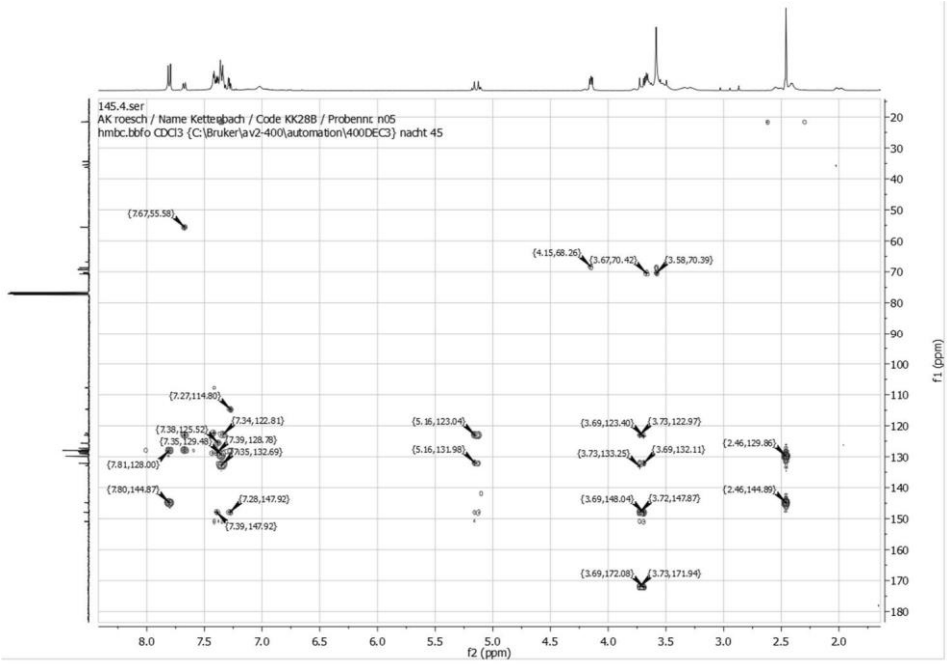

COSY-2D-NMR

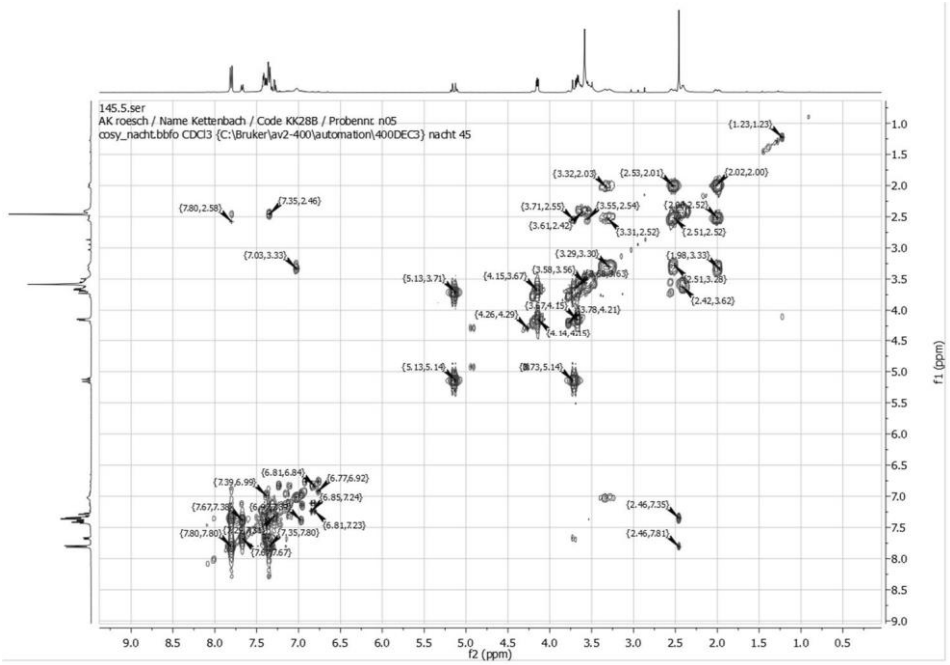

3-(2-(2-(2-mesyloxyethoxy)ethoxy)ethoxy)-N-[3-oxo-N-(DBCO)propyl]propanamid (10)

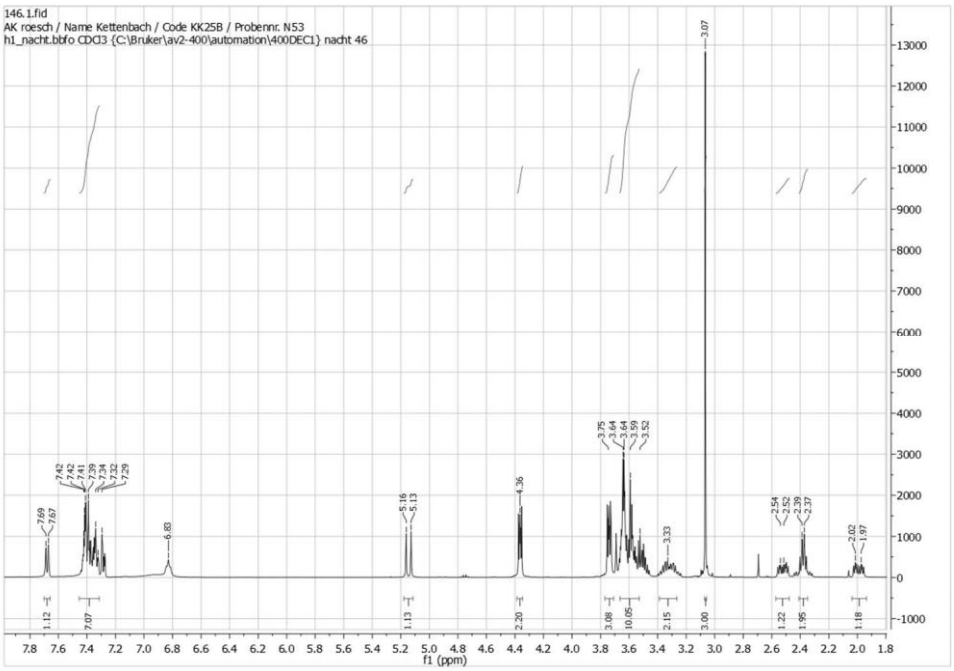

^{1}H-NMR (400 MHz, $CDCl_3$, Me_4Si): ω [ppm] = 1.97 – 2.02 (1H, m, N-CO-C*H*$_2$-CH_2-NH-CO) und 2.52. – 2.54 (1H, m, N-CO-C*H*$_2$-CH_2-NH-CO), 2.37 (2H, dd, 5.6 HZ & 6.6 Hz, PEG-C*H*$_2$-CO-N), 3.07 (3H, s, MesylC*H*$_3$), 3.3 (2H, m, DBCO-CO-CH_2-C*H*$_2$), 3.52 – 3.64 (10 H, m, PEG-C*H*$_2$), 3.75 (3 H, m, Mesyl-PEG-C*H*$_2$$CH_2$-CO und DBCO-C*H*$_2$), 4.36 (2H, t, 4.6 Hz, N-CO-CH_2-C*H*$_2$-N-CO), 5.13 – 5.16 (1H, d, 13.7 Hz, DBCOC*H*$_2$), 7.32 – 7.42 (7H, m, DBCO- und Tos-C*H*), 7.67 – 7.69 (1H, d, 7.5 Hz, DBCO-C*H*).

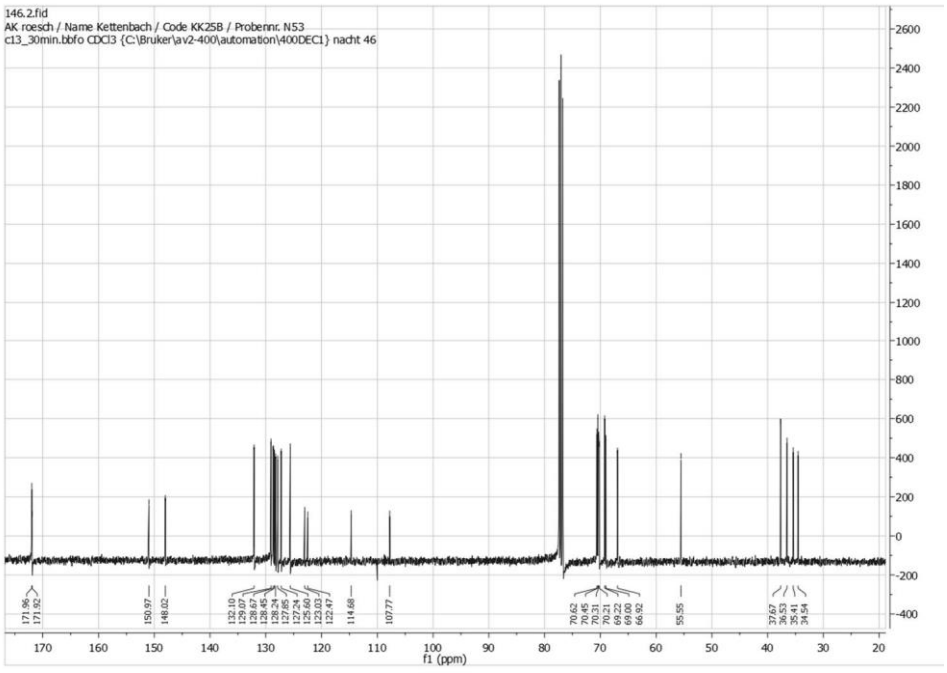

^{13}C-NMR (400 MHz, $CDCl_3$, Me_4Si): ω [ppm] = 34.54 (DBCO-CO-*C*H_2-CH_2-N-CO), 35.41 (DBCO-CO-CH_2*C*H_2-N-CO), 36.56 (N-CO-*C*H_2-CH_2-PEG-Mesyl), 37.67 (Mesyl-*C*H_3), 55.55 (DBCO-*C*H_2), 66.92 – 70.62 (PEG-*C*H_2), 107.77 (Alkyne-C), 114.68 – 150.97 (aromatic C-atoms), 171.92 (*C*O).

HSQC-2D-NMR

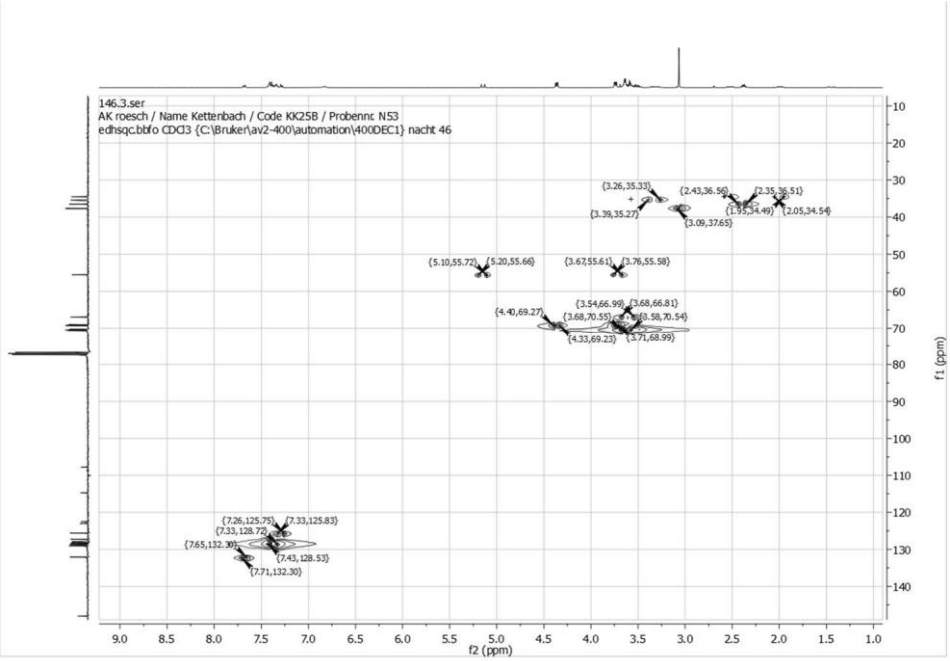

HMBC-2D-NMR

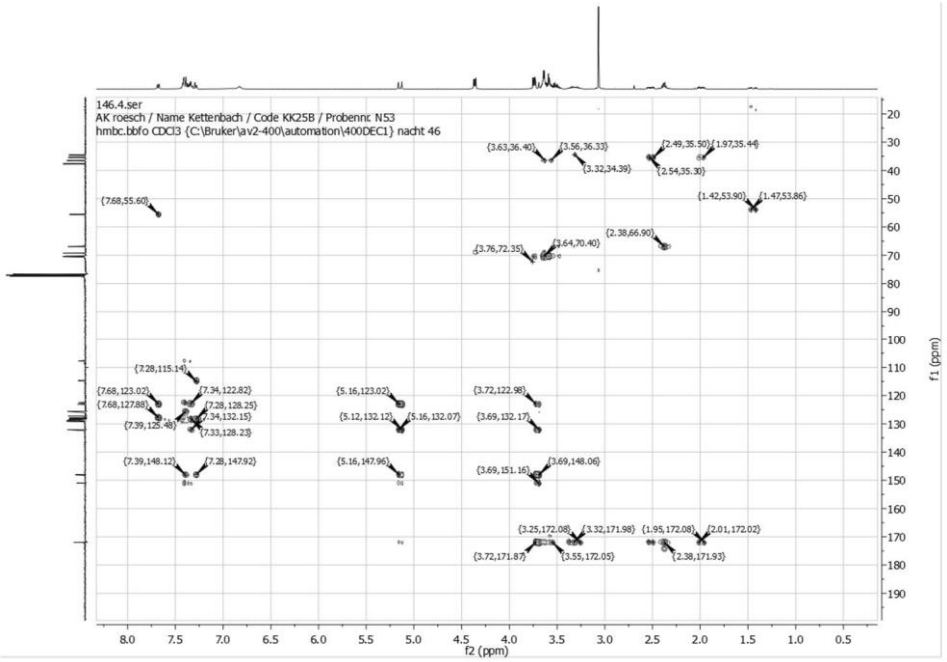

3-(2-(2-(2-fluoroethoxy)ethoxy)ethoxy)-N-[3-oxo-N-(DBCO)propyl]propanamid (11)

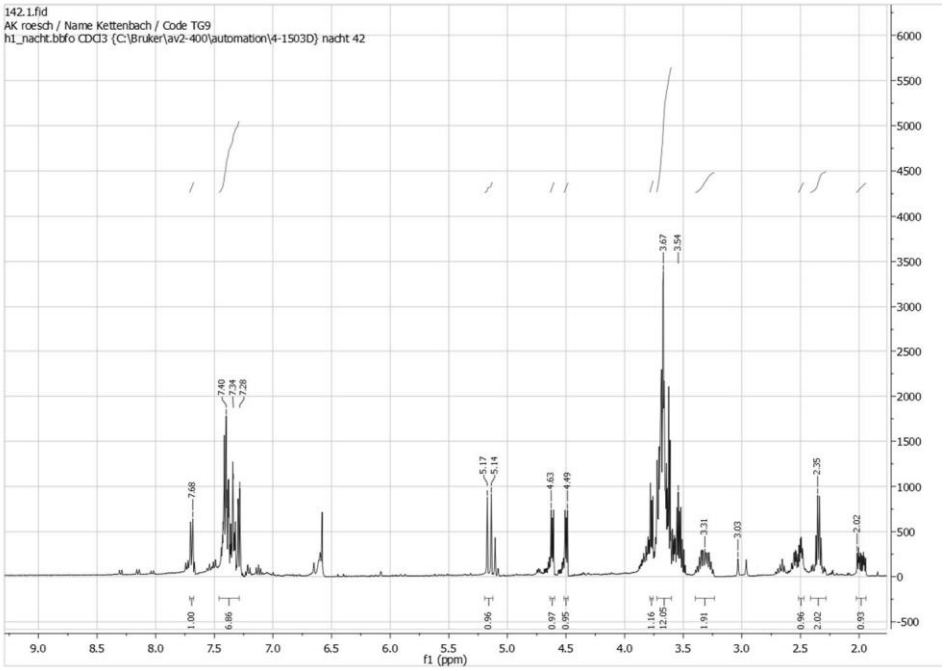

^{1}H-NMR (400 MHz, $CDCl_3$, Me_4Si): ω [ppm] = 1.95 – 2.02 (1H, m, N-CO-C*H*$_2$-CH_2-NH-CO), 2.35 (2H, dd, 5.6 Hz und 6.7 Hz, PEG-C*H*$_2$-CO-NH), 2.50 (1H, dd, 2.8 Hz und 4.7 Hz, N-CO-C*H*$_2$-CH_2-NH-CO), 3.24 – 3.40 (2H, m, N-CO-CH_2-C*H*$_2$-NH-CO), 3.61 – 3.72 (12H, m, PEG-CH_2), 3.77 (1H, t, 4.2 Hz, DBCO-C*H*$_2$), 4.50 (1H, t, 4.1 Hz, PEG-C*H*$_2$-F), 4.62 (1H, t, 4.4 Hz, PEG-C*H*$_2$-F), 5.11 (1H, d, 14.4 Hz, DBCO-C*H*$_2$), 7.29 – 7.44 (7 H, m, DBCO-C*H*), 7.68 (1H, d, 7.2 Hz, DBCO-C*H*).

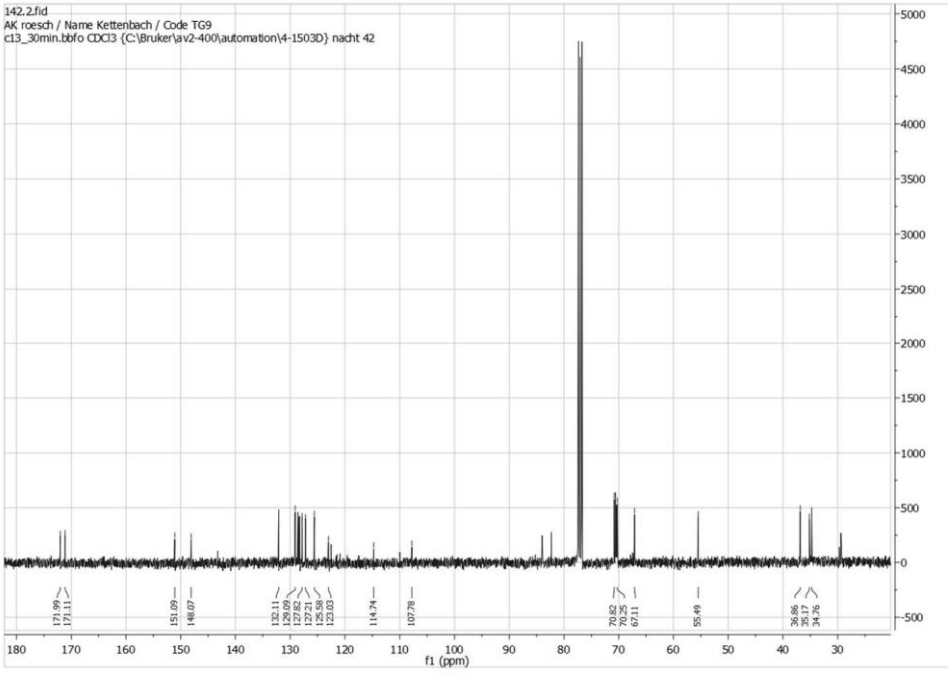

^{13}C-NMR (400 MHz, $CDCl_3$, Me_4Si): ω [ppm] = 34.76 (DBCO-CO-*C*H_2-CH_2-NH-CO), 35.17 (DBCO-CO-CH_2*C*H_2-NH-CO), 36.86 (NH-CO-*C*H_2-CH_2-PEG), 55.49 (DBCO-*C*H_2), 67.11 – 70.82 (PEG-*C*H_2), 107.56 (Alkyne-*C*), 125.70 – 132.37 (aromatic *C*-atoms).

HSQC-2D-NMR

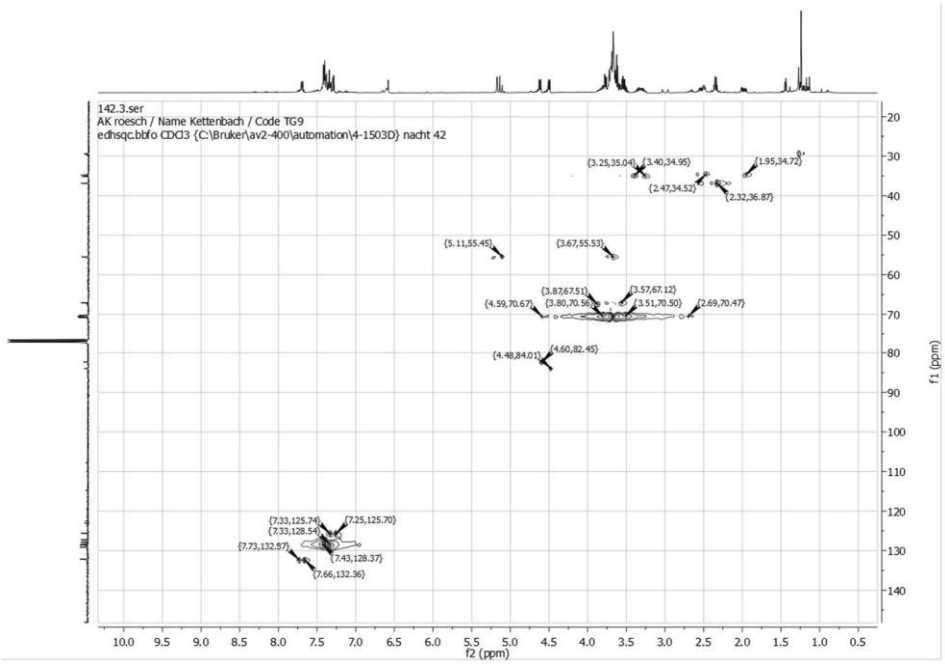

HMBC-2D-NMR

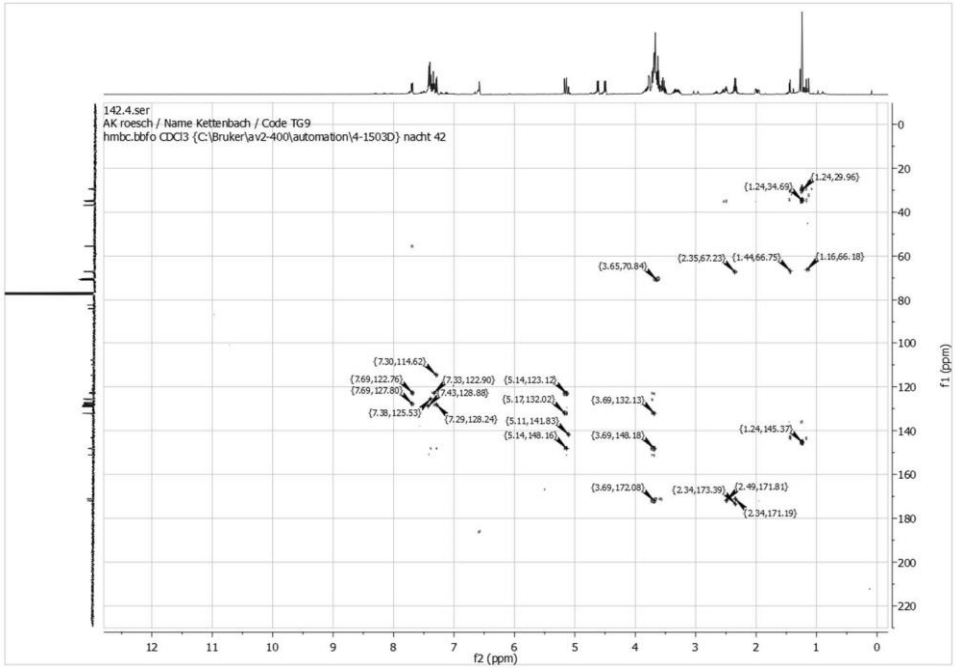

^{19}F-NMR

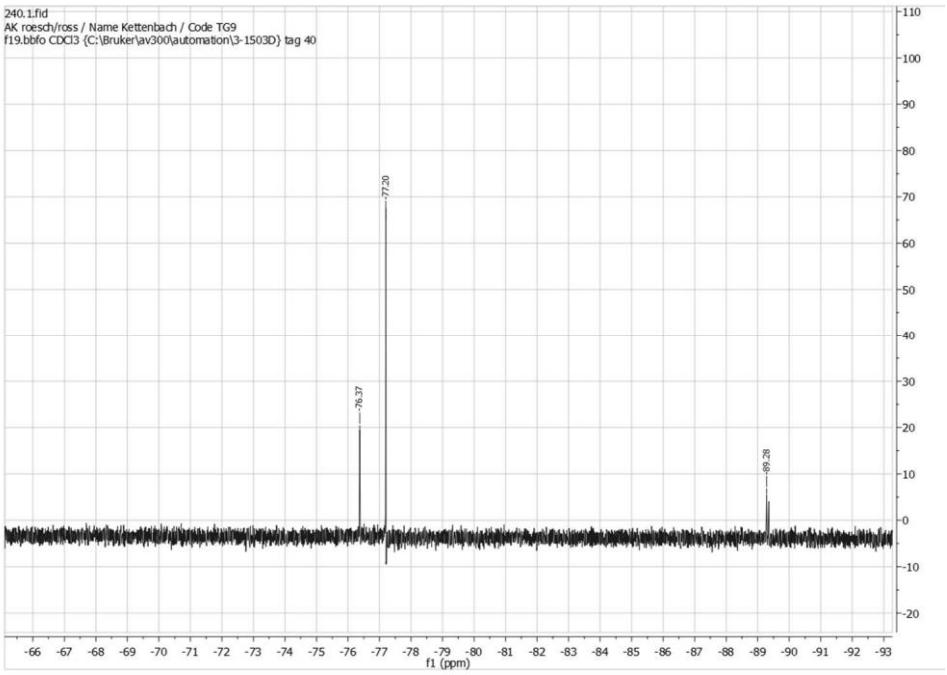

^{19}F-NMR (400 MHz, $CDCl_3$, CCl_3F): ω [ppm] = -77.20.

IV.II. Radio-HPLC data

[^{18}F]11

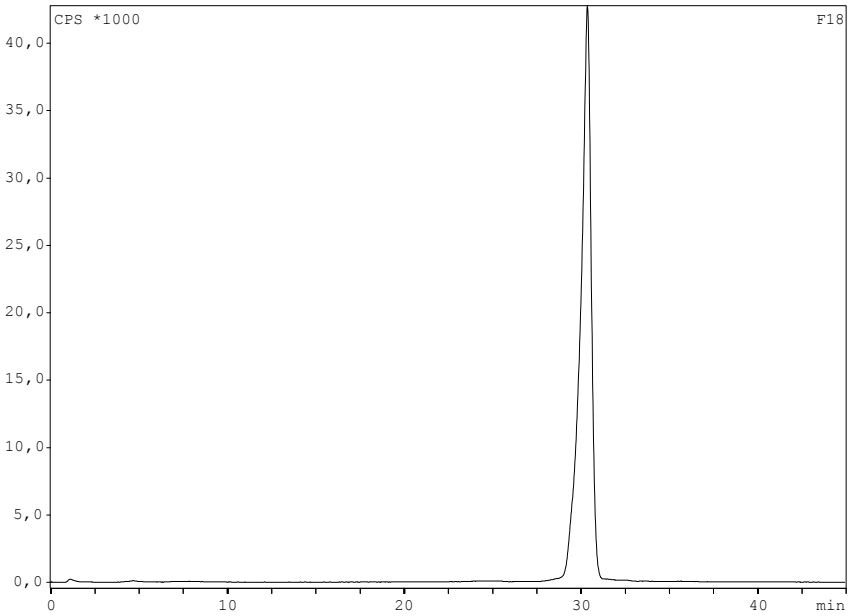

Scheme 1: Analytical radio-HPLC chromatogram [^{18}F]11. Analytical radio-HPLC was performed with a Phenomenex Luna C18 column (5 µm, 250x20 mm) using the following conditions: Flow 0.7 ml min-1, with eluent A was water with 0.1 % TFA (trifluoroacetic acid) and eluent B was acetonitrile with 0.1 % TFA. The following method was used: 0 - 40 min, 5 – 95 % eluent B (gradient).

[^{18}F]13

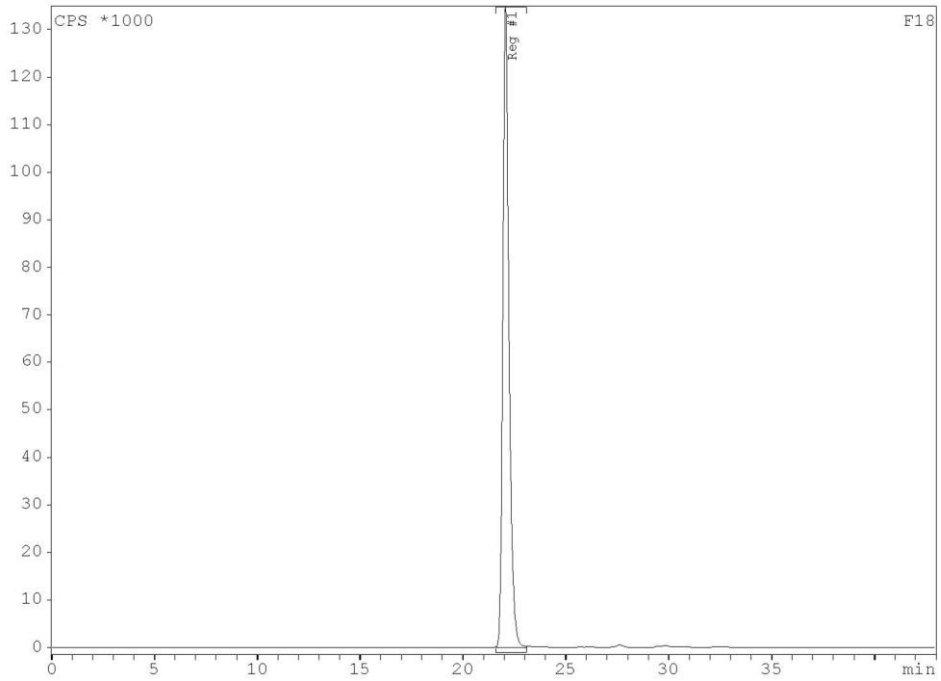

Scheme 2: Analytical radio-HPLC chromatogram [^{18}F]13. Analytical radio-HPLC was performed with a Phenomenex Luna C18 column (5 µm, 250x20 mm) using the following conditions: Flow 0.7 ml min-1, with eluent A was water with 0.1 % TFA (trifluoroacetic acid) and eluent B was acetonitrile with 0.1 % TFA. The following method was used: 0 - 40 min, 5 – 95 % eluent B (gradient). [^{18}F]15

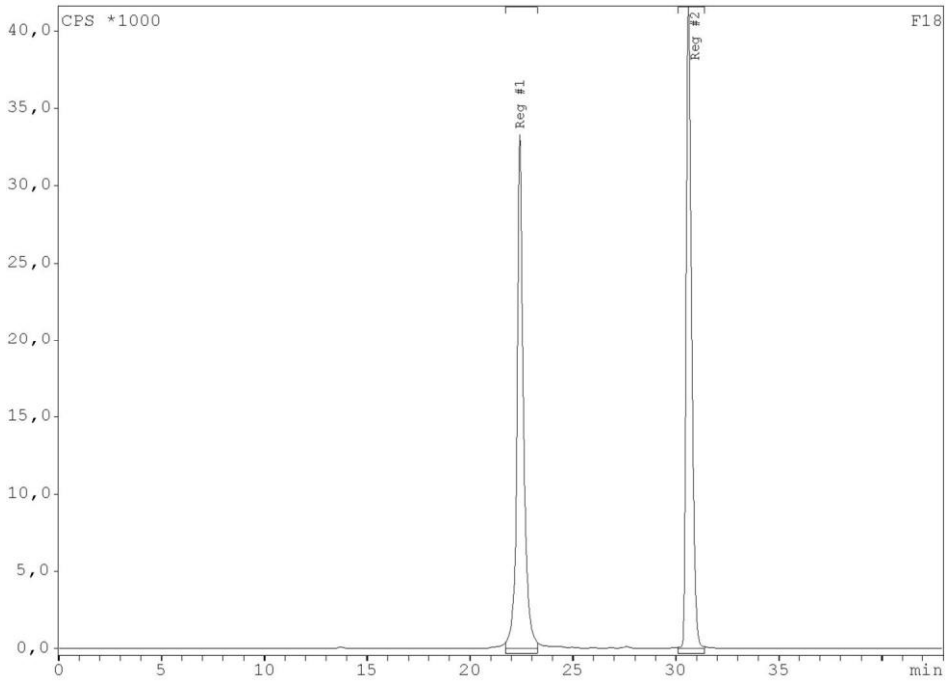

Scheme 3: Analytical radio-HPLC chromatogram [^{18}F]15. Analytical radio-HPLC was performed with a Phenomenex Luna C18 column (5 µm, 250x20 mm) using the following conditions: Flow 0.7 ml min-1, with eluent A was water with 0.1 % TFA (trifluoroacetic acid) and eluent B was acetonitrile with 0.1 % TFA. The following method was used: 0 - 40 min, 5 – 95 % eluent B (gradient).

[^{18}F]17

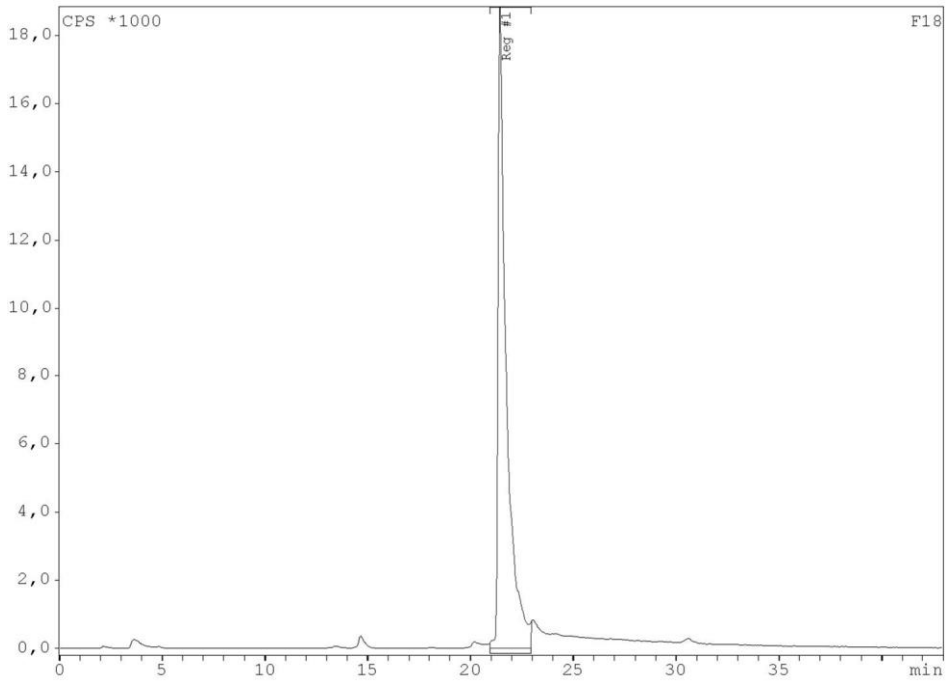

Scheme 4: Analytical radio-HPLC chromatogram [^{18}F]17. Analytical radio-HPLC was performed with a Phenomenex Luna C18 column (5 µm, 250x20 mm) using the following conditions: Flow 0.7 ml min-1, with eluent A was water with 0.1 % TFA (trifluoroacetic acid) and eluent B was acetonitrile with 0.1 % TFA. The following method was used: 0 - 40 min, 5 – 95 % eluent B (gradient). IV.III. Mass spectrometry

3-(2-(2-(2-tosyloxyethoxy)ethoxy)ethoxy)-N-[3-oxo-N-(DBCO)propyl]propanamid (9)

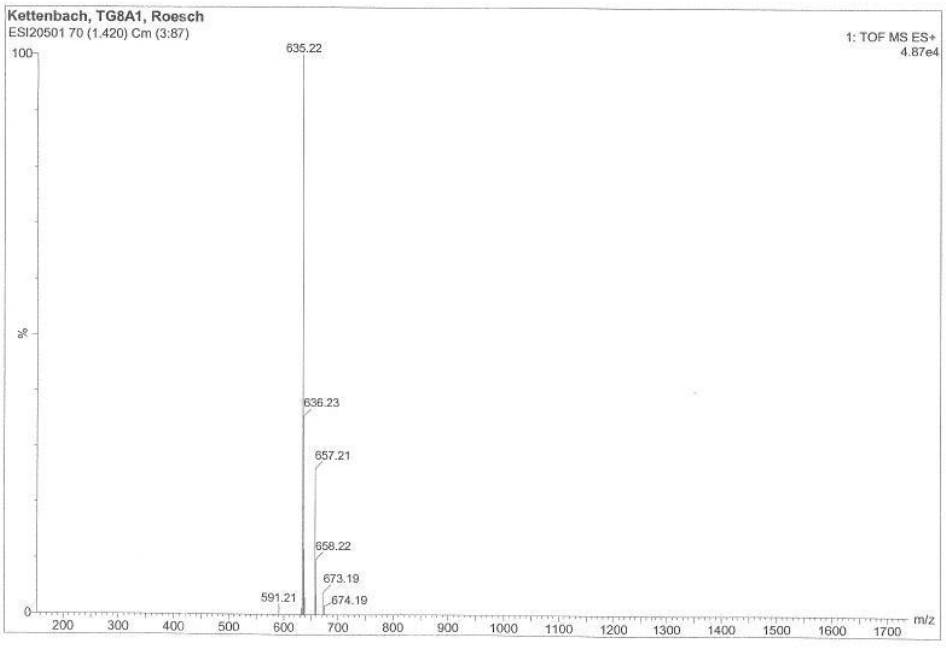

MS (ESI positive): m/z 635.22 ([M]$^+$, 100 %), 657.21 ([M+Na]$^+$), 673.19 ([M+K]$^+$,); m/z (high resolution) 657.2259 ([M+Na]$^+$, 100 %); calculated for $C_{34}H_{38}N_2O_8S$: 634.23.

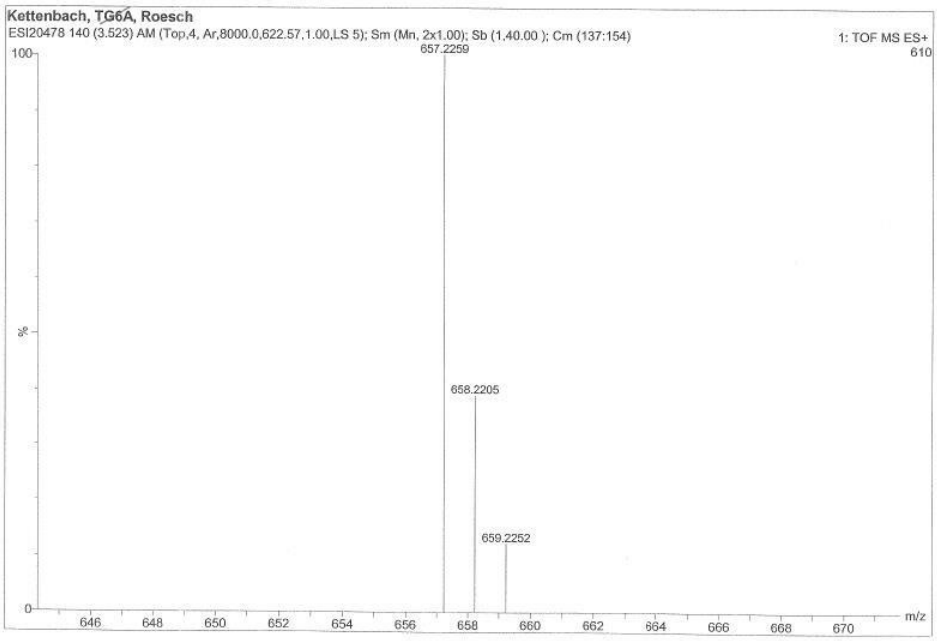

Elemental Composition Report Page 1

Single Mass Analysis
Tolerance = 10.0 PPM / DBE: min = -1.5, max = 200.0
Isotope cluster parameters: Separation = 1.0 Abundance = 1.0%

Monoisotopic Mass, Odd and Even Electron Ions
308 formula(e) evaluated with 1 results within limits (up to 50 closest results for each mass)

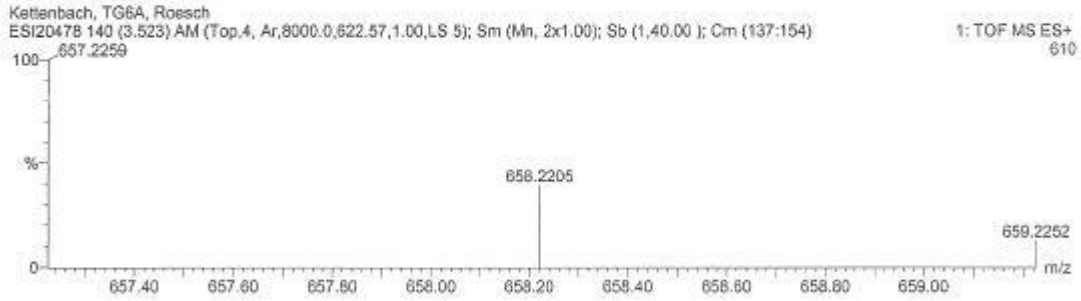

Minimum:				-1.5		
Maximum:		200.0	10.0	200.0		
Mass	Calc. Mass	mDa	PPM	DBE	Score	Formula
657.2259	657.2247	1.2	1.9	16.5	1	C34 H38 N2 O8 23Na S

3-(2-(2-(2-mesyloxyethoxy)ethoxy)ethoxy)-N-[3-oxo-N-(DBCO)propyl]propanamid (10)

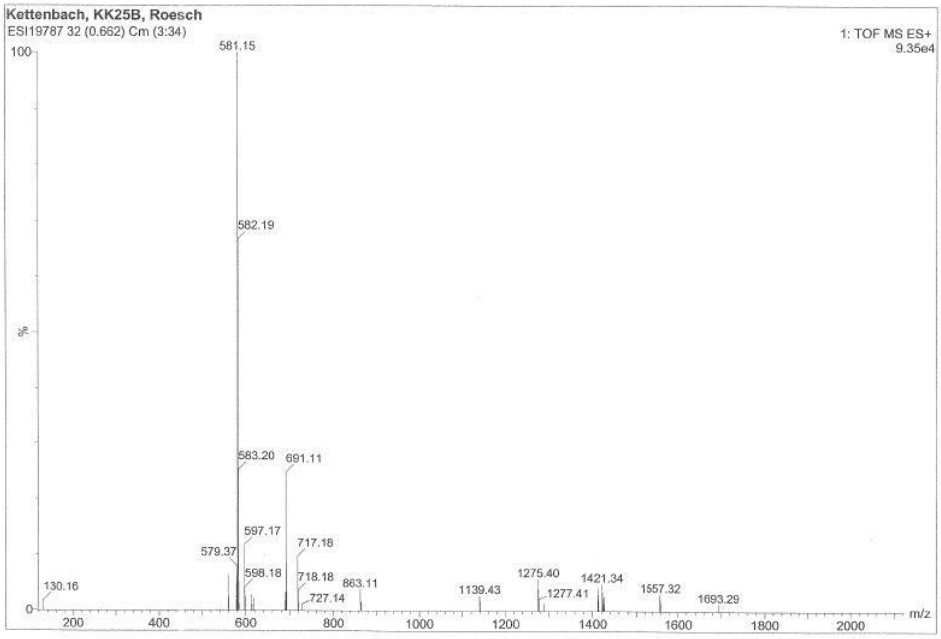

MS (ESI positive): m/z 581.15 ($[M+Na]^+$, 100 %); calculated for $C_{28}H_{34}N_2O_8S$: 558.20.

3-(2-(2-(2-fluoroethoxy)ethoxy)ethoxy)-N-[3-oxo-N-(DBCO)propyl]propanamid (11)

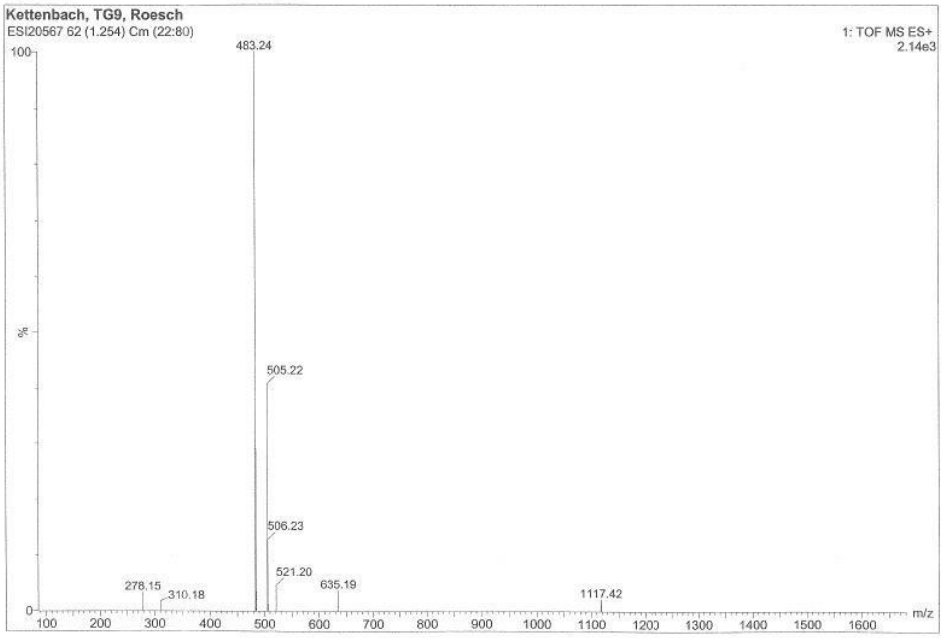

MS (ESI positive): m/z 483.24 ($[M]^+$, 100 %), 505.22 ($[M + Na]^+$); m/z (high resolution) 483.2306 ($[M]^+$, 100 %); 505.2107 ($[M+Na]^+$, 100 %); calculated for $C_{27}H_{31}FN_2O_5$: 482.22.

In vitro and *in vivo* comparison study of a folate derivative labeled with fluorine-18 via copper-free and copper-catalyzed cycloaddition

Kathrin Kettenbach[1], Hanno Schieferstein[1], Stefanie Pektor[2], Raphael Eckert[1], Laura M. Reffert[3], Georg Otto[2], Matthias Miederer[2], Frank Rösch[1]. Tobias L. Ross[1,3]

[1] Institute of Nuclear Chemistry, Johannes Gutenberg University Mainz, 55128 Mainz, Germany

[2]Department of Nuclear Medicine, University Medical Centre Mainz, 55131 Mainz, Germany

[3] Radiopharmaceutical Chemistry, Department of Nuclear Medicine, Hannover Medical School, 30625 Hannover, Germany

Abstract

The folate receptor (FR) is known as an oncological target for diagnosis and therapy over many years due to its upregulation in various epithelial cancer types (ɲ-FR) while its expression in healthy tissues is restricted to the kidneys. Moreover, due to its expression on activated macrophages the ɴ-FR isoform plays an important role in inflammatory and autoimmune diseases. Within the last decades, several folic acid-based radiopharmaceuticals for Single Photon Emission Computed Tomography (SPECT) and Positron Emission Tomography (PET) were evaluated, however, there is still a lack of suitable [^{18}F]fluoro-folates for clinical PET imaging. Herein, we report the synthesis and evaluation of two novel folic acid conjugates regiospecifically labeled with novel ^{18}F-prosthetic groups. [^{18}F]fluorodibenzocyclooctyne-folate ([^{18}F]24) was synthesized via copper-free click cycloaddition using [^{18}F]fluoro-dibenzocyclooctyne and an azido-folate. The novel, high FR-affine (IC_{50} = 11.2 ± 3.7 nM and K_i = 6.3 ± 1.4 nM) radiotracer was achieved within 120 min and radiochemical yields of 3 %.
Determination of the octanol/water partition coefficient showed a quite high lipophilicity of [^{18}F]24 (logD = 0.69 ± 0.08) reflected by a high unspecific binding in cell internalization studies using KB cells (FR positive) and OC 316 cells (FR negative). Biodistribution studies of the copper-free labeled [^{18}F}]fluoro-click-folate in KB tumor-bearing mice showed a low uptake of the radiotracer in FRpositive tumors (0.48 ± 0.14 % ID/g, 60 min p.i.) and kidneys (3.95 ± 0.38 % ID/g, 60 min p.i.). The tumor was not visualizable in PET imaging studies, due to a high abdominal background of the relatively lipophilic radiotracer [^{18}F]24. To improve *in vivo* the pharmacokinetic profile by increasing the polarity of the radiotracer, the azido-folate was radiolabeled via copper-catalyzed cycloaddition of an alkyne and an azide using a highly polar alanine-based ^{18}F-prosthetic group. [^{18}F]fluoro-alaninefolate ([^{18}F]25) was synthesized using [^{18}F]fluoro-alakyne and the azido-folate within 150 min in high radiochemical yields of 20 %. Compared to the [^{18}F]fluoro-DBCO-folate, an increased hydrophilic character (logD = -1.43 ± 0.08) was achieved while maintaining high affinity to the FR (IC_{50} = 6.4 ± 0.5 nM and K_i = 5.5 ± 0.4 nM). PET and biodistribution studies using KB tumor-bearing mice showed a moderate FR-specific uptake of [^{18}F]25 in the tumor (1.68 ± 0.13 % ID/g, 60 min p.i.) and the kidneys (14.38 ± 3.39 % ID/g, 60 min p.i.). The image quality could be significantly improved with a good signalto-noise-contrast. Unspecific uptake was only observed in the liver (1.71 ± 1.02 % ID/g, 60 min p.i.) and the intestines (5.05 ± 4.98 % ID/g, 60 min p.i.), due to the partial hepatobiliary excretion pathway of the tracer.

Introduction

Folic acid (vitamin B_9), is an essential nutrient for the *de novo* DNA synthesis. [1,2] In the beginning of this one-carbon metabolism, folic acid is reduced to tetrahydrofolate (THF), which is then converted into 5-methyl-5,6,7,8-tetrahydrofolate. The coenzyme 5-methyl-THF plays an important role as onecarbon donor by carrying methylene and formyl groups. [3] To ensure sufficient supply of folic acid and folates, tetrahydrofolate (THF) is transported via the anionic reduced folate carrier (RFC) across the cellular membrane. Furthermore, the proton-coupled folate transporter (PCFT) carries reduced folates directly into the cell cytosol. [4] These transporters can easily be reached by folates circulating in the blood stream. [5] In contrast, the folate receptor (FR) transports oxidized folates via receptorshows high affinities to the ɲ-FR ($k_D \sim 1$ nM), which is associated with various epithelial malignancies mediated endocytosis into cells and is overexpressed on highly proliferating cancer cells. [6] Folic acid

of the ovaries, uterus, lung and breast. [7] On the other hand, the ɴ-FR plays an important role in inflammatory and autoimmune diseases due to its expression on activated macrophages. [8-10] However, in healthy tissue the expression of the FR is strictly limited to a few sites such as the kidneys, chroid plexus, lung, salivary glands and the placenta, making it an ideal oncological target for imaging and therapy. [7, 11, 12]

Within the past ten years, several ^{18}F-labeled folate derivatives have been developed using either ^{18}Flabeled prosthetic groups [13-17] or direct labeling strategies. [18, 19] In 2008 the first [^{18}F]fluoroclick-folate was reported, resulting in excellent overall yields of up to 35 %, but unfavorable *in vivo* behavior due to the lipophilic character. [14]To increase the polarity, an [^{18}F]fluoro-click-folate with an oligoethylene glycol spacer was developed in our group. [17] This radiotracer showed significantly reduced hepatobiliary excretion, while maintaining the tumor uptake. Further approaches provided directly labeled [^{18}F]fluoro-folate derivatives with high affinities to the folate receptor (K_i=1.8 ± 0.1 mM), but very poor overall radiochemical yields of less than 9 %. [18] As these examples show, the major goal in [^{18}F]fluoro-folate research is to achieve the right balance between pharmacokinetics (reduced abdominal background) and radiochemistry. This aim was first achieved by Fischer *et al.* in 2012 by using [^{18}F]FDG as a remarkable polar ^{18}F-prosthetic group, which was attached to a folate derivative via copper-catalyzed azide-alkyne click cycloaddition (CuAAC). They obtained for the first time good RCYs of 25 % AND a high tumor uptake of 10 %ID/g tissue. Solely the long preparation time of 180 min can be seen as a drawback. [15] The fact that radiolabeled amino acids show great potential for clinical useful radiotracers and that most relevant biomolecules are based on amino acids, encouraged Schieferstein *et al.* in 2014 to develop a novel ^{18}F-prosthetic group based on alanine. [20] This approach offers the introduction of a very hydrophilic ^{18}F-prosthetic group with a minor effect on the physiological behavior, especially in case of very polar biomolecules. ^{18}F-labeled folate derivatives

are great examples where prosthetic groups usually impair pharmacokinetics. Enhanced blood circulation time and an increased tumor-to kidney-ratio (0.88 ± 0.12 compared to 0.23 ± 0.04) were achieved by attaching an albumin-binding moiety to the [^{18}F]fluoro-folate radiotracer. [21]

One disadvantage of these click reactions is the need of a cytotoxic copper catalyst. Therefore, a multitude of strained ^{18}F-prosthetic groups have been developed, which can be attached without the need of a copper species (strain-promoted azide alkyne cycloaddition, SPAAC). Recently, a new ^{18}Fprosthetic group based on a dibenzocyclooctyne has been developed in our group. We already applied this [^{18}F]fluoro-dibenzocyclooctyne (DBCO) for the radiolabeling of a folate derivative among other biomolecules such as RGD-azide and azide-functionalized peptides. [22]

The aim of this work was to compare a copper-free and a copper-catalyzed labeling approach. Both, the novel copper-free labeled [^{18}F]fluoro-DBCO-folate and the very hydrophilic [^{18}F]fluoro-ala-folate were investigated with regard to their *in vitro* characteristics and *in vivo* biodistribution in KBxenograft bearing mice.

Material and methods

General

Reagents and solvents were purchased from Acros Organics, Alfa Aesar, Fisher Scientific, Fluka, Merck, Sigma Aldrich and VWR and used without further purification. [3´,5´,7,9-^{3}H]folic acid diammonium salt was purchased from Hartmann Analytics (Germany). Reactions were monitored using thin layer chromatography (Merck silica gel 60 F254) or high-performance liquid chromatography (HPLC). Nuclear magnetic resonance spectra (^{1}H and ^{19}F) were recorded using an AC-300-Spectrometer (300MTh-T-NMR-spectrometer AC 300, Bruker Analytik GmbH) in $DCCl_3$, DMSO-d_6 or CD_3OD and an Avance II-400-Spectrometer (400 MHz) for ^{13}C-NMR. Chemical shifts are reported in parts per million (ppm) relative to tetramethylsilane (0.00 ppm) for ^{1}H- and ^{13}C-NMR and trichloro-fluoro-methane (0.00 ppm) for ^{19}F-NMR. Coupling constants (J) are given in hertz (Hz) and the following abbreviations are used for the description of the NMR: singlet (s), doublet (d), triplet (t), quartet (q), multiplet (m), doublet of doublet (dd). FD and ESI mass spectrometry were performed on a MAT 95-MS 7500 CE and a HP 4500 (Agilent Technologies and Hewlett-Packard, respectively, both Santa Clara, Ca, USA).

Semi preparative and analytical HPLC was performed with a Dinoex HPLC system equipped with a 680 HPLC pump and a UVD170U UV-detector (210 nm, 230 nm, 254 nm and 286nm) using a reversedphase column (semi preparative column: Luna, C18, 5 µm, 250x10 mm; analytical column: Luna, C18, 5 µm, 250x4.6 mm; Gemini, C18, 5 µm, 250x4.6 mm and Synergi, C12, max-RP column, 4 µm, 250x10 mm) at a flow rate of 3.5 mL/min for the semi preparative column and 1.0 mL/min for the analytical column.

Analytical radio-HPLC was performed on a Dionex P680A pump and a Dionex UVD 170U (254 nm), equipped with a 2 mL-loop and a GabiStar radiodetector (Raytest). An analytical column (Luna, C18, 5 µm, 250x4.6 mm and a Gemini, C18, 5 µm, 250x4.6 mm) was used at a flow rate of 1.0 mL/min. Dionex Chromeleon software was used for UV-data analysis and Raytest Gina star software for radioactivity detection.

Purification of the radiolabeled products was performed on a semi preparative radio-HPLC system with a Dinoex HPLC system equipped with a 680 HPLC pump and a UVD170U UV-detector (210 nm, 230 nm, 254 nm and 286nm), equipped with a 2 mL-loop and a GabiStar radiodetector (Raytest). A semi preparative column (Luna, C18, 5 µm, 250x20 mm and a Synergi, C12, max-RP, 250x10 mm) was used at a flow rate of 3.5 mL/min. All HPLC methods are described in the Supporting Information.

Specific activity (SA) was determined from a calibration curve obtained from different concentrations of the nonradioactive reference compounds [^{19}F]fluoro-DBCO-folate 24 and [^{19}F]fluoro-ala-folate 25.

PET imaging studies were performed on a nanoScan PET/MRI (Mediso, Budapest, Hungary) and PET data were dynamically reconstructed with Teratomo 3D (4 iterations, 6 subsets, voxel size 0.4mm) using user defined frames (3x10; 3x30; 3x60; 5x300; 3x600sec). Afterwards the PET images were coregistered to the MR and analyzed with pmod software (version 3.6).

Organic Chemisty

3-(2-(2-(2-tosyloxyethoxy)ethoxy)ethoxy)-N-[3-oxo-N-(DBCO)propyl]propanamide (6)

The (aza)dibenzocyclooctyne-based precursor was synthesized as previously reported. [22] For reduced lipophilicity, a triethyl glycol spacer was introduced. The synthesis started from commericially available triethylene glycol 2 and (aza)dibenzocyclooctyne (DBCO)-amine (scheme 1). Triethylene glycol was first reacted with *tert*-butylacrylate 1 to enable amide-coupling to the DBCO. In the second step a tosyl-group as leaving group was introduced for ^{18}F-labeling reaction. Finally, amide-coupling between the tosylated linker and the DBCO-amine was performed using 2-(1H-benzotriazol-1-yl)1,1,3,3-tetramethyluronium-hexafluorophosphat (HBTU) as activating agent and DIPEA.

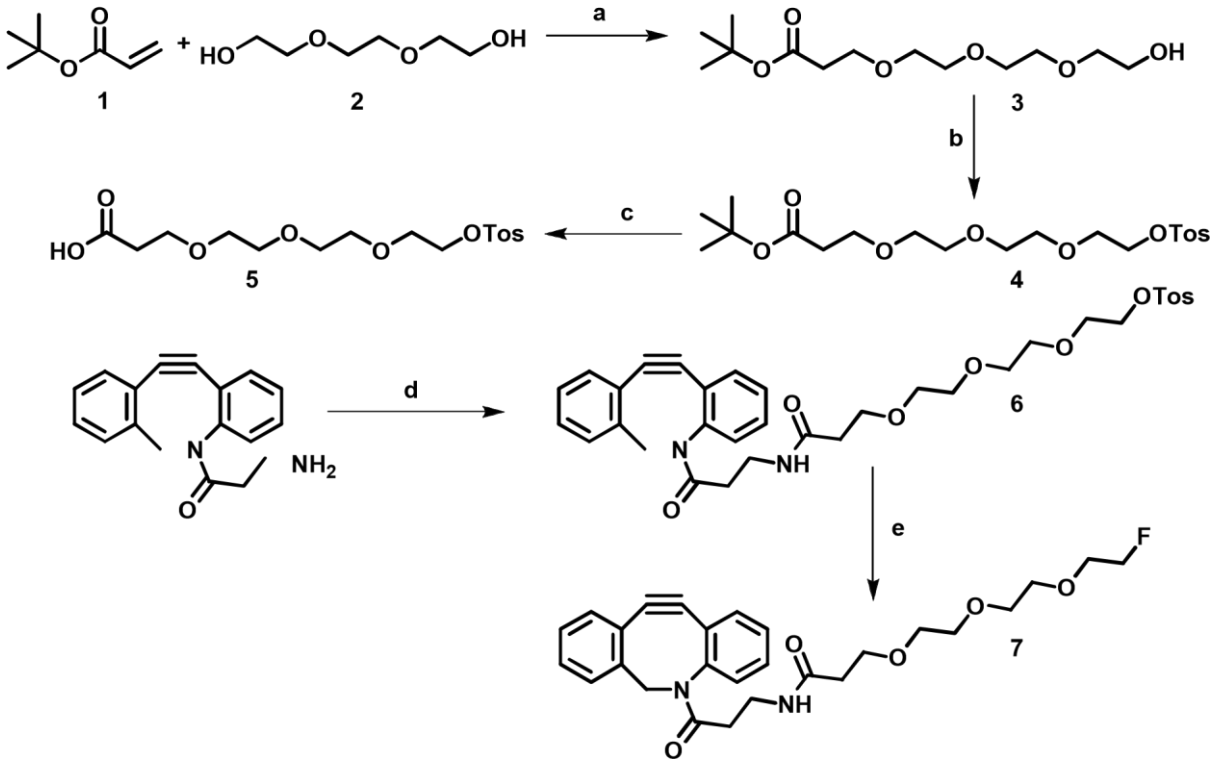

Scheme 1: Synthesis of alkyne-functionalized reference compound 7 and labeling precursor 6. Regents and conditions: a) sodium, THF, 24 h, rt; b) TEA, *p*-toluenensulfonyl chloride, DCM, 1 h, 0 °C, rt; c) TFA, DCM, 4 h, rt; d) TEG-carboxylic acid, *N,N,N´,N´*-tetramethyl-*O*-(1*H*-benzotriazol-1-yl)uranium-hexafluorophoyphate (HBTU), *N,N*-diisopropylethylamine (DIPEA), DMF, 24 h, rt; e) tetrabutylammoniumfluoride, THF, 2 h, 80 °C.

3-(2-(2-(2-fluoro-oxyethoxy)ethoxy)ethoxy)-N-[3-oxo-N-(DBCO)propyl]propanamide (7)

The cold reference compound 7 was obtained via the reaction of precursor 6 and tetrabutylammonium fluoride (TBAF) in tetrahydrofurane (THF) at 70 °C as depicted in scheme 1.

Methyl-3-chloro-2-((2,4-dimethoxybenzyl)(prop-2-yn-1-yl)amino)-propanoate (13)

The labeling precursor 13 was synthesized according to Schieferstein *et al.* and shown in scheme 2. [21] he synthesis started with the reductive amination of *L*-serine methyl ester hydrochloride 8 using 2,4-dimethoxybenzyl and sodium cyanoborohydride. To ensure *N*-regioselectivity during the alkylation, the hydroxyl function of 9 was first protected using triisopropylsilyl chloride. Subsequently, 3-bromo-1-(trimethylsilyl)-1-propyne was used to attach an alkyne to the secondary amine 10, enabling the molecule 11 to participate in copper-catalyzed cycloadditions. The alkyne group and the hydroxyl function were deprotected using tetrabutylammonium fluoride (1M). Intermediate 12 can be used for both, synthesis of the labeling precursor 13 as well as the reference compound 16. The preferred leaving group was meant to be a sulfonic-based one (tosyl or mesyl), but as previously reported it was not possible to synthesize and isolate the tosylated precursor due to the high reactivity within the molecule. [20] Therefore, a chloro-precursor 13 was employed and was synthesized using *p*-toluenesulfonyl chloride.

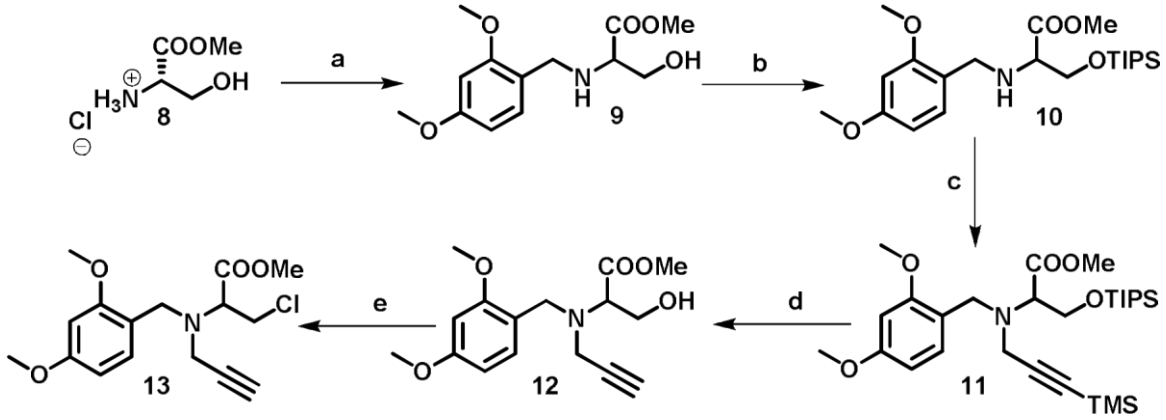

Scheme 2: Synthesis of alkyne-functionalized labeling precursor 13. Conditions and regents: a) 2,4-dimethoxybenzaldehyde, methanol, sodium cyanoborohydride, rt, 24 h; b) triisopropylsilyl chloride, DMF, imidazole, 0 °C, 30 min, rt, 24 h; c) 3-bromo1-(trimethylsilyl)-1-propyne, MeCN, Cs_2CO_3, 100 °C, 12 h; d) tetrabutylammonium fluoride in THF (1M), rt, 12 h; e) *p*toluenesulfonyl chloride, MeCN, TEA, 60 °C, 12 h.

3-fluoro-2-(prop-2-yn-1-ylamino)propanoic acid (16)

At first, compound 12 was fluorinated using DAST ((diethylamino)sulfur trifluoride) at 0 °C as depicted in scheme 3. In the following two reaction steps full deprotection of the molecule was performed using

lithium hydroxide solution (1 M) and trifluoroacetic acid. Purification of the cold reference compound 16 was performed using a C18 cartridge.

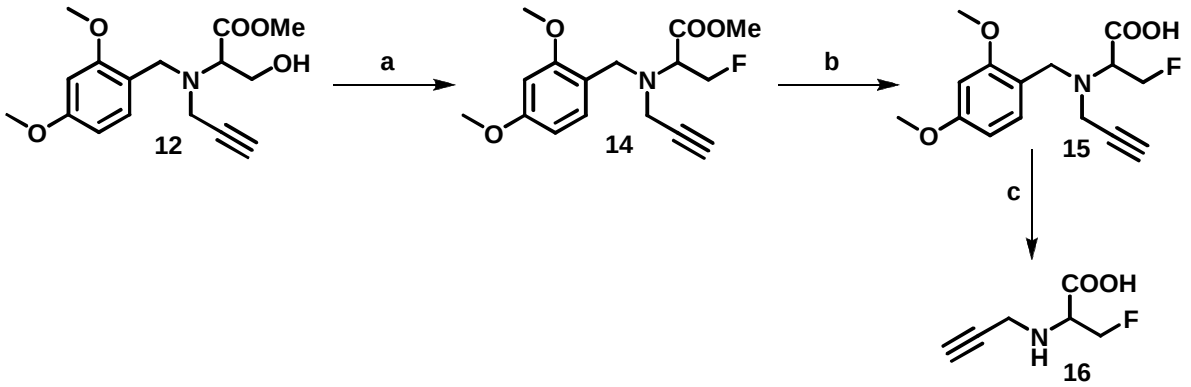

Scheme 3: Synthesis of alkyne-functionalized reference compound 16. Conditions and regents: a) (diethylamino)sulphur trifluoride, DCM, 0 °C, 1 h; b) lithium hydroxide (1M, aq.), THF, *tert*-butyl alcohol, 40 °C, 2 h; c) TFA, DCM, rt, 16h, 50 °C, 2h.

N_{α}-(2-(2-(2-(2-Azidoethoxy)ethoxy)ethoxy)ethyl)-pteroyl-*L*-glutamine (23)

Direct functionalization with the linker would lead to a mixture of γ- and α-functionalized folate derivatives. To enable a regiospecific build-up synthesis, folic acid first was degraded to pteroic acid and glutamate. Subsequently, a α-functionalized glutamate 19 can be attached giving the folate derivative shown in scheme 4. The synthesis of acetyl-pyrofolic acid was performed according to Temple *et al.* [23] using acetic anhydride and acetic acid. The final decomposition yielding acetylpteroic acid 21 was done using a sodium hydroxide solution. The azido-functionalized glutamate was synthesized according to El-Faham *et al.* [24] starting with *N*-(tert-butoxycarbonyl)-*L*-glutamic acid-γmethylester 17 which was coupled to 11-zzido-3,6,9-trioxyundecan-1-amine through amide bond formation using 1-cyano-2-ethoxy-2-oxoethylidenaminooxy)dimethylamino-morpholino-carbenium hexafluoro phosphate (COMU) and DIPEA. After cleavage of the *tert*-butyl group with hydrochloride acid solution in dioxane the glutamate linker 19 was coupled to the acetyl-pteroic acid 22 using again COMU and DIPEA. Final deprotection of the folate derivative was performed on hydrochloride acid solution (aq.) at pH 2 at rt.

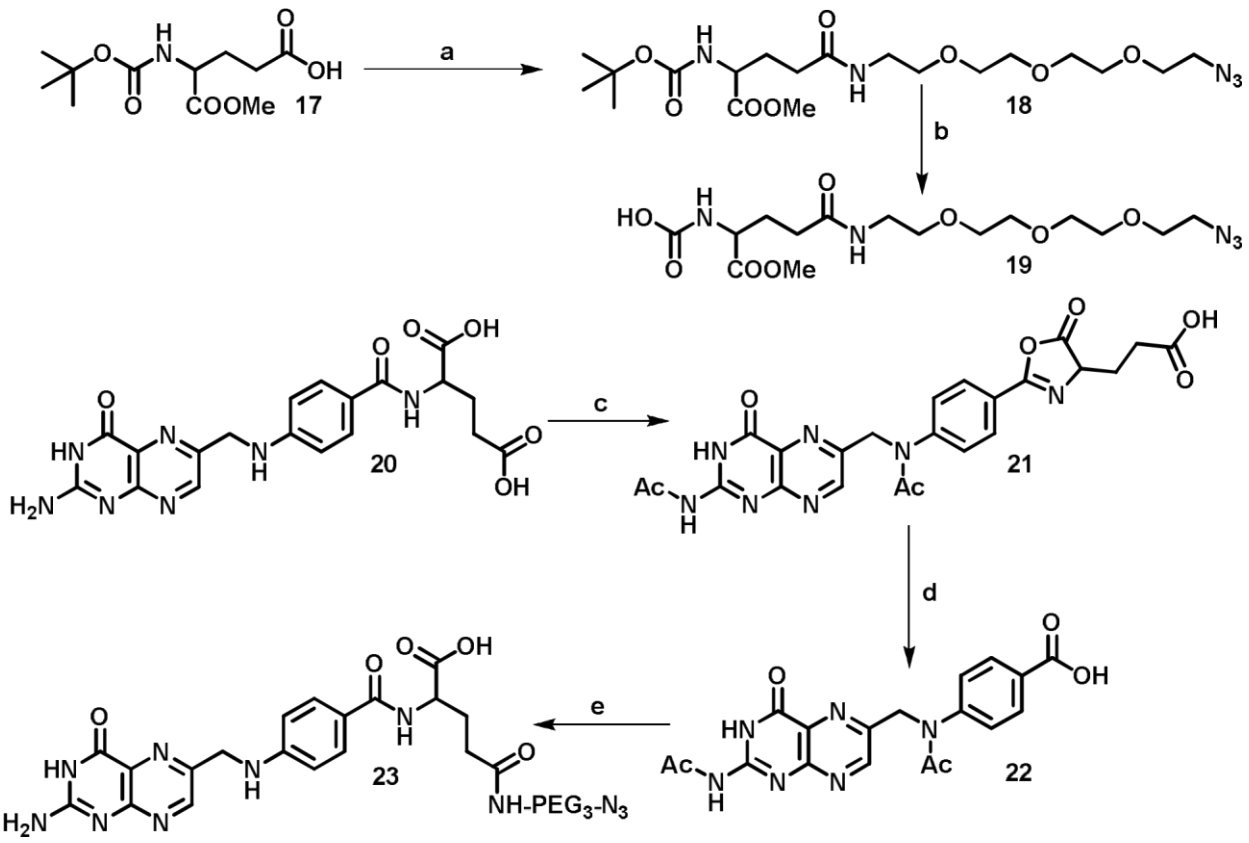

Scheme 4: Synthesis of azide-functionalized glutamate linker 19 and folic acid 23. Conditions and reagents: a) (1-cyano-2ethoxy-2-oxoethylidenaminooxydimethylamino-morpholino-carbenium hexafluorophosphat (COMU), *N,N*-diisopropyl ethylamine (DIPEA), MeCN, 11-azido-3,6,9-trioxyundecan-1-amin, rt, 16 h; b) hydrochloride acid (4M in dioxane), rt, 16 h; c) acetic anhydride, acetic acid, reflux, 2 h; d) water, sodium hydroxide solution (1M), rt, 48 h; e) (1-cyano-2-ethoxy-2oxoethylidenaminooxydimethylamino-morpholino-carbenium hexafluorophosphat (COMU), *N,N*-diisopropylethylamine (DIPEA), DMF, glutamate linker 19, 50 °C, 16h.

11-(1,2,3-Triazo-4-N-ethyl-(3-(2-(2-(2-fluoro-oxyethoxy)ethoxy)ethoxy)-N-[3-oxo-N(DBCO)propyl] propanamide)3,6,7-trioxaundecan-1-yl)folic acid amide (24)

The strain-promoted azide-alkyne cycloaddition (SPAAC) of 7 and 23 (scheme 5) was performed without copper species as catalyst at rt in phosphate-buffered saline (PBS). For purification of product 24 a semi-preparative HPLC system was used.

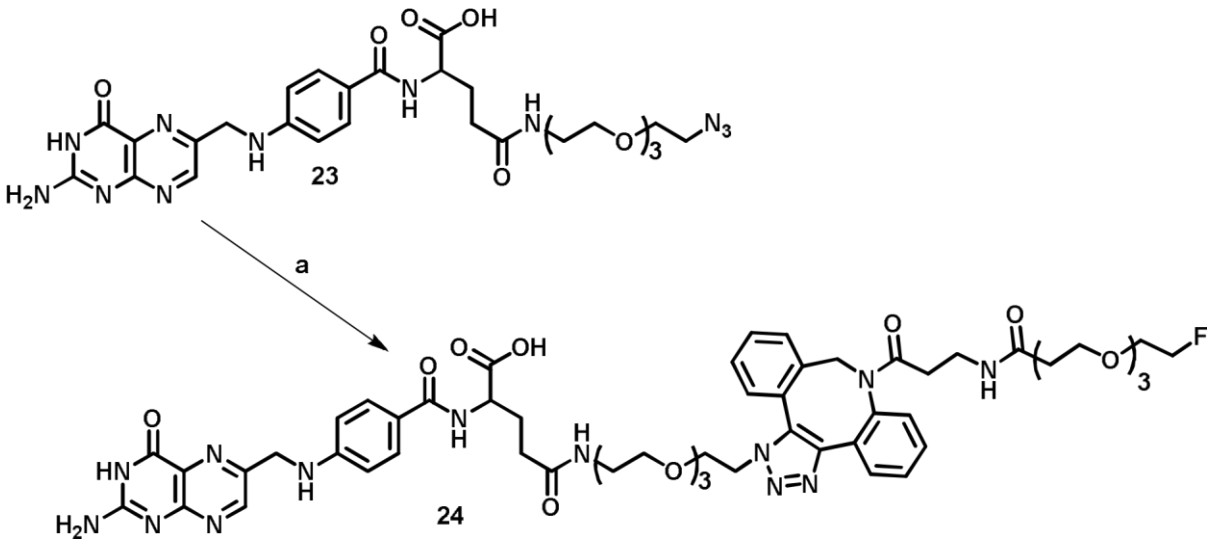

Scheme 5: Synthesis of reference compound 24. Conditions and reagents: a) [^{19}F]fluoro-DBCO, PBS, rt, 2 h.

11-(1,2,3-Triazo-4-N-ethyl-(3-fluoro-2-(prop-2-yn-1-ylamino)propanoic acid)3,6,7trioxaundecan-1-yl)folic acid amide (25)

The reference compound 25 was synthesized via copper(I)-catalyzed azide-alkyne-cycloaddition (CuAAC) of 16 and 23 using copper(II) and sodium ascorbate system in a PBS/EtOH-mixture (1:1) as depicted in scheme 6. Purification of product 25 was performed with a semi-preparative HPLC system.

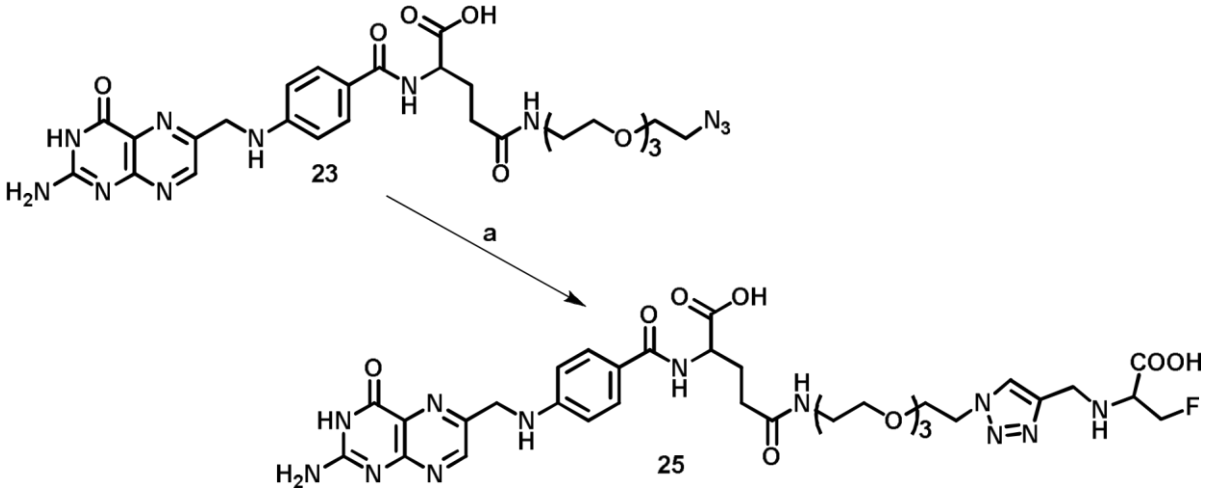

Scheme 6: Synthesis of reference compound 25. Conditions and reagents: a) [^{19}F]fluoro-ala-folate, $CuSO_4$, sodium ascorbate, ethanol, PBS/EtOH (1:1), rt, 16 h.

Radiochemistry

Radiosyntheses were performed hands-on (starting activities ч 8 GBq) or in a manipulator-equipped hot cell (starting activities > 8GBq) using conventional heating. The procedure for the production of dried [^{18}F]fluoride is described in the supporting information.

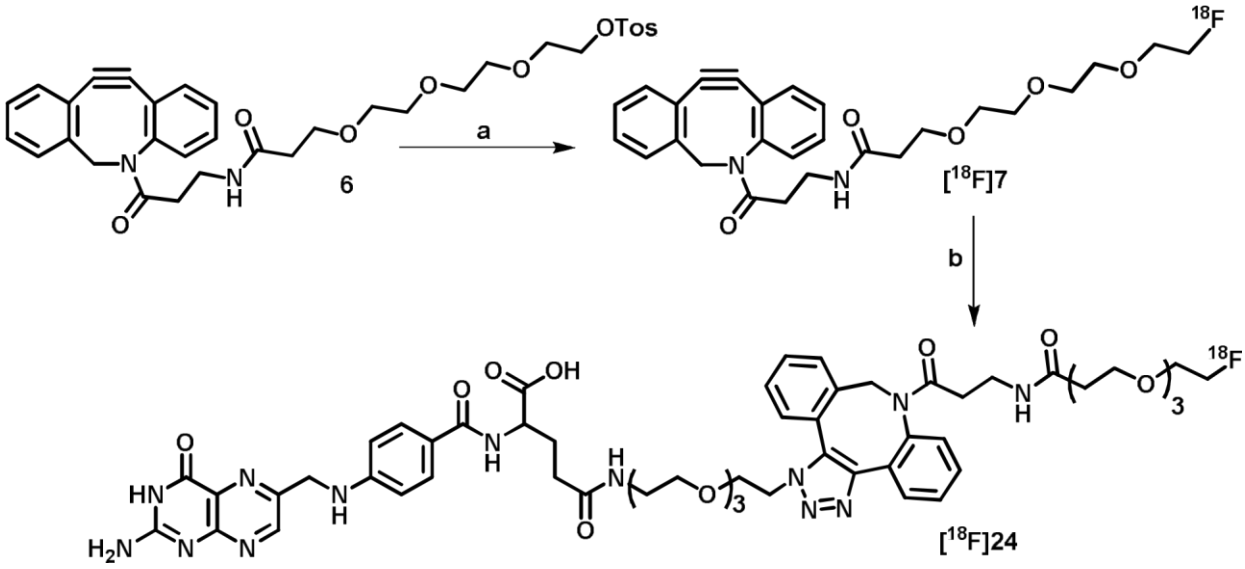

Scheme 7: Synthesis of ^{18}F-prosthetic group [^{18}F]7 and ^{18}F-labeled folate derivative [^{18}F]24. Conditions and reagents: a) n.c.a. [^{18}F]fluoride, Et_4NHCO_3, dry MeCN, 100 °C, 10 min; b)Folate-azide 23, PBS, 40 °C, 15 min.

[^{18}F]fluoro-TEG-DBCO

The DBCO-based ^{18}F-prosthetic group [^{18}F]7 was prepared as previously reported in the literature. [23] Tetraethylammonium bicarbonate was used as a base and the radiolabeling reaction was performed at 100 °C for 15 min. Purification of the [^{18}F]fluoro-DBCO was performed using semi-preparative HPLC and C18 cartridge. [22]

[^{18}F]fluoro-TEG-DBCO-folate

The final product [^{18}F]fluoro-DBCO [^{18}F]24 was prepared as previously reported in the literature. [22] Copper-free click cycloaddition was performed in PBS at 40 °C for 15 min. Purification of the product was performed using semi-preparative HPLC and C18 cartridge.

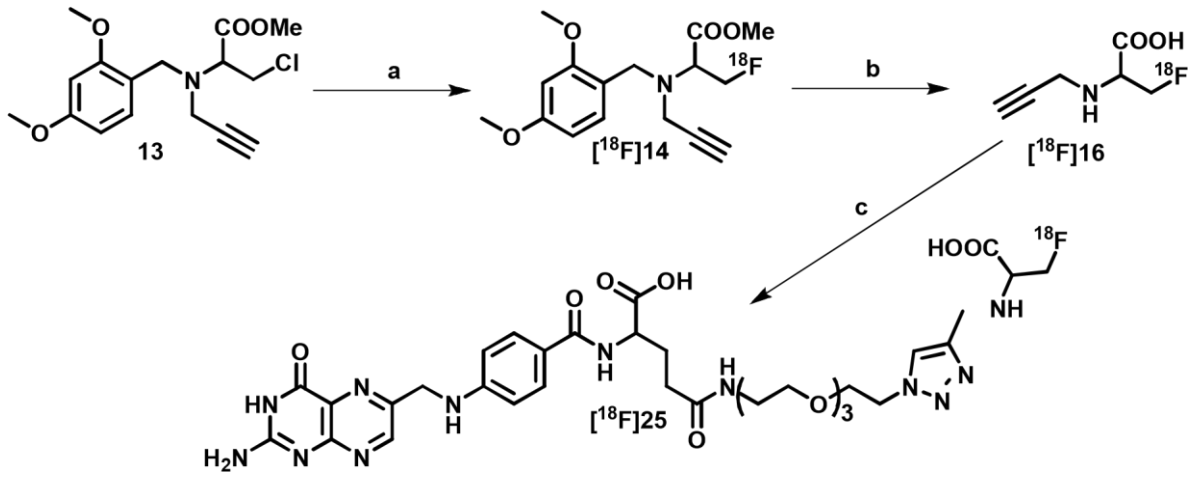

Scheme 8: Synthesis of ^{18}F-prosthetic group [^{18}F]16 and ^{18}F-labeled folate derivative [^{18}F]25. Conditions and reagents: a) n.c.a. $^{18}F^-$, K_{222}, K_2CO_3, DMF, 140 °C, 15 min; b) hydrochloride acid (3.3M), 120 °C, 15 min; c) Folate-azide 23, $CuSO_4$, sodium ascorbate, ethanol, PBS/EtOH (1:1), 70 °C, 15 min.

[^{18}F]fluoro-alanine

The synthesis of the alanine-based ^{18}F-prosthetic group [^{18}F]16 was performed as previously reported by Schieferstein *et al.* (scheme 8) with some minor changes. [20] The [^{18}F]fluoride was eluted from the QMA cartridge with a solution of Kryptofix (5 mg) and potassium carbonate (1 mg, 7.5 µmol) in 600 µL (acetonitrile:water/1:1). The labeling reaction was carried out in dry DMSO at 140 °C using conventional heating. Sparing the transfer of dried [^{18}F]fluoride from a reaction vial into a microwave vial, which reduced the loss of activity. Methyl-3-[^{18}F]fluoro-2-((2,4-dimethoxybenzyl)(prop-2-yn-1yl)amino)-propanoate can be separated from unreacted [^{18}F]fluoride using a C18 cartridge instead of semi-preparative HPLC saving additional time. The protected prosthetic group was deprotected using 3.3M hydrochloride acid solution at 120 °C for 15 min, followed by semi-preparative HPLC purification. However, an effective separation from the non-radioactive precursor was not achievable, resulting in a high load of non-radioactive material. The final product [^{18}F]16 group was isolated by evaporation of the HPLC solvents.

[^{18}F]fluoro-ala-folate

The CuAAC of the ^{18}F-prosthetic group [^{18}F]16 and the azido-folate 23 was performed in a PBS/EtOHmixture using $CuSO_4$ and sodium ascorbate at 70 °C for 15 min. Purification of the final product [^{18}F]25 was performed with a semi-preparative HPLC system and evaporation of the HPLC solvents. For lipophilicity and cell experiments the [^{18}F]fluoro-folate was dissolved in phosphate-buffered saline, for stability tests and *in vivo* application sterile sodium chloride solution was used.

Lipophilicity

Octanol-water partition coefficient

The lipophilicity of the [^{18}F]fluoro-alakyne [^{18}F]16 itself and the ^{18}F-labeled folate derivatives [^{18}F]24 and [^{18}F]25 was determined using the shake-flask method (octanol-water partition). Approximately 20 MBq of the radiolabeled prosthetic group were diluted in 0.7 mL phosphate-buffered saline (PBS). An equal volume of 1-octanol was added to obtain a binary phase system. After stirring the samples at 1.500 1/min for 2 min, the two layers were separated by centrifuge (12.000 U/min for 2 min). 300µLsamples were taken from each layer and radioactivity of both layers was measured using a Curiemeter. Besides, activity was also determined using a TLC plate. A log*D* value of 1.20 ± 0.07 has been previously reported for the [^{18}F]fluoro-DBCO [^{18}F]7. [22]

Relative lipophilicity (k´ value)

To determine the relative lipophilicity a reversed-phase HPLC with an acetonitrile-phosphoric acid buffer eluent system at pH 2.4 was used. [18] The relative lipophilicity was calculated as capacity factor k´: $k' = (t_{retention}-t_{solvent})/t_{solvent}$. Native folic acid and both folate-based reference compounds 24 and 25 were dissolved in PBS and their retention time was measured with an analytical HPLC system (see supporting information). To obtain the dead time of the HPLC system a $NaNO_2$ solution was used.

In vitro studies

For *in vitro* biological evaluation human KB cells derived from human cervical carcinoma were used. The cell line was obtained from DSMZ (German Collection of Microorganisms and Cell Cultures). As a negative control we used OC316 (human ovarian adenocarcinoma, epithelial) cells (for FACS analysis data see supporting information, figure 2). This cell line was kindly provided by the group of Prof. Dr. Müller-Klieser (Institute of Pathophysiologie, Universitätsmedizin of the Johannes Gutenberg University Mainz). The cells were cultured in RPMI medium containing 10 % FCS and Hepes (10 mM, 5 mL) grown at 37 °C in a humidified atmosphere containing 5 % CO_2.

Stability studies in human serum albumin

Solutions of [^{18}F]fluoro-DBCO-folate [^{18}F]24 and [^{18}F]fluoro-ala-folate [^{18}F]25 (200 µL, approximately 4 MBq) were incubated with 500 µL of human serum albumin (HSA) at 37 °C for 1 and 2 h. After incubation, plasma proteins were precipitated using 600 µL of ice-cold acetonitrile and centrifugation (10.000 rpm, 10 min). An aliquot (200 µL) of both time points was injected into the analytical radio-HPLC system (Gemini, C18, 5 µm, 250x4.6 mm, 1mL/min). Each experiment was carried out in triplicates.

binding affinity studies

To determine the IC_{50} and K_i values of both [^{18}F]fluoro-folate derivatives and to demonstrate specific binding to the receptor, displacement assays using [^{3}H]folic acid were performed as described elsewhere. [25] *internalization studies*

The ^{18}F-labeled folate derivatives were dissolved in PBS buffer at different concentrations (1 and 5 nM). Cells were used in suspension (1 Mio.) and incubated for 1 h at 4 °C and 37 °C. After incubation the supernatant was removed and cells were washed 2-times with PBS and 2-times with an acidic glacial buffer (pH 3). Each experiment was carried out minimum three times in triplicates for each setup (incubation temperature and concentration). Blocking experiments using native folic acid on receptor-positive KB cells were performed. Thus, cells were pre-incubated with 100 µg native folic acid in 100 µL PBS buffer right before the radiotracer was added.

Animal experiments

Male and female balb/c and balb/c nude (Balb/c AnNRj-Foxn1nu) mice were purchased from Janvier labs and housed under specific pathogen-free conditions in the animal care facility in Mainz according to the guidelines of the regional animal care committee. All experiments were performed in accordance with federal guidelines and approved by the ethical committee of the state of Rheinland Pfalz (according to §8 Abs. 1 Tierschutzgesetz, Landesuntersuchungsamt; permission no. 2317707/G15-1-033). Mice were kept on a folate-deficient rodent diet for two weeks to reduce the level of folate in the blood to the level found in humans. Healthy and KB tumor bearing mice were used. After 7 days of acclimatization, human KB tumor cells (2.5 x 10^6 cells) were inoculated in the right shoulder of each mouse. All *in vivo* treatments and imaging experiments were done under isoflurane anesthesia to minimize suffering.

Ex vivo biodistribution studies

Eleven to twelve days after inoculation, animals were intravenously injected with [^{18}F]fluoro-DBCOfolate [^{18}F]24 and [^{18}F]fluoro-ala-folate [^{18}F]25 with 5-8 MBq in 100-200 µL sodium chloride solution. Blocking studies were performed with native folic acid (100 µg in 100 µL PBS) injected directly prior administration of the tracer. Animals were sacrificed 1 h after injection and selected organs were dissected, weighed and measured in a œ-counter. The incorporated radioactivity was expressed as percentage of injected activity per gram of tissue [% ID/g].

In vivo PET studies

Eleven or twelve days after inoculation animals were anesthetized with 2 % isoflurane in an air/oxygen mixture (70 % O2) and intravenously injected with [^{18}F]fluoro-DBCO-folate [^{18}F]24 and [^{18}F]fluoro-alafolate [^{18}F]25 (5-8 MBq, 100-200 µL). For blocking studies mice were injected with native folic acid (100 µg in 100 µL PBS) prior to the radiotracer injection. MRI measurements (Material Map for coregistration of the PET scan; 3D Gradient Echo External Averaging (GRE-EXT), Multi Field of View (FOV); slice thickness: 0.6 mm; TE: 2 ms; TR: 15 ms; flip angle: 25 deg) were performed before the whole body-PET scans were acquired over 60 min post-injection (p.i.) or over 10 min 50 min p.i.. PET data were dynamically reconstructed with Teratomo 3D (4 iterations, 6 subsets, voxel size 0.4mm) in user-defined frames using (3x10; 3x30; 3x60; 5x300; 3x600sec) or statically using one 10 min frame. Afterwards the PET images were coregistered to the MR and analyzed with pmod software (version 3.6). Manually drawn regions of interest (ROIs) were used to calculate the accumulated activity in tumor, liver and kidney (cortex and complete) as SUV (standardized uptake value).

Results and Discussion

Organic Chemistry

The tosylated DBCO-based labeling precursor 6 was obtained in a very good overall yield of 28 % over four steps. The first step yielded ethylene glycolate 3 in 74 %, enabling amide coupling. To generate a suitable leaving group, intermediate 3 was reacted with p-toluenensulfonyl chloride to obtain compound 4 in 67 %. After quantitative deprotection the tosylated linker 5 was coupled to the DBCOamine via amide bond formation, obtaining the radiolabeling precursor 6 with 56 %. To facilitate the whole synthesis as well as to minimize side reaction the DBCO-amine was introduced during the last synthesis step. Finally, reference compound 7 was obtained via the reaction with tetrabutylammonium fluoride in 82 % giving a high overall yield of 23 % over five steps. [22]

The chlorinated alanine-based labeling precursor 13 was obtained with an overall yield of 15 % over five steps. To ensure regioselective functionalization of serine, an extensive protecting group chemistry was necessary starting with the protection of the amino functionality using 2,4dimethoxybenzaldehyde obtaining intermediate 9. Pre-incubation of the aldehyde with triethylamine resulted in a slightly higher yield of 60 % than reported by Schieferstein *et al.*[20] Protection of the hydroxyl function with triisopropylsilyl in quantitative yields led to intermediate 10, which was Nalkylated using 3-bromo-1-(trimethylsilyl)-1-propyne giving compound 11 in 51 % yield. Tetrabutylammonium fluoride was used to cleave the TMS protecting group at the alkyne-function 12 (yield: 67 %), which subsequently was chlorinated to give the labeling precursor by using ptoluenesulfonyl chloride in 79 % yield. As already pointed out before, it was not possible to isolate the tosylated precursor due to the high reactivity of the tosyl group next to multiple electron withdrawing functionalities. Reference compound 16 was synthesized by fluorination of intermediate 12 using DAST [(diethylamino)sulfur trifluoride)] obtaining compound 14 in 62 %. Complete deprotection was performed using lithium hydroxide (1M, 60 %) and trifluoroacetic acid (86 %) obtaining the reference compound 16 with an overall yield of 6 % over seven steps. Both, labeling precursor and reference could be obtained in good overall yields and a good stability of the labeling precursor at room temperature and under air.

Folate azide 23 was prepared by amide coupling of protected pteroic acid 22 and an azidefunctionalized glutamate 19. The glutamate 19 was synthesized according to El-Faham et al. [24] in an overall yield of 70 % over two steps. To synthesize the pteroic acid part of the final tracer, folic acid was stepwise degraded following the procedure published by Temple *et al*. [23] Acetic anhydride and acetic acid was used to obtain acetyl-pyrofolic acid 21 with 79 % followed by the addition of sodium hydroxide to give acetyl-pteroic acid 22 in 57 %. The synthesis of the folate azide 23 was facilitated through amide

coupling of pteroic acid 22 and the glutamate derivative 19 using COMU and DIPEA (66 %) and an overall yield of 30 % over three steps.

The final reference compound 24 was obtained via copper-free cycloaddition of the folate azide 23 and prosthetic group 7 in aqueous phosphate-buffered saline (PBS) followed by semi-preparative HPLC in 9 % yield.The Cu(I)-catalyzed cycloaddition of the folate azide 23 and the prosthetic group 16 was performed in aqueous ethanol using the $CuSO_4$ and sodium ascorbate system and purification via semi-preparative HPLC yielding reference compound 25 in a good yields of 26 %.

Radiochemistry

The DBCO-based prosthetic group [^{18}F]7 was obtained by nucleophilic substitution of the tosylprecursor 6 in overall RCYs of 17.1 ± 4.2 % (purity ш99 %) including HPLC and C18 cartridge purification within 60 min. After evaporation of the solvent the ^{18}F-prosthetic group participated in a copper-free click reaction with the azido-folate 23 in PBS at 40 °C giving a RCY of 76 % within 15 min. After HPLC ;ш95 % purity, for HPLC chromatogram see supporting information) and C18 cartridge purification the final product [^{18}F]24 was obtained with an overall radiochemical yield of 3.2 ± 1.8 % and a total synthesis time of 120 min giving 60-190 MBq (specific activity: 1.8 – 2.4 GBq/µmol) of the formulated product [^{18}F]24. Coinjection of reference compound 24 into the analytical HPLC system confirmed the identity of the tracer, which is the first copper-free labeled [^{18}F]fluoro-click-folate evaluated in µPET and biodistribution studies.

Furthermore, the protected alanine-based prosthetic group [^{18}F]14 was obtained by nucleophilic substitution of the respective chloro-precursor 13 with 80 % ^{18}F-incorporation. After quantitative deprotection with hydrochloride acid, the crude product [^{18}F]16 was neutralized and purified via semipreparative HPLC giving the ^{18}F-prosthetic group in good overall RCY of 29.4 ± 7.7 % within 90 min and a purity of ш99 %.The product fraction of [^{18}F]16 was evaporated and used for Cu(I)-catalyzed click reaction with the azido-folate 23 using the Cu(II) and sodium ascorbate system in aqueous ethanol. After 15 min at 70 °C, almost quantitative conversion could be observed yielding [^{18}F]25 in good overall RCY of 19.3 ± 2.8 % after HPLC purification (ш97 % purity, for HPLC chromatogram see supporting information) and formulation. However, a complete separation of [^{18}F]16 from the nonradioactive precursor 13 was not achievable, resulting in a high load of non-radioactive material in the product. Consequently, the specific activity of [^{18}F]25 was very low (2 – 2.6 GBq/µmol). Maximum activity amounts of 480 - 610 MBq within 150 min could be obtained. [^{18}F]25 was identified by coinjection with reference compound 25 by analytical HPLC. The combination of the click chemistry approach with this novel alanine-based prosthetic group provides a highly efficient procedure to synthesize hydrophilic

folic acid derivatives without sophisticated protecting groups. Compared to previously reported [^{18}F]fluoro-click-folate derivatives [16,18,27] excellent radiochemical yields of up to 22 % were achieved. However, the enduring synthesis time of 150 min can be reduced by automatization, which would make the novel hydrophilic radiotracer accessible for routine production and translation into clinics.

Lipophilicity

octanol-water partition coefficient

The shake flask method was used to determine the distribution of the [^{18}F]fluoro-DBCO [^{18}F]7 and [^{18}F]fluoro-alakyne [^{18}F]16, as well as the two novel [^{18}F]fluoro-folate derivatives [^{18}F]24 and [^{18}F]25 in an octanol/PBS system under physiological pH conditions. From the distribution coefficients the $logD_{7.4}$ value was calculated being 1.25 ± 0.21 for [^{18}F]7 and 0.69 ± 0.08 for [^{18}F]24, indicating a rather lipophilic character of the [^{18}F]fluoro-DBCO-folate compared to published folate derivatives (Table 1). In contrast, the alanine-based derivatives, as expected, showed a much lower $logD_{7.4}$ value of -1.18 ± 0.03 for [^{18}F]16 and -1.43 ± 0.08 for [^{18}F]25. These findings indicate the favorable hydrophilic character of [^{18}F]25. Additionally, for the [^{18}F]fluoro-ala-folate the lipophilicity was also determined at pH 2.4 using a phosphoric acid solution. As expected, a much lower logD value of -3.56 ± 0.17 was obtained due to protonation of the amine moieties within the molecule. Table 1 gives an overview of logD values reported for several folate derivatives in the literature. By comparing these results, first hints on the excretion pathway pattern *in vivo* of both folate derivatives could be received. The copper-free labeled [^{18}F]fluoro-DBCO-folate has a more lipophilic character triggering a predominant hepatobiliary excretion. In contrast, the [^{18}F]fluoro-ala-folate seems to be promising due to its more polar character in comparison the DBCO-folate indicating a predominant renal excretion pathway, and thus, an improved image quality.

Table1: Overview of logD values obtained for different fluorinated folate derivatives at pH 7.4.

Folate derivative	$logD_{7.4}$ value	Literature
[^{19}F]fluoro-TEG-DBCO-TEG-folate	0.69 ± 0.08	*this work*
[^{19}F]fluoro-ala-folate	-1.43 ± 0.08 (-3.56 ± 0.17) *	*this work*
[^{18}F]FDG-folate	-1.54 ± 0.03	[16]
[^{18}F]fluorobutyl-folate	-2.7 ± 0.1	[27]
[^{18}F]fluoroethyl-folate	-3.0 ± 0.1	[27]
Albumin-binding[^{18}F]FDG-folate	-3.2 ± 0.4	[21]
3´-Aza-2´[^{19}F]fluorofolic acid	-4.2 ± 0.1	[19]
[^{18}F]FDG(click)folate	-4.2 ± 0.1	[15]

*determined at pH 2.4

Relative lipophilicity (k´ value)

The relative lipophilicity can be used to compare different radiofolates based on their polarity. Therefore, the capacity factor (k´ value) was determined using a standardized reversed-phase HPLC system. By comparing literature examples (table 2) an idea regarding liver uptake, hepatobiliary excretion and abdominal background of the [^{18}F]fluoro-folate derivative can be given. The retention time (t_R) for the [^{19}F]fluoro-ala-folate was 2.89 min, which equals a k´ value of 0.27. This is even lower than the value found for native folic acid (t_R=3.07 min, k´=0.30) and the 2´-[^{18}F]fluorofolic acid (k´=0.53), which already showed excellent *in vivo* behavior. [18] The reason for this very low value is due to the acidic HPLC eluent (pH 2.4), which leads to protonation of the extra amine function of the [^{19}F]fluoro-ala-folate. The k´ value on a neutral pH HPLC showed a k' value of 0.40, which is still lower than the one found for 2´-[^{18}F]fluorofolic acid. This suggests that the use of the alanine moiety as a prosthetic group has a rather negligible influence on the polarity compared to folic acid and therefore, [^{18}F]fluoro-ala-folate might be a very promising candidate for *in vivo* µPET imaging. In contrast the copper-free labeled [^{18}F]fluoro-DBCO-folate showed a slightly higher k´ value of 0.50 ± .10 (t_R=3.26 min). Especially, the value obtained on a neutral HPLC system of 0.88 ±0.13 reveals that this folate derivative might show a predominant hepatobiliary excretion leading to a higher abdominal background and an impaired image quality as already observed for the [^{18}F]fluoro-TEG-triazol-TEGfolate (k´value of 1.12). [17] The [^{18}F]fluoro-DBCO-folate also has a secondary amine function that can be protonated explaining the lower k´value of 0.50 at pH 2.4.

Table2: Overview of k´values obtained for different fluorinated folate derivatives obtained at pH 2.

Folate derivative	k´ value (relative lipophilicity)	Literature
^{19}F-Ala-folate	0.27 (0.40*)	*this work*
native folic acid	0.30	[14]
^{19}F-TEG-DBCO-TEG-FS	0.50 ± 0.10 (0.88 ± 0.13*)	*this work*
2´[^{19}F]fluorofolic acid	0.53	[18]
^{19}F-Benzyl-FS	0.67	[14]
^{19}F-TEG-triazol-TEG-FS	1.12	[17]
^{19}F-Propyl-triazol-FS	2.28	[14]

*determined at pH 7.4 (phosphate buffer)

In vitro studies

stability studies in human serum albumin

To test the stability of the two novel ^{18}F-labeled folate-based radiotracers, they were incubated in human serum albumin (HSA) at 37 °C for 1 and 2 h, respectively. No degradation nor defluorination of the radiotracers was observed over a period of 2 h indicating no considerable stability problem for the duration of a µPET scan as shown in figure 1 in the supporting information.

binding affinity studies

Figure 1 shows the displacement curve of [^{3}H]folic acid (8 x 10^{-7} M) with reference compound 24 and 25 in various concentrations ranging from 10^{-4} to 10^{-12} M giving the inhibitory concentration of 50 % inhibition (IC_{50}). For the DBCO-folate 24 we obtained a slightly higher IC_{50} value of 11.2 ± 3.7 nM (pIC_{50} value of 7.98 ± 0.21) than for native folic acid (1.9 nM). From the Cheng-Prusoff equation a K_i value of 6.3 ±1.4 nM was calculated for the DBCO-folate 24 and 1.6 nM for native folic acid, assuming a K_D value of 1 nM for [^{3}H]folic acid. These results indicate a very high affinity of DBCO-folate 24 to the folate receptor. As expected, the derivatization of the folate molecule shows no significant influence on the binding affinity to the folate receptor, since the pharmacophore is the pteroic part of the molecule.

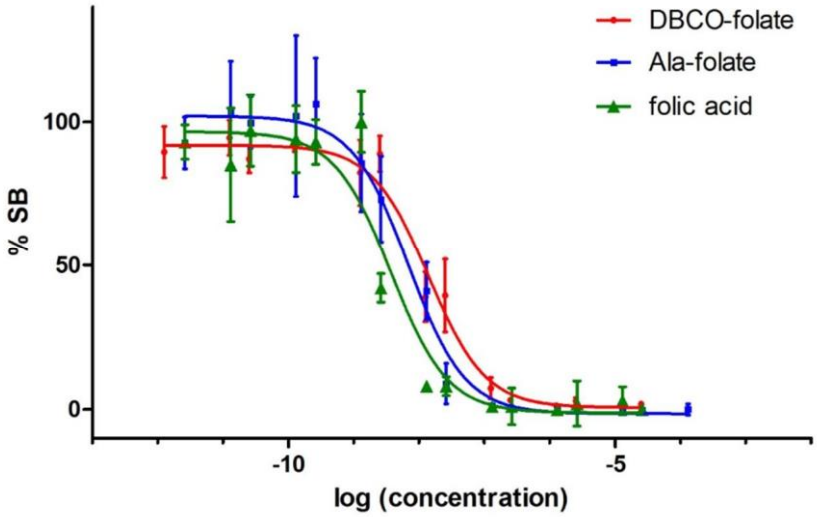

Figure 1: Curve of the displacement assay of [^{3}H]folic acid with [^{19}F}]fluoro-DBCO-folate 24 and [^{19}F]fluoro-ala-folate 25, using different concentrations of folate derivative ranging from 10^{-4} to 10^{-12} M. Errors are given as standard deviation representing n=3.

For the Ala-folate 25 an IC_{50} value of 6.4 ± 0.5 (pIC_{50} value of 8.20 ± 0.05) was obtained and from these values a K_i value of 5.5 ± 0.4 was calculated. These data demonstrate again that the FR tolerates even very bulky derivatization such as boron cluster with no loss in affinity at the non-pteroic acid part of the molecule. [25]

Tabel 3 provides an overview of IC_{50} and pIC_{50} values for various [^{18}F]fluoro-folate derivatives. The pIC_{50} value displays the negative logarithm of the IC_{50} value in molar in analogy to the pH value. The pIC_{50}

value is much more appropriate to describe a logarithmic phenomenon such as the dose dependent displacement of a novel radiotracer and eases the comparison between the different compounds. This is especially very helpful if the values vary in a wide range over a few potencies. In the case of the [^{18}F]fluoro-folate derivatives shown in table 3, the pIC_{50} values are quiet similar, representing the high affinity to the FR of all presented compounds.

Table 3: Overview of IC_{50} and pIC_{50} valued obtained for different fluorinated folate derivatives using KB cells and [^{3}H]folic acid.

Folate derivative	IC_{50}	pIC_{50}	Literature
3´-Aza-2´[^{18}F]fluorofolic acid	0.8 ± 0.2 nM	9.11 ± 0.16	[19]
[^{18}F]fluoroethyl-folate	1.4 ± 0.2 nM	8.86 ± 0.08	[27]
[^{18}F]FDG-folate	1.5 ± 0.3 nM	8.84 ± 0.12	[27]
native folic acid	1.9 nM	8.72	*this work*
[^{18}F]fluorobutyl-folate	2.1 ± 0.2 nM	8.68 ± 0.06	[27]
2´-[^{18}F]fluorofolic acid	3.4 ± 0.3 nM	8.75 ± 0.04	[18]
[^{18}F]fluoro-ala-folate	6.4 ± 0.5 nM	8.20 ± 0.05	*this work*
[^{18}F]fluoro-DBCO-folate	11.2 ± 3.7 nM	7.98 ± 0.21	*this work*
[^{18}F]fluoro-click-folate	18.0 ± 7.1 nM	7.78 ± 0.26	[14]
Folate-NOTA-Al[^{18}F]F	18.7 nM	7.73	[28]

internalization studies

Both [^{18}F]fluoro-folate radiotracer [^{18}F]24 and [^{18}F]25 were tested using FR-positive KB cells including blockade studies with an excess of native folic acid as well as FR-negative OC316 cells. Figure 2 displays the results of internalization studies with the [^{18}F]fluoro-DBCO-folate [^{18}F]24 at concentrations of 1 and 5 nM for 1 h at 4 °C and 37 °C, respectively. It could be confirmed that the internalization rate is reduced at 4 C compared to 37 °C. Furthermore, a concentration depended increase of activity in the cells was observed when increasing the concentration from 1 to 5 nM. Especially, for incubation at 5 nM and 37 °C an increased receptor-specific internalization of [^{18}F]24 in the KB cells was observed. Due to the quite lipophilic character of this [^{18}F]fluoro-folate derivative, a distinct unspecific binding was detected for the blocked KB cells and especially for the FR-negative OC316 cells which led to an increased background signal. However, these experiments proof the tolerant receptor-mediated internalization of [^{18}F]24 into the FR-positive KB cells. Figure 3 shows the distribution of [^{18}F]24 in the uptake assay at 5 nM and 37 °C indicating that only about 3 % of the tracer was actually taken up und about 7 % were receptor bound. Thus, about 90 % of [^{18}F]24 were not binding.

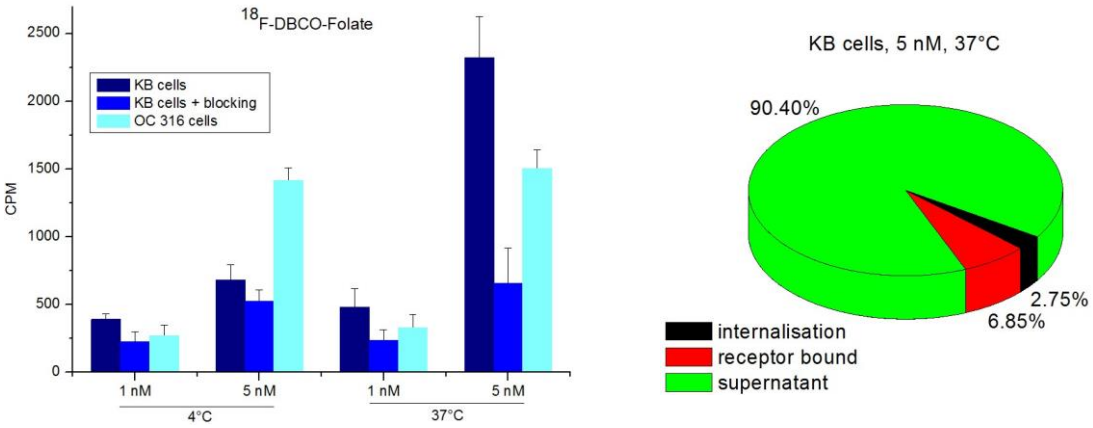

Figure 2: Internalization of [^{18}F]24 and blockade studies with excess of folic acid in FR-positive KB cells and FR-negative OC316 cells at 4 °C and 37 °C for 1h. Errors are given as standard deviation representing n=3 (left). Pie chart of the [^{18}F]24 distribution after incubation (1h) with 5 nM within one sample of KB cells (right).

In contrast, Figure 3 shows the results of internalization studies with the [^{18}F]fluoro-ala-folate [^{18}F]25 at incubation concentrations of 1 and 5 nM for 1 h at 4 °C and 37 °C. As for the more hydrophilic folate derivative [^{18}F]25 expected, a much lower unspecific binding was observed which resulted in an improved background signal. A clearly visible blocking effect using native folic acid (95 %) underlines the specificity in FR-positive KB cells. However, the overall receptor-bound and internalized fraction are similar to [^{18}F]24.

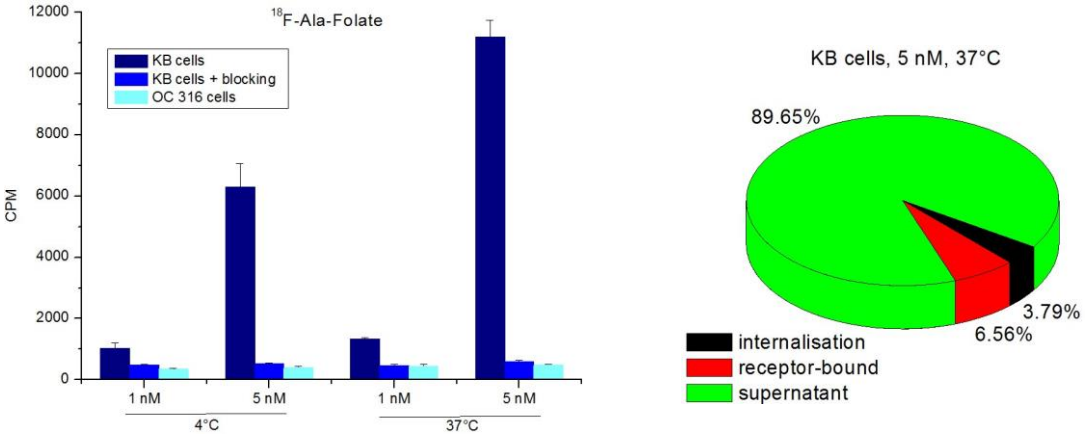

Figure 3: Internalization of [^{18}F]25 and blockade studies with excess folic acid in FR-positive KB cells and FR-negative OC316 cells at 4 °C and 37 °C for 1h. Errors are given as standard deviation representing n=3 (left). Pie chart of the [^{18}F]25 distribution after incubation (1h) with 5 nM within one sample of KB cells (right).

Animal studies

Ex vivo biodistribution studies

The results of the biodistribution studies of the DBCO-folate derivative [^{18}F]24 are shown in table 4 and figure 4. Groups of healthy and KB-tumor bearing mice (n=4) were sacrificed 60 min p.i. after injection of 5-7 MBq [^{18}F]24. Furthermore, healthy mice and KB-tumor bearing mice (n=5) which received a pre-block of native folic acid (100 µg in 100 µL PBS) were sacrificed 60 min p.i.

Table 4: *Ex vivo* biodistribution studies of [^{18}F]fluoro-DBCO-folate [^{18}F]24 in healthy and KB tumor bearing balb/c and balb/c nu/nu mice after 60 min p.i. Errors are given as standard deviation.

	healthy balb/c mice		balb/c mice, KB xenograft	
%ID/g	60 min p.i. (n = 4)	60 min p.i. Blockade[a] (n = 5)	60 min p.i. (n = 4)	60 min p.i. Blockade[a] (n = 5)
Pancreas	0.08 ± 0.01	0.09 ± 0.05	0.07 ±0.01	0.03 ± 0.02
ing LN	0.18 ± 0.08	0.10 ± 0.08	0.48 ± 0.14	0.04 ± 0.02
Lung	0.35 ± 0.27	0.36 ± 0.11	0.17 ±0.06	0.13 ± 0.05
Blood	0.08 ± 0.01	0.12 ± 0.05	0.09 ± 0.04	0.06 ± 0.04
Heart	0.09 ± 0.01	0.11 ± 0.06	0.08 ± 0.02	0.04 ± 0.02
Liver	0.24 ± 0.02	0.33 ± 0.08	0.18 ± 0.07	0.14 ± 0.06
Intestines (empty)	0.87 ± 0.57	0.33 ± 0.22	0.42 ± 0.52	0.56 ± 0.81
Spleen	0.07 ± 0.02	0.11 ± 0.06	0.06 ± 0.02	0.05 ± 0.03
Left kidney	3.90 ± 0.38	0.40 ± 0.07	4.83 ± 0.90	0.30 ± 0.04
Right kidney	3.99 ± 0.37	0.38 ± 0.07	4.76 ± 0.89	0.30 ± 0.02
urine	50.08 ± 15.09	89.19 ± 0.253	31.03 ± 34.67	25.91 ± 43.73
testes	0.18 ± 0.03	0.12 ± 0.07	0.19 ± 0.07	0.03 ± 0.02
muscle	0.06 ± 0.01	0.07 ± 0.05	0.07 ± 0.01	0.02 ± 0.01
Stomach (empty)	n.d.	n.d.	0.82 ± 0.64	0.22 ± 0.09
appendix	n.d.	n.d.	0.13 ± 0.02	0.07 ± 0.01
tumor			0.48 ± 0.14	0.09 ± 0.04
tumor/blood			5.61	
tumor/liver			2.58	
tumor/kidney			0.05	
tumor/muscle			6.86	

[a]In the blocking group, each animal received 100 µg/100 µL of folic acid in phosphate buffered saline (PBS) 2 min before radiotracer injection. n.d., no data

FR-specific uptake was found in the tumor (0.48 ± 0.14 %ID/g tissue) and other FR-positive tissues such as the kidneys (4.80 ± 0.90 %ID/ g tissue) where the FR is expressed in the proximal tubule cells. [7] Significantly reduced uptake (81 %) of the radiotracer in tumor tissue (0.09 ± 0.04 %ID/g tissue) was observed by using native folic acid as blocking agent. The same findings were observed for the kidneys (94 %, 0.30 ± 0.03 %ID/g tissue). The highest uptake was found in the urine confirming the fast and predominant renal clearance of this radiotracer. Also the radioactivity in the blood was very low after 60 min p.i. (0.09 ± 0.04 %ID/g tissue) indicating a fast clearance of [^{18}F]24 from the blood pool. The tumor-to-kidney-ratio was quiet low (0.05), but a good tumor-to-liver-ratio (2.6) was observed. Surprisingly, no strong accumulation of the tracer was observed in the liver although [^{18}F]24 showed a relatively high lipophilicity compared to other ^{18}F-labeled folates. In general the uptake values in FRpositive tissues are low due to reduced specific activities (1.8 – 2.4 GBq/µmol).

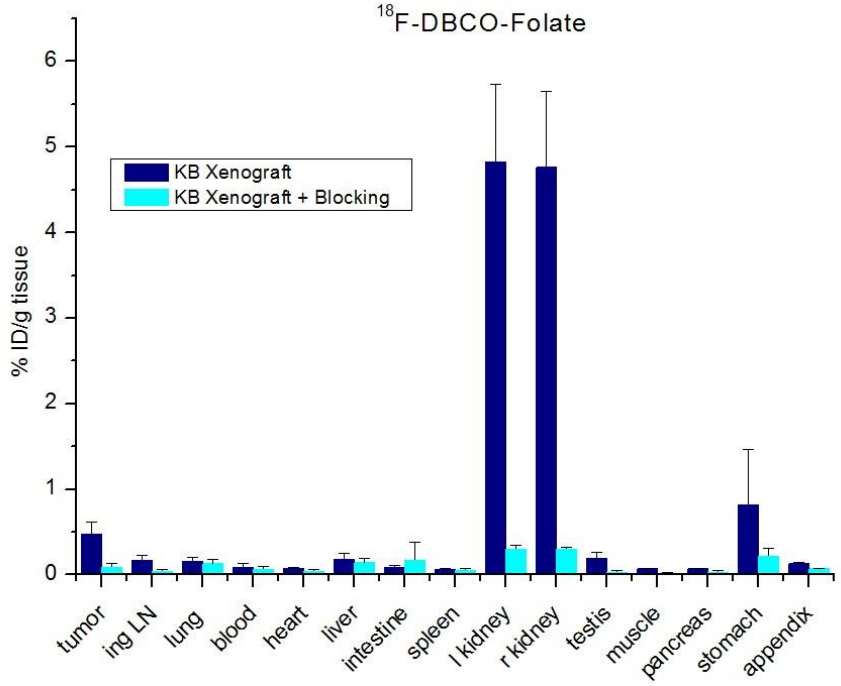

Figure 4: Results of biodistribution study at 60 min p.i. of [^{18}F]24.

The results of the biodistribution studies with the [^{18}F]fluoro-ala-folate derivative [^{18}F]25 are shown in table 5 and figure 5. Groups of healthy (n=3) and KB-tumor bearing mice (n=5) were sacrificed 60 min p.i. of 5-8 MBq [^{18}F]25. Furthermore, healthy mice (n=3) and KB-tumor bearing mice (n=4) received a pre-block of native folic acid (100 µg in 100 µL PBS) and were sacrificed 60 min p.i. of [^{18}F]25.

Table 5: *Ex vivo* biodistribution studies of [^{18}F]fluoro-ala-folate [^{18}F]25 in healthy and KB tumor bearing balb/c and balb/c nu/nu mice after 60 min p.i. Errors are given as standard deviation.

	healthy balb/c mice		balb/c mice, KB xenograft	
%ID/g	60 min p.i. (n = 3)	60 min p.i. Blockade[a] (n = 3)	60 min p.i. (n = 5)	60 min p.i. Blockade[a] (n = 4)
Pancreas	0.33 ± 0.20	0.16 ± 0.04	0.26 ± 0.11	0.12 ± 0.08
ing LN	0.93 ± 0.67	0.27 ± 0.15	0.57 ± 0.15	0.17 ± 0.12
Lung	0.36 ± 0.16	0.38 ± 0.05	0.28 ± 0.05	0.19 ± 0.10
Blood	0.29 ± 0.29	0.18 ± 0.01	0.17 ± 0.05	0.13 ± 0.06
Heart	0.32 ± 0.21	0.14 ± 0.04	0.22 ± 0.09	0.09 ± 0.05
Liver	1.51 ± 1.26	1.63 ± 0.32	1.71 ± 1.02	1.34 ± 0.67
Intestines (empty)	1.67 ± 1.12	4.86 ± 3.97	3.42 ± 2.18	1.49 ± 1.23
Spleen	0.15 ± 0.09	0.14 ± 0.03	0.16 ± 0.04	0.11 ± 0.06
Left kidney	19.90 ± 8.63	1.88 ± 0.44	14.49 ± 3.42	1.07 ± 0.49
Right kidney	20.55 ± 9.71	1.72 ± 0.58	14.27 ± 3.35	1.00 ± 0.36
urine	83.99 ± 32.64	n.d.	419.81 ± 302.77	0.30 ± 0.42
muscle	0.26 ± 0.13	0.15 ± 0.02	0.22 ± 0.02	0.22 ± 0.13
Stomach (empty)	0.71 ± 0.24	1.99 ± 1.68	0.95 ± 0.50	2.50 ± 1.80
appendix	0.20 ± 0.11	3.11 ± 1.71	0.39 ± 0.22	0.13 ± 0.04
tumor			1.68 ± 0.13	0.26 ± 0.06
tumor/blood			10.11	2.02
tumor/liver			0.98	0.19
tumor/kidney			0.12	0.24
tumor/muscle			7.64	1.18

[a]In the blocking group, each animal received 100 µg/100 µL of folic acid in phosphate buffered saline (PBS) 2 min before radiotracer injection. n.d., no data

By comparing the DBCO-folate [^{18}F]24 with the Ala-folate [^{18}F]25 a 3-times higher tumor uptake (1.68 ±

0.13 %ID/g tissue) was observed for the Ala-folate. Additionally, the specific kidney uptake (14.38 ± 3.39 %ID/g tissue) could be significantly reduced by 93 % for the kidneys and 85 % for tumor tissue via blocking with native folic acid, demonstrating high specificity of the [^{18}F]fluoro-ala-folate. However, all FR positive tissues still show rather low uptake values, which might be due to the high load of nonradioactive mass deriving from the presence of the "clickable" precursor 13 in the product [^{18}F]16. As a consequence, 13 is inherently clicked to the azido-folate, and thus, adds cold mass to the [^{18}F]fluoroala-folate able to bind to the folate receptor. The tumor-to-blood-ratio was twice as high for the [^{18}F]fluoro-ala-folate (10.11) than for the [^{18}F]fluoro-DBCO-folate (5.61), which seems to be due to the lipophilic character of the DBCO-moiety. Furthermore, the tumor-to-kidney and the tumor-to-muscle ratios are clearly higher for the [^{18}F]fluoro-ala-folate derivative, leading to a much better image quality due to the reduced noise during the image acquisition. Compared to the recently reported [^{18}F]fluoroPEG-folate [18], a slightly increased tumor-to-kidney-ratio was observed and furthermore, the unspecific accumulation in the liver, the feces and the empty intestines could be decreased for [^{18}F]fluoro-ala-folate. These observations correlate with the three times lower k´ value as an indicator of lipophilicity with regard to [^{18}F]25.

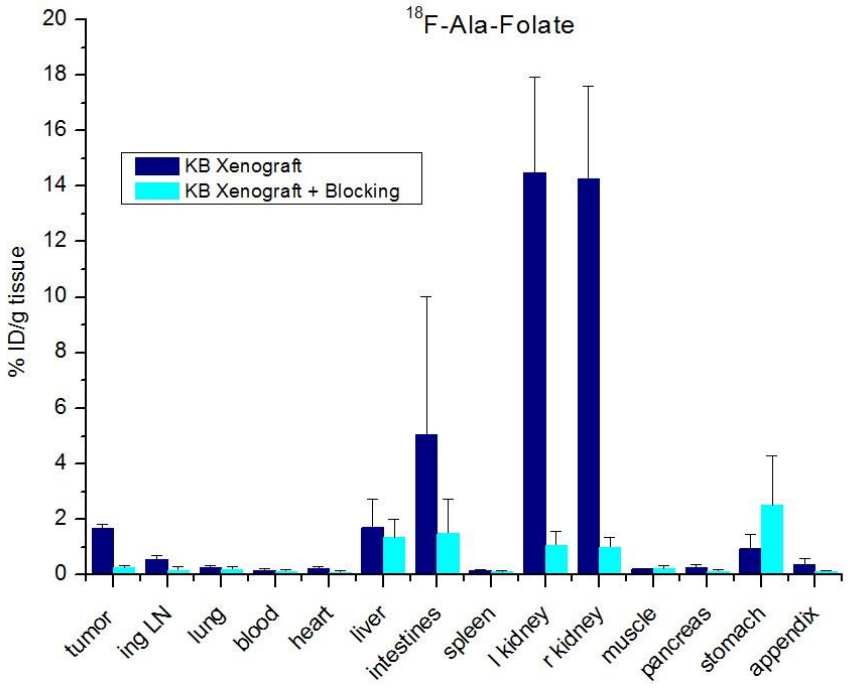

Figure 5: Results of biodistribution study at 60 min p.i. of [^{18}F]25.

In vivo PET studies

Healthy and KB tumor-bearing mice with the tumor located at the right shoulder were used for µPET imaging studies. To obtain the pharmacokinetic profiles of the radiotracers, dynamic scans were performed over 60 min with one mouse each. These dynamic scans showed that the equilibrium in the tumor was already reached after 5 min giving a constant signal in the tumor. Therefore, static scans over 10 min were performed 50 min after injection to allow the animals to efficiently clear the unbound tracer, which led to an improved background signal. The low accumulation of the tracer in the tumors shown in the *ex vivo* biodistribution of the [^{18}F]fluoro-DBCO-folate [^{18}F]24, revealed that the tumor is not detectable in a maximum intensity projection (MIP, data not shown). Additionally, the kidneys are not clearly visible indicating no or low binding to the receptors in the proximal tubule cells. Furthermore, a considerable amount of activity was found in the abdominal region, more precisely in the intestines due to the metabolism/excretion of lipophilic folates via gallbladder, liver and feces. [29,30]

In contrast, [^{18}F]fluoro-ala-folate [^{18}F]25 displayed the tumor clearly in the MIP (figure 6) as expected from *ex vivo* biodistribution. Furthermore, a clear visualization of the kidney cortex proofs folate receptor specific uptake of the [^{18}F]fluoro-ala-folate in the kidneys. Additionally, a distinct abdominal accumulation can be seen, but the tumor-to-background contrast is much higher compared to the [^{18}F]fluoro-DBCO-folate [^{18}F]24 and the recently reported [^{18}F]fluoro-TEG-folate due to a reduced lipophilicity resulting in the improved image quality.

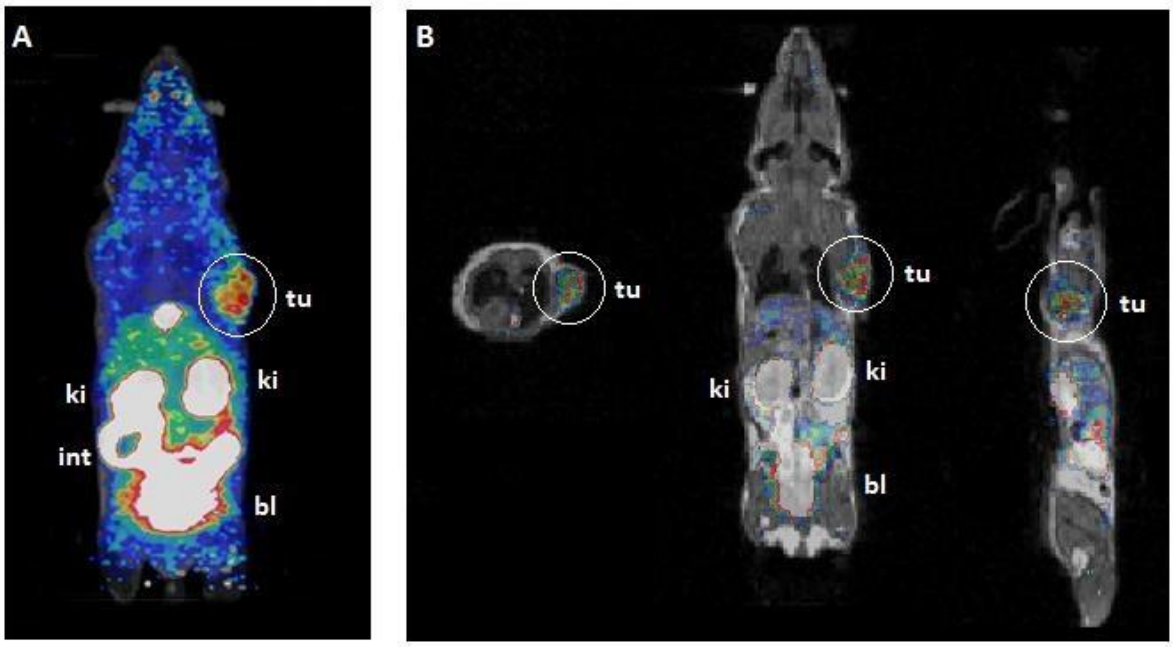

Figure 6: PET images of a KB-tumor bearing mouse. Static scan over 10 min 50 min p.i. of [^{18}F]fluoro-ala-folate [^{18}F]25 (approximately 7 MBq). (A) Maximal intensity projection (B) representative sagittal, coronal and transversal slice. tu, tumor; ki, kidneys; bl, bladder.

Under blockade conditions, the tumor and kidney uptake was negligible, whereas activity in the gallbladder was not reduced or rather slightly reduced for the liver. In contrast to previous findings where the accumulation was only observed in the outer rim of the tumors [17], the novel radiofolate showed a more homogeneous uptake. PET quantification resulted in mean SUV in the tumors of 0.3, but further revealed “hot spots” in the tumor with SUV of up to 2.5. These results were achieved due to reduced cell number inoculation and the usage of matrigel (CORNING MATRIGEL, growth factor reduced), which is thought to retard tumor growth of xenograft models. This should result in a lower internal tumoral pressure and an improved tumor vascularization. [^{18}F]25 showed a reduced hepatobiliary excretion and abdominal background compared to the [^{18}F]fluoro-TEG-folate.

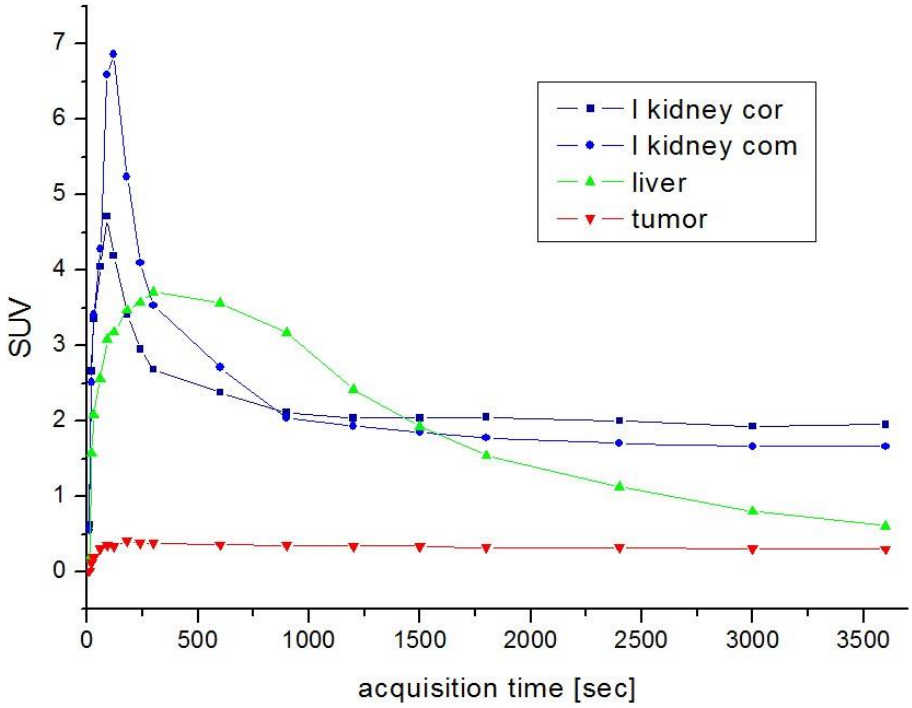

Figure 7: Accumulation kinetic of [^{18}F]25 in the kidneys, the liver and the KB tumor. Analysis of a dynamic PET scan over 60 min p.i. of approximately 6 MBq of [^{18}F]25.

Figure 7 shows the dynamic of the accumulation (time activity curves) of [^{18}F]25 within 60 min p.i. in a KB-tumor bearing mouse. The tumor uptake stays constant over time while the kidney accumulation reduces to the amount of receptor-specific uptake due to renal clearance of the radiotracer. Also the liver uptake is reduced over time through hepatobiliary excretion via liver, gallbladder and intestines.

Conclusions

Two novel ^{18}F-labeled folic acid derivatives [^{18}F]24 and [^{18}F]25 were synthesized using a DBCO-based ^{18}F-prosthetic group for copper free click chemistry and a hydrophilic alanine entity for coppercatalyzed cycloaddition. The DBCO-based ^{18}F-prosthetic group [^{18}F]7 was investigated with the aim to develop a catalyst free but fast, regioselective and bioorthogonal labeling method for folate derivatives using the well-established click chemistry approach. In contrast, the alanine entity was used as a ^{18}F-prosthetic

group ([^{18}F]16) to increase the overall polarity of the ^{18}F-labeled folate radiotracer. Furthermore, it showed clear advantages over the DBCO-based ^{18}F-prosthetic group ([^{18}F]7) such as high radiochemical yields of the radiolabeling and click reaction. Both radiotracers showed high affinity to the folate receptor, but unspecific binding was significantly reduced through the hydrophilic alanine moiety resulting in an improved image quality. However, due to an incomplete separation of [^{18}F]16 form its precursor, the [^{18}F]fluoro-ala-folate carries a high load of non-radioactive mass able to bind to folate receptor, indicating that the given results might even underestimate the potential of [^{18}F]25. Further work to develop an improved precursor for [^{18}F]16 is in warranted. In summary, the alanine folate derivative [^{18}F]25 was clearly superior to [^{18}F]24 and showed good and FRspecific tumor uptake *in vivo* and would consequently be a promising candidate for PET imaging of FRpositive cancer as well as inflammatory diseases.

Ethical statement

All experiments with commercial available human serum (Sigma Aldrich, H4522, from human male AB plasma) were conducted in accordance with the local law and national and institutional guidelines and ethics. The officer for biological safety has approved the performed experiments and informed consent was obtained for any experiment with commercial available human serum. All animal experiments were performed in accordance with federal guidelines and approved by the ethical committee of the state of Rheinland Pfalz (according to §8 Abs. 1 Tierschutzgesetz, Landesuntersuchungsamt; permission no. 23177-07/G15-1-033).

Acknowledgments

The authors thank the Max Planck Graduate Center and the Graduate School of the SFB 1066 for supporting Kathrin Kettenbach.

References

[1] V. Schirch, and W. B. Strong, "Interaction of Folylpolyglutamates with enzymes in one-carbon metabolism," *Archives of Biochemistry and Biophysics*, vol. 269, pp.3 71-80, 1989.

[2] A. C. Antony, "Folate Receptors," *Annual Review of Nutrition,* vol. 16, pp. 501-21, 1996.

[3] J. W. Locasale, "Serine, glycine and one-carbon units: Cancer metabolism in full circle," *Nature Reviews Cancer*, vol. 13, no. 8, pp 572-583, 2013.

[4] H. Yuasa, K. Inoue, and Y. Hayashi, "Molecular and functional characteristics of protoncoupled folate transporter," *Journal of Pharmaceutical Sciences*, vol. 98, no- 5, pp. 16081616, 2009.

[5] J. R. Whetstine, R. M. Flatley, L. H. Matherly, "The human reduced folate carrier gene is ubiquitously and differentially expressed in normal human tissue: identification of seven noncoding exons and characterization of a novel promoter," *Biochemical Journal*, vol. 367, pp. 629-40, 2002.

[6] C.-Y. Ke, C. J. Mathias, and M. A. Green, "The folate receptor as a molecular target for tumorselective radionuclide delivery," *Nuclear Medicine and Biology*, vol. 30, no. 8, pp. 811-817, 2003.

[7] N. Parker, M. J. Turk, E. Westrick, J. D. Lewis, P. S. Low, and C. P. Leamon, "Folate receptor expression in carcinomas and normal tissues determined by a quantitative radioligand binding assay," *Analalytical Biochemistry*, vol. 338, no. 2. pp. 284-293, 2005.

[8] J. W. van der Heijden, R. Oerlemans, B. A. Dijkmans, H. Qi, C. J. van der Laken, W. F. Lems, A. L. Jackman, M. C. Kraan, P. P. Tak, M. Ratnam, and G. Jansen, "Folate receptor beta as a

potential delivery route for novel folate antagonists to macrophages in the synovial tissue of rheumatoid arthritis patients," *Arthritis & Rheumatology*, vol. 60, no. 1, pp. 12-21, 2009.

[9] P. S. Low, W. A. Henne, and D. D. Doorneweerd, "Discovery and development of folic-acidbased receptor targeting for imaging and therapy of cancer and inflammatory diseases," *Accounts of Chemical* Research, vol- 41, no. 1. pp. 120-129, 2008.

[10] E. I. Sega, and P. S. Low, "Tumor detection using folate receptor-targeted imaging agents," *Cancer Metastasis* Review, vol. 27, no. 4, pp. 655-664, 2008.

[11] S. D. Weitmann, A. G. Weinberg, L. R. Coney, V. R. Zurawski, D. S. Jennings, and B. A. Kamen, "Cellular Localisation of the Folate Receptor: Potential Role in Drug Toxicity and Folate Homeostasis," *Cancer Research*, vol- 52, no. 23, pp. 6708-11, 1992.

[12] S. D. Weitmann, R. H. Lark, L. R. Coney, D. W. Fort, V. Frasca, and V. R. Zurawski, "Distribution of the Folate Reecptor GP38 in Normal and Maligant Cell Lines and Tissues," *Cancer Research*, vol. 52, no. 12, pp. 3396-401, 1992.

[13] A. Bettio, M. Honer, C. Müller, M. Brühlmeier, U. Müller, R. Schibli, V. Groehn, A P. Schubiger, amd S. M. Ametamey, "Synthesis and Preclinical Evaluation of a Folic Acid Derivative Labeled with 18F for PET Imaging of Folate Receptor-Positive Tumors," *Journal of Nuclear Medicine*, vol. 47, no. 7, pp. 1153-60, 2006.

[14] T. L. Ross, M. Honer, P. H. Lam, T. L. Mindt, V. Groehn, R. Schibli, P. A. Schubiger, and S. M. Ametamey, "Fluorine-18 click radiosynthesis and preclinical evaluation of a new ^{18}F-labeled folic acid derivative," *Bioconjugate Chemistry*, vol. 19, no. 12, pp. 2462-2470, 2008.

[15] C. R. Fischer, C. Müller, J. Reber, A. Müller, S. D. Krämer, S. M. Ametamey, and R. Schibli, "[^{18}F]Fluoro-Deoxy-Glucose Folate: A Novel PET Radiotracer with Improved in Vivo Properties for Folate Receptor Targeting," *Bioconjugate Chemistry*, vol. 23, no. 4, pp. 805-813, 2012.

[16] I. Al Jammaz, B. Al-Otaibi, S. Amer, N. Al-Hokbany, and S. Okarvi, "Novel synthesis and preclinical evaluation of folic acid derivatives labeled with (18)F-FDG for PET imaging of folate receptor-positive tumors," *Nuclear Medicine and Biology*, vol. 39, no. 6, pp. 864-870, 2012.

[17] H. Schieferstein, T. Betzel, C. R. Fischer, and T. L. Ross, "^{18}F-click labeling and preclinical evaluation of a new ^{18}F-folate for PET imaging," *EJNMMI research*, vol. 3, no. 1, pp. 68, 2013.

[18] T. L. Ross, M. Honer, C. Muller, V. Groehn, R. Schibli, and S. M. Ametamey, "A new ^{18}F-labeled folic acid derivative with improved properties for the PET imaging of folate receptor-positive tumors," *Journal of Nuclear Medicine*, vol. 51, no. 11, pp. 1756-1762, 2010.

[19] T. Betzel, C. Muller, V. Groehn, A. Müller, J. Reber, C. R. Fischer, S. D. Krämer, R. Schibli, and S. M. Ametamey, "Radiosynthesis and preclinical evaluation of 3'-Aza-2'-(18)Ffluorofolic acid: a novel PET radiotracer for folate receptor targeting," *Bioconjugate Chemistry*, vol. 24, no. 2, pp. 205-214, 2013.

[20] H. Schieferstein, T. L. Ross, "A Polar ^{18}F-Labeled Amino Acid Derivative for Click Labeling of Biomolecules," *European Journal of Organic Chemistry*, vol. 2014, no. 17, pp. 3546-3550, 2014.

[21] C. R. Fischer, V. Groehn, J. Reber, R. Schibli, S. M. Ametamey, and C. Muller, "Improved PET imaging of tumors in mice using a novel (18) F-folate conjugate with an albumin-binding entity," *Molecular Imaging and Biology*, vol. 16, no. 6, pp. 649-654, 2013.

[22] K. Kettenbach, and T. L. Ross, "A ^{18}F-labeled dibenzocyclooctyne (DBCO) derivative for copper-free click labeling of biomolecules" *Med Chem* Comm, vol. 7, no. 4, pp. 654-657, 2016.

[23] C. Temple, J. D. Rose, and J. A. Montgomery, "Chemical Conversion of Folic Acid to Pteroic Acid," *The Journal of Organic Chemistry*, vol. 46, no. 18, pp. 3666-3667, 1981.

[24] A. El-Faham, and F. Albericio, "COMU: a third generation of uronium-type coupling reagents," *Journal of Peptide Science*, vol. 16, no. 1, pp. 6-9, 2010.

[25] K. Kettenbach, H. Schieferstein, C. Grunewald, D. Iffland, L. M. Reffert, G. Hampel, C. L. Schütz, N. H. Bings, and T. L. Ross, "Synthesis and evaluation of boron folates for Boron-Neutron-Capture-Therapy (BNCT)," *Radiochimica Acta*, vol. 103, no. 11,pp. 799-809, 2015.

[26] T. L. Ross, M. Honer, P. H. Lam, T. L. Mindt, V. Groehn, R. Schibli, P. A. Schubiger, and S. M-Ametamey, "Fluorine-18 Click Radiosynthesis and Preclinical Evaluation of a New ^{18}F-Labeled Folic Acid Derivative," *Bioconjugate Chemistry*, vol. 19, no. 12, pp. 2462-2470, 2008.

[27] S. D. Boss, T. Betzel, C. Müller, C. R. Fischer, S. Haller, J. Reber, V. Groehn, R. Schibli, and S. M. Ametamey, "Comparative Studies of Three Pairs of ɲ- and œ-Conjugated Folic Acid Derivatives Labeled with Fluorine-18," *Bioconjugate Chemistry*, vol. 27, no. 1, pp. 74-86, 2016.

[28] Q. Chen, X. Meng, P. McQuade, D. Rubins, S.-A. Lin, Z. Zeng, H. Haley, P. Miller, D. G. Trotter, and P. S. Low, "Synthesis and Preclinical Evaluation of Folate-NOTA-Al(18)F for PET Imaging of Folate-Receptor-Positive Tumors," *Molecular Pharmaceutics*, vol. 13, no. 5, pp. 1520-1527, 2016.

[29] F. Horn, "*Biochemie des Menschen: Das Lehrbuch für das Medizinstudium,"* 4. Auflage: Georg Thieme Verlag; 2009.

[30] P. J. Stover, "Physiology of Folate and Vitamin B_{12} in Health and Disease," *Nutrition Reviews*, vol. 62, no. 6, pp. 3-12, 2004.

Supplementary data

In vitro and *in vivo* comparison study of a folate derivative labeled with fluorine-18 via copper-free and copper-catalyzed cycloaddition

Kathrin Kettenbach[1], Hanno Schieferstein[1], Stefanie Pektor[2], Raphael Eckert[1], Laura M. Reffert[3], Georg Otto[2], Matthias Miederer[2], Frank Rösch[1]. Tobias L. Ross[1,3]

[1] Institute of Nuclear Chemistry, Johannes Gutenberg University Mainz, 55128 Mainz, Germany

[2]Department of Nuclear Medicine, University Medical Centre Mainz, 55131 Mainz, Germany

[3] Radiopharmaceutical Chemistry, Department of Nuclear Medicine, Hannover Medical School, 30625 Hannover, Germany

Content

I. ORGANIC SYNTHESES OF DBCO-DERIVATIVES

I.1. Synthesis of DBCO-based labeling precursor

I.2. Synthesis of DBCO-based reference compound

This content can be found in supplementary information "A ^{18}F-labeled Dibenzocyclooctyne(DBCO)Derivative for Copper-free Click Labeling of Biomolecules".

II. ORGANIC SYNTHESES OF ALANINE-DERIVATIVES

II.1. Synthesis of Alanine labeling precursor

Methyl-2-((2,4-dimethoxybenzyl)amino)-3-(oxy)-propanoate (9)

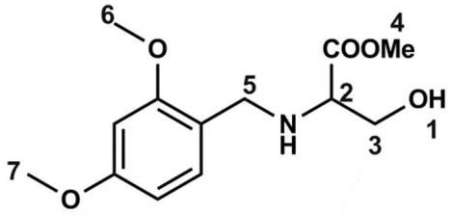

L-serine methylester hydrochloride 8 (2 g, 12.84 mmol) and 2,4-dimethoxybenzaldehyde (2.12 mg, 12.84 mmol) were dissolved in dry methanol (30 mL). Triethylamine (1.08 mL, 1.3 g, 12.84 mmol) was added and the reaction mixture was stirred for 30 min at rt. Sodium cyanoboronhydride (1.6 g, 25.46 mmol) was added and the mixture was stirred at rt for additionally 24 h. Dichloromethane (40 mL) was added and the organic layer was extracted 3-times (10 mL) with sodium bicarbonate solution (1M). The organic layers were dried over magnesium sulfate and the solvent was removed under reduced pressure. The product was purified by column chromatography (ethylacetate, R_f = 0.29) obtaining 9 as yellow oil (2.08 g, 7.73 mmol, 60 %).

^{1}H-NMR (300 MHz, $CDCl_3$, Me_4Si): ω [ppm] = 2.75 (br, 1H, H-1), 3.42 (dd, 1H, $^3J_{H-H}$ = 4.5 Hz, H-2), 3.63 (q, 1H, $^3J_{H-H}$ = 6.3 Hz, H-3), 3.70 (s, 3H, H-4), 3.75 – 3.77 (d, 2H, $^3J_{H-H}$ = 5.7 Hz, H-5), 3.79 – 3.81 (d, 1H, $^3J_{H-H}$ = 6.4 Hz, H-3), 3.82 (s, 3H, H-6), 3.84 (s, 3H, H-7), 6.43 – 6.47 (m, 2H, Ar-H), 7.10 (d, 1 H, $^3J_{H-H}$ = 7.8 Hz, Ar-H).

MS (ESI positive): m/z 270.1 ($[M]^+$, 100 %) ,calculated for $C_{13}H_{19}NO_5$: 269.1.

Methyl-2-((2,4-dimethoxybenzyl)amino)-3-((triisopropylsilyl)oxy)-propanoate (10)

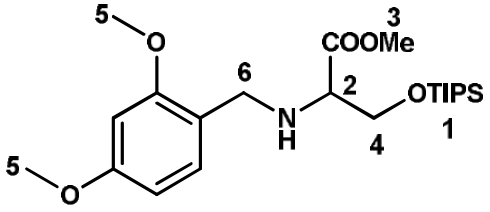

A solution of 9 (1.28 g, 3.87 mmol) and triisopropylsilyl chloride (1.12 mL, 1.02 g, 5.08 mmol) in dry dimethylformamide (60 mL) was cooled to 0 °C. Then imidazole (643 mg, 9.44 mmol) was added and the reaction mixture was stirred at rt for 12 h. The solvent was removed under high vacuum and the residue was resolved in dichloromethane (30 mL) and extracted 3-times with water (5 mL). The organic phase was dried over magnesium sulfate and the solvent was removed under reduced pressure. The product was purified by column chromatography (n-hexane:ethyl acetate/4:1, R_f = 0.3) obtaining 10 as a yellow oil (1.47 g, 3.68 mmol, 95 %).

^{1}H-NMR (300 MHz, $CDCl_3$, Me_4Si): ω [ppm] = 1.05 (m, 21H, H-1), 3.46 (t, 1H, $^3J_{H-H}$ = 5.7 Hz, H-2), 3.69 (s, 3H, H-3), 3.73 (s, 1H, H-4), 3.81 (s, 6H, H-5), 3.86 – 3.97 (m, 3H, H-4 und H-6), 6.42 – 6.45 (m, 2H, ArH), 7.15 (d, 1H, $^3J_{H-H}$ = 8.7 Hz, Ar-H).

MS (ESI positive): m/z 426.6 ([M]$^+$, 100 %),calculated for $C_{22}H_{39}NO_5Si$: 425.3.

Methyl-2-((2,4-dimethoxybenzyl)(3-(trimethylsilyl)prp-2-yn-1-yl)amino)-3-((triisopropylsilyl)propanoate (11)

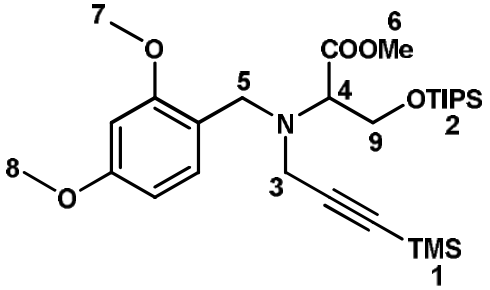

To a solution of 10 (1.47 g, 3.68 mmol) in dry acetonitrile (60 mL) 3-bromo-1-(trimethylsilyl)-1propyne (900 µL, 0.77 g, 4.03 mmol) was added and the reaction mixture was stirred for 10 min at 60 °C. Then cesium carbonate (2.48 g, 7.61 mmol) was added and the reaction mixtures was stirred at 100 °C for additionally 12 h. The reaction was quenched with water (200 mL) and extracted 3-times with dichloromethane (10 mL). The organic layer was dried over magnesium sulfate and the solvent was removed under reduced pressure. The product was purified by colum chromatography (nhexane:ethyl acetate/7:1, R_f = 0.4) obtaining 11 as a colorless oil (997 mg, 1.86 mmol, 51 %).

^{1}H-NMR (300 MHz, $CDCl_3$, Me_4Si): ω [ppm] = 0.19 (s, 9H, H-1), 1.06 (s, 21H, H-2), 3.51 (s, 2H, H-3), 3.73 (s, 1H, H-4), 3.71-3.79 (m, 2H, H-5), 3.74 (2, 3H, H-6), 3.80 (s, 3H, H-7), 3.81 (s, 3H, H-8), 4.07-4.16 (m, 2H, H-9), 6.44-6.47 (m, 2H, Ar-H), 7.28 (d, 1H, $^3J_{H-H}$ = 8.7 Hz, Ar-H).

MS (ESI positive): m/z 536.3 ([M]$^+$, 100 %),calculated for $C_{28}H_{49}NO_5Si_2$: 535.3.

Methyl 2-((2,4-dimethoxybenzyl)(prop-2-yn-1-yl)amino)-3-hydroxy-propanoate (12)

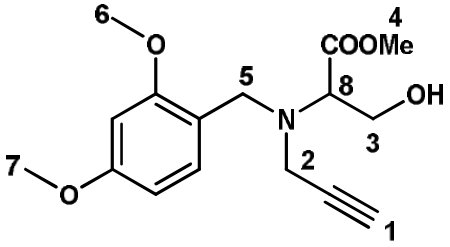

Compound 11 (1.17 g, 2.18 mmol) was dissolved in tetrahydrofurane (5 mL). Then tetrabutylamonniumfluoride (9.4 mL, 1 M in THF) was added and the reaction mixture was stirred at rt for 12 h. The solvent was removed under reduced pressure and the product was purified using column chromatography (n-hexane:ethylacetate/3:1, R_f = 0,18) obtaining 12 as a colorless oil (447 mg, 1.46 mmol, 67 %).

^{1}H-NMR (300 MHz, $CDCl_3$, Me_4Si): ω [ppm] = 2.22 (t, 1H, $^3J_{H-H}$ = 2.3 Hz, H-1), 3.39-3.49 (dd, 2H, $^3J_{H-H}$ = 2.7 Hz, H-2), 3.57 (d, 1H, $^3J_{H-H}$ = 13.3 Hz, H-3), 3.72 (s, 3H, H-4), 3.77-3.79 (m, 2H, H-5), 3.80 (s, 3H, H6), 3.81 (s, 3H, H-7), 3.90 (d, 1H, $^3J_{H-H}$ = 9 Hz, H-8), 4.02-4.06 (d, 1H, $^3J_{H-H}$ = 12.8 Hz, H-3), 6.42-6.47 (m, 2H, Ar-H), 7.13 (d, 1H, $^3J_{H-H}$ = 8.1 Hz, Ar-H).

MS (ESI positive): m/z 308.1 ([M]$^+$, 100 %),calculated for $C_{16}H_{21}NO_5$: 307.3.

Methyl 3-chloro-2-((2,4-dimethoxybenzyl)(prop-2-yn-1-yl)amino)-propanoate (13)

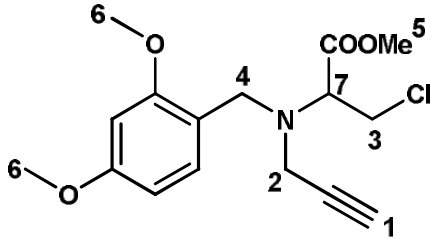

A solution of compound 12 (208 mg, 0.68 mmol) and *p*-toluenesulfonyl chloride (259 mg, 1.36 mmol) in dry acetonitrile (5 mL) was cooled to 0 °C. Then triethylamine (252 µL, 184 mg, 1.82 mmol) was added and the reaction mixture was stirred at 60 °C for 12h. The solvent was removed under reduced pressure and the product was purified using column chromatography (n-hexane:ethylacetate/5:1, R_f = 0.39) obtaining 13 as a yellow oil (175 mg, 0.54 mmol, 79 %).

^{1}H-NMR (300 MHz, $CDCl_3$, Me_4Si): ω [ppm] = 2.25 (t, 1H, $^3J_{H-H}$ = 2.7 Hz, H-1), 2.96-3.22 (ddd, 2H, $^3J_{H-H}$ = 19 Hz, H-1), 3.34 (s, 2H, H-3), 2.68 (s, 2H, H-4), 3.76 (s, 3 H, H-5), 3.80 (s, 6H, H-6), 4.05 (dd, 1H, $^3J_{H-H}$ = 5.7 Hz, H-7), 6.42-6.44 (m, 2H, Ar-H), 7.14 (d, 1H, $^3J_{H-H}$ = 8.8 Hz, Ar-H).

MS (ESI positive): m/z 326.1 ([M]$^+$, 100 %),calculated for $C_{16}H_{20}ClNO_4$: 325.1.

I.2. Synthesis of Alanine-alkyne reference compound

Methyl 2-((2,4-Methoxybenzyl)(prop-2-yn-1-yl)amino)-3-fluoro-propanoate (14)

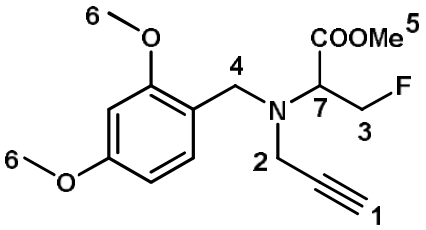

Compound 12 (438 mg, 1.46 mmol) dissolved in dry dichloromethane (29 mL) and (diethylamino)sulfur trifluoride (189 µL, 0.15 mmol) was added at room temperature. The reaction mixture was stirred for one hour, quenched with water (30 mL) and extracted 3-times with dichloromethane (15 mL). The organic layer was dried over magnesium sulfate and the solvent was removed under reduced pressure. The product was purified by colum chromatography (nhexane:ethyl acetate/4:1, R_f = 0.3) obtaining 14 as a colorless oil (280 mg, 0,91 mmol, 62 %).

^{1}H-NMR (400 MHz, $CDCl_3$, Me_4Si): ω [ppm] = 2.27 (t, 1H, $^3J_{H-H}$ = 2.3 Hz, H-1), 3.05 (m, 2H, H-2), 3.45 (dd, 2H, $^3J_{H-H}$ = 2.5 Hz, H-3), 3.72 (s, 2H, H-4), 3.78 (s, 3 H, H-5), 3.82 (s, 6H, H-6), 5.04 (dd, 1H, $^3J_{H-H}$ = 3.8 Hz, H-7), 6.46-6.49 (m, 2H, Ar-H), 7.22 (d, 1H, $^3J_{H-H}$ = 8.8 Hz, Ar-H).

MS (ESI positive): m/z 310.2 ([M]$^+$, 100 %),calculated for $C_{16}H_{20}FNO_4$: 309.1.

2-((2,4-Methoxybenzyl)(prop-2-yn-1-yl)amino)-3-fluoropropanoic acid (15)

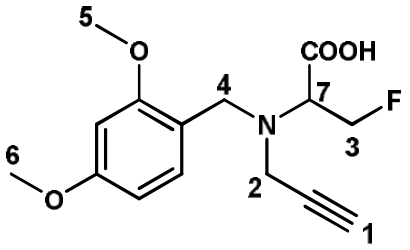

To a solution of 14 (90 mg, 0.28 mmol) in tetrahydrofuran (1 mL) and *tert*-butanol (1 mL) a 1 M lithium hydroxide solution (water) was added. The reaction mixture was stirred at 40 °C for 2 h followed by the separation of the two layers. The solvents of the organic layer were removed under reduced pressure,

the residue was resolved in dichloromethane and filtered. The product 15 (50 mg, 0,17 mmol, 60 %) was obtained as a yellow solvent after removing the solvents under reduced pressure.

^{1}H-NMR (400 MHz, $CDCl_3$, Me_4Si): ω [ppm] = 2.20 (t, 2H, $^3J_{H-H}$ = 2 Hz, H-1), 2.99 (m, 2H, H-2), 3.24 (2, 2H, H-3), 3.58 (s, 2H, H-4), 3.67 (2, 3H, H-5), 3.68 (s, 3H, H-6), 4.88-5.09 (dd, 1H, $^3J_{H-H}$ = 7.1 Hz, H-7), 6.33 (m, 2H, Ar-H), 7.12 (d, 1H, $^3J_{H-H}$ = 9.3 Hz, Ar-H).

MS (ESI positive): m/z 296.2 ([M]$^+$, 100 %),calculated for $C_{15}H_{18}FNO_4$: 295.1.

3-fluoro-2-(prop-2-yn-1-ylamino)propanoic acid (16)

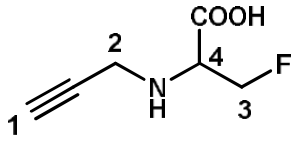

Compound 15 (150 mg, 0.51 mmol) was solved in dry dichloromethane (7 mL) and trifluoroacetic acid (15 mL) was added. The reaction mixture was stirred at room temperature for 48 h followed by coevaporation with toluene (3-times, 2 mL). The residue was resolved in methanol (2 mL) and filtered. The filtrate was diluted with water (40 mL) and a C18 cartridge was used to separate the product from side products. The solvent was removed under reduced pressure and the product 16 (TFA-salt, 114 mg, 0.44 mmol, 86 %) was obtained as a yellow oil.

^{1}H-NMR (400 MHz, CD_3OD, Me_4Si): ω [ppm] = 3.25 (t, 1H, $^3J_{H-H}$ = 2.6 Hz, H-1), 3.52-3.85 (m, 2H, H-2), 4.02 (d, 2H, $^3J_{H-H}$ = 2.3 Hz, H-3), 5.08-5.27 (dd, 1H, $^3J_{H-H}$ = 7.6 Hz, H-4).

MS (ESI positive): m/z 146.1 ([M]$^+$, 100 %),calculated for $C_6H_8FNO_2$: 145.05 und $C_8H_9FN4_2$: 259.1.

Tert-Butyl-3-(2-(2-(2-(2-ethoxy)ethoxy)ethoxy)ethylcarbamoylazid)-1-(methoxycarbonyl)propylcarbamate (18)

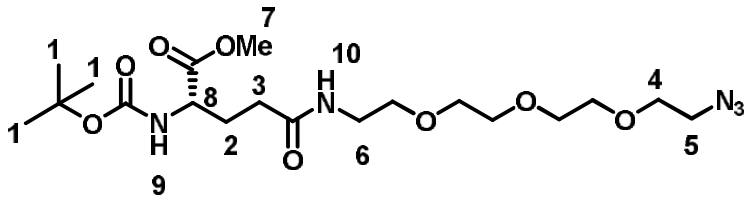

N-(tert-Butoxycarbonyl)-*L*-glutaminsäure-ɲ-methylester 17 (500 mg, 1.90 mmol) was solved in dry acetonitrile (17 mL) and DIPEA (332 µL, 246 mg, 1.90 mmol) and (1-Cyano-2-ethoxy-2oxoethylidenaminooxy)dimethylamino-morpholino-carbenium hexafluorophosphate (COMU, 813 mg, 1.90 mmol) were added. After 10 min 11-Azido-3,6,9-trioxyundecan-1-amin (377 µL, 415 mg, 1.90 mmol) and another equivalent DIPEA (332 µL, 246 mg, 1.90 mmol) were added and the reaction mixture was stirred at rt for 16 h. The solvent was removed under reduced pressure and the residue was resolved in ethylacetate (35 mL). The organic layer was washed with HCl (0.5 M, 3 x 20 mL), $NaHCO_3$ solution (1M, 3 x 20 mL) and NaCl solution (saturated, 3 x 20 mL). The organic layer were dried over $MgSO_4$, filtered and the solvent was removed under reduced pressure. The product was purified by colum chromatography (ethyl acetate, R_f = 0.18) obtaining 18 as a pale yellow oil (670 mg, 1.45 mmol, 76 %).

^{1}H-NMR (400 MHz, $CDCl_3$, Me_4Si): ω [ppm] = 1.43 (s, 9H, H-1), 1.91 – 1.99 (m, 1H, H-2), 2.14 – 2.22 (m, 1H, H-2), 2.25 – 2.30 (m, 2H, H-3), 3.39 (t, 2H, $^3J_{H-H}$ = 5.0 Hz, H-4), 3.44 – 3.48 (m, 2H, H-5), 3.56 (t, 2H, $^3J_{H-H}$ = 4.8 Hz, H-6), 3.61 – 3.70 (m, 10H, PEG-H), 3.73 (s, 3H, H-7), 4.28 (br, 1H, H-8), 5.35 (br, 1H, H-9), 6.32 (br, 1H, H-10).

MS (ESI positive): m/z 462.3 ([M]$^+$, 100 %),calculated for $C_{19}H_{35}N_5O_8$: 461.25.

Methyl-4-(2-(2-(2-(2-ethoxy)ethoxy)ethoxy)ethylcarbamoylazid)-3-aminobutanoate (19)

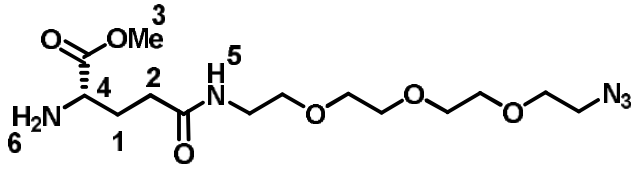

Compound 18 was dissolved in HCl (4M in dioxane, 15 mL) and the reaction mixture was stirred at rt for 16 h. The solvent was removed under reduced pressure and product 19 was obtained as a yellow oil (483 mg, 1.34 mmol, 92 %).

^{1}H-NMR (400 MHz, $CDCl_3$, Me_4Si): ω [ppm] = 2.40 (m, 2H, H-1), 2.59 (m, 2H, H-2), 3.41 – 3.67 (m, 16H, PEG-H), 3.81 (s, 3, H-3), 4.24 (br, 1H, H-4), 7.61 (br, 1H, H-5), 8.75 (br, 2H, H-6).

MS (ESI positive): m/z 362.2 ([M]$^+$, 100 %), calculated for $C_{14}H_{27}N_5O_6$: 361.20.

Acetyl-pyrofolic acid (21)

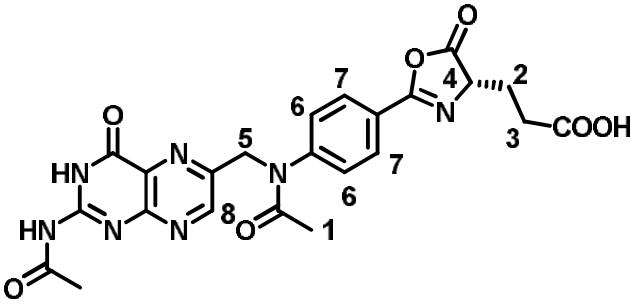

Folic acid 20 (5.00 g, 11.3 mmol) was suspended in acetic anhydride (87.5 mL) and acetic acid (12.5 mL) and heated to reflux for 2 h. The reaction mixture was poured into diethyl ether (500 mL) and filtered. The residue was resolved with water (50 mL) and lyophilized. The product 21 was obtained as a pale brown solid (4.52 g, 8.90 mmol, 79 %).

^{1}H-NMR (400 MHz, $CDCl_3$, Me_4Si): ω [ppm] = 2.09 (s, 3H, H-1), 2.35 (s, 2H, H-2), 2.58 – 2.80 (m, 2H, H3), 4.99 (m, 1H, H-4), 5.28 (s, 2H, H-5), 7.62 (d, 2H, $^3J_{H-H}$ = 8.5 Hz, H-6), 7.76 (d, 2H, $^3J_{H-H}$ = 8.6 Hz, H-7), 9.01 (s, 1H, H-8).

MS (ESI positive): m/z 508.1 ([M]$^+$, 100 %), 1015.3 (65%, [2M]$^+$, 95 %), calculated for $C_{23}H_{21}N_7O_7$: 507.15

Acetyl-pteroic acid (22)

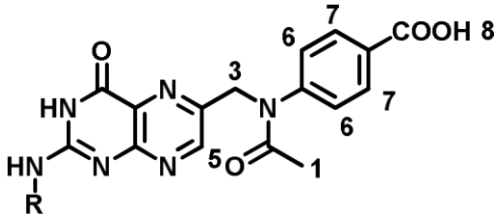

10: R = Ac 2
10a: R = H 4

Acetyl-pyrofolic aicd 21 (1.72 g, 3.386 mmol) was suspended in degased water (170 mL) and was slowly dissolved by adding NaOH solution (1M), keeping the pH below 11. The reaction mixture was stirred under argon atmosphere and light exclusion at rt for 48 h. After 5 and 22h the pH was readjusted to pH 10. After 48 h the pH was adjusted to 3.5 by using HCl solution (6M and 0.5M). The resulting residue

was filtered. The mono- and diacetyl-pyrofolic acid 22a and 22 was obtained as a brown solid (742 mg, 57 % (27 % 22a, 73 % 22)).

^{1}H-NMR (300 MHz, DMSO-d_6, Me_4Si): ω [ppm] = 1.92 (s, 3H, H-1), 2.19 (s, 3H, H-2), 5.02 (s, 2H, H-3), 5.12 (s, 2H, H-3), 6.92 (br, 2H, H-4), 7.52 – 7.60 (m, 2H, H-6), 7.91 – 7.95 (m, 2H. H-7), 8.63 (s, 1H, H-5), 11.94 (s, 1H, H-8), 12.27 (s, 1H, H-8).

MS (ESI positive): m/z 397.1 ([M(10a)]$^+$, 100 %), 355.1 ([M(10)]$^+$, 55 %), 793.3 ([2M(10)]$^+$, 40 %), calculated for $C_{18}H_{16}N_6O_5$: 396.12 and calculated for $C_{16}H_{14}N_6O_4$: 354.11.

N_{α}-(2-(2-(2-(2-Azidoethoxy)ethoxy)ethoxy)ethyl)-pteroyl-L-glutamine (23)

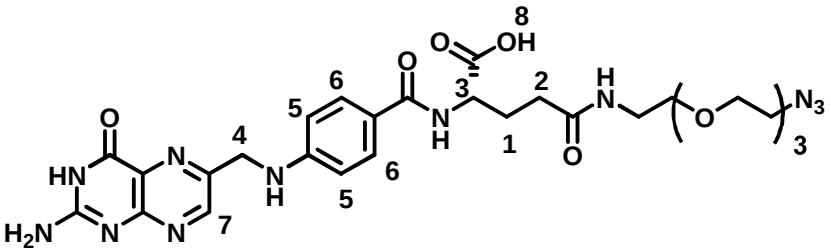

The mixture of compound 22a and 22 (148 mg, 0.373 mmol) was disolved in dry dimethylformamide (6 mL) and COMU (159 mg, 0.373 mmol) and DIPEA (35.6 µL, 26.4 mg, 0.373 mmol) were added. The reaction mixture was stirred for 30 min. Subsequently the amine 11 (135 mg, 0.373 mmol) in dry dimethylformamide (6 mL) and DIPEA (35.6 µL, 26.4 mg, 0.373 mmol) were added and the solution was stirred at 50 °C for 16h. The solvent was removed under reduced pressure and the residue was was washed with diethyl ather (2 x 10 mL). After the solid was dried *in vacuo*, NaOH solution (1M, 20mL) was aded and the reaction mixture was at RT for 16h. Subsequently the pH was adjusted to 2 using HCl solution (2M). The precipitated solid was filtered and washed with water (2 x 10 mL). The yellow product 23 (158 mg, 0.246 mmol, 66 %) was dried *in vacuo*.

^{1}H-NMR (400 MHz, CD_3OD, Me_4Si): ω [ppm] = 1.89 (m, 2H, H-1), 2.18 (m, 2H, H-2), 3.33 – 3.59 (m, 16 H, PEG-CH_2), 4.26 (m, 1H, H-3), 4.48 (s, 2H, H-4), 6.62 (d, 2H, $^3J_{H\text{-}H}$ = 8.4 Hz, H-5), 7.64 (d, 2H, $^3J_{H\text{-}H}$ = 8.4 Hz, H-6), 8.64 (s, 1H, H-7), 11.45 (s, 1H, H-8)

MS (ESI positive): m/z 321.7 ([M]$^{2+}$, 100 %), 642.3 ([M]$^+$, 70 %), calculated for $C_{27}H_{35}N_{11}O_8$: 641.27.

11-(1,2,3-Triazo-4-N-ethyl-(3-(2-(2-(2-fluoro-oxyethoxy)ethoxy)ethoxy)-N-[3-oxo-N-(DBCO)propyl] propanamide)3,6,7-trioxaundecan-1-yl)folic acid amide (24)

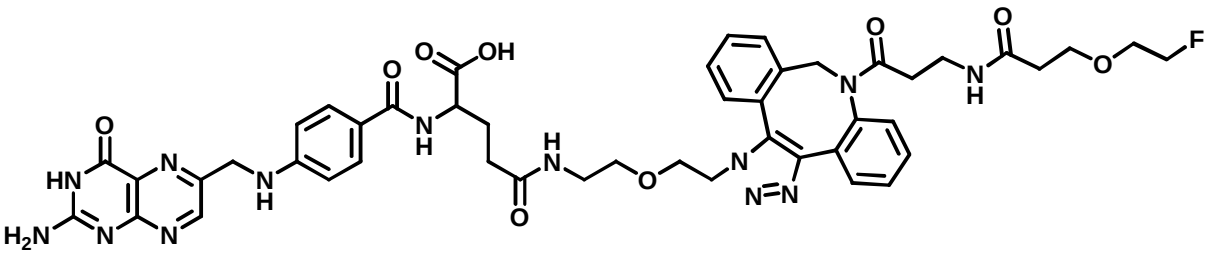

Compound 7 (4.2 mg, 8.7 µmol) and compound 23 (3.4 mg, 5.3 µmol) were dissolved in dry dimethylformamide (1mL). The reaction mixture was stirred at rt for 12 h followed by purification using semi-preparative HPLC (Luna, C18, 5 µm, 250x10 mm, flow of 3.5 mL/min, whereas A is water and B is acetonitrile. The following method was used: 0-17 min 5-95 % B (gradient), 17-19 min 95 % B (isocratic), 19-20 min 5-95 % A (gradient)) obtaining product 24 (0.5 mg, 0.45 µmol, 8.5 %) as a pale yellow solid.

MS (ESI positive): m/z 562.3 ([M]2+, 100 %), 1123.3 ([M]+, 10 %),calculated for C54H66FN13O13: 1123.5.

11-(1,2,3-Triazo-4-*N*-ethyl-(3-fluoro-2-(prop-2-yn-1-ylamino)propanoic acid)3,6,7,-trioxa unde-can-1-yl)folic acid amide (25)

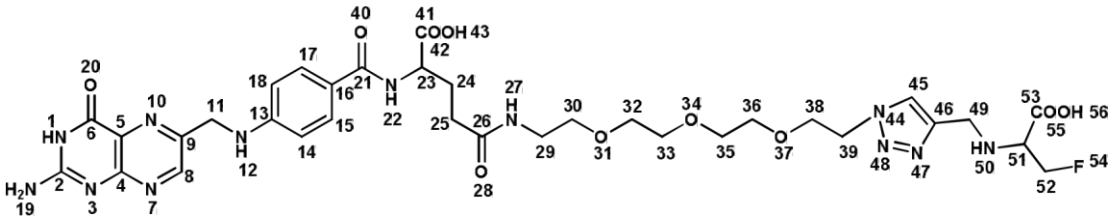

Compound 16 (20.2 mg, 0.078 mmol) was dissolved in ethanol (4 mL) and copper(II)sulfate (4.9 mg, 0.031 mmol) in phosphate buffered saline (0.5 mL), 11-azido-3,6,9-trioxaundecan-1-yl-folic acid amide 23 (50 mg, 0.078 mmol) in phosphate buffered saline (3.3 mL) and sodium ascorbate (24.8 mg, 0.125 mmol) in phosphate buffered saline (0.5 mL) were added. The reaction mixture was stirred at room temperature for 30 min. Because no product formation was observed, some more copper(II)sulfate (4.9 mg, 0.031 mmol) was added. After additionally 16 h the reaction mixture was purified using semipreperative HPLC system at a flow of 3.6 mL/min, whereas A is water and B is acetonitrile. The following method was used: 0-5 min 100 % A (isocratic), 5-114 min 0-60 % B (gradient), 14-17 min 95 % B (gradient),17-18 min 95 % B (isocratic), 18-19 min 5-100 % A (gradient). obtaining product 25 (9.2 mg, 0,021 mmol, 26 %) as a yellow solid.

^{1}H-NMR (600 MHz, DMSO-d_6, Me_4Si): ω [ppm] = 1.90 – 2.04 (m, 2H, H-24), 2.19 (m, 2H, H-25), 3.34 – 3.58 (m, 13H, H-30 – H-38 and H-51), 3.80 – 3.81 (m, 2H, H-29), 4.25 – 4.28 (m, 1H, H-23), 4.35 (s, 2H, H-49), 4.50 (s, 1H, H-50), 5.04 (s, 1H, H-12), 4.56 – 4.58 (m, 2H, H-39), 4.71 – 4.74 (m, 2H, H-11), 5.36 – 5.48 (m, 2H,H-52), 6.64 (d, 2H, $^{3}J_{H-H}$ = 8.5 Hz, H-14/18), 7.07 (s, 1H, H-27), 7.15 (s, 1H, H-1), 7.24 (s, 1H, H-22), 7.65 (d,2H, $^{3}J_{H-H}$ = 8.5 Hz, H-15/17), 8.20 (s, 1H, H-45), 8.67 (s, 1H, H-8), 9.57 (br, 2H, H-19).

^{13}C-NMR (600 MHz, DMSO-d_6) ω [ppm] = 26.9 & 27.1 (C24), 32.3 (C25), 42.0 (C49), 47.3 (C51), 50.3 (C39), 52.7 (C23), 66.9 (C11), 69.1 (C29), 69.5 – 70.1 (C30 – C38), 111.6 (C14/18), 126.5 (C45), 128.5 (C16), 129.4 (C15/17), 132.1 (C9), 138.3 (C46), 148.9 (C8), 151.2 (C13), 154.1 (C4), 158.5 (C2/5), 158.7 (C2/5), 166.8 (C21), 168.1 (C6/53), 168.2 (C6/53), 172.3 (C26), 174.1 (C41).

^{19}F-NMR (400 MHz, DMSO-d_6) ω [ppm] = -194.3 (F-54)

MS (ESI positive): m/z (% rel Int): 394.2 ($[M]^{2+}$, 100 %), 787.3 ($[M]^{+}$, 80 %), calculated for $C_{33}H_{43}FN_{12}O_{10}$: 786.32.

IV. ^{18}F-RADIOLABELING

IV.1. General radiolabeling methods

N.c.a. [^{18}F]fluoride ion was produced using the ^{18}O(p,n)^{18}F nuclear reaction. The aqueous ^{18}F-solution was then trapped on an anion exchange resin (Sep Pak light Waters Accell Plus QMA cartridge), which was pre-conditioned with 1 M potassium carbonate solution (10 mL) and rinsed with millipore water (10 mL). For the elution of the QMA a solution of tetraethylammonium bicarbonate (3.4 mg, 17 µmol) dissolved in acetonitrile (405 µL) and water (45 µL) was used for the preparation of [^{18}F]7 and a solution of Kryptofix (5 mg) and potassium carbonate (1 mg, 7.5 µmol) in 600 µL (acetonitrile:water/1:1) for the preparation of [^{18}F]16. The azeotropic drying was performed using a helium stream and heating to 85 °C for 20 min under reduced pressure (250 mbar) and helium flow. Within this time, dry acetonitrile (3 x 1 mL) was added and evaporated to yield final dry [^{18}F]fluoridebase mixture. The radiolabeling reaction was optimized concerning different heating methods (conventional and micro-wave assisted) and purification pathways.

IV.2. Synthesis of [^{18}F]7

After azeotropic drying of the [^{18}F]fluoride ion, the [^{18}F]fluoride-base mixture was dissolved in acetonitrile (0.5 mL) and transferred into a 5-mL sealed reaction vial containing the DBCO-precursor 9 dissolved in acetonitrile (0.5 mL). The reaction mixture was heated to 100 °C for 15 min (30 min for determining the kinetics) followed by quenching the labeling reaction with water (1 mL) and injection into a semi-preperative HPLC system at a flow of 2.5 mL/min, whereas A is water and B is acetonitrile. The following method was used: 50 % A (isocratic).After purification using semi-preparativ HPLC (figure 2), the fraction was diluted with water (10 mL) and fixed on a Sep-Pak light SPE cartridge (Sep Pak Light tC18). The fixed ^{18}F-prosthetic group was eluted with acetonitrile (1 mL) into a reaction vessel and the acetonitrile was removed using helium steam at 85 °C under reduced pressure (500 mbar) within 15 min. The dried prosthetic group was solved in the preferred reaction solvent to perform the click reaction. The ^{18}F-prosthetic group was prepared in an overall reaction time of 60 min with an overall yield (n.d.c.) of (11.4±2.8) % (n=4).

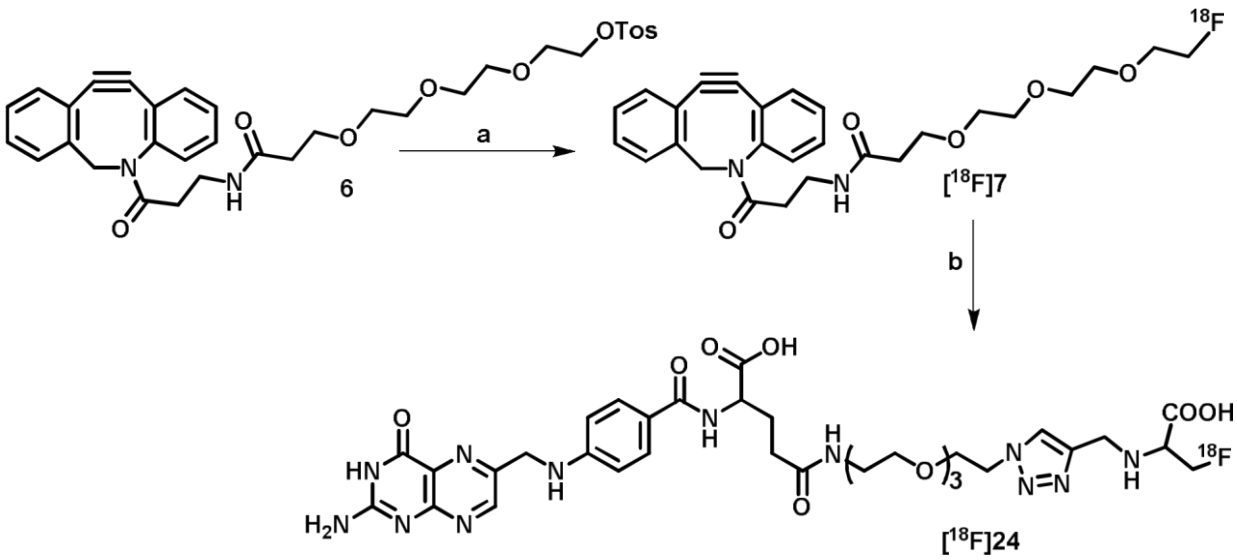

IV.3. Synthesis of [^{18}F]16

After azeotropic drying of the [^{18}F]fluoride ion, the [^{18}F]fluoride-base mixture was dissolved in dimethylsulfoxide (0.25 mL) and transferred into a 5-mL sealed reaction vial containing the alanineprecursor 7 dissolved in dimethylsulfoxide (0.25 mL). The reaction mixture was heated to 140 °C for 15 min followed by quenching the labeling reaction with ammonium formiate buffer (50 mM, 20 mL). A C18 cartridge was used to separate the unreacted [^{18}F]Fluoride from the reaction mixture followed by elution of the protected product [^{18}F]14 with dry acetonitrile (1.5 mL). The solvent was removed under reduced pressure and [^{18}F]14 was resolved with hydrochloride solution (3.3 M, 500 µL) and heated to 120 °C for 15 min. After cooling the reaction mixture was neutralized with sodium hydroxide solution (3.3 M, 500 µL) and injected into a semi-preperative HPLC system at a flow of 3.6

mL/min, whereas A is ammonium formiate solution (50 mM) and B is acetonitrile. The following method was used: 0-5 min 100 % A (isocratic), 5-18 min 0-95 % B (gradient), 18-22 min 95 % B (isocratic), 22-25 min 5-100 % A (gradient). After purification using semi-preparativ HPLC, the fraction was evaporated. The dried prosthetic group was solved in the preferred reaction solvent to perform the click reaction. The ^{18}Fprosthetic group was prepared in an overall reaction time of 90 min with an overall yield (n.d.c.) of (16.8±7.4) % (n=3).

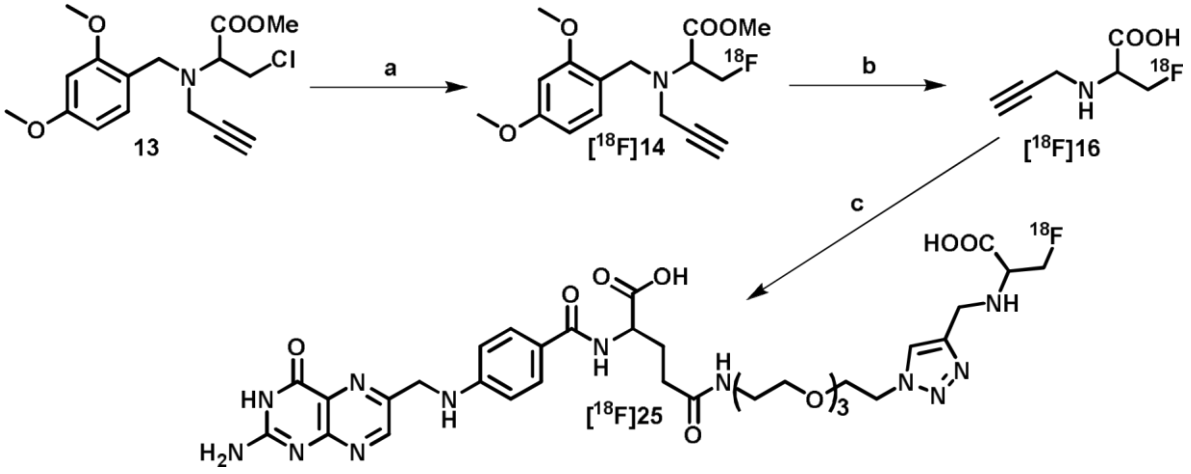

IV.4. Octanol-water partition coefficient (logD octanol/water)

To determine the lipophilicity of the radiolabeled ^{18}F-prostehtic group and the ^{18}F-labeled folate derivatives, approximately 0.55 mCi of the radiolabeled prosthetic group were diluted in 0.7 mL phosphate-buffered saline (PBS). An equal volume of 1-octanole was added to obtain a binary phase system. After stirring the samples at 1.500 1/min for 2 min, the two layers were separated by centrifuge (12.000 U/min for 2 min). 300-µL samples were taken from each layer and radioactivity was measured using a curimeter. Besides activity was also determined using a TLC plate.

IV.5. Relative lipophilicity (k´ value)

Native folic acid 20 and both reference compound 24 and 25 were dissolved in PBS (1 mg/mL). To 150 mL of these solutions 10 µL of a $NaNO_2$ solution (1M) were added and the resulting mixture were analyzed by analytical HPLC (Gemini-NX, 5 µ, C18, 110A, 250x4.60 mm, 80 % phosphoric acid (0.013 M, pH 2.4), 20 % MeCN, isocratic, 1 mL/min flow). Sodium nitrite was added to determine the dead time of the column. The relative lipophilicity was calculated using following equation.

□ =ي_____ ?يي□

ي

V. RADIOLABELUNG OF BIOMOLECULES

V.1. Copper-free cycloaddition of [^{18}F]7 and azido-functionalized folate-derivative

The prosthetic group [^{18}F]7 was dissolved in PBS buffer (200 µL) and azide-funktionalized folatederivative 23 (0.5 mg, 1 µmol) in 200 µL PBS was added.). The reaction mixtures was heated to 40 C for 15 min followed by injection into a semi-preperative HPLC system at a flow of 2.5 mL/min, whereas A is water and B is acetonitrile. The following method was used: 50 % A (isocratic).After purification using semi-preparativ HPLC, the fraction was diluted with water (20 mL) and fixed on a Sep-Pak light SPE cartridge (Sep Pak Light tC18). The fixed [^{18}F]fluoro-folate was eluted with EtOH/water (1:1, 1 mL) into a reaction vessel and the ethanol was removed using helium steam at 95 °C within 15 min. The [^{18}F]fluoro-DBCO-Folate was prepared in an overall reaction time of 120 min with an overall yield (n.d.c.) of (1.6±0.9) % (n=4).

V.2. Copper-catalyzed cycloaddition of [^{18}F]16 and azido-functionalized folate-derivative

The prosthetic group [^{18}F]16 was dissolved in PBS buffer:ethanol (1:1, 1 mL) and $CuSO_4$ (20 µmol in 40 µL PBS was added followed by the azide-functionalized folate derivative 23 (0.5 mg, 0.6 µmol) and sodium ascorbate (100 µmol in 40 µL PBS). The reaction mixtures was heated to 70 °C for 15 min followed by injection into a semi-preperative HPLC system at a flow of 3.6 mL/min, whereas A is ammonium formiate solution (50 mM) and B is acetonitrile. The following method was used: 0-5 min 100 % A (isocratic), 5-18 min 0-95 % B (gradient), 18-22 min 95 % B (isocratic), 22-25 min 5-100 % A (gradient). After purification using semi-preparativ HPLC, the fraction was evaporated. The [^{18}F]fluoroala-Folate was prepared in an overall reaction time of 150 min with an overall yield (n.d.c.) of (7.7±1.1) % (n=3).

VI. IN VITRO STUDIES

VI.1. Stability in human serum albumin

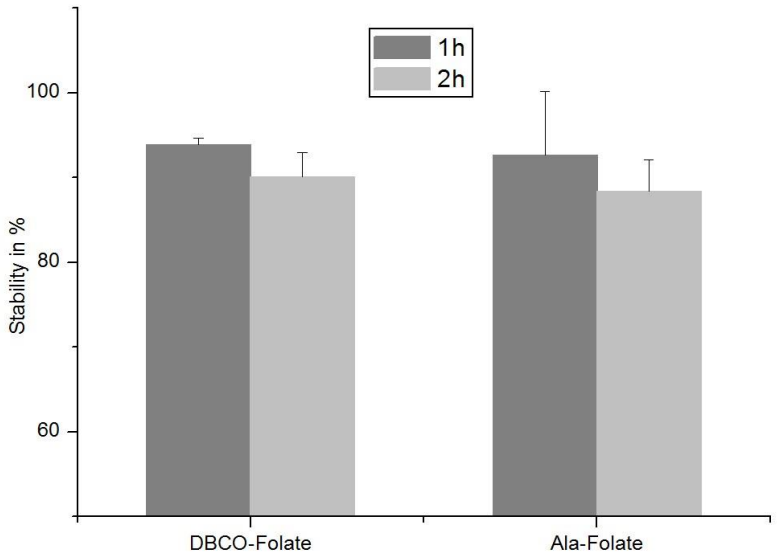

Figure 1: Stability of [^{18}F]24 and [^{18}F]25 in human serum albumin at 37 °C over 1 and 2h. Errors are given as standard deviation representing n=3.

VI.2. FACS analysis of human KB and OC316 cells

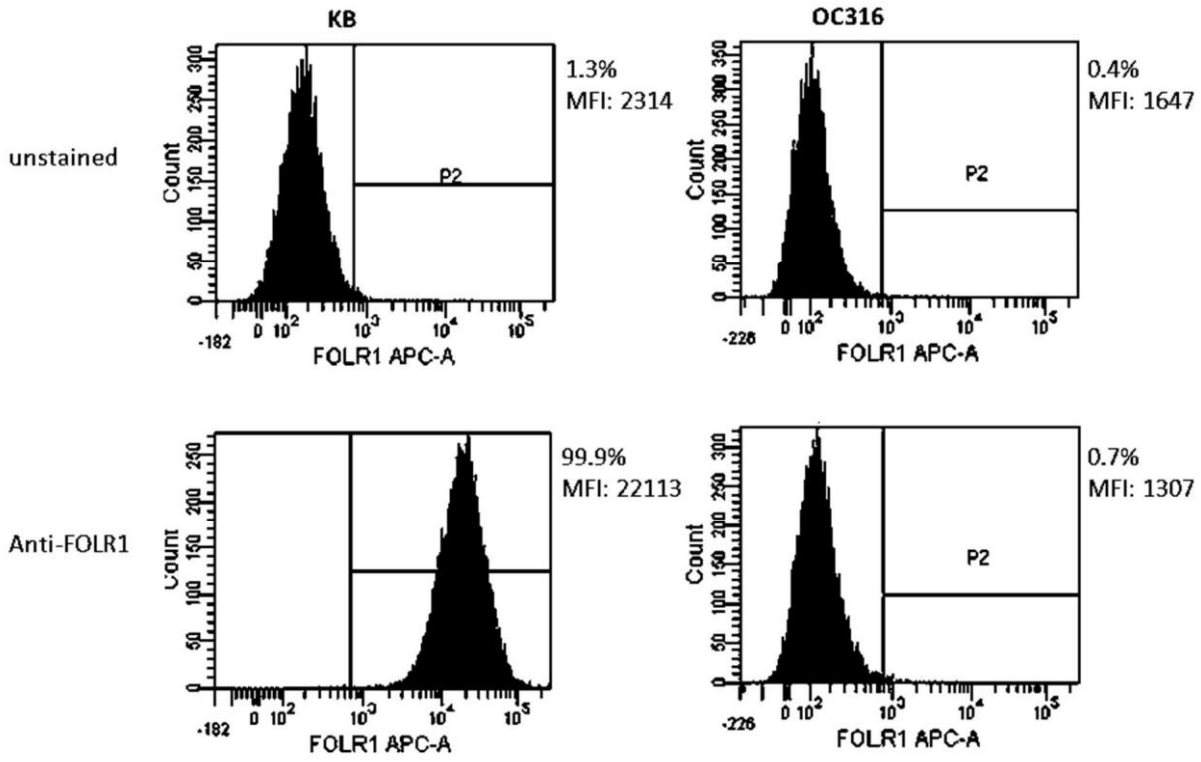

Figure 2: FACS analysis of human KB and OC316 cells. 1x10^6 cells were stained with 0.25 µg of anti-human FOLR1-APC (R&D System) and analysed by a LSRII (Becton Dickinson) flow sytometer equipped with DIVA software (version 6.0).

VII. ANALYTICS

VII.I. NMR data

Tert-butyl-3-(2-(2-(2-hydroxyethoxy)ethoxy)ethoxy)propanoate (3)

Tert-butyl-3-(2-(2-(2-tosyloxyethoxy)ethoxy)ethoxy)propanoate (4)

3-(2-(2-(2-tosyloxyethoxy)ethoxy)ethoxy)propanoate (5)

3-(2-(2-(2-tosyloxyethoxy)ethoxy)ethoxy)-N-[3-oxo-N-(DBCO)propyl]propanamid (6)

3-(2-(2-(2-fluoroethoxy)ethoxy)ethoxy)-N-[3-oxo-N-(DBCO)propyl]propanamid (7)

This content can be found in supplementary information "A [1] [8]F-labeled Dibenzocyclooctyne(DBCO)Derivative for Copper-free Click Labeling of Biomolecules".

Methyl 2-((2,4-dimethoxybenzyl)-3-hydroxypropanoate (9)

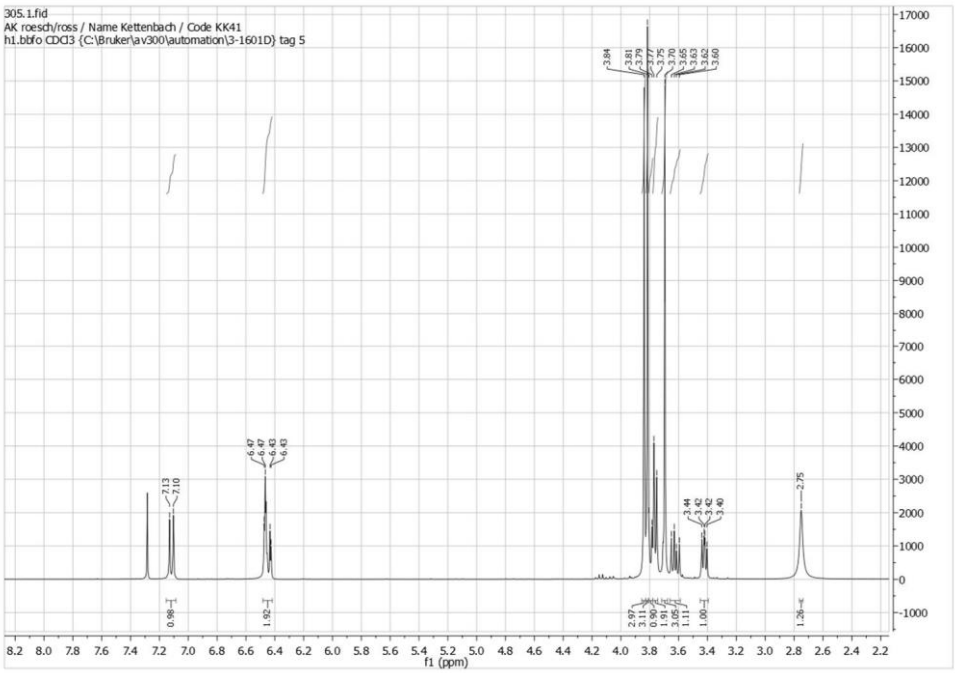

Methyl-2-((2,4-dimethoxybenzyl)amino)-3-((triisopropylsilyl)oxy)-propanoate (10)

[1] H-NMR (300 MHz, $CDCl_3$, Me_4Si): ω [ppm] = 2.75 (br, 1H, H-1), 3.42 (dd, 1H, $^3J_{H-H}$ = 4.5 Hz, H-2), 3.63 (q, 1H, $^3J_{H-H}$ = 6.3 Hz, H-3), 3.70 (s, 3H, H-4), 3.75 – 3.77 (d, 2H, $^3J_{H-H}$ = 5.7 Hz, H-5), 3.79 – 3.81 (d, 1H, $^3J_{H-H}$ = 6.4 Hz, H-3), 3.82 (s, 3H, H-6), 3.84 (s, 3H, H-7), 6.43 – 6.47 (m, 2H, Ar-H), 7.10 (d, 1 H, $^3J_{H-H}$ = 7.8 Hz, Ar-H).

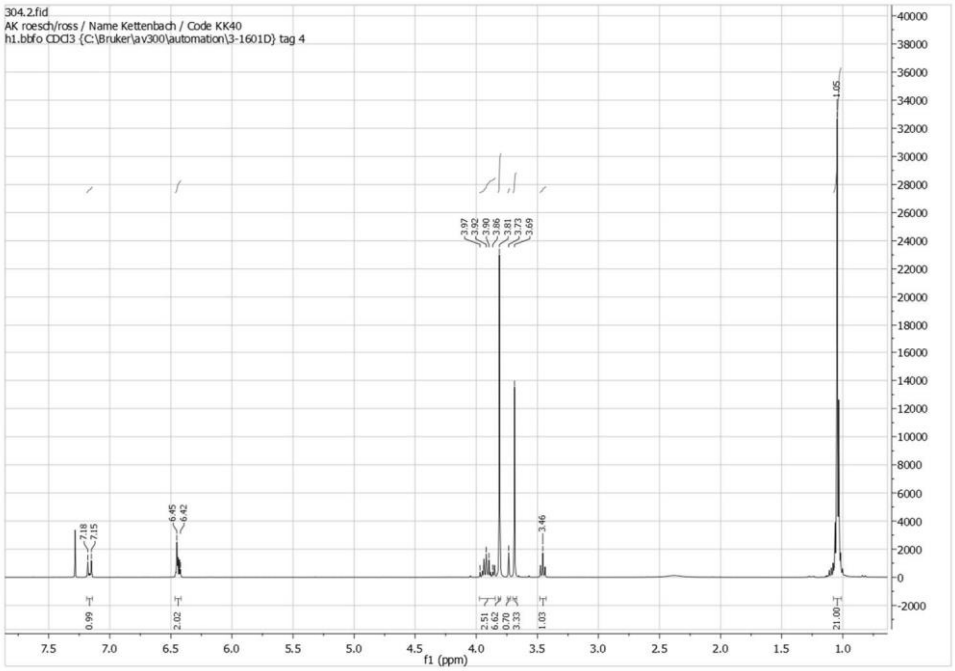

^{1}H-NMR (300 MHz, $CDCl_3$, Me_4Si): ω [ppm] = 1.05 (m, 21H, H-1), 3.46 (t, 1H, $^{3}J_{H-H}$ = 5.7 Hz, H-2), 3.69 (s, 3H, H-3), 3.73 (s, 1H, H-4), 3.81 (s, 6H, H-5), 3.86 – 3.97 (m, 3H, H-4 und H-6), 6.42 – 6.45 (m, 2H, ArH), 7.15 (d, 1H, $^{3}J_{H-H}$ = 8.7 Hz, Ar-H).

Methyl-2-((2,4-dimethoxybenzyl)(3-(trimethylsilyl)prp-2-yn-1-yl)amino)-3-((triisopropylsilyl)propanoate (11)

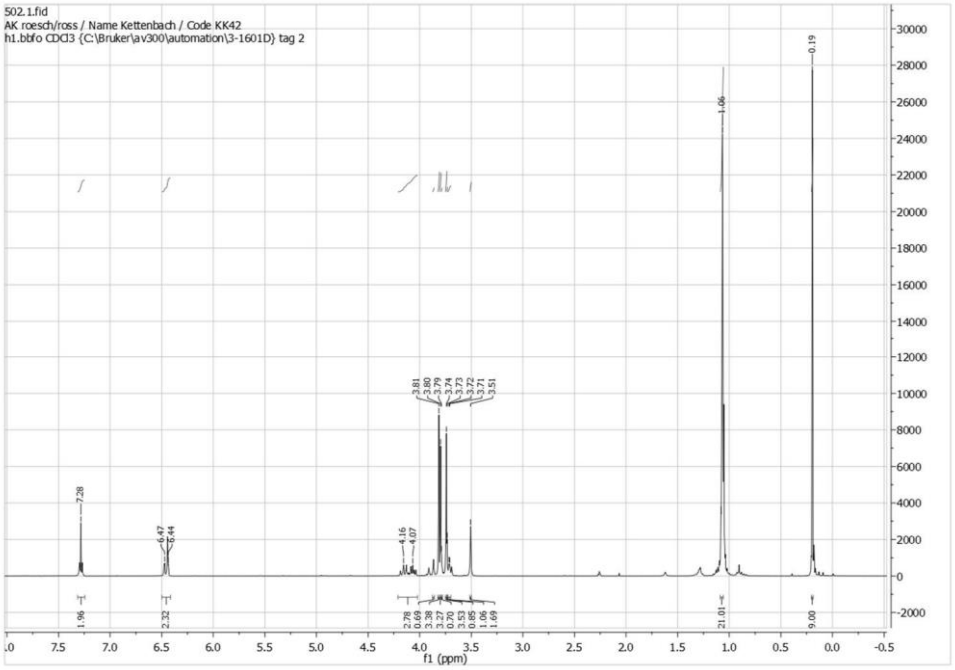

[1] H-NMR (300 MHz, $CDCl_3$, Me_4Si): ω [ppm] = 0.19 (s, 9H, H-1), 1.06 (s, 21H, H-2), 3.51 (s, 2H, H-3), 3.73 (s, 1H, H-4), 3.71-3.79 (m, 2H, H-5), 3.74 (2, 3H, H-6), 3.80 (s, 3H, H-7), 3.81 (s, 3H, H-8), 4.07-4.16 (m, 2H, H-9), 6.44-6.47 (m, 2H, Ar-H), 7.28 (d, 1H, $^{3}J_{H-H}$ = 8.7 Hz, Ar-H).

Methyl 2-((2,4-dimethoxybenzyl)(prop-2-yn-1-yl)amino)-3-hydroxy-propanoate (12)

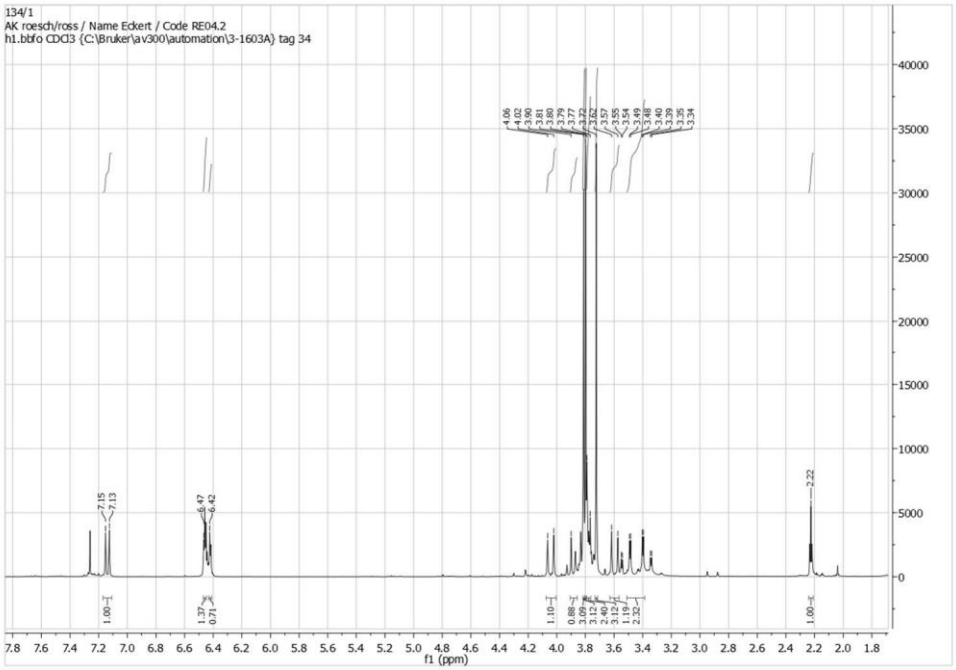

^{1}H-NMR (300 MHz, $CDCl_3$, Me_4Si): ω [ppm] = 2.22 (t, 1H, $^{3}J_{H-H}$ = 2.3 Hz, H-1), 3.39-3.49 (dd, 2H, $^{3}J_{H-H}$ = 2.7 Hz, H-2), 3.57 (d, 1H, $^{3}J_{H-H}$ = 13.3 Hz, H-3), 3.72 (s, 3H, H-4), 3.77-3.79 (m, 2H, H-5), 3.80 (s, 3H, H6), 3.81 (s, 3H, H-7), 3.90 (d, 1H, $^{3}J_{H-H}$ = 9 Hz, H-8), 4.02-4.06 (d, 1H, $^{3}J_{H-H}$ = 12.8 Hz, H-3), 6.42-6.47 (m, 2H, Ar-H), 7.13 (d, 1H, $^{3}J_{H-H}$ = 8.1 Hz, Ar-H).

Methyl 3-chloro-2-((2,4-dimethoxybenzyl)(prop-2-yn-1-yl)amino)-propanoate (13)

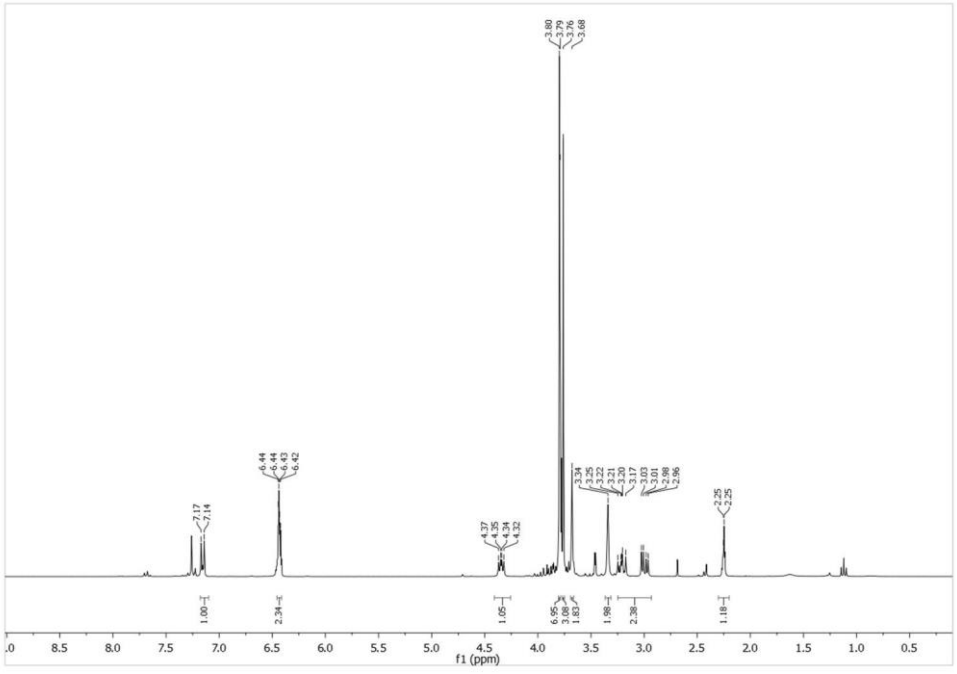

^{1} , Me_4Si): ω
^{3}
H-NMR (300 MHz, CDCl [ppm] = 2.25 (t, 1H, $^3J_{H-H}$ = 2.7 Hz, H-1), 2.96-3.22 (ddd, 2H, $^3J_{H-H}$ = 19 Hz, H-1), 3.34 (s, 2H, H-3), 2.68 (s, 2H, H-4), 3.76 (s, 3 H, H-5), 3.80 (s, 6H, H-6), 4.05 (dd, 1H, $^3J_{H-H}$ = 5.7 Hz, H-7), 6.42-6.44 (m, 2H, Ar-H), 7.14 (d, 1H, $^3J_{H-H}$ = 8.8 Hz, Ar-H).

Methyl 2-((2,4-Methoxybenzyl)(prop-2-yn-1-yl)amino)-3-fluoro-propanoate (14)

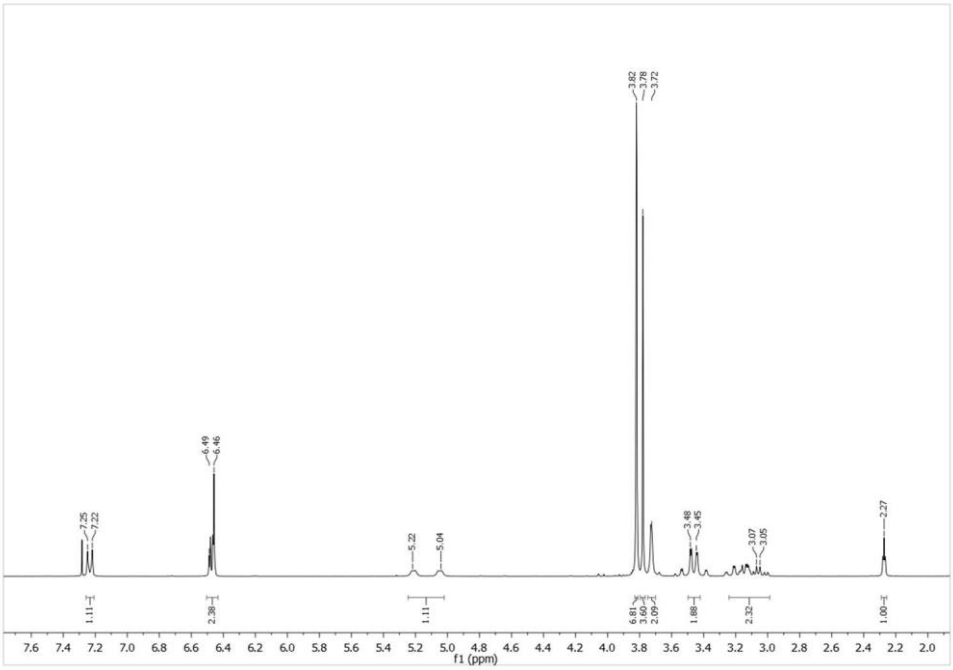

^{1}H-NMR (400 MHz, $CDCl_3$, Me_4Si): ω [ppm] = 2.27 (t, 1H, $^3J_{H-H}$ = 2.3 Hz, H-1), 3.05 (m, 2H, H-2), 3.45 (dd, 2H, $^3J_{H-H}$ = 2.5 Hz, H-3), 3.72 (s, 2H, H-4), 3.78 (s, 3 H, H-5), 3.82 (s, 6H, H-6), 5.04 (dd, 1H, $^3J_{H-H}$ = 3.8 Hz, H-7), 6.46-6.49 (m, 2H, Ar-H), 7.22 (d, 1H, $^3J_{H-H}$ = 8.8 Hz, Ar-H).

2-((2,4-Methoxybenzyl)(prop-2-yn-1-yl)amino)-3-fluoropropanoic acid (15)

^{1}H-NMR (400 MHz, $CDCl_3$, Me_4Si): ω

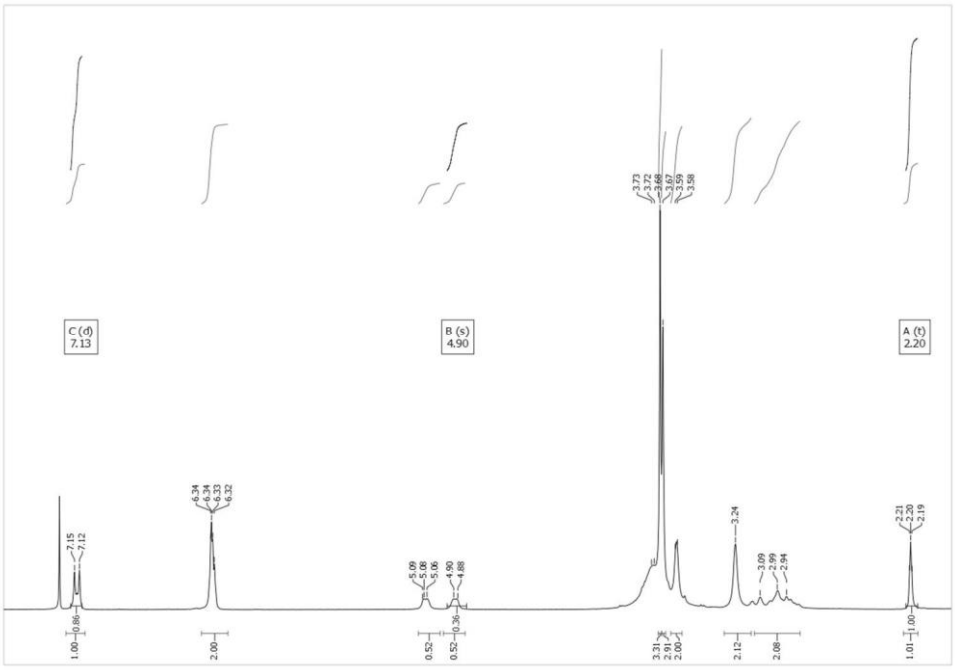

[ppm] = 2.20 (t, 2H, $^3J_{H-H}$ = 2 Hz, H-1), 2.99 (m, 2H, H-2), 3.24 (2, 2H, H-3), 3.58 (s, 2H, H-4), 3.67 (2, 3H, H-5), 3.68 (s, 3H, H-6), 4.88-5.09 (dd, 1H, $^3J_{H-H}$ = 7.1 Hz, H-7), 6.33 (m, 2H, Ar-H), 7.12 (d, 1H, $^3J_{H-H}$ = 9.3 Hz, Ar-H).

3-fluoro-2-(prop-2-yn-1-ylamino)propanoic acid (16)

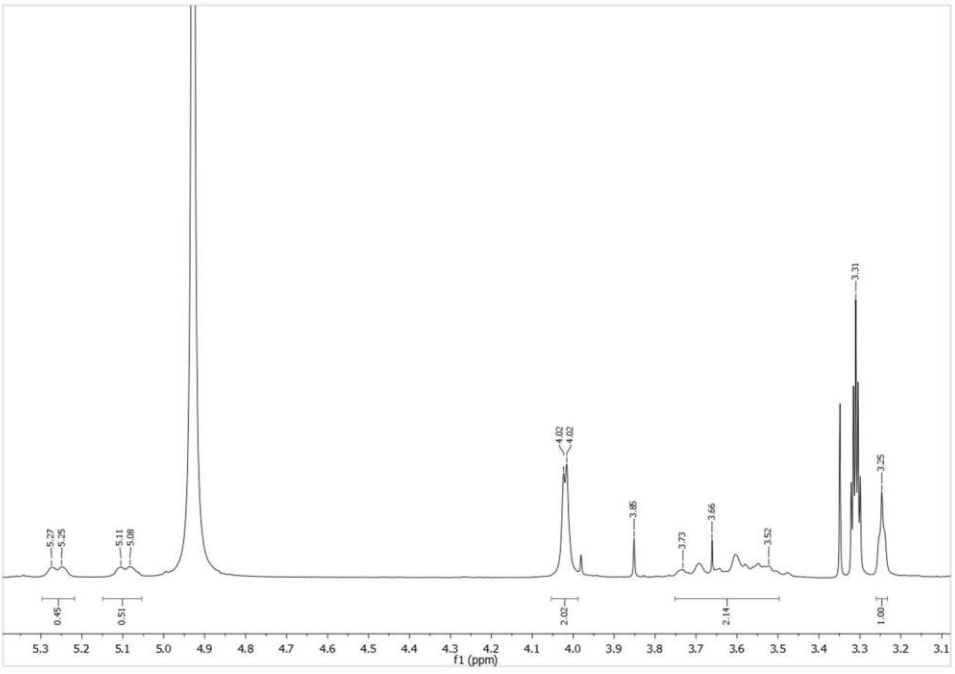

^{1}H-NMR (400 MHz, CD_3OD, Me_4Si): ω [ppm] = 3.25 (t, 1H, $^3J_{H-H}$ = 2.6 Hz, H-1), 3.52-3.85 (m, 2H, H-2), 4.02 (d, 2H, $^3J_{H-H}$ = 2.3 Hz, H-3), 5.08-5.27 (dd, 1H, $^3J_{H-H}$ = 7.6 Hz, H-4).

Tert-Butyl-3-(2-(2-(2-(2-ethoxy)ethoxy)ethoxy)ethylcarbamoylazid)-1-(methoxycarbonyl)propylcarbamate (18)

^{1}H-NMR (400 MHz, $CDCl_3$, Me_4Si): ω

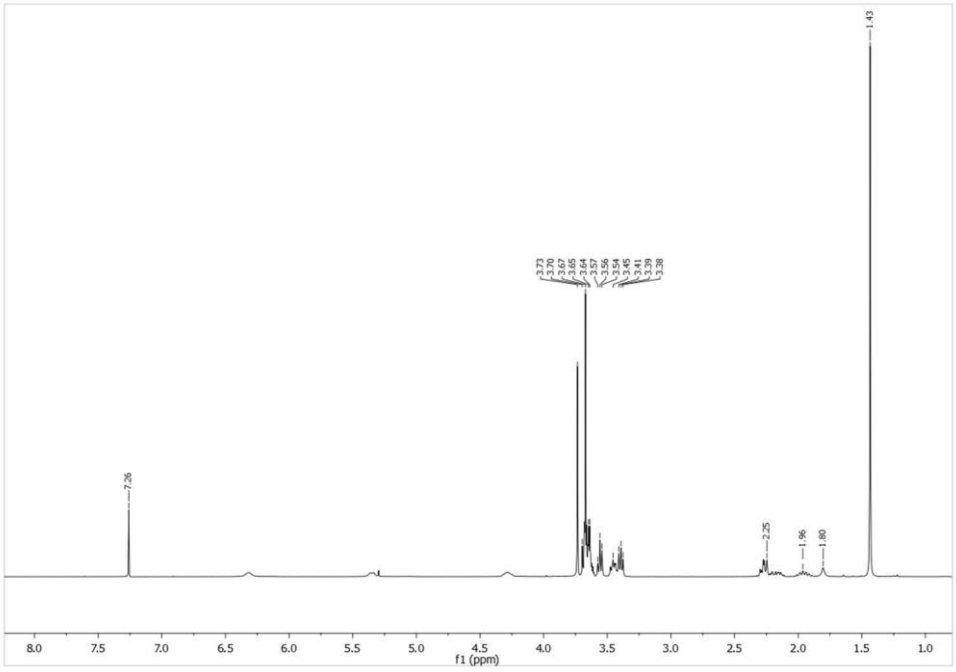

[ppm] = 1.43 (s, 9H, H-1), 1.91 – 1.99 (m, 1H, H-2), 2.14 – 2.22 (m, 1H, H-2), 2.25 – 2.30 (m, 2H, H-3), 3.39 (t, 2H, $^{3}J_{H-H}$ = 5.0 Hz, H-4), 3.44 – 3.48 (m, 2H, H-5), 3.56 (t, 2H, $^{3}J_{H-H}$ = 4.8 Hz, H-6), 3.61 – 3.70 (m, 10H, PEG-H), 3.73 (s, 3H, H-7), 4.28 (br, 1H, H-8), 5.35 (br, 1H, H-9), 6.32 (br, 1H, H-10).

Methyl-4-(2-(2-(2-(2-ethoxy)ethoxy)ethoxy)ethylcarbamoylazid)-3-aminobutanoate (19)

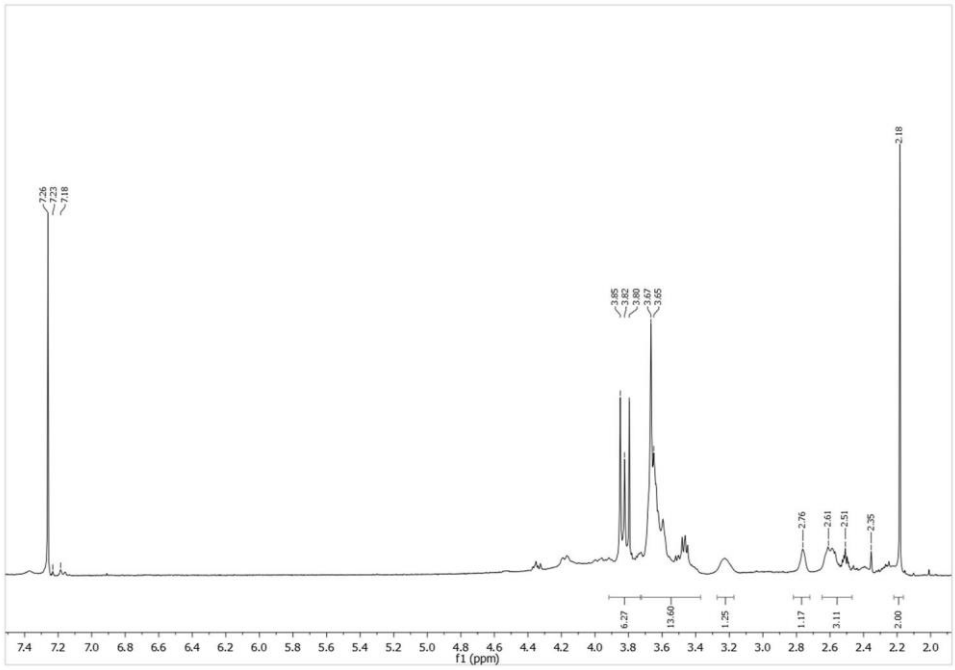

^{1}H-NMR (400 MHz, $CDCl_3$, Me_4Si): ω [ppm] = 2.40 (m, 2H, H-1), 2.59 (m, 2H, H-2), 3.41 – 3.67 (m, 16H, PEG-H), 3.81 (s, 3, H-3), 4.24 (br, 1H, H-4), 7.61 (br, 1H, H-5), 8.75 (br, 2H, H-6). Acetyl-pyrofolic acid (21)

^{1}H-NMR (400 MHz, $CDCl_3$, Me_4Si): ω

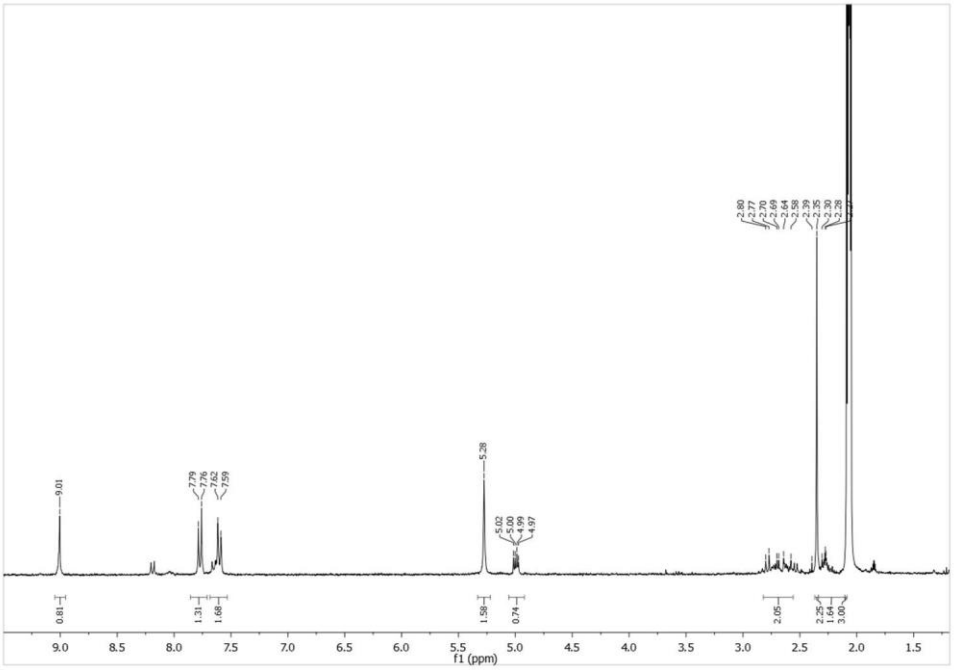

[ppm] = 2.09 (s, 3H, H-1), 2.35 (s, 2H, H-2), 2.58 – 2.80 (m, 2H, H3), 4.99 (m, 1H, H-4), 5.28 (s, 2H, H-5), 7.62 (d, 2H, $^3J_{H\text{-}H}$ = 8.5 Hz, H-6), 7.76 (d, 2H, $^3J_{H\text{-}H}$ = 8.6 Hz, H-7), 9.01 (s, 1H, H-8).

Acetyl-pteroic acid (22)

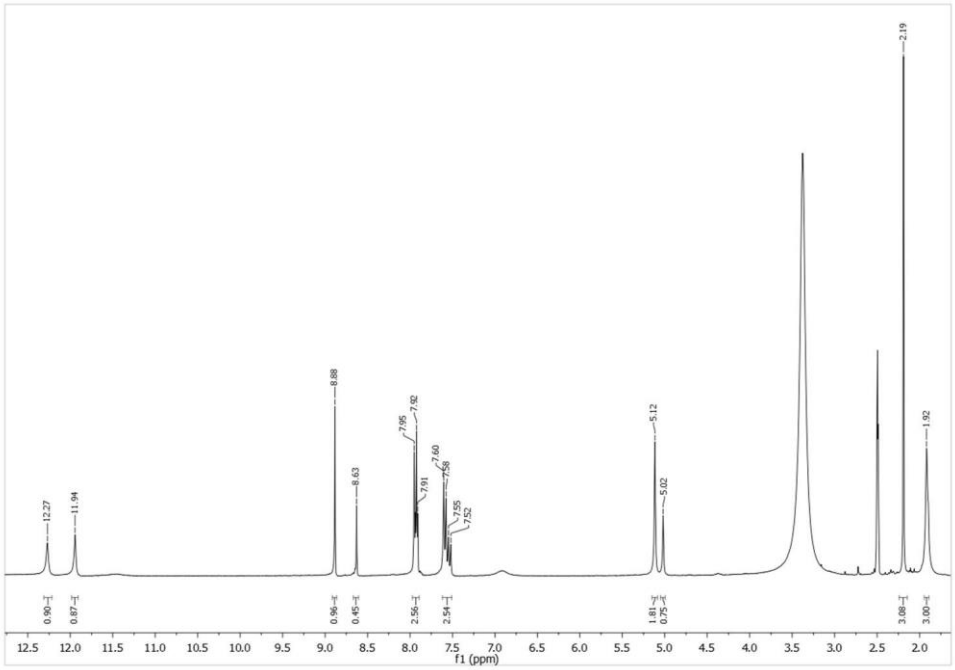

^{1}H-NMR (300 MHz, DMSO-d_6, Me_4Si): ω [ppm] = 1.92 (s, 3H, H-1), 2.19 (s, 3H, H-2), 5.02 (s, 2H, H-3), 5.12 (s, 2H, H-3), 6.92 (br, 2H, H-4), 7.52 – 7.60 (m, 2H, H-6), 7.91 – 7.95 (m, 2H. H-7), 8.63 (s, 1H, H-5), 11.94 (s, 1H, H-8), 12.27 (s, 1H, H-8).

N_{α}-(2-(2-(2-(2-Azidoethoxy)ethoxy)ethoxy)ethyl)-pteroyl-L-glutamine (23)

^{1}H-NMR (400 MHz, $CDCl_3$, Me_4Si): ω

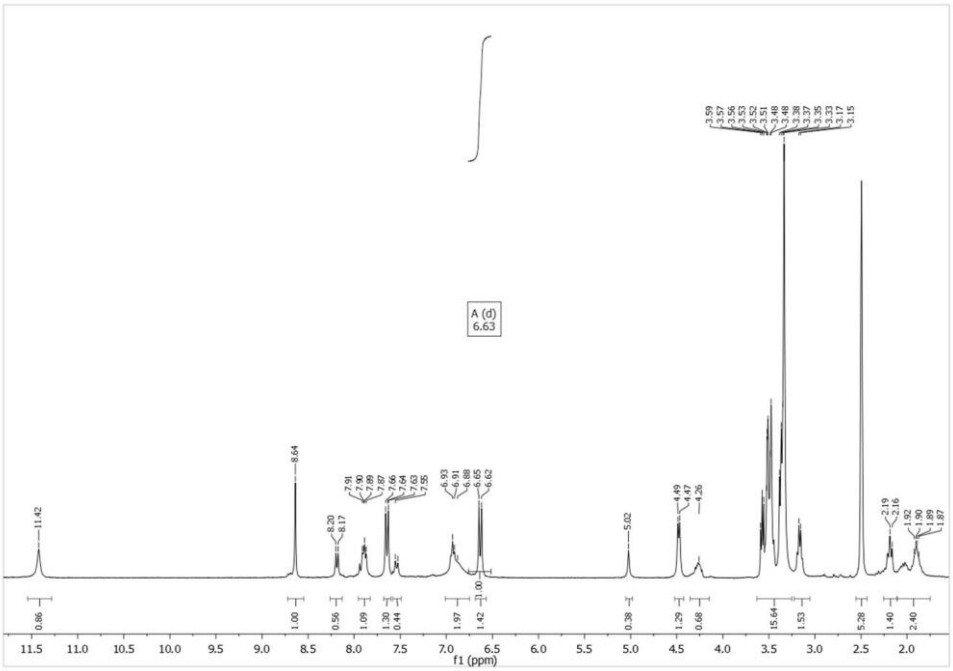

[1]H-NMR (400 MHz, CD_3OD, Me_4Si): ω [ppm] = 1.89 (m, 2H, H-1), 2.18 (m, 2H, H-2), 3.33 – 3.59 (m, 16 H, PEG-CH_2), 4.26 (m, 1H, H-3), 4.48 (s, 2H, H-4), 6.62 (d, 2H, $^3J_{H-H}$ = 8.4 Hz, H-5), 7.64 (d, 2H, $^3J_{H-H}$ = 8.4 Hz, H-6), 8.64 (s, 1H, H-7), 11.45 (s, 1H, H-8).

11-(1,2,3-Triazo-4-*N*-ethyl-(3-fluoro-2-(prop-2-yn-1-ylamino)propanoic acid)3,6,7,-trioxa unde-can-1yl)folic acid amide (25)

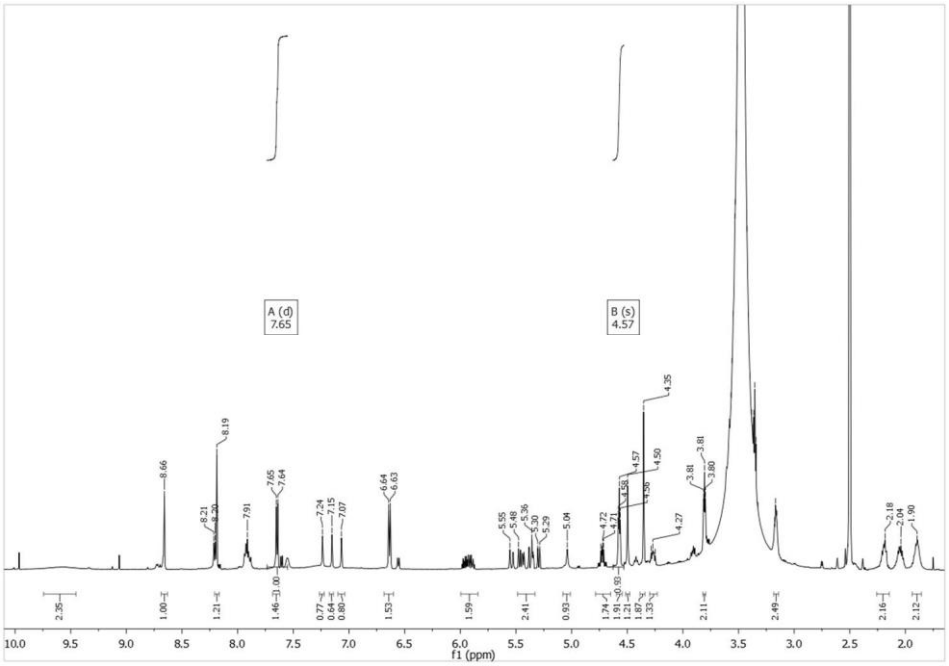

^{1}H-NMR (600 MHz, DMSO-d_6, Me_4Si): ω [ppm] = 1.90 – 2.04 (m, 2H, H-24), 2.19 (m, 2H, H-25), 3.34 – 3.58 (m, 13H, H-30 – H-38 and H-51), 3.80 – 3.81 (m, 2H, H-29), 4.25 – 4.28 (m, 1H, H-23), 4.35 (s, 2H, H-49), 4.50 (s, 1H, H-50), 5.04 (s, 1H, H-12), 4.56 – 4.58 (m, 2H, H-39), 4.71 – 4.74 (m, 2H, H-11), 5.36 – 5.48 (m, 2H,H-52), 6.64 (d, 2H, $^3J_{H-H}$ = 8.5 Hz, H-14/18), 7.07 (s, 1H, H-27), 7.15 (s, 1H, H-1), 7.24 (s, 1H, H-22), 7.65 (d,2H, $^3J_{H-H}$ = 8.5 Hz, H-15/17), 8.20 (s, 1H, H-45), 8.67 (s, 1H, H-8), 9.57 (br, 2H, H-19).

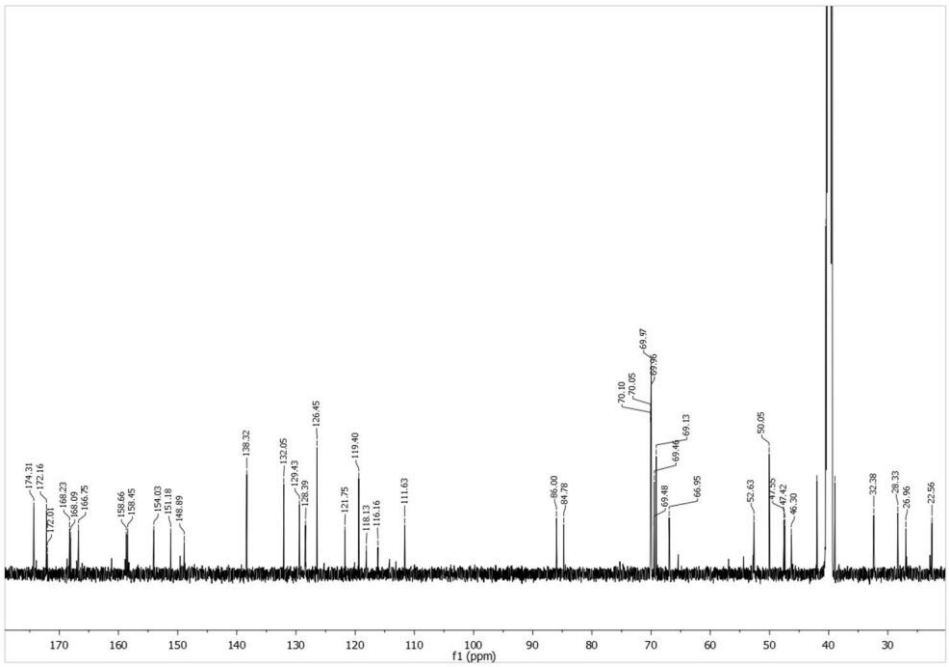

^{13}C-NMR (600 MHz, DMSO-d_6) ω [ppm] = 26.9 & 27.1 (C24), 32.3 (C25), 42.0 (C49), 47.3 (C51), 50.3

(C39), 52.7 (C23), 66.9 (C11), 69.1 (C29), 69.5 – 70.1 (C30 – C38), 111.6 (C14/18), 126.5 (C45), 128.5 (C16), 129.4 (C15/17), 132.1 (C9), 138.3 (C46), 148.9 (C8), 151.2 (C13), 154.1 (C4), 158.5 (C2/5), 158.7 (C2/5), 166.8 (C21), 168.1 (C6/53), 168.2 (C6/53), 172.3 (C26), 174.1 (C41). HSQC

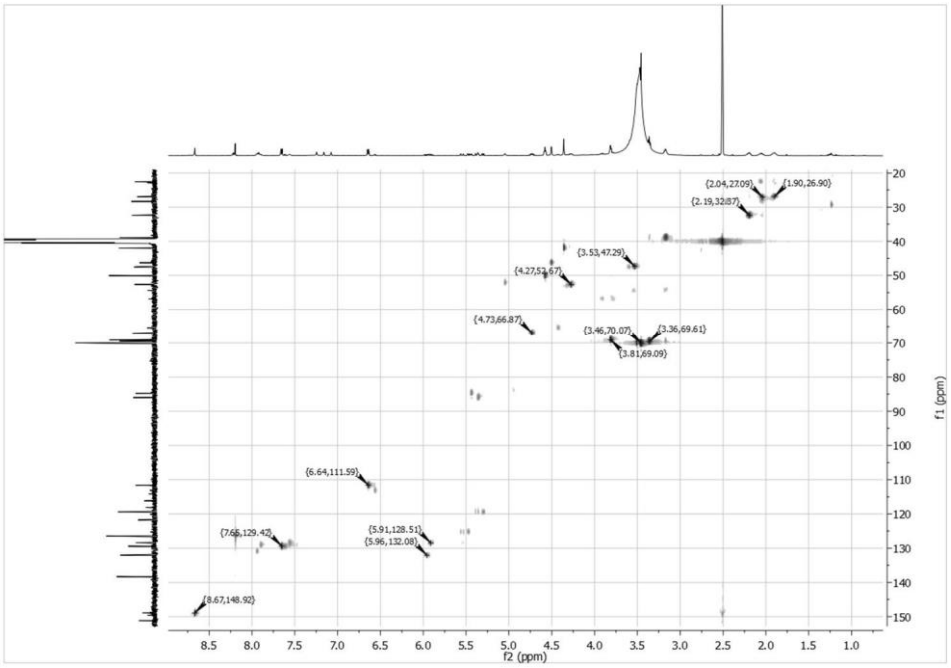

HMBC

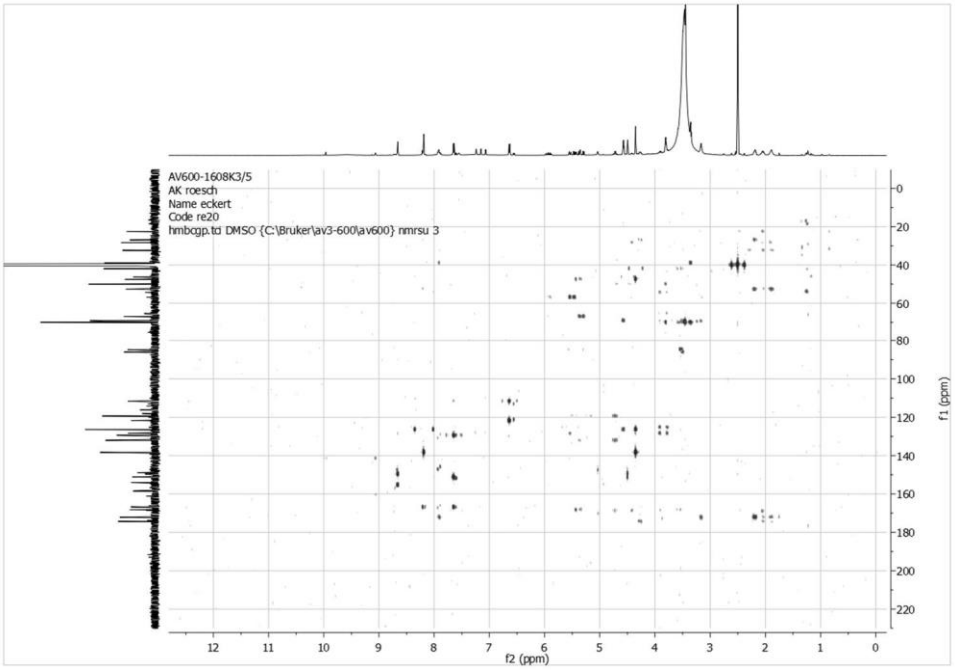

^{19}F-NMR

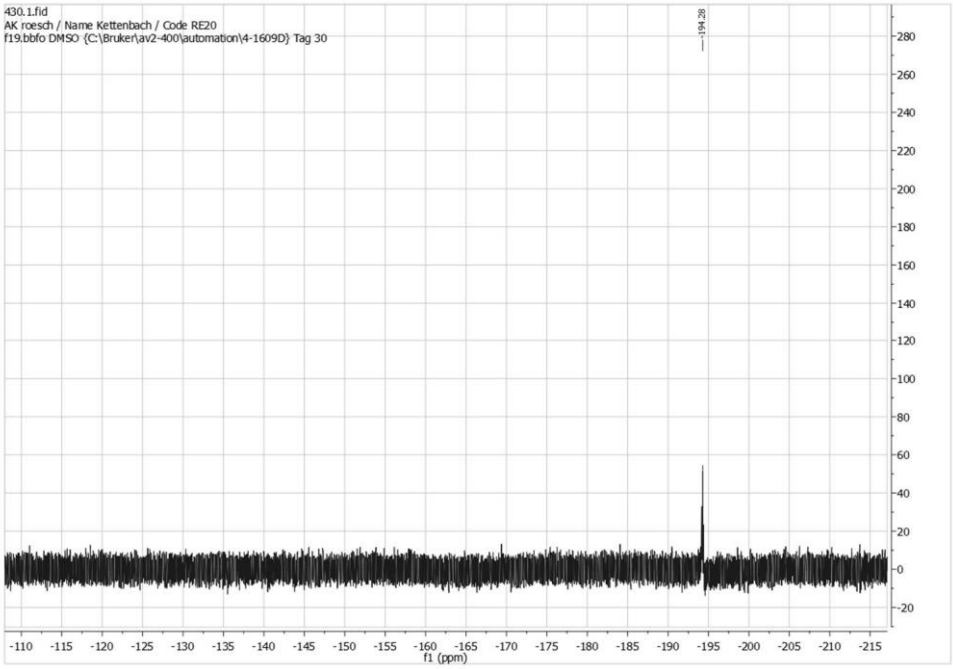

^{19}F-NMR (600 MHz, DMSO-d_6) ω [ppm] = -194.3 (F-54).

VII.2. Mass spectrometry (ESI)

3-(2-(2-(2-tosyloxyethoxy)ethoxy)ethoxy)-N-[3-oxo-N-(DBCO)propyl]propanamid (7)

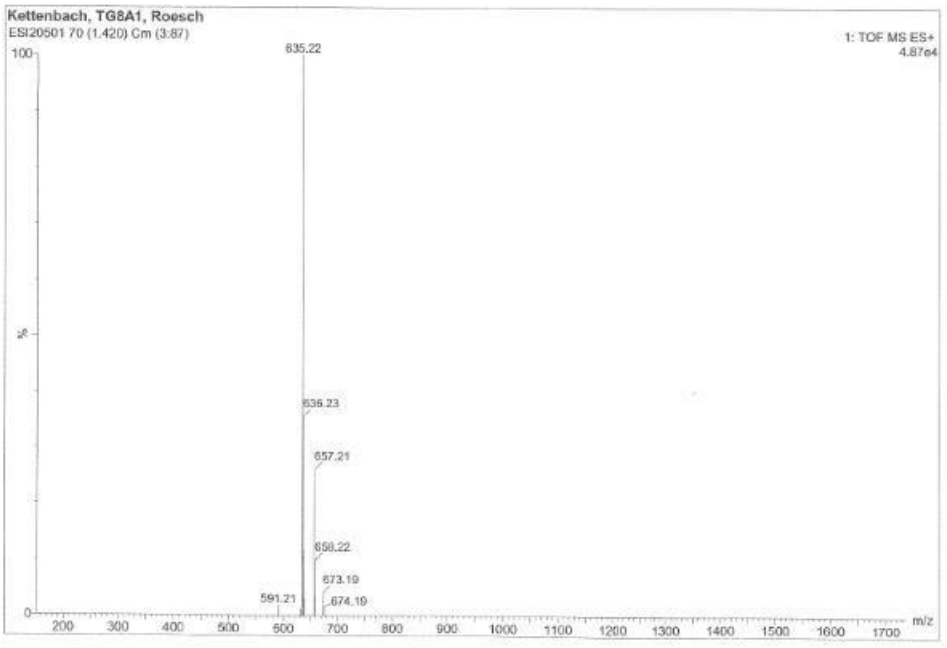

MS (ESI positive): m/z 635.22 ([M]$^+$, 100 %), 657.21 ([M+Na]$^+$, 30 %), 673.19 ([M+K]$^+$, 10 %); m/z (high resolution) 657.2259 ([M+Na]$^+$, 100 %); calculated for $C_{34}H_{38}N_2O_8S$: 634.23.

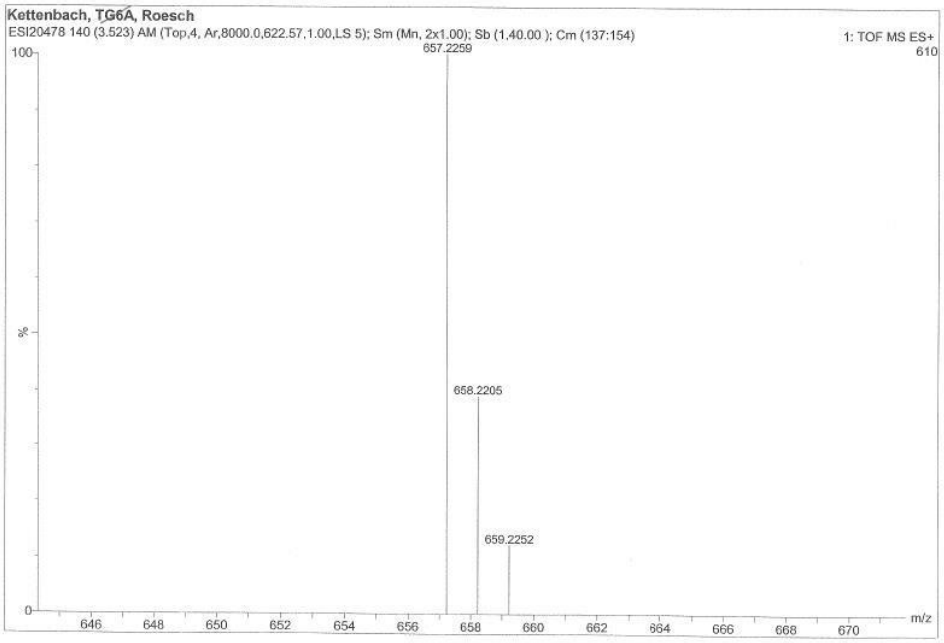

Elemental Composition Report Page 1

Single Mass Analysis
Tolerance = 10.0 PPM / DBE: min = -1.5, max = 200.0
Isotope cluster parameters: Separation = 1.0 Abundance = 1.0%

Monoisotopic Mass, Odd and Even Electron Ions
308 formula(e) evaluated with 1 results within limits (up to 50 closest results for each mass)

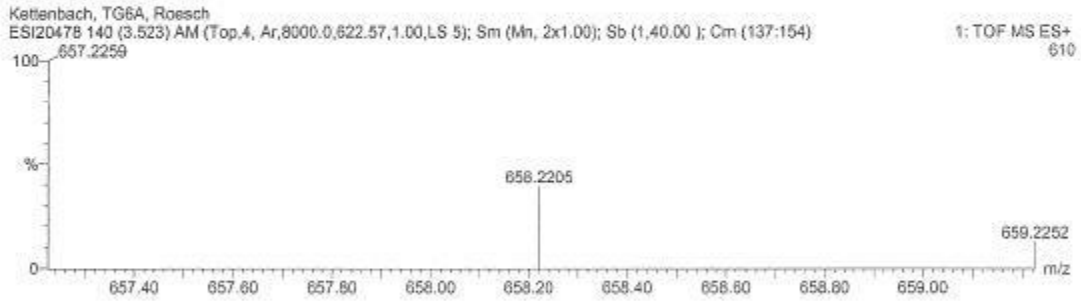

Minimum:				-1.5		
Maximum:		200.0	10.0	200.0		
Mass	Calc. Mass	mDa	PPM	DBE	Score	Formula
657.2259	657.2247	1.2	1.9	16.5	1	C34 H38 N2 O8 23Na S

3-(2-(2-(2-fluoroethoxy)ethoxy)ethoxy)-N-[3-oxo-N-(DBCO)propyl]propanamid (11)

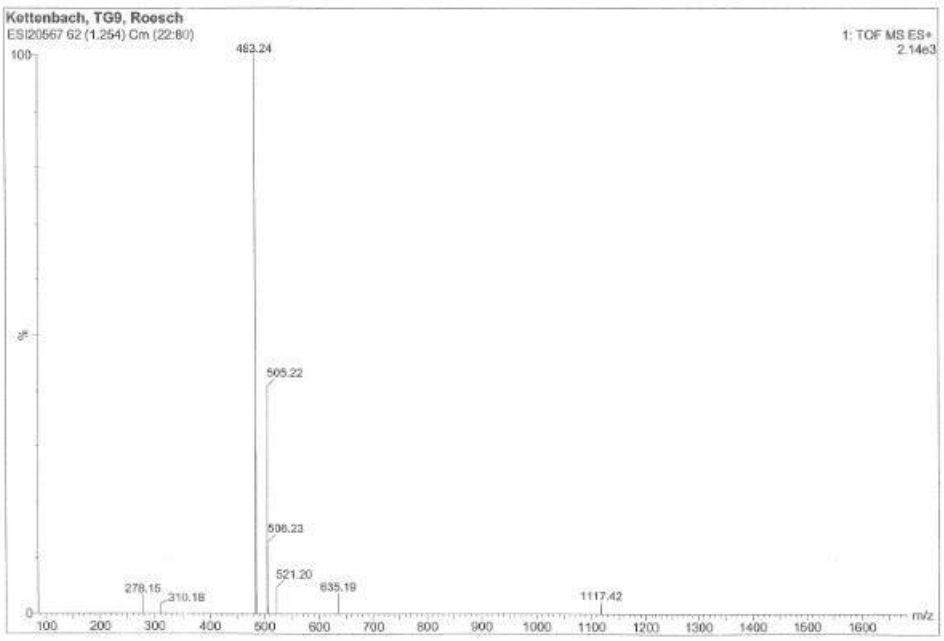

MS (ESI positive): m/z 483.24 ($[M]^+$, 100 %), 505.22 ($[M + Na]^+$, 40 %); m/z (high resolution) 483.2306 ($[M]^+$, 100 %); 505.2107 ($[M+Na]^+$, 100 %); calculated for $C_{27}H_{31}FN_2O_5$: 482.22

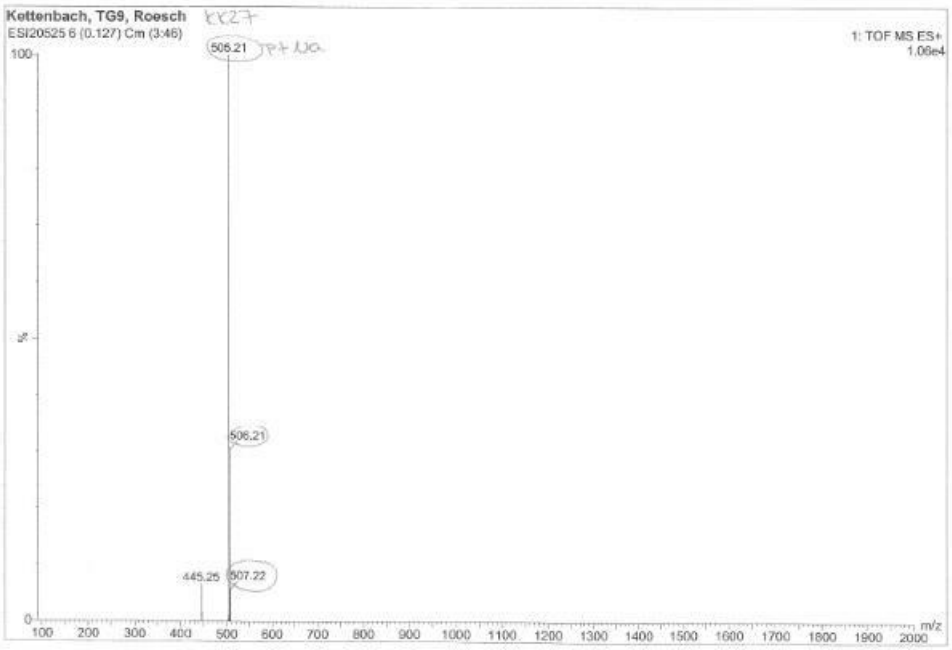

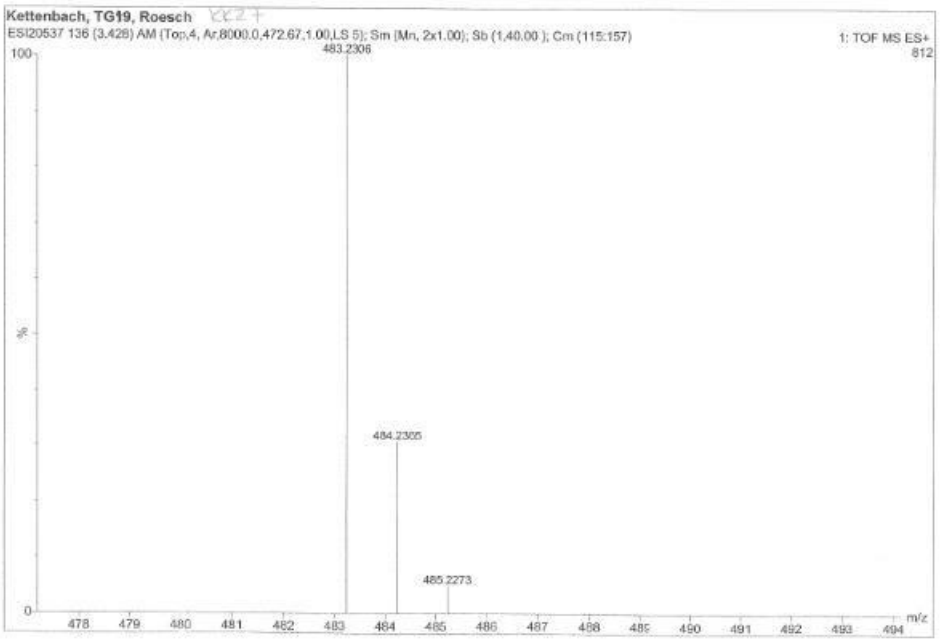

Elemental Composition Report Page 1

Single Mass Analysis
Tolerance = 10.0 PPM / DBE: min = -1.5, max = 200.0
Isotope cluster parameters: Separation = 1.0 Abundance = 1.0%

Monoisotopic Mass, Odd and Even Electron Ions
171 formula(e) evaluated with 2 results within limits (up to 50 closest results for each mass)

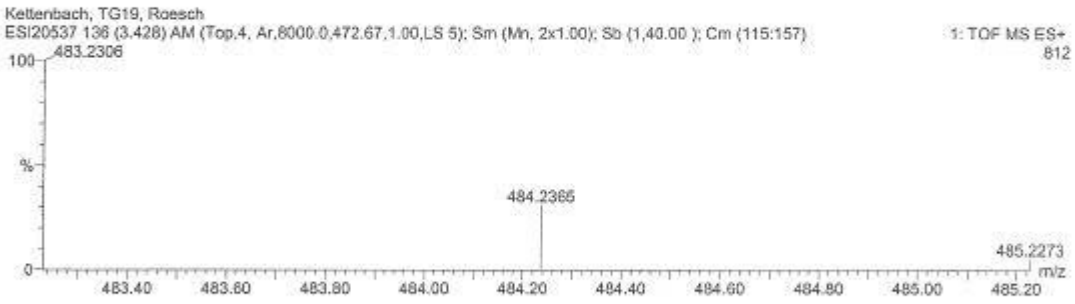

Minimum:				-1.5		
Maximum:		200.0	10.0	200.0		
Mass	Calc. Mass	mDa	PPM	DBE	Score	Formula
483.2306	483.2295	1.1	2.2	12.5	1	C27 H32 N2 O5 F
	483.2333	-2.7	-5.7	13.0	2	C27 H31 N3 O3 F2

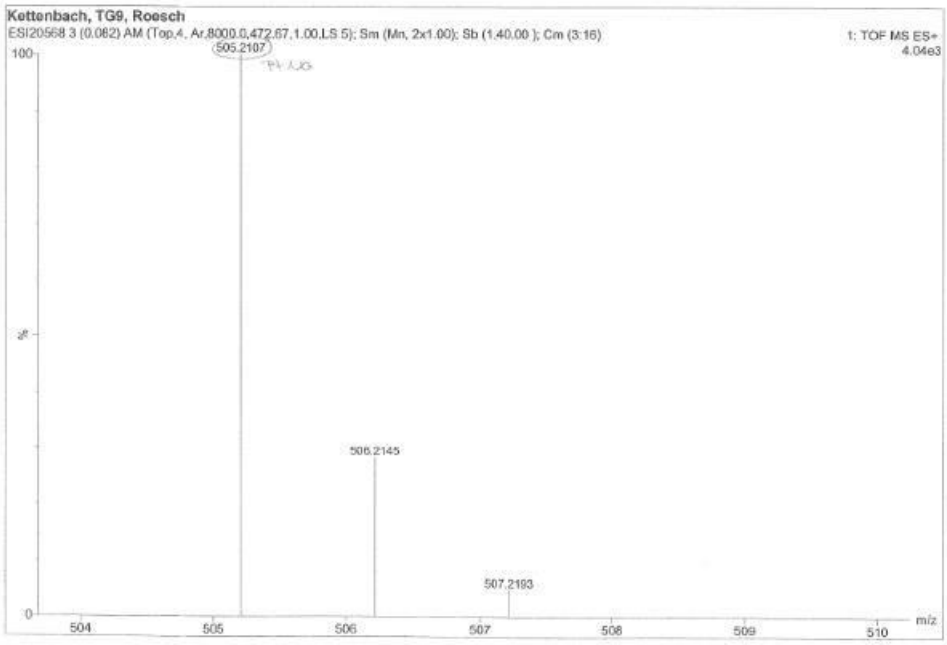

Elemental Composition Report Page 1

Single Mass Analysis
Tolerance = 20.0 PPM / DBE: min = -1.5, max = 200.0
Isotope cluster parameters: Separation = 1.0 Abundance = 1.0%

Monoisotopic Mass, Odd and Even Electron Ions
54 formula(e) evaluated with 3 results within limits (up to 50 closest results for each mass)

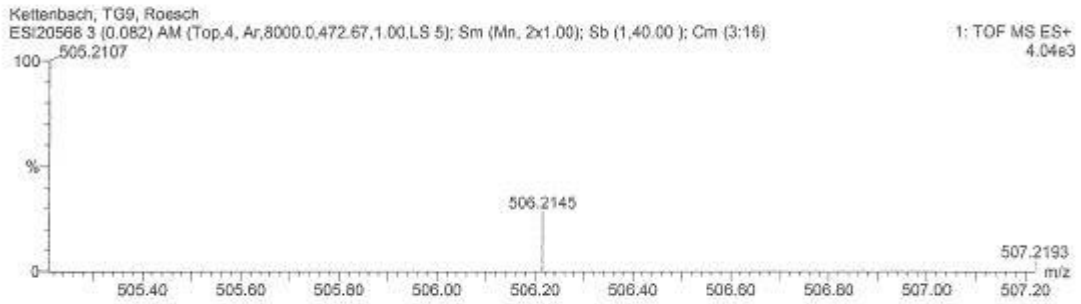

Minimum:				-1.5		
Maximum:		200.0	20.0	200.0		
Mass	Calc. Mass	mDa	PPM	DBE	Score	Formula
505.2107	505.2115	-0.8	-1.5	12.5	3	C27 H31 N2 O5 23Na F
	505.2076	3.1	6.1	12.0	1	C27 H30 N O5 P3
	505.2153	-4.6	-9.1	13.0	2	C27 H30 N3 O3 23Na F2

VII.3. (Radio-)chromatograms

[^{18}F]fluoro-DBCO

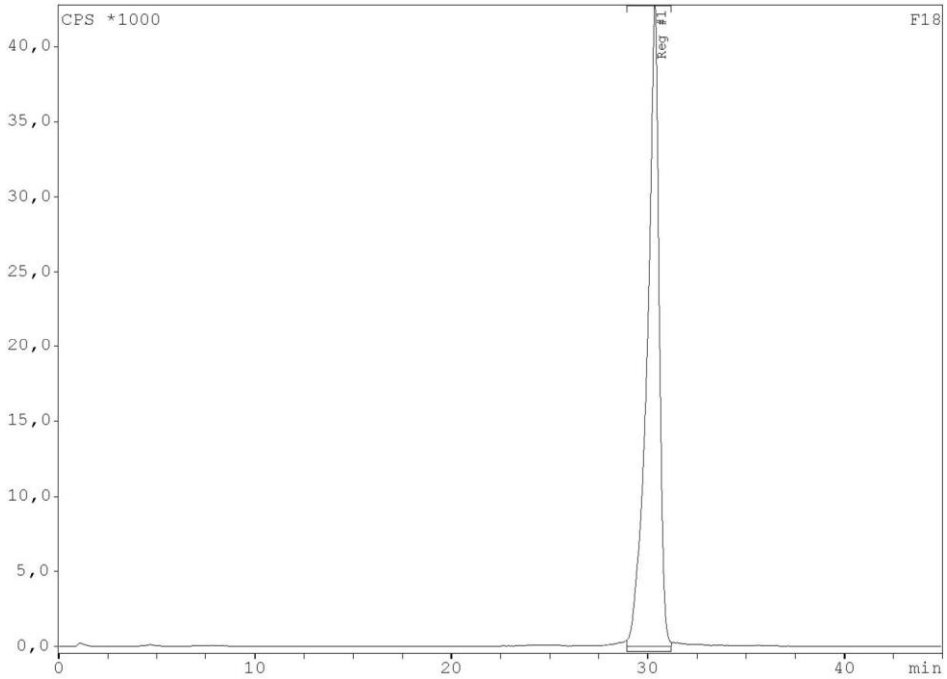

Figure 1: Analytical radio-HPLC chromatogram [^{18}F]7. Analytical radio-HPLC was performed with a Phenomenex Luna C18 column (5 µm, 250x20 mm) using the following conditions: Flow 0.7 mL/min, with eluent A was water with 0.1 % TFA (trifluoroacetic acid) and eluent B was acetonitrile with 0.1 % TFA. The following method was used: 0 - 40 min, 5 – 95 % eluent B (gradient). Retention time 30.08 min, purity ɯ99 %.

[^{18}F]fluoro-DBCO-folate

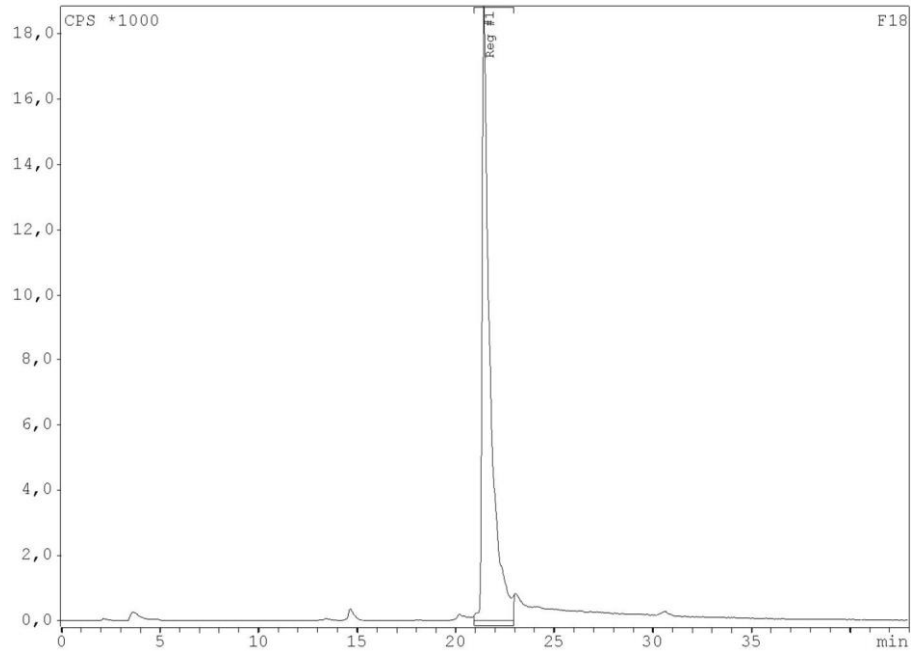

Figure 2: Analytical radio-HPLC chromatogram [^{18}F]24. Analytical radio-HPLC was performed with a Phenomenex Luna C18 column (5 µm, 250x20 mm) using the following conditions: Flow 0.7 ml min-1, with eluent A was water with 0.1 % TFA (trifluoroacetic acid) and eluent B was acetonitrile with 0.1 % TFA. The following method was used: 0 - 40 min, 5 – 95 % eluent B (gradient). Retention time 21.89 min, purity ɯ95 %.

[^{18}F]fluoro-alakyne

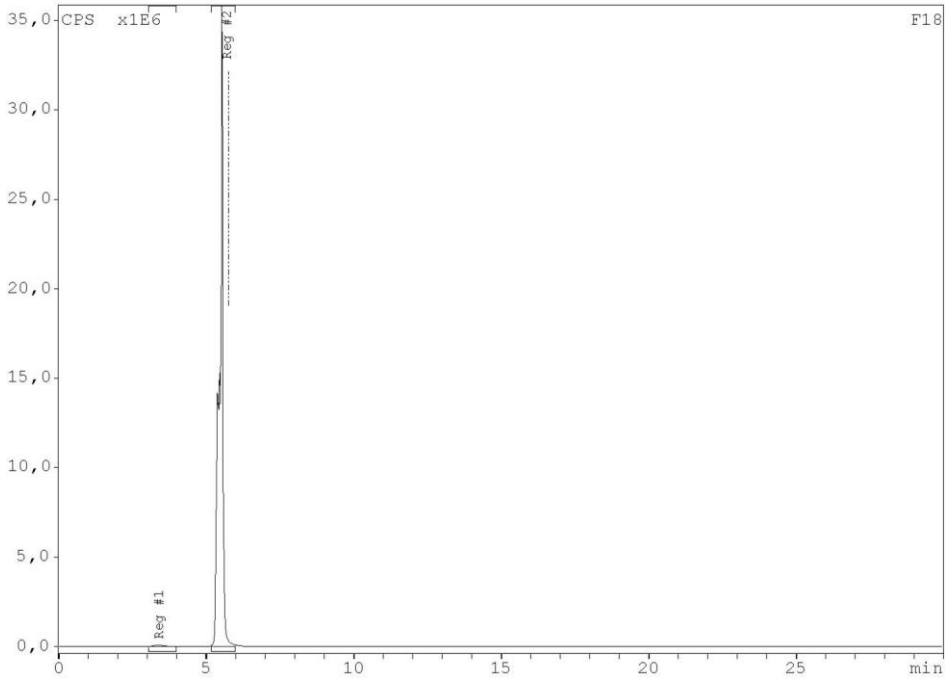

Figure 3: Analytical radio-HPLC chromatogram [^{18}F]16 . Analytical radio-HPLC was performed with a Phenomenex gemini C18 column (5 µm, 250x4.6 mm) at a flow of 3.6 mL/min, whereas A is ammonium formiate solution (50 mM) and B is acetonitrile. The following method was used: 0-5 min 100 % A (isocratic), 5-18 min 0-95 % B (gradient), 18-22 min 95 % B (isocratic), 22-25 min 5-100 % A (gradient). Retention time 5.50 min, purity ш99 %.

[^{18}F]fluoro-ala-Folate

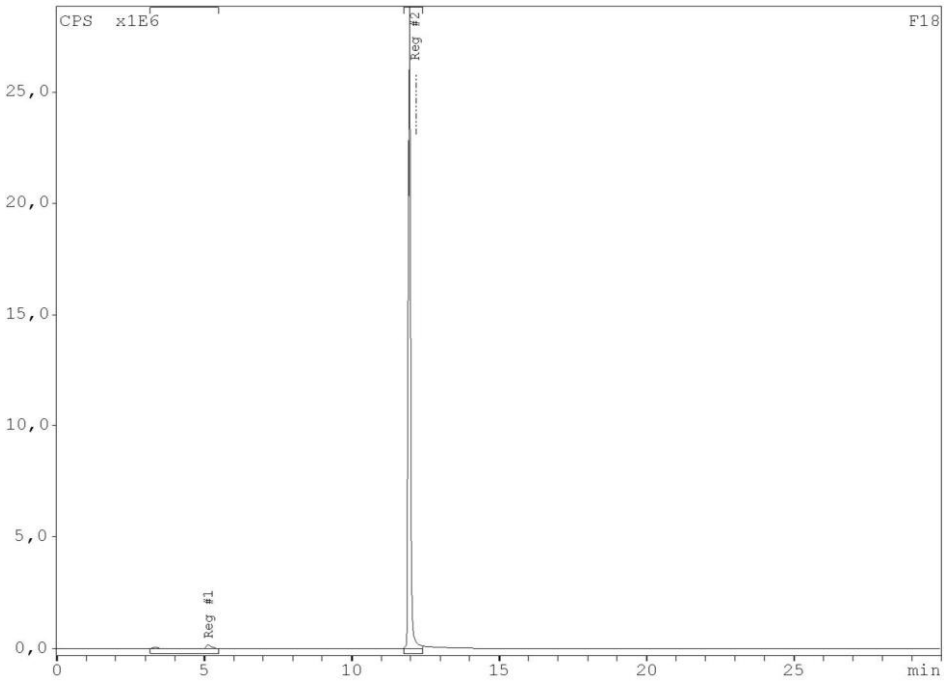

Figure 4: Analytical radio-HPLC chromatogram [^{18}F]25. Analytical radio-HPLC was performed with a Phenomenex gemini C18 column (5 µm, 250x4.6 mm) at a flow of 3.6 mL/min, whereas A is ammonium formiate solution (50 mM) and B is acetonitrile. The following method was used: 0-5 min 100 % A (isocratic), 5-18 min 0-95 % B (gradient), 18-22 min 95 % B (isocratic), 22-25 min 5-100 % A (gradient). Retention time 11.93 min, purity ш97 %.

[^{18}F]fluoro-alakyne: not only a prosthetic group, but also a potent tumor imaging candidate!

Kathrin Kettenbach[1], Hanno Schieferstein[1], Nicole Bausbacher[2], Barbara Biesalski[3], Wolfgang Müller-Klieser[3], Frank Rösch[1]. Tobias L. Ross[1,4]

Abstract

The use of radiolabeled amino acids enables the differentiation between tumors and inflammatory processes using positron emission tomography (PET). Highly proliferating cells such as cancer cells show a higher demand on amino acids due to increased protein synthesis rate. This fact makes ^{18}Flabeled amino acid derivatives an ideal oncological biomarker. Herein we report the synthesis and evaluation of a ^{18}F-labeled alanine derivative, which can be used in both ways, as a prosthetic group and as a radiotracer for tumor imaging itself. [^{18}F]fluoro-alakyne ([^{18}F]9) was radiolabeled using the K_2CO_3/Kryptofix system followed by a quantitative acidic deprotection step. After HPLC purification a RCY of 29.4 ± 7.7 % and a purity of ш97 % were achieved. Time-dependent uptake studies with nonsmall cell lung cancer (nsclc) cells (NCI-H1975) showed fast uptake and an early equilibrium. Competition assays showed significant inhibition of [^{18}F]fluoro-alakyne uptake for coincubation with L⁄D-alanine, –serine and fluoro-alakyne. *In vivo* small animal biodistribution studies with NCI-H1975 xenograft mice showed a low tumor uptake (0.28 ± 0.06 % ID/g tissue), but an extraordinary tumor-tobackground contrast. Despite the tumor only kidneys and bladder are visible in the µPET imaging. A very favorable tumor-to-blood (3.50) and tumor-to-liver ratio (2.55) were observed, which results in a clear-cut image quality. Further studies with other tumor cell lines and xenografts are under current investigation.

Introduction

Amino acids are the building blocks in protein biosynthesis, wherefore high proliferating cells such as tumor cells have a higher demand on amino acids. Several Na^+-dependent and –independent transporter systems are known to be responsible for the uptake of various amino acids into the cells. [1] The Na^+-independent systems (e.g. LAT1 – 4) transport amino acids by an 1:1-exchange with other amino acids into the cells. Therefore, a second transporter system and a substrate for both transporter systems are necessary. LAT1 mainly transports large amino acids, whereas LAT2 in general provides broader substrate specificity. For Na^+-dependent transporters, the electrochemical gradient across the cell membrane can be used to transport amino acids into the cells. In 2000, a novel protein (ASC-1) with the highest structural similarity to LAT2 was identified. A particularity of ASC-1 is the fact that it also accepts D-amino acids and amino acid-related compounds. [2]

In general, malignant cells show a higher demand on amino acids due to their increased proliferation rate, which results in a higher protein synthesis rate (PSR). [3] It is thought, that tumors can upregulate the amino acid transporter expression and the transporter activity to ensure sufficient supply of these nutrients. [4] Therefore, radiolabeled amino acids can be used to investigate the incorporation of amino acids into proteins by measuring the PSR (L-[^{11}C]leucine) [5] or only the tumor uptake using PET. [6-8] For many years, ^{11}C-labeled amino acids have been the research focus because of their easy labeling properties. [5] The most investigated amino acid usable for PET is certainly [^{11}C]methionine, which can be used for the imaging of brain, head and neck, lung and breast cancer. [9] Since the short half-life of carbon-11 does not allow the transportation of ^{11}C-labeled radiotracers to remote sites, the interest in ^{18}F-labeled radiopharmaceuticals increased. Distinct research activities focused on^{18}F-labeled tyrosine derivatives, frequently *O*-(2-[^{18}F]fluoroethyl)-L-tyrosine ([^{18}F]FET). [8,10-14] Unfortunately, most of these radiotracers showed some disadvantages such as poor stability [13] or high abdominal background due to accumulation in the pancreas and the kidneys. [11]

Instead of using radiofluorinated substrates for system L, Koglin *et al.* reported in 2011 an ^{18}F-labeled glutamate derivative, which is a substrate for system x_c^-. [15] In contrast to the oncological standard [^{18}F]FDG, this radiotracer enables the differentiation between tumors and inflammatory tissue, and allows the imaging of brain tumors. System x_c^- is overexpressed in many tumors, ensuring increased access to L-cysteine. Since this system is not able to discriminate between L-cysteine and L-glutamate, this novel radiotracer is a promising candidate for tumor imaging. (4S)-4-(3-[^{18}F]fluoropropyl)-Lglutamate alias [^{18}F]FSPG showed high uptake in several tumor cell lines and in PET studies. A fast and high tumor uptake combined with a rapid blood clearance was observed. Clinical studies with [^{18}F]FSPG in comparison with [^{18}F]FDG in non-small cell lung cancer (nsclc) patients showed that they were able

to identify all nsclc lesions and that 59 of 67 (88 %) [^{18}F]FDG lesions were detected. [16] These examples prove the high potential of amino acid-based radiotracers for tumor diagnosis using PET.

In 2014, Schieferstein *et al.* developed a novel ^{18}F-prosthetic group based on alanine to improve the metabolic and pharmacokinetic properties of hydrophilic radiotracers. [17] [^{18}F]fluoro-alakyne has already been applied as a prosthetic group for the radiolabeling of a folate derivative with fluorine-18 followed by *in vitro* and *in vivo* evaluation. [18] The aim of this work was to evaluate the [^{18}F]fluoroalakyne as a tumor imaging candidate itself. Therefore, non-small cell lung cancer (ncsls) cells (NCIH1975) and xenografts were used. *In vitro* uptake and trans-stimulating assays as well as *in vivo* µPET imaging studies have been performed.

This novel approach enables the synthesis of two different radiotracers, the [^{18}F]fluoro-ala-folate (e.g.) and the [^{18}F]fluoro-alakyne within one radiosynthesis.

Experimental procedure

General

Reagents and solvents were purchased from Acros Organics, Alfa Aesar, Fisher Scientific, Fluka, Merck, Sigma Aldrich and VWR and used without further purification. Reactions were monitored using thin layer chromatography (Merck silica gel 60 F254) or high-performance liquid chromatography (HPLC). Nuclear magnetic resonance spectra (^{1}H and ^{19}F) were recorded using an AC-300-Spectrometer (300MTh-T-NMR-spectrometer AC 300, Bruker Analytik GmbH) in $DCCl_3$, DMSO-d_6 or CD_3OD and an Avance II-400-Spectrometer (400 MHz) for ^{13}C-NMR. Chemical shifts are reported in parts per million (ppm) relative to tetramethylsilane (0.00 ppm) for ^{1}H- and ^{13}C-NMR and trichloro-fluoro-methane (0.00 ppm) for ^{19}F-NMR. Coupling constants (J) are given in hertz (Hz) and the following abbreviations are used for the description of the NMR: singlet (s), doublet (d), triplet (t), quartet (q), multiplet (m), doublet of doublet (dd). FD and ESI mass spectrometry were performed on a MAT 95-MS 7500 CE and a HP 4500 (Agilent Technologies and Hewlett-Packard, respectively, both Santa Clara, Ca, USA).

Semi preparative and analytical HPLC was performed with a Dionex HPLC system equipped with a 680 HPLC pump and a UVD170U UV-detector (210 nm, 230 nm, 254 nm and 286nm) using a reversedphase column (semi preparative column: Synergi, C12, max-RP column, 4 µm, 250x10 mm) at a flow rate of 3.5 mL/min for the semi preparative column.

Analytical radio-HPLC was performed on a Dionex P680A pump and a Dionex UVD 170U (254 nm), equipped with a 2 mL-loop and a GabiStar radiodetector (Raytest). An analytical column (Gemini, C18, 5 µm, 250x4.6 mm) was used at a flow rate of 1.0 mL/min. Dionex Chromeleon software was used for UV-data analysis and Raytest Gina star software for radioactivity detection.

Purification of the radiolabeled products was performed on a semi preparative radio-HPLC system with a Dinoex HPLC system equipped with a 680 HPLC pump and a UVD170U UV-detector (210 nm, 230 nm, 254 nm and 286nm), equipped with a 2 mL-loop and a GabiStar radiodetector (Raytest). A semi preparative column (Synergi, C12, max-RP, 250x10 mm) was used at a flow rate of 3.5 mL/min.
All HPLC methods are described in the Supporting Information.

Organic Chemisty

Methyl-3-chloro-2-((2,4-dimethoxybenzyl)(prop-2-yn-1-yl)amino)-propanoate (6)

The labeling precursor 6 was synthesized according to Schieferstein *et al.* as shown in scheme 1. [17] The synthesis started with the reductive amination of L-serine methyl ester hydrochloride 1 using 2,4dimethoxybenzyl and sodium cyanoborohydride. To ensure *N*-regioselectivity during the alkylation, the hydroxyl function of 2 was first protected using triisopropylsilyl chloride. Subsequently, 3-bromo1-(trimethylsilyl)-1-propyne was used to attach an alkyne to the secondary amine 3, enabling the molecule 4 to participate in copper-catalyzed cycloadditions. The alkyne group and the hydroxyl function were deprotected using tetrabutylammonium fluoride (1M). Intermediate 5 can be used for both, synthesis of the labeling precursor 6 as well as the reference compound 9. The preferred leaving group was meant to be a sulfonic-based one (tosyl or mesyl), but as previously reported it was not possible to synthesize and isolate the tosylated precursor due to the high reactivity within the small molecule. [17] Therefore, a chloro-precursor 6 was employed and was synthesized using *p*toluenesulfonyl chloride.

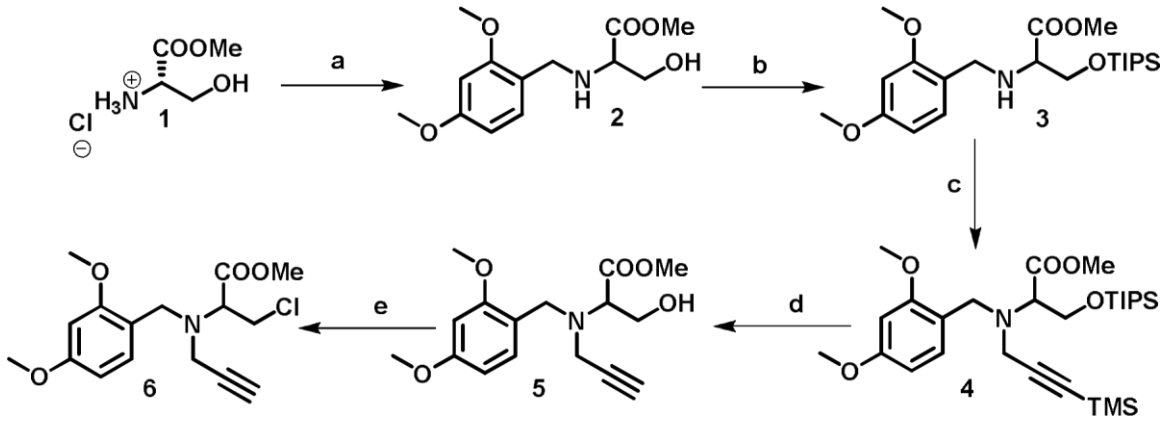

Scheme 1: Synthesis of alkyne-functionalized labeling precursor 6. Conditions and reagents: a) 2,4-Dimethoxybenzaldehyde , methanol, sodium cyanoborohydride, rt, 24 h; b) triisopropylsilyl chloride, DMF, imidazole, 0 °C, 30 min, rt, 24 h; c) 3-bromo1-(trimethylsilyl)-1-propyne, MeCN, Cs_2CO_3, 100 °C, 12 h; d) tetrabutylammonium fluoride in THF (1M), rt, 12 h; e) *p*toluenesulfonyl chloride, MeCN, TEA, 60 °C, 12 h.

Radiosyntheses were performed manually (starting activities ч 8 GBq) using conventional heating. The procedure for the production of dried [^{18}F]fluoride is described in the supporting information.

[^{18}F]fluoro-alakyne

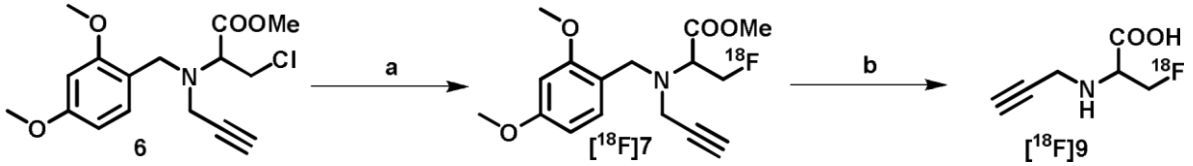

Scheme 2: Synthesis of ^{18}F-prosthetic group [^{18}F]9. Conditions and reagents: a) n.c.a. $^{18}F^-$, K_{222}, K_2CO_3, DMF, 140 °C, 15 min; b) hydrochloric acid (3.3M), 120 °C, 15 min.

The synthesis of the alanine-based ^{18}F-prosthetic group [^{18}F]9 was performed as previously reported by Schieferstein *et al.* (scheme 2) with some minor adjustments. [17] The [^{18}F]fluoride was eluted from the QMA cartridge with a solution of Kryptofix (5 mg) and potassium carbonate (1 mg, 7.5 µmol) in 600 µL (acetonitrile:water/1:1). The labeling reaction was carried out in dry DMSO at 140 °C using conventional heating. Sparing the transfer of dried [^{18}F]fluoride from a reaction vial into a microwave vial, which reduced the loss of activity. Methyl-3-[^{18}F]fluoro-2-((2,4-dimethoxybenzyl)(prop-2-yn-1yl)amino)propanoate can be separated from unreacted [^{18}F]fluoride using a C18 cartridge instead of semi-preparative HPLC saving additional time. The protected prosthetic group was deprotected using 3.3 M hydrochloric acid solution at 120 °C for 15 min followed by semi-preparative HPLC purification. The final product [^{18}F]9 group was isolated by evaporation of the HPLC solvents.

Stability test in human serum albumin

A solution of [^{18}F]9 (200 µL, approximately 4 MBq) was incubated with 500 µL human serum albumin (HSA) at 37 °C for 1 and 2 h. After incubation, plasma proteins were precipitated using 600 µL of icecold acetonitrile and centrifugation (10.00 rpm, 10 min). An aliquot (200 µL) of both time points was injected into the analytical radio-HPLC system (Gemini, C18, 5 µm, 250x4.6 mm, 1 mL/min). Each experiment was carried out in triplicates.

In vitro studies

For *in vitro* biological evaluation human non-small cell lung cancer cells (NCI-H1975) were used. The cell line was obtained from ATCC. The cells were cultured in RPMI medium containing 10 % FCS and Hepes (10 nM, 5 mL). For uptake, competition and trans-stimulating assays approximately 30.000 cells were seeded in 24-well plates two days in advance of the cell experiments and grown under standard conditions (37 °C, 5 % CO_2).

Uptake, competition and trans-stimulation studies

Prior to the application of [^{18}F]fluoro-alakyne [^{18}F]9, the medium was removed and the cells were washed one time with PBS buffer. The radiotracer solution was diluted with PBS buffer and 500 kBq/well were applied to the cells and they were incubated for 1 h at 37 °C. For the time dependency assay, cells were incubated for different time points from 5 to 120 min. For competition assays cells were coincubated with competitors either in excess at 5 mmol/L or in a dose-dependent manner (0.001 – 1 mmol/L). For trans-stimulation assays, cells were incubated with [^{18}F]9 for 60 min, washed and incubated with different compounds at 1 mmol/L for 45 min in PBS. After incubation the supernatant was removed, the cells were washed two times with PBS and lysed using sodium hydroxide solution (1M). Each experiment was carried out at minimum three times in triplicates for each setup. Radioactivity of the cell samples was determined using a gamma counter (Wizard, Perkin Elmer).

Animal studies

Female NMRI nude mice were purchased from Janvier and housed under specific pathogen-free conditions in the animal care facility in Mainz according to the guidelines of the regional care committee. All experiments were performed in accordance with the federal guidelines and approved by the ethical committee of the state of Rhineland-Palatinate (according to §8 Abs. 1 Tierschutzgesetz, Landesuntersuchungsamt). After seven days of acclimatization, human non-small cell lung cancer cells (NCI-H1975) were inoculated in the left shoulder of each mouse. All *in vivo* treatments and imaging experiments were done under isofluorane anesthesia.

Ex vivo biodistribution studies

Sixteen days after inoculation, animals were intravenously injected with [^{18}F]9 with 6-8 MBq in 150200 µL sodium chloride solution. Animals were sacrificed 90 min after injection and selected organs were dissected, weighed and measures in a gamma counter. The incorporated radioactivity was expressed as percentage of injected dose per gram of tissue [% ID/g tissue].

In vivo PET studies

Sixteen days after inoculation, animals were anesthetized with 2 % isofluorane in an air/oxygen mixture (70 % O_2) and intravenously injected with [^{18}F]9 (6-8 MBq, 150-200 µL). Whole body-PET scans were acquired over 10 min 50 min p.i. followed by MRI measurements (Material Map coregistration of the PET scan, 3D Gradient Echo External Averaging (GRE-EXT), Multi Filed of View (FOV); slice thickness: 0.6 mm, TE: 2 ms; TR: 15 ms; flip angle: 25 deg). Afterwards the PET images were coregistered to the MR and analyzed with pmod software.

Results and Discussion

Organic Chemistry

The chlorinated alanine-based labeling precursor 6 was obtained with an overall yield of 15 % over five steps. To ensure regioselective functionalization of serine, an extensive protecting group chemistry was necessary starting with the protection of the amino functionality using 2,4-dimethoxybenzaldehyde obtaining intermediate 2. Pre-incubation of the aldehyde with triethylamine resulted in a slightly higher yield of 60 % than reported by Schieferstein *et al.* [17] Protection of the hydroxyl function with triisopropylsilyl in quantitative yields led to intermediate 3, which was *N*alkylated using 3-bromo-1-(trimethylsilyl)-1-propyne giving compound 4 in 51 % yield. Tetrabutylammonium fluoride was used to cleave the TMS protecting group at the alkyne-function 5 (yield: 67 %), which subsequently was chlorinated to give the labeling precursor by using *p*-toluenesulfonyl chloride in 79 % yield. As already pointed out before, it was not possible to isolate the tosylated precursor due to the high reactivity of the tosyl group next to multiple electron withdrawing functionalities. Reference compound 9 was synthesized by fluorination of intermediate 5 using DAST (*N,N*-diethylaminosulfur trifluoride) obtaining compound 7 in a yield of 62 %. Complete deprotection was performed using lithium hydroxide (1M, 60 %) and trifluoroacetic acid (86 %).The reference compound 9 was obtained in an overall yield of 6 % over seven steps. Both, labeling precursor and reference could be obtained in good overall yields, and the labeling precursor exhibited a good stability at room temperature.

In our hands, the [^{18}F]fluoro-alakyne ([^{18}F]9) could not be separated quantitatively from the chlorinated precursor molecule 6 by HPLC. 1-naphthalenesulfonyl could be used as a leaving group instead to ensure high “specific activities”. Therefore, 1-naphthalenesulfonyl chloride was first converted into the silver salt using silver(II)oxide and then reacted with alanine-chloride 6. [19] The novel 1-naphthalenesulfonyl alanine precursor 10 was obtained after semi-preparative HPLC in 38 % yield.

Radiochemistry

The protected alanine-based prosthetic group [^{18}F]7 was obtained by nucleophilic substitution of the respective chloro-precursor 6 with 80 % ^{18}F-incorporation. After quantitative de-protection with 3.3M hydrochloric acid, the crude product [^{18}F]9 was neutralized and purified via semi-preparative HPLC giving the ^{18}F-prosthetic group in good overall RCY of 29.4 ± 7.7 % within 90 min.

Stability studies in human serum albumin

To test the stability of the novel amino acid based radiotracer [^{18}F]9, it was incubated in human serum albumin (HSA) at 37 °C for 1 and 2 h. No significant degradation of the radiotracer was observed over a period of 2 h by analytical radio-HPLC. Therefore, this novel radiotracer can be considered to be stable for the duration of a µPET scan.

In vitro studies

Uptake studies

The uptake of [^{18}F]fluoro-alakyne ([^{18}F]9) was investigated in non-small cell lung cancer cells (NCIH1975). Figure 1 shows the time-dependency of the uptake, reaching equilibrium after 30 min of incubation. Therefore, for all following experiments cells were incubated with the radiotracer [^{18}F]9 for 1 h.

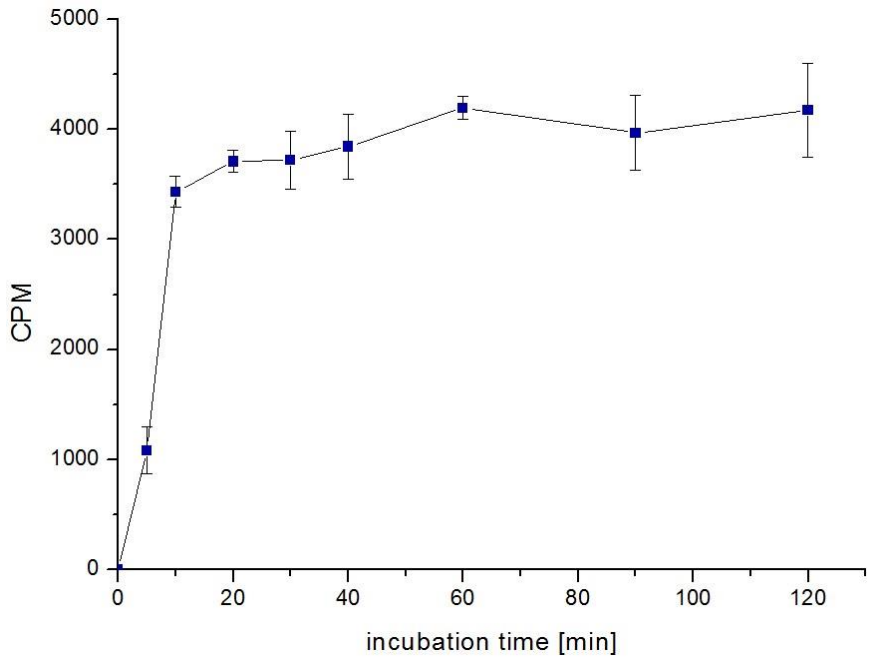

Figure 1: Time-dependent uptake of [^{18}F]9 in human NCI-H1975 non-small cell lung cancer cells was monitored over 120 min.

The fast uptake and early equilibrium of [^{18}F]9 into NCI-H1975 cells suggests an amino acid transporter with an 1:1 exchange of another amino acid by [^{18}F]fluoro-alakyne.

Competition assay

To further characterize the responsible transporter system for cellular uptake of [^{18}F]9, the tracer uptake was investigated in the presence of different amino acids and the cold reference compound 9

in a competition assay. We assume that the [^{18}F]fluoro-alakyne might be transported by either the Na^+-independent LAT2 [1,20,21], which transports large and small neutral amino acids into cells and/or by the ASC-1, which prefers small amino acids and also accepts D-isomers. [2] Therefore, the cells were coincubated with L-alanine, D-alanine, L-serine and D-serine (substrates for LAT2 and ASC1), the cold reference compound 9 as well as with L-aspartate, L-glutamate (substrates for the GLutamate/ASpartate transporter, GLAST) [22], lysine and proline (substrates for the neutral brush border (NBB) system and IMINO carrier). [23] Inhibition of [^{18}F]fluoro-alakyne uptake (y 50 %) was observed for coincubation with an excess of L-alanine, D-alanine, L-serine, D-serine and cold reference 9 but not for L-aspartate, L-glutamate, lysine or proline (figure 2).

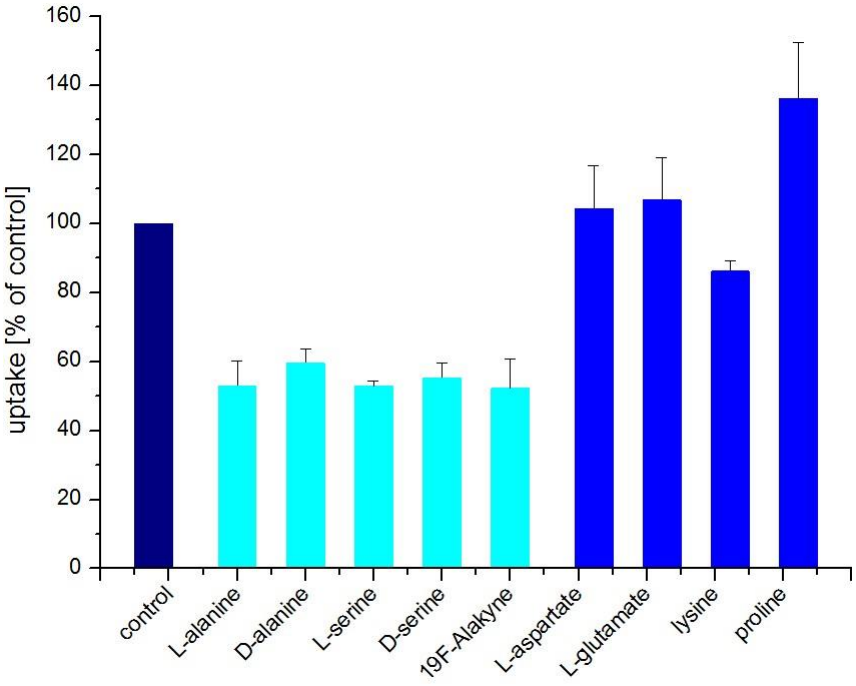

Figure 2: Coincubation of NCI-H1975 cells with [^{18}F]9 and other amino acids as well as with the cold reference compound 9 for 60 min.

For the coincubation with proline an even increased uptake of [^{18}F]9 (130 %) was observed. This suggests the transportation of proline into the NCI-H1975 cells by another pathway (NBB system or IMINO carrier) followed by an 1:1 exchange with [^{18}F]9. This preloading of the cells with another amino acid might than enable an increased radiotracer uptake.

Trans-stimulating assay

To study the intracellular retention of [^{18}F]9 in NCI-H1975 cells, the [^{18}F]fluoro-alakyne-loaded cells were investigated under efflux conditions for 45 min. Therefore, the cells were trans-stimulated with PBS, medium, the cold reference compound 9 and various amino acids. For all conditions the cells

showed an almost complete release (ɯ90 %) of [^{18}F]9 after 45 min as shown in figure 3. A slightly stronger retention was observed for PBS (20 %) and trans-stimulation with phenylalanine (30 %). The conclusion of this experiment is, that - as expected - the [^{18}F]fluoro-alakyne ([^{18}F]9) is not trapped in the cells by incorporation into proteins, but can also be exchanged by other amino acids.

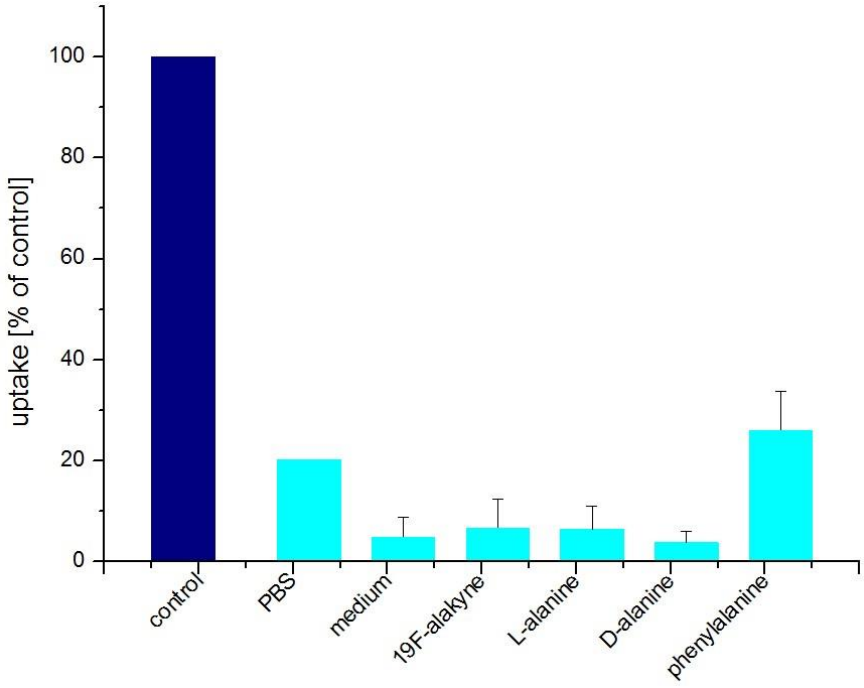

Figure 3: Intracellular retention of [^{18}F]9 for trans-stimulation for 45 min with PBS, medium, compound 9, L-alanine, D-alanine and phenylalanine. *In vivo* studies

Ex vivo Biodistribution

The results of the biodistribution studies of [^{18}F]9 are shown in table 1 and figure 4. NCI-H1975-tumor bearing mice (n=5) were sacrificed 90 min p.i. after injection of [^{18}F]9 (5-8 MBq). The high uptake in the urine (406.80 ± 56.00 %ID/g tissue) confirms the expected exclusively renal clearance of this radiotracer. Also the radioactivity found in the blood was very low after 90 min p.i. (0.08 ± 0.03 %ID/g tissue) indicating also a very fast clearance of [^{18}F]9 from the blood pool. Despite the low tumor uptake (0.28 ± 0.06 %ID/g tissue) very favorable tumor-to-kidney (0.70) and especially tumor-to-liver (2.55) and tumor-to-blood ratios (3.50) were achieved. The low background leads to an extraordinary high tumor-to-background contrast already at 90 min p.i.

Table 6: *Ex vivo* biodistribution studies of [^{18}F]9 in NCI-H1975 tumor bearing NMRI nu/nu mice after 90 min p.i. Errors are given as standard deviation.

	NMRI nu/nu mice NCI-H1975 xenograft	NMRI nu/nu mice NCI-H1975 xenograft
	90 min p.i. 90 min p.i. %ID/g tissue (n=5)	%ID/g tissue (n=5)

pancreas 0.10 ± 0.06 muscle 0.15 ± 0.07 ing LN 0.14 ± 0.08

urine	406.80 ± 56.00

tumor	0.28 ± 0.06
tumor/blood	3.50
tumor/liver	2.55
tumor/kidney	0.70
tumor/muscle	1.87

lung	0.09 ± 0.03	stomach	0.71 ± 0.88
blood	0.08 ± 0.03	appendix	0.25 ± 0.19
heart	0.08 ± 0.02	feces	0.32 ± 0.32

liver 0.11 ± 0.02 intestines 0.10 ± 0.07 spleen 0.08 ± 0.03 left kidney 0.38 ± 0.19 right kidney 0.42 ± 0.21

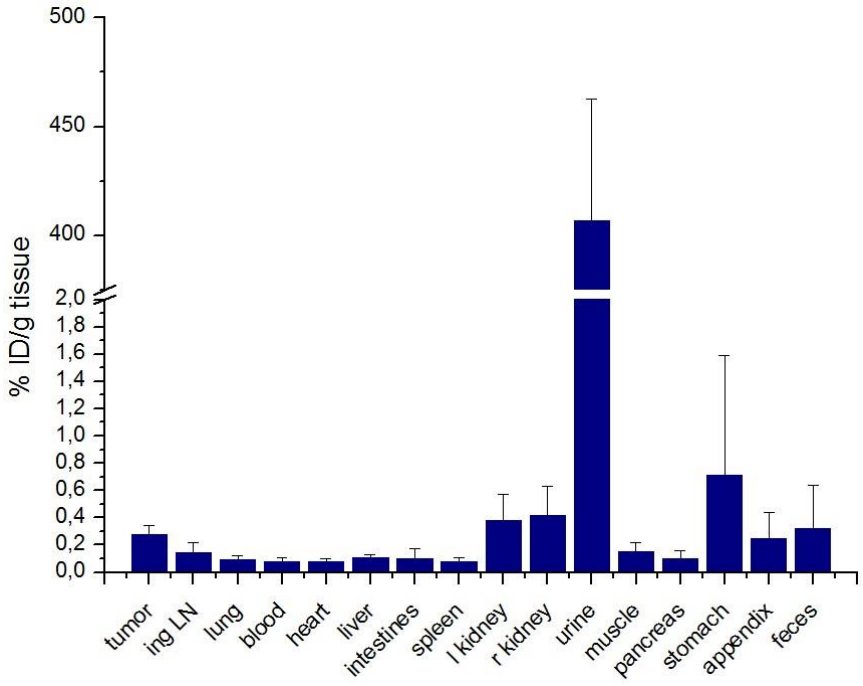

Figure 4: Results of the *ex vivo* biodistribution study at 90 min p.i. of [^{18}F]9.

In vivo PET studies

NCI-H1975 tumor bearing mice with the tumor located at the left shoulder were used for µPET imaging studies. Statistic scans over 10 min were performed 50 min after injection to allow the animals to efficiently clear the unbound tracer, which led to an improved background signal. As expected from the *ex vivo* biodistribution data, [^{18}F]9 provided a very low background and only negligible uptake in other organs. Therefore, an excellent clear-cut tumor visialization was achieved in spite of a low absolute uptake of activity in the tumor.

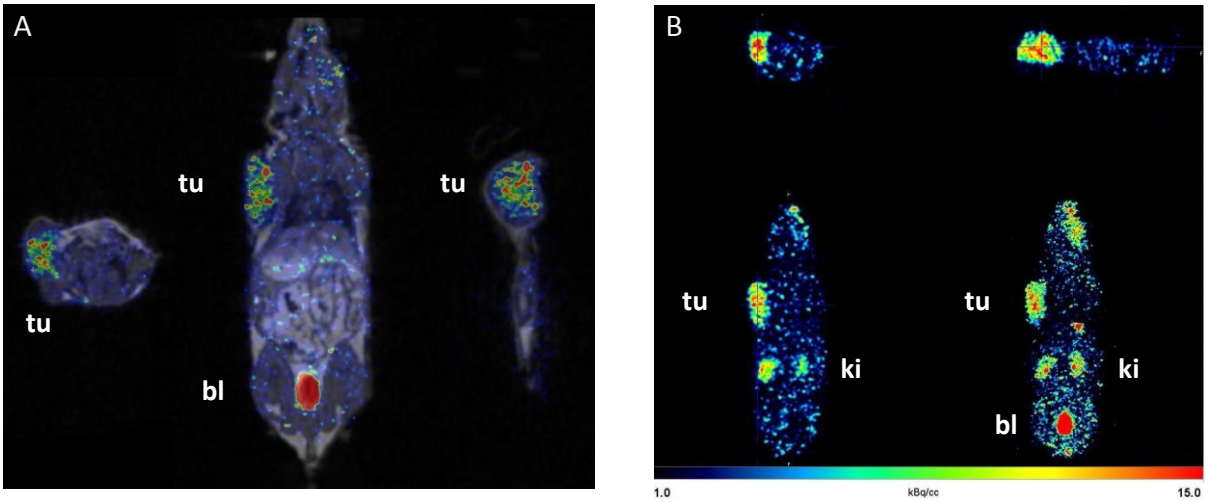

Figure 5: PET images of a NCI-H1975-tumor bearing mouse. Static scan over 10 min 50 min p.i. of [^{18}F]fluoro-alakyne **[^{18}F]9** (approximately 7 MBq), **A** PET/MRI sagittal, coronal and transversal slices and **B** PET sagittal, transversal, coronal slices and MIP.

Conclusions

A novel ^{18}F-labeled amino acid derivative [^{18}F]9 was synthesized in high yields and purity. Its high potential as a hydrophilic prosthetic group for the ^{18}F-labelling of biomolecules with fluorine-18 has already been shown before. [18] [^{18}F]fluoro-alakyne shows great improvements in comparison to other ^{18}F-labeled amino acid derivatives in terms of undesirable accumulation in the pancreas, the liver or the intestines. [^{18}F]9 provided only a low tumor uptake but an extraordinary tumor-tobackground contrast. Consequently, the tumor was clearly visible in the µPET imaging. Further investigations concerning the differentiation between tumors and inflammatory processes using [^{18}F]fluoro-alakyne are planned.

Ethical statement

All experiments with commercial available human serum albumin (Sigma Aldrich, H4522, from human male AB plasma) were conducted in accordance with the local law and national and institutional guidelines and ethics. The officer for biological safety has approved the performed experiments and informed consent was obtained for any experiment with commercial available human serum. All animal experiments were performed in accordance with federal guidelines and approved by the ethical committee of the state of Rheinland Pfalz (according to §8 Abs. 1 Tierschutzgesetz, Landesuntersuchungsamt).

Acknowledgments

The authors thank the Max Planck Graduate Center, the Graduate School of the SFB 1066 and the Ci3Cluster of Excellence for supporting Kathrin Kettenbach.

References

[1] E. M. del Amo, A. Urtti, and M. Yliperttula, “Pharmacokinetic role of L-type amino acid transporters LAT1 and LAT2,” *European Journal of Pharmaceutical Sciences*, vol. 35, no. 3, pp. 161–174, 2008.

[2] Y. Fukasawa, H. Segawa, J. Y. Kim, A. Chairoungdua, D. K. Kim, H. Matsuo, S. H. Cha, H. Endou, and Y. Kanai, “Identification and Characterization of a Na^+-independent Neutral Amino Acid Transporter That Assiciates with the 4F2 Heavy Chaina and Exhibits Substrate Selectivity for Small Neutral D- and L- Amino Acids,” *Journal of Biological Chemistry*, no. 13, pp. 9690–9698, 2000.

[3] A. L. Lehninger, "*Biochemistry", 2nd edition,* New York, Worth, 1976.

[4] T. Miyagawa,T. Oku, H. Uehara, R. Desai, B. Beattie, J. Tjuvajev, and R. Blasberg, “"Facilitated" amino acid transport is upregulated in brain tumors,” *Journal of Cerebral Blood Flow and Metabolism*, vol. 18, no. 5, pp. 500–509, 1998.

[5] W. Vaalburg, H. H. Coenen, C. Crouzel, P. H. Elsinga, B. Lanström, C. Lemaire, and G. J. Meyer, “Amino acids for the measurement of protein synthesis in vivo by PET,” *International Journal of Radiation Applications and Instrumentation*, vol. 19, no. 2, pp. 227–237, 1992.

[6] H. J. Wester, M. Herz, W. Weber, P. Heiss, R. Senekowitsch-Schmidtke, M. Schaiger, and G. Stöcklin, “Synthesis and Radiopharmacology of O-(2-[^{18}F]fluoroethyl-L-tyrosine for tumor imaging,” *The Journal of Nuclear Medicine*, vol. 40, no. 1, pp. 205-212, 1999.

[7] H. Uehara, T. Mijagawa, J. Tjuvajev, R. Joshi, and B. Beattie, “Imaging experimental brain tumors with 1-aminocyclopentane carboxylic acid and alpha-aminoisobutyric acid: comparison to fluorodeoxyglucose and diethylenetriaminepentaacetic acid in morphologically defined tumor regions,” *Journal of Cerebral Blood Flow and Metabolism*, vol. 17, no. 11, pp. 1239–1253, 1997.

[8] T. M. Shoup, J. Olson, J. M. Hoffman, J. Votaw, D. Eshima, L. Eshima, V. M. Camp, D. Votaw, and M. M. Goodman, “Synthesis and evaluation of ^{18}F-1-Amino-3-fluorocyclobutane-1-carboxylic acid to image brain tumors,” *The Journal of Nuclear Medicine*, no. 40, pp. 331–338, 1999.

[9] T. Inoue, K. Tomiyoshi, T. Higuichi, K. Ahmed, M. Sarwar, K. Aoyagi, S. Amano, S. Alyafei, H. Zhang, and K. Endo, “Biodistribution Studies on L-3-Fluorine-18-Fluoro-alpha-methyl tyrosine,” *The Journal of Nuclear Medicine*, no. 39, pp. 663–667, 1998.

[10] N. Koglin, A. Mueller, M. Berndt, H. Schmitt-Willich, L. Toschi, A. W. Stephens, V. Gekeler, M. Friebe, and L. M. Dinkelborg, “Specific PET imaging of xC- transporter activity using a ^{18}F-labeled glutamate derivative reveals a dominant pathway in tumor metabolism,” *Clinical Cancer Research*, vol. 17, no. 18, pp. 6000–6011, 2011.

[11] P. D. Shreve, Y. Anzai, and R. L. Wahl, “Pitfalls in oncologic diagnosis with FDG PET imaging: physiologic and benign variants,” *Radiographics*, vol. 19, no. 1, 61-77, pp. 150-1, 1999.

[12] B. Chin *et al.,* “Synthesis and priliminary evaluation of 5-[18F)fluoroleucine: a novel LAT1 substrate,” *The Journal of Nuclear Medicine*, no. vol. 57, suppl 2, p. 1390, 2016.

[13] P. Heiss, D. McDougald, D. Weitzel, T. Hawk, R. Reiman, M. Zalutsky, and G. Vaidyanathan, “Investigation of Transport Mechanism and Uptake Knietics of O-2-^{18}F-Fluoroethyl-L-tyrosine in vitro and in vivo,” *The Journal of Nuclear Medicine*, no. 40, pp. 1367–1373, 1999.

[14] T. Inoue, T. Shibasaki, N. oriuchi, K. Aoyagi, K. Tomiyoshi, S. Amano, M. Mikuni, I. Ida, J. Aoki, and K. Endo, "^{18}F alpha-methy tyrosine PET studies in patients with brain tumors," *The Journal of Nuclear Medicine*, no. 40, pp. 399–405, 1999.

[15] R. N. Krasikova, O. F. Kuznetsova, O. S. Fedorova, Y. N. Belokon, V. I. Maleev, L. Mu, S. Ametamey, P. A. Schubiger, M. Friebe, M. Berndt, N. Koglin, A. Mueller, K. Graham, L. Lehmann, and L. M. Dinkelborg, "4-[^{18}F]fluoroglutamic acid (BAY 85-8050), a new amino acid radiotracer for PET imaging of tumors: synthesis and in vitro characterization," *Journal of Medicinal Chemistry*, vol. 54, no. 1, pp. 406–410, 2011.

[16] S. Baek, C.-M. Choi, S. H. Ahn, J. W. Lee, G. Gong, J.-S. Ryu, S. J. Oh, C. Bacher-Stier, L. Fels, N. Koglin, C. Hultsch, C. A. Schatz, L. M. Dinkelborg, E. S. Mittra, S. S. Gambhir, and D. H. Moon, "Exploratory Clinical Trial of (2S)-4-(3-[^{18}F]fluoropropyl)-Lglutamate for Imaging x_c^- Transporter Using Positron Emission Tomography in Patients with Non-Small Cell Lung or Breast Cancer," *Clinical Cancer Research*, vol. 18, no. 19, pp. 5427-37, 2012.

[17] H. Schieferstein, and T. L. Ross, "A Polar ^{18}F-Labeled Amino Acid Derivative for Click Labeling of Biomolecules," *European Journal of Organic Chemistry*, vol. 2014, no. 17, pp. 3546–3550, 2014.

[18] K. Kettenbach, H. Schieferstein, S. Pektor, R. Eckert, L. M. Reffert, G. Otto, M. Miederer, F. Rösch, and T. L. Ross, "*In vitro* and *in vivo* comparison study of folate derivatives labeled with fluorine-18 via copper-free and copper-catalyzed click cycloadditions: the lipophilicity makes the difference!," *Bioorganic & Medicinal Chemistry* (under review).

[19] R. Loser, S. Fischer, A. Hiller, M. Köckerling, U. Funke, A. Maisonial, P. Brust, and J. Steinbach, "Use of 3-(18)Ffluoropropanesulfonyl chloride as a prosthetic agent for the radiolabelling of amines: Investigation of precursor molecules, labelling conditions and enzymatic stability of the corresponding sulfonamides," *Beilstein Journal of Organic Chemistry*, vol. 9, pp. 1002–1011, 2013.

[20] M. Pineda, E. Fernandez, D. Torrents, R. Estevez, C. Lopez, M. Camps, J. lloberas, A. Zorzano, and M. Palacin, "Identification of a Membrane, LAT2, That Co-expresses with aF2 Heavy Chain L-type
Amino Acid Transport Activity with Broad Specificity for Small and Large Zwitterionic Amino Acids," *Biochemical Journal*, vol. 349, pp. 787-95, 2000

[21] H. Segawa, Y. Fukasawa, K. Miyamoto, E. Takeda, H. Endou, and Y. Kanai, "Identification and functional characterization of a na idenpendent neutral amino acid transporter with broad substrate slelectivity,"*The Journal of Biological Chemistry*, vol. 274, no. 28, pp. 19745-51, 1999.

[22] Y. Kanai, and M. A. Hediger, "The glutamate/neutral amino acid transporter family SLC1: molecular, physiological and pharmacological aspects," *Pflugers Archiv : European Journal of Physiology*, vol. 447, no. 5, pp. 469–479, 2004.

[23] B. R. Stevens, E. M. and Wright, "Substrate specificity of the intestinal brush-border proline/sodium (IMINO) transporter," *The Journal of Membrane Biology,* vol. 87, no. 1, pp. 27–34, 1985.

Supplementary data

[^{18}F]fluoro-alakyne: not only a prosthetic group, but also a potent tumor imaging candidate!

Kathrin Kettenbach[1], Hanno Schieferstein[1], Nicole Bausbacher[2], Barbara Biesalski[3], Wolfgang Müller-Klieser[3], Frank Rösch[1]. Tobias L. Ross[1,4]

[1] Institute of Nuclear Chemistry, Johannes Gutenberg University Mainz, 55128 Mainz, Germany

[2] Clinic and Policlinic of Nucear Medicine, Johannes Gutenberg University Medicine, 55131 Mainz, Germany

[3] Institute of Pathophysiology, Johannes Gutenberg University Mainz, 55128 Mainz, Germany

[4] Radiopharmaceutical Chemistry, Department of Nuclear Medicine, Hannover Medical School, 30625 Hannover, Germany

Content

I. ORGANIC SYNTHESES OF ALANINE-DERIVATIVES

I.1. Synthesis of Alanine labeling precursor

I.2. Synthesis of Alanine-alkyne reference compound

This content can be found in supplementary data "In vitro and in vivo comparison study of a folate derivative labeled with fluorine-18 via copper-free and copper-catalyzed cycloaddition".

Methyl-2-((2,4-dimethoxybenzyl)(prp-2-ynyl)amino)-3-(naphthalene-1-ylsulfonyloxy)prpanoate (10)

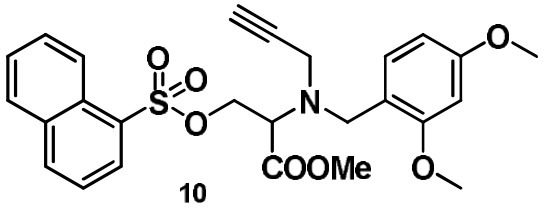

10

To a solution of 1-naphthalenesulfonyl chloride (159 mg, 0.7 mmol) in acetonitrile (5 mL) was added silver(II)oxide (300 mg, 1.3 mmol). The resulting suspension was stirred for 3 days at room temperature under the exclusion of light. The solid material was filtered off and washed with acetonitrile. The solvent of the combined filtrates was removed under reduced pressure. The 1naphthalenesulfonyl silver salt was used without further purification. To a solution of 6 (12 mg, 0.04 mmol) in acetonitrile (5 mL) was added silver 1-naphthalensulfonyl (19 mg, 0.06 mmol) and the resulting mixture was stirred at room temperature for 3 days under the exclusion of light. After semipreparative HPLC purification product 9 (7 mg, 0.014 mmol, 38 %) was obtained as a yellow oil.

^{1}H-NMR (400 MHz, $CDCl_3$, Me_4Si): ω [ppm] = 2.19 (s, 1H, H-1), 2.68 (s, 2H, H-2), 3.48 (d, J = 2.37 Hz, 1H, H-3), 3.76 (s, 2H, H-4), 3.78 (s, 3H, H-5), 3.80 (s, 3H, H-6), 3.82 (s, 3H, H-7), 3.84 (s, 1H, H-8), 4.87 (s, 1H, H-8), 6.42 (m, 2H, H-9 and H-10), 7.42 (dd, J = 1 Hz and 7.3 Hz, 1H, H-11), 7.55 (m, 1H, H-12), 7.85 – 7.89 (q, J = 8Hz, 3H, H-13, H-14 and H-15), 8.16 (d, J = 7.23 Hz, 1H, H-16), 8.89 (d, J = 8.53 Hz, 1H, H17).

^{13}C-NMR (400 MHz, $CDCl_3$, Me_4Si): ω [ppm] =30.83 (C-2), 30.90 (C-1), 52.90 (C-4), 55.32 (C-8), 55.40 (C5), 55.44 (C-3), 55.44 (C-6), 55.59 (C-7), 98.70 (C-10), 104.95 (C-9), 126.40 (C-11), 127.10 (C-12), 128.26 (C-13), 128.26 (C-14), 131.37 (C-15), 125.88 (C-16), 126.96 (C-17),

MS (ESI positive): m/z 301.13 ($[M+Na]^+$, 73.12 %), 317.13 ($[M+K]^+$, 62.19 %), calculated for $C_{13}H_{26}O_6$: 278.34.

II. ^{18}F-RADIOLABELING

II.1. General radiolabeling methods

II.2. Synthesis of [^{18}F]9

This content can be found in supplementary data "In vitro and in vivo comparison study of a folate derivative labeled with fluorine-18 via copper-free and copper-catalyzed cycloaddition". III. ANALYTICS

III.I. NMR data

Methyl-2-((2,4-dimethoxybenzyl)amino)-3-oxy-propanoate (2)

Methyl-2-((2,4-dimethoxybenzyl)amino)-3-((triisopropylsilyl)oxy)-propanoate (3)

Methyl-2-((2,4-dimethoxybenzyl)(3-(trimethylsilyl)prp-2-yn-1-yl)amino)-3-((triisopropylsilyl)propanoate (4)

Methyl 2-((2,4-dimethoxybenzyl)(prop-2-yn-1-yl)amino)-3-hydroxy-propanoate (5)

Methyl 3-chloro-2-((2,4-dimethoxybenzyl)(prop-2-yn-1-yl)amino)-propanoate (6)

Methyl 2-((2,4-Methoxybenzyl)(prop-2-yn-1-yl)amino)-3-fluoro-propanoate (7)

2-((2,4-Methoxybenzyl)(prop-2-yn-1-yl)amino)-3-fluoropropanoic acid (8)

3-fluoro-2-(prop-2-yn-1-ylamino)propanoic acid (9)

This content can be found in supplementary data "In vitro and in vivo comparison study of a folate derivative labeled with fluorine-18 via copper-free and copper-catalyzed cycloaddition".

Methyl-2-((2,4-dimethoxybenzyl)(prp-2-ynyl)amino)-3-(naphthalene-1-ylsulfonyloxy)prpanoate (10)

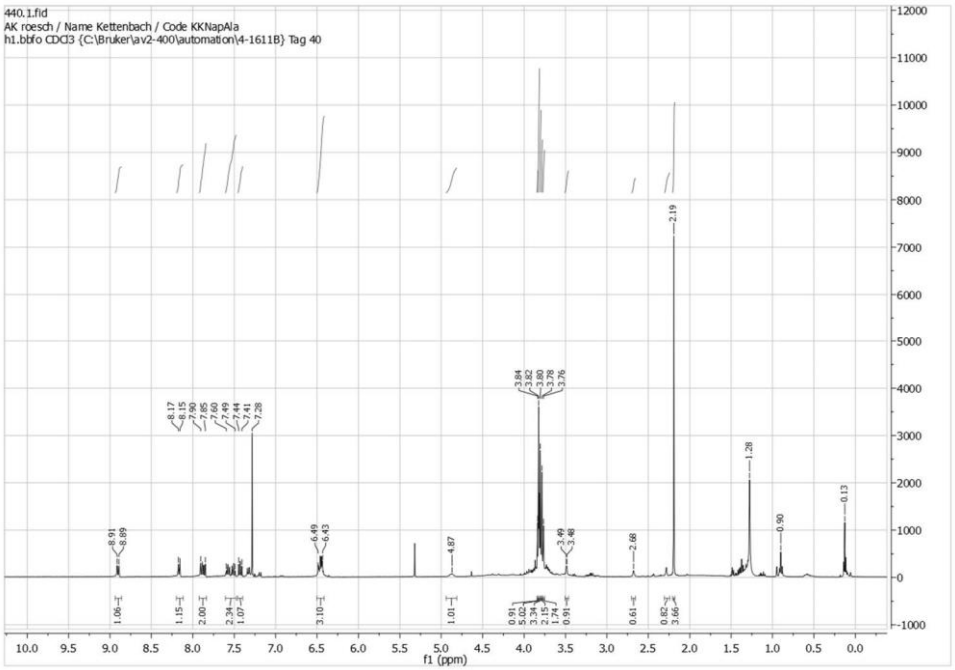

^{1}H-NMR (400 MHz, $CDCl_3$, Me_4Si): ω [ppm] = 2.19 (s, 1H, H-1), 2.68 (s, 2H, H-2), 3.48 (d, J = 2.37 Hz, 1H, H-3), 3.76 (s, 2H, H-4), 3.78 (s, 3H, H-5), 3.80 (s, 3H, H-6), 3.82 (s, 3H, H-7), 3.84 (s, 1H, H-8), 4.87 (s, 1H, H-8), 6.42 (m, 2H, H-9 and H-10), 7.42 (dd, J = 1 Hz and 7.3 Hz, 1H, H-11), 7.55 (m, 1H, H-12), 7.85 – 7.89 (q, J = 8Hz, 3H, H-13, H-14 and H-15), 8.16 (d, J = 7.23 Hz, 1H, H-16), 8.89 (d, J = 8.53 Hz, 1H, H17).

Radiolabeling of a FAP specific microprotein

Kathrin Kettenbach[1], Benedikt Sandhöfer [1], Joycelyn Wüstehube-Lausch[2], Matin Daneschdar[2], Ugur Sahin[2], Frank Rösch[1]. Tobias L. Ross[1,3]

[1] Institute of Nuclear Chemistry, Johannes Gutenberg-University Mainz, 55128 Mainz, Germany

[2]BioNTech AG, An der Goldgrube 12, 55131 Mainz, Germany

[3] Radiopharmaceutical Chemistry, Department of Nuclear Medicine, Hannover Medical School, 30625 Hannover, Germany

Abstract

The serine protease FAP (fibroblast activation protein alpha, also named seprase) is known as an oncological target for therapy and diagnosis for many years due to its upregulation in reactive stromal fibroblast of more than 90 % of human epithelial tumors. While FAP is found in breast, lung and colorectal cancers, no expression is observed in normal tissues as well as bone and soft tissue sarcomas. Within the last decades, many monoclonal antibodies with selectivity to FAP have been developed for therapeutic applications, but there is still a lack of FAP specific radiopharmaceuticals for precise and early diagnosis using positron emission tomography (PET). Herein, we report the synthesis and preclinical evaluation of a novel FAP specific microbody labeled with gallium-68. The novel microbody MC-FA-012 was identified by the BioNTech AG using a phage display system followed by recombinant production in *E. coli*.. For radiolabeling with gallium-68 the microbody was derivatized with a DOTA chelator in very good yields. The radiolabeling reaction was carried out in sodium acetate buffer at 90 °C for 10 min, resulting in almost quantitative incorporation of gallium-68 into the chelator. [^{68}Ga]Ga-DOTA-MC-FA-012 showed a fast and specific uptake in FAP-positive cells (CHO-K1huFAP) compared to FAP-negative cells (CHO-K1-MOCK). An average of 1.5 % of the applied activity was internalized into CHO-K1-huFAP cells and additionally 3 % were surface bound, which also adds to a diagnostic or therapeutic effect of the novel radiotracer. To investigate the formation of a tetramer, neutrAvidin, which shows high affinity to biotin, was derivatized with a deferoxamine chelator (DFO, *p*isothiocyanato-benzyl-deferoxamine) and radiolabeled with gallium-68. [^{68}Ga]Ga-DFO-neutrAvidin was investigated in combination with the biotinylated non-binder MC-Myc-Bio as well as with the FAPbinder MC-FA-010-bio. Due to tetramer formation a more than 12-fold higher uptake (12.13 %) was observed for the CHO-K1-huFAP cells. Furthermore, a strongly increased avidity was achieved for the MC-FA-010-biotin-avidin-tetramer.

Introduction

The most accurate and early diagnosis of tumors is essential for a promising approach to individualized therapy in cancer. Functional molecular imaging techniques such as positron emission tomography (PET) can provide critical information about the presence and quantity of tumor associated proteins using cancer-specific structures. The pharmacological properties of radiopharmaceuticals, consisting of a biomolecule (targeting vector) and a radionuclide, are comtrolled mainly by the targeting vector. Especially small molecules show very favorable pharmacokinetics and provide a high contrast in tumor imaging. Otherwise, only a few small molecules are able to supply high tumor selectivity and specificity, as for example biomacromolecules such as monoclonal antibodies and proteins. [1] On the other hand, biomacromulecules generally show slow pharmacokinetics and long circulation times, which is

unfavorable for PET imaging using short-lived radionuclides. Therefore, smaller molecules such as peptides and peptidomimetics as well as fragmented antibodies (Fab) are of interest. Though those molecules show attractive pharmacokinetics, they are very sensitive in biological systems and to chemical influences. To further improve the thermal and proteolytic stability of peptides, cysteineknot microbodies have been developed within the last years offering very fast pharmacokinetics as well as biological, metabolical and chemical stability. [2-4] These highly selective and cancer-specific molecules enable not only a clear localization and distribution of tumors, but can also be used to select patients for a cancer therapy with specific ligands binding to the detected associated tumor proteins. Classical anti-cancer therapy normally suffers from poor selectivity and toxic side effects to healthy tissue. The use of toxins conjugated to specific ligands would not harm healthy cells and therefore optimize the therapy results for the patient. [5]

The serine protease FAP (fibroblast activation protein alpha, also named seprase) is selectively overexpressed in reactive stromal fibroblasts in more than 90 % of human epithelial tumors such as breast, lung and colorectal cancers with little to no expression in normal fibroblasts or other normal tissues [6] as well as in bone and soft tissue sarcomas [7-9] making it an attractive target for cancer therapy and diagnosis of a variety of carcinomas.

Already in 1994, a ^{131}I-labeled murine monoclonal antibody ([^{131}I]I-mAbF19) was reported with selectivity to FAP and accumulation in tumor stromal tissue. [10] Due to the formation of anti-mouse antibodies in patients after application of repeated doses, *sibrotuzumab*, a human monoclonal antibody was developed from F19. [11] After several phase I and II studies, sibrotuzmab failed in 2003 because the minimum of at least one complete or partial remission of four patients with stable disease was not met. [12] But still, FAP displays a very potential target for high precise diagnostic and efficient therapy due to selective expression at various epithelial cancer types. Therefore, new targeting vectors such as microbodies need to be identified and evaluated as radiolabeled derivatives.

Microbodies, so called "*knottins*", are based on 30-50 amino acids and show a remarkable chemical and thermal stability due to a unique knotted topology of three disulfide bonds. [2-4, 13-14] Hereby these cystine-knot peptide-based molecules combine bioactivity with very high stability. Due to their small size these polypeptides generally provide fast tumor targeting and short *in vivo* half-lifes compared to biomacromulecules such as monoclonal antibodies. [6] The first engineered cystine knot peptide was reported by Kimura *et al.* in 2009, showing high affinities to $\alpha_V\beta_3$ integrins. [15,16] Derivatives of this microbodies 2.5 labeled with optical and positron emission tomography (copper-64, fluorine-18) imaging probes have been later on evaluated by various groups. [6,17-20] Furthermore, first preliminary studies using ^{177}Lu-labeled knottin peptides (2.5D and 2.5F) for integrin receptormediated radionuclide therapy have been reported. [21] The latest approach deals with tumor

targeted drug delivery using knottin peptides conjugated to gemcitabine, a chemotherapeutic agent. The EETI-2.5-Val-Ala-PAB-gemcitabine showed selective binding to tumor associated integrins and releases its cytotoxic payload inside the tumor tissue. [5]

These examples show impressively the high potential of knotted peptides for tumor imaging and therapy. In the following, we present a novel ^{68}Ga-labeled microbody, which can be used for FAPbased tumor imaging via positron emission tomography.

Experimental procedure

General

Regents and solvents were purchased from Acros Organics, Alfa Aesar, Fisher Scientific, Fluka, Merck, Sigma Aldrich and VWR and used without further purification. 1,4,7,10-tetraazacyclododecane1,4,7,10-tetraacetic acid (DOTA was purchased from CheMatech and NeutrAvidin from Thermo Fisher Scientific. Reactions were monitored using thin layer chromatography (Merck silica gel 60 F254) or high-performance liquid chromatography (HPLC). FD and ESI mass spectrometry were performed on a MAT 95-MS 7500 CE and a HP 4500 (Agilent Technologies and Hewlett-Packard, respectively, both Santa Clara, Ca, USA).

Semi preparative and analytical HPLC was performed with a Dionex HPLC system equipped with a 680 HPLC pump and a UVD170U UV-detector (210 nm, 230 nm, 254 nm and 286nm) using a reversedphase column (semi preparative column: Luna, C18, 5 µm, 250x10 mm; analytical column: Luna, C18, 5 µm, 250x4.6 mm) at a flow rate of 3.5 mL/min for the semi preparative column and 1.0 mL/min for the analytical column.

Analytical radio-HPLC was performed on a LaChrom HPLC (Merck) equipped with a Hitachi pump L7100, a UV detector L7400 and a GabiStar radiodetector (Raytest). An analytical column (Chromolith performance, RP-18e, 100-4.6 mm) was used at a flow rate of 2.5 mL/min.

Microbody synthesis

The synthesis of the presented microbodies was carried out by the BioNTech AG. In principle, new engineered target specific microbodies can be achieved by three possible methods: (1) molecular modeling, (2) grafting of a known binding motif into established microbodies (*peptide* grafting) or (3) evolutionary protein design (*library screening*). The BioNTech AG established a phage display system that allows functional microbodies presentation and generated a combinatorial library with a high clonal diversity of > 10^{10}. After phage selection against the extracellular domain of human FAP, enriched pools are sub-cloned into an expression vector for recombinant production in *E. coli*. After purification

of the variants and expression analysis via SDS-PAGE hit identification is done by ELISA. Identified binders are finally produced in a higher scale and characterized in depth using different protein and cell based assays.

Organic Chemistry

MC-FA-012

The first binder with affinity to the human FAP in nanomolar range produced by the BioNTech AG was MC-FA-010. This microbody showed effective binding in non-radioactive binding assays (data not shown). Since selective modification at the N-terminus was not possible with this derivative due to a lysine moiety, the alanine-substituted derivative MC-FA-012 has been developed. This derivative still exhibits a favorable receptor affinity (data not shown) and was now derivatized with a DOTA chelator (1,4,7,10-tetraazacyclododecane-1,4,7,10-tetraacetic acid) for radiolabeling with gallium-68.

DOTA-MC-FA-012

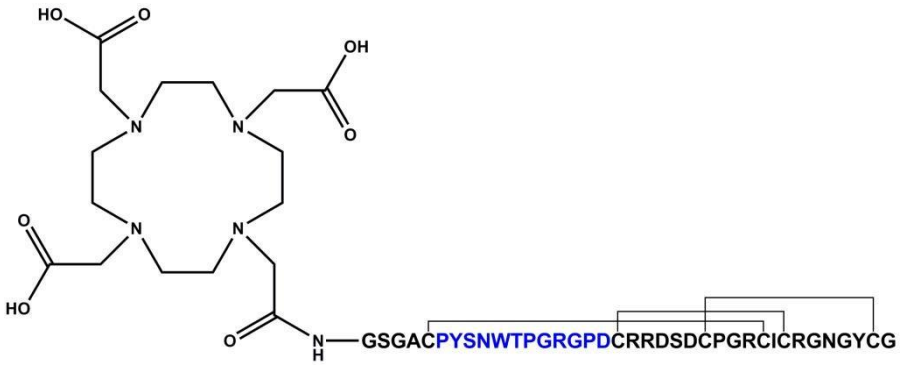

Scheme 1: Chemical structure of DOTA-MC-FA-012.

MC-FA-012 (3.2 mg, 0.82 µmol) was dissolved in a 2:1 mixture (1 mL) of a 0.25M phosphate buffer (pH 7.8) and acetonitrile. DOTA-NHS ester (2.3 mg, 3.08 µmol) in water (1 mL) was added and the pH of the reaction mixture was adjusted to 8 using sodium hydroxide solution (2M). After 2 h of stirring, HPLC-MS showed only the mass of DOTA-MC-FA-012. After semi-preparative HPLC purification (15 % to 35 % MeCN in 25 min, 3.5 mL/min, R_t: 12.8 min) and lyophilization the product (2.59 mg, 0.61 µmol, 74 %) was obtained as a colorless solid.

DFO-NeutrAvidin

NeutrAvidin, a glycolsylated version of avidin with a mass of 60 kDa, is a tetramer with a high affinity to biotin (K_D=10^{-15}M). Due to the removal of carbohydrate, the binding affinity to lectin is reduced to a not detectable level while the affinity to biotin is maintained. Due to a near-neutral isoelectric point

(pH 6.3) NeutrAvidin shows reduced non-specific interactions with the negatively charged cell surface compared to avidin. The lysine residue enables derivatization such as conjugation of a chelator molecule. [22,23]

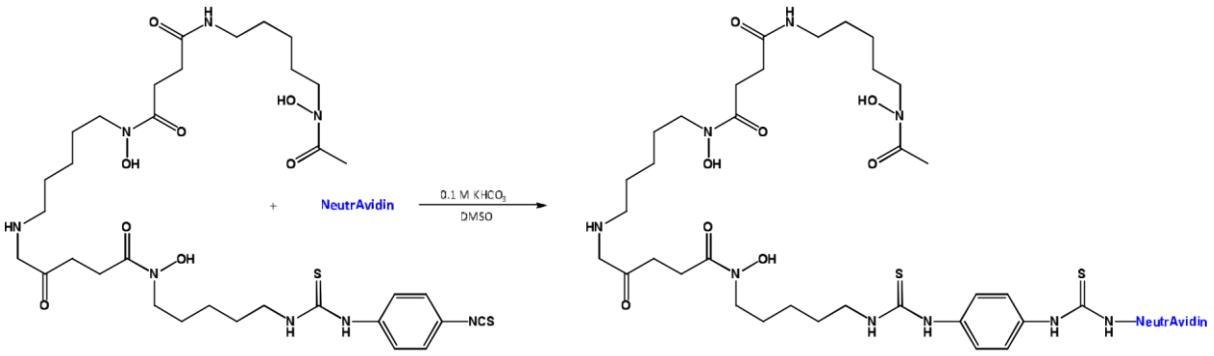

Scheme 2: Synthesis of DFO-NeutrAvidin.

NeutrAvidin (4 mg, 50 nmol) was dissolved in $KHCO_3$ (0.1 M, 500 µL) and *p*-isothiocyanato-benzyldesferroxamine *(DFO,* Df-*p*-Bn-NCS, 0.18 mg, 250 nmol) in DMSO (500 µL) was added. After adjusting the pH to 9 using K_2CO_3 (0.2M) the reaction mixture was stirred for 1 h. Afterwards the reaction was purified using a PD10 desalting column (GE Healthcare Life Sciences). The column was eluted using 250 µL portions of acetate buffer (0.1M, pH 5.5). The fractions were analysed using thin-layer chromatography. After lyophilisation of the product fractions DFO-NeutrAvidin (2.3 mg, 28 nmol, 56 %) was obtained as a colorless solid.

Radiochemistry

Cation exchange based post processed gallium-68 was used for radiolabeling. Generators produced by Cyclotron Obninsk Ltd. Co. (Russia) and Eckert & Ziegler AG, Berlin (Germany) were used. First, the generator was eluted with hydrochloric acid solution (0.1M, 5 mL) and the gallium-68 was loaded on a cation exchange column (30 mg bed, DOWEX 50WX8). The cation exchange resin was flushed with N1 solution (80 % acetone, 20 % 0.1 M HCl, 1 mL) and 1 mL of air to remove impurities. Then, N2 solution (97.6 % acetone, 2.4 % 0.05 M HCl, 400µL) was applied and incubated for 2 min before eluting the gallium-68. Afterwards the cation exchange resin was regenerated using hydrochloric acid solution (4M, 1 mL) and water (1 mL).

[^{68}Ga]Ga-DOTA-MC-FA-012

After removing the acetone from the N2 fraction of gallium-68 elution, sodium acetate buffer (1 mL, 0.2 M, pH 4.5) and DOTA-MC-FA-012 (40 µL, 40 nmol) in water were added. The reaction mixture was stirred for 10 min at 90 °C. Due to RCYs ш98 % the reaction mixture was used without further purification and only neutralized using sodium hydroxide solution (2M) and PBS for dilution.

[^{68}Ga]Ga-DFO-NeutrAvidin

The radiolabeling of NeutrAvidin was performed using the N2 fraction of gallium-68 elution (after removing of acetone) and DFO-NeutrAvidin (100 µL, 130 µg) in sodium acetate buffer (500 µL, 0.05M). The mixture was heated at 40 °C for 10 min and used without any further purification due to RCY ш95 %.

Stability test in human serum albumin

Solutions of [^{68}Ga]Ga-DOTA-MC-FA-012 and [^{68}Ga]Ga-DFO-NeutrAvidin (200 µL, approximately 4 MBq) were incubated with 500 µL human serum albumin (HSA) at 37 °C for 1 and 2 h. After incubation plasma proteins were precipitated using 600 µL cold acetonitrile and centrifugation (10.00 rpm, 10 min). An aliquot (100 µL) of both time points was injected into an analytical radio-HPLC system (Chromolith performance, RP-18e, 100-4.6 mm, with the following conditions: flow 2.5 mL/min, 0 – 0.5 min isocratic 95 % A, 0.5 – 0.6 min gradient 60 % A, 0.6 – 5 min isocratic 60 % A, 5 – 5.5 min gradient 95 % A, 5.5 – 7 min isocratic 95 %, with eluent A was H_2O + 0.1 % TFA and eluent B was acetonitrile + 0.1 % A). Each experiment was carried out in triplicates.

In vitro studies

For first *in vitro* studies of the novel radiolabeled FAP-binding microbody MC-FA-012/010, targetpositive CHO-K1-huFAP and target-negative CHO-K1-MOCK cells were used adherent in 24 well-plates (0.5 x 10^6 cells per well). The aim of this study was to show specific uptake of MC-FA-012 in FAPpositive cells and investigate the effect of NeutrAvidin-mediated tetramerization of MC-FA-010 on the uptake of this microbody.

uptake studies

First, DOTA-MC-FA-012 was radiolabeled with gallium-68 and the cells were incubated with three different tracer concentrations (4nM, 40nM and 400nM) for 45 min at 37 °C. For the second part of the study [^{68}Ga]Ga-DOTA-MC-FA-012 (794nM) and [^{68}Ga]Ga-DFO-NeutrAvidin (43 nM) alone and in combination with the biotinylated non-binder MC-Myc-010-Bio (225nM) and the FAP-binder MC-FA010-Bio (225nM) (figure 1) were applied to both cell types. Biotinylated microbodies were used in a ratio ш 5 compared to NeutrAvidin. The [^{68}Ga]Ga-DFO-NeutrAvidin alone and in combination with the non-binder should not bind at all to both cell types, while an increased uptake was expected for the [^{68}Ga]Ga-DFO-NeutrAvidin in combination with MC-FA-010-Bio due to the formation of a tetramer (avidity effect, figure 1).

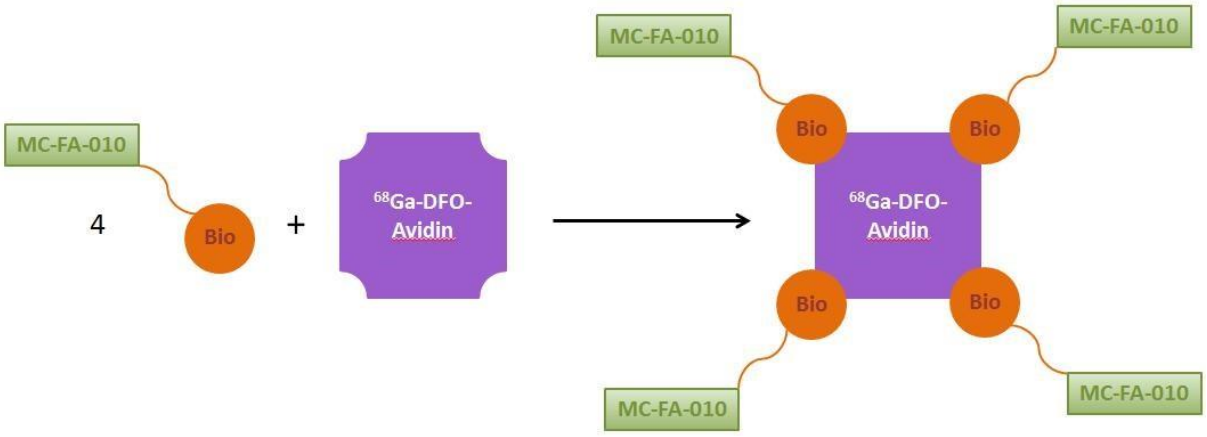

Figure 1: Schematic diagram of the avidin-biotin interaction. NeutrAvidin can bind up to four biotin molecules, which are here conjugated to the microbody MC-FA-010.

After incubation the cells were washed two-times with PBS and two-times with an acidic stripping buffer (pH 3, 0.1M acetic acid, 0.15M sodium chloride). The activity of the supernatant, the stripping buffer (extracellular signal) and the cells (intracellular signal) were measured in a gamma counter.

Results and Discussion

Organic Chemistry

The conjugation between the MC-FA-012 amine and the DOTA-NHS ester was performed in phosphate buffer with a twofold excess of DOTA-NHS. Higher buffer concentrations (0.25 M) resulted in a very effective and robust synthesis strategy. Analytical evaluation using LC-MS measurements confirmed very good yields of ш90 %.

NeutrAvidin was conjugated to the DFO-chelator via its lysine residue and the isothiocyanato group of Df-*p*-Bn-NCS. A $KHCO_3/K_2CO_3$ buffer system was used for the reaction and PD 10 desalting columns for purification of the product.

Radiochemistry

Radiolabeling reaction of both derivatives proceeded with excellent radiochemical yields ш95 % (determined by analytical radio-HPLC and TLC, figure 2) and radiolabeled products were used without further purification. For cell experiments the labeling solution was neutralized using sodium hydroxide solution (2M) and diluted with PBS.

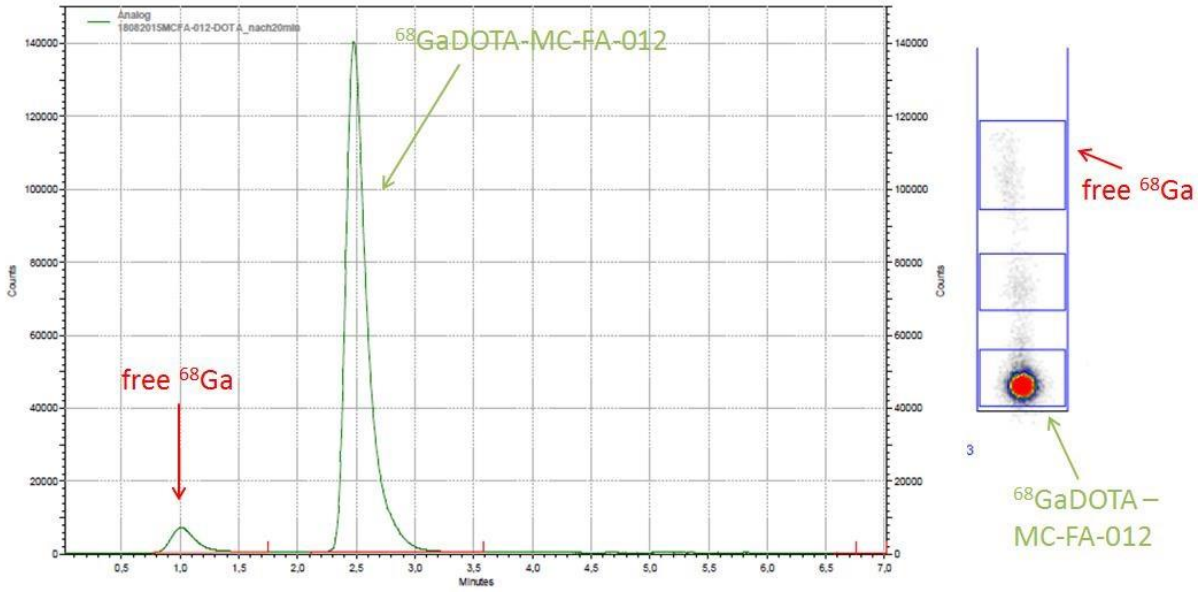

Figure 2: Analytical radio-HPLC chromatogram and TLC of the crude reaction mixture of the radiosynthesis of [^{68}Ga]Ga-DOTAMC-FA-012. Analytical radio-HPLC was performed with a Chromolith performance column, RP-18e, 100-4.6 mm, with the following conditions: flow 2.5 mL/min, 0 – 0.5 min isocratic 95 % A, 0.5 – 0.6 min gradient 60 % A, 0.6 – 5 min isocratic 60 % A, 5 – 5.5 min gradient 95 % A, 5.5 – 7 min isocratic 95 %, with eluent A was H_2o + 0.1 % TFA and eluent B was acetonitrile + 0.1 % A. For the TLC a citrate buffer was used.

Stability studies in human serum albumin

To evaluate the stability of [^{68}Ga]Ga-DOTA-MC-FA-012 and [^{68}Ga]Ga-DFO-NeutrAvidin (200 µL, approximately 4 MBq) they were incubated in human serum albumin (HSA) at 37 °C for 1 and 2h. Both

radiolabeled molecules showed a stability of ш95 % and no significant release of gallium-68 from the chelator was observed. Therefore, they can both be considered to be stable for the general duration of cell studies and µPET scans (1-2h) as shown in figure 3.

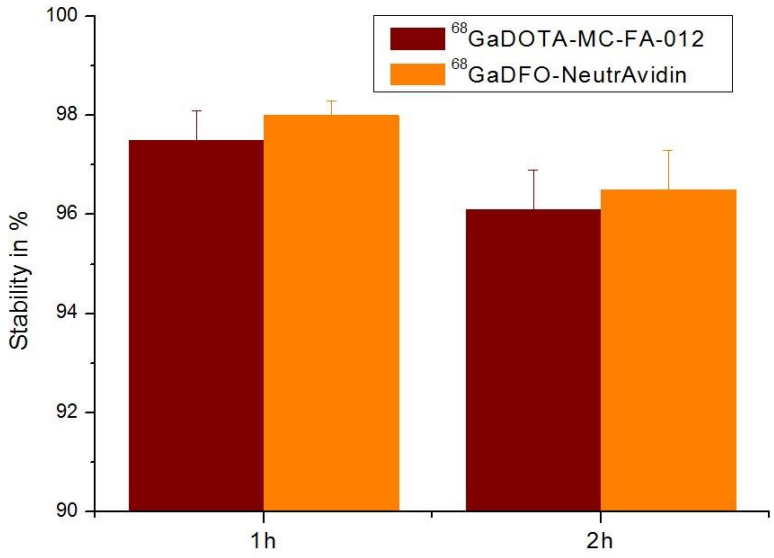

Figure 3: Stability of [^{68}Ga]Ga-DOTA-MC-FA-012 and [^{68}Ga]Ga-DFO-NeutrAvidin in human serum albumin at 37 °C over 1 and 2 h. Error are given as standard deviation representing n=3.

In vitro studies

Uptake studies

The ^{68}Ga-labeled FAP binder DOTA-MC-FA-012 was tested using human FAP positive (CHO-K1-huFAB) and FAP negative (CHO-K1-MOCK) cells. First we performed a time-dependency uptake study varying the time points from 5 to 120 min with an incubation concentration of 400nM. Figure 4 shows the activity in the cells (intracellular signal), which was obtained after washing with the acidic stripping buffer. Within the first 30 min after tracer application, a strong increase of radioactivity in the CHO-K1huFAP cells was observed. Much longer incubation did not yield in a significant higher uptake. Therefore, for the following experiments, the cells were incubated with the tracer solution for 45 min.

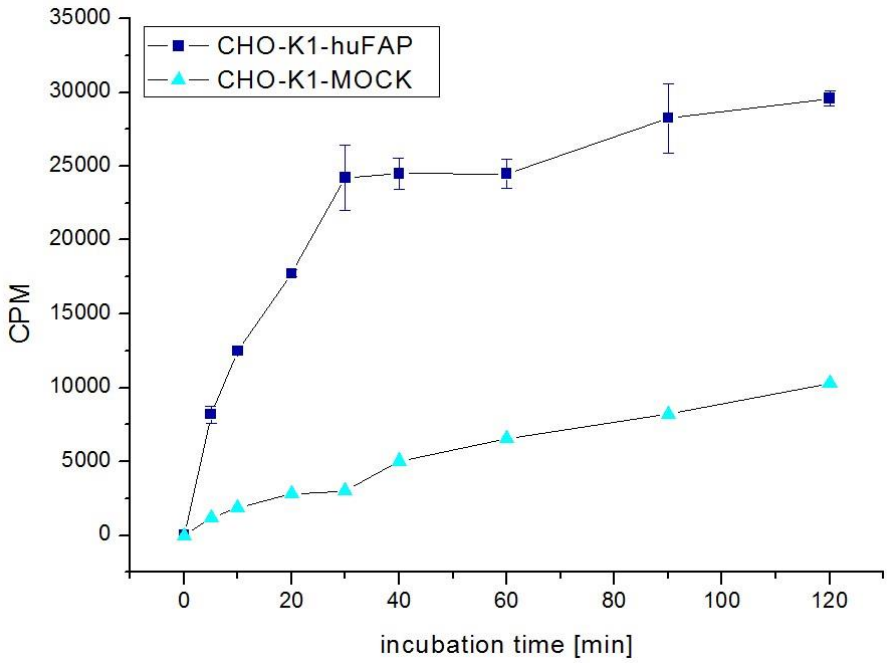

Figure 4: Internalization (intracellular signal) of [^{68}Ga]Ga-DOTA-MC-FA-012 (400 nM) in huFAP positive CHO-K1-huFAPcells and huFAP negative CHO-K1-MOCK cells at 37 °C from 5 to 120 min. Errors are given as standard deviation representing n-3.

Figure 5 displays the results of uptake studies with [^{68}Ga]Ga-DOTA-MC-FA-012 at concentrations of 4, 40 and 400nM for 45 min at 37 °C. A concentration-dependent increase of activity in FAP positive cells was observed when increasing the incubation concentration from 4 to 400nM. For FAP negative cells, a clearly reduced internalization of the radiotracer was observed. However, these experiments prove the FAP specific uptake of FAP binder MC-FA-012 into target positive cells (CHO-K1-huFAP).

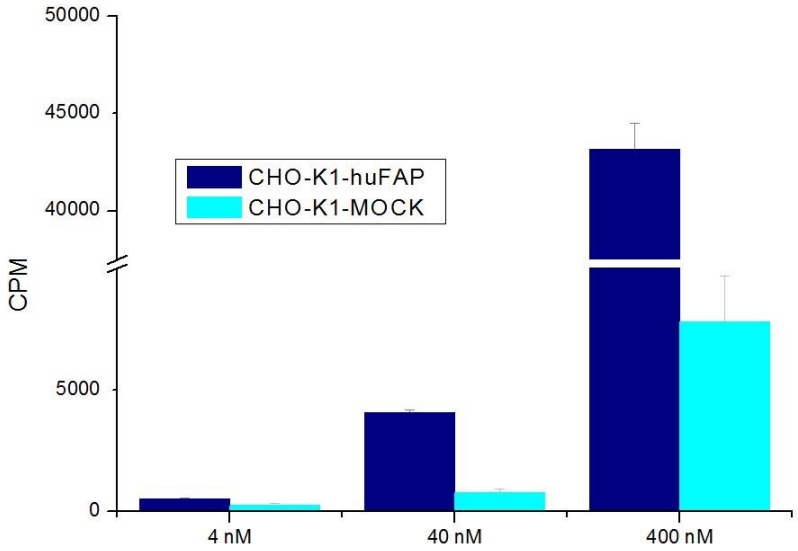

Figure 5: Internalization of [^{68}Ga]Ga-DOTA-MC-FA-012 in huFAP positive CHO-K1-huFAP cells and huFAP negative CHO-K1MOCK cells at 37 °C for 45 min. Errors are given as standard deviation representing n=3.

Table 1: Comparative results of the CHO-K1-huFAP and CHO-K1-MOCK cell-based assay in 24-well plates.

		[^{68}Ga]Ga-DOTA-MC-FA-012		
% binding (specific)	internal	4 nM (2 pmol)	40 nM (20 pmol)	400 nM (200 pmol)
	external	2.05 ± 0.16	1.50 ± 0.03	1.27 ± 0.04
		4.11 ± 0.15		
		3.49 ± 0.05	2.44 ± 0.00	
neg/pos ratio	internal	47.31 %	20.67 %	18.11 %
	external	23.60 %	4.87 %	8.61 %
pmol peptide binding	internal	0.04	0.30	2.54
	external	0.08	0.70	4.88

Table 1 and figure 6 provide an overview of the percentage uptake and distribution of the applied activity between internalized and surface-bound amount of [^{68}Ga]Ga-DOTA-MC-FA-012. An average of 1.5 % of the applied activity was internalized into CHO-K1-huFAP cells, which equals a peptide amount between 0.04 pmol for an incubation concentration of 4nM and 2.54 pmol for 400nM. Additionally, around 3 % (0.08 – 4.88 pmol peptide) of [^{68}Ga]Ga-DOTA-MC-FA-012 were surface-bound (extracellular signal), which adds also to a diagnostic or therapeutic effect of the radiotracer. Interestingly, the difference between unspecific and specific tracer uptake becomes more distinctive with higher tracer concentrations (from around 50 % for 4nM to fewer than 20 % for 400nM). This means that the tracer uptake becomes somehow more specific with higher concentrations. Normally, the unspecific binding is expected to increase lineary with tracer concentration, but showed a saturation effect. Finally, about 94 % of [^{68}Ga]Ga-DOTA-MC-FA-012 were not bound.

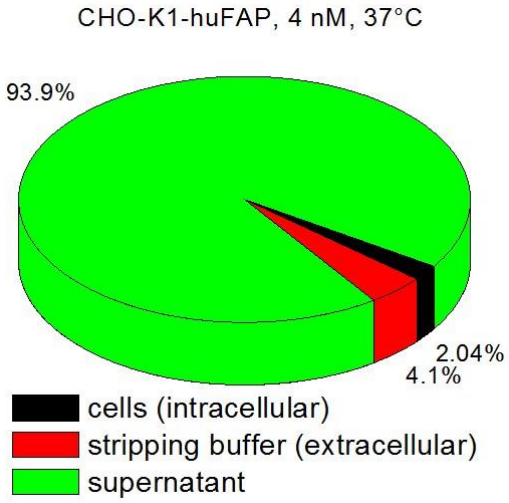

Figure 6: Pie chart of the [^{68}Ga]Ga-DOTA-MC-FA-012 distribution after incubation (45 min) within one sample of CHO-K1huFAP cells.

To investigate the influence of the formation of a MC-FA-010 tetramer, CHO-K1-huFAP and CHO-K1-

MOCK cells were incubated with [^{68}Ga]Ga-DFO-NeutrAvidin in combination with the non-binder MCMyc-010-Bio as well as with the FAP binder MC-FA-010-Bio for 45 min. As expected, for NeutrAvidin alone as well as in combination with the non-binder MC-Myc-010-Bio no binding (neither intracellular nor extracellular) was observed for both cell lines. Table 2 shows that due to the formation of a tetramer an almost 4-fold higher (pmol peptide) accumulation (intracellular signal) of MC-FA-010 was observed in FAP positive cells. The effect becomes even clearer when comparing the percentage uptake of applied activity into the cells (12.13 % compared to 0.84 %) due to the formation of a tetramer. For this experiment, [^{68}Ga]Ga-DOTA-MC-FA-012 was applied in a concentration of almost 800nM to the cells. This higher concentration additionally improved the uptake ratio between negative and positive cells (7.14 %) and therefore increases the specificity of the uptake.

Table 2: Comparative results of the CHO-K1-huFAP and CHO-K1-MOCK cell-based assay in 24-well plates.

		[^{68}Ga]Ga-DFO-MC-FA-012	[^{68}Ga]Ga-DFO-NeutrAvidin	[^{68}Ga]Ga-DOTA-NeutrAvidin + MC-Myc-010-Bio	[^{68}Ga]Ga-DFO-NeutrAvidin + MC-FA-010-Bio
% binding (specific)	pos	0.84 ± 0.05	0.05 ± 0.01	0.05 ± 0.00	12.13 ± 2.59
	neg	0.06 ± 0.01	0.04 ± 0.01	0.04 ± 0.01	0.06 ± 0.01
neg/pos ratio		7.14 %			0.49 %
pmol peptide binding	pos	3.68	0.01	0.05	13.04
	neg	0.26	0.01	0.04	0.06

Figure 7 illustrates again the effect of tetramer formation on the uptake of gallium-68 into FAP positive cells. With [^{68}Ga]Ga-DFO-NeutrAvidin alone as well as with the non-binder MC-Myc-010-Bio only background signal was observed for the positive and negative cells. In addition, for the NeutrAvidin-biotin–tetramer not only the uptake was higher but also the difference between positive and negative cells. The unspecific binding was reduced to below 1 % compared to the uptake in target positive cells.

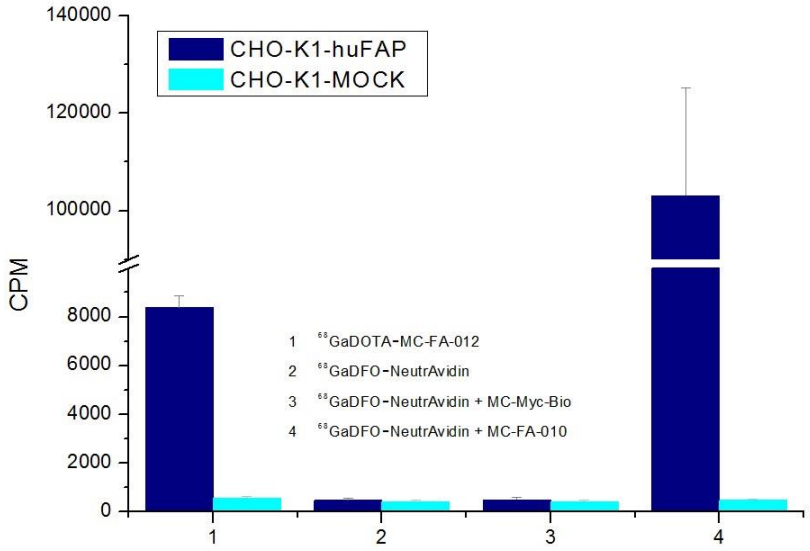

Figure 7: Internalization (intracellular signal) of ^{68}Ga-labeled MC-FA derivatives in FAP positive CHO-K1-huFAP cells and FAP negative CHO-K1-MOCK cells at 37 °C for 45 min. Errors are given as standard deviation representing n-3.

Conclusions

A novel microbody with selectivity to the fibroblast activation protein was identified and produced in higher scale by the BioNTech AG. It was then derivatized with a chelator for complexation of gallium68 respectively with biotin for the binding to avidin. For the indirect radiolabeling of MC-FA-010-Bio, NeutAvidin was derivatized with DFO for complexation of gallium-68. Almost quantitative radiolabeling (ш95 %) was observed for [^{68}Ga]Ga-DOTA-MC-FA-012 and [^{68}Ga]Ga-DFO-NeutrAvidin, wherefore no further purification was necessary. *In vitro* evaluation showed very high specific accumulation of the direct as well as of the indirect labeled MC-FA-012/010 in target positive cells. The formation of a NeutrAvidin-biotin tetramer further increased the accumulation of applied activity in CHO-K1-huFAP cells. Furthermore, an enhanced specificity was achieved due to the MC-FA-010biotin-avidin-tetramer. In conclusion, this novel FAP-specific microbody is a very promising candidate for further *in vivo* evaluation as diagnostic and therapeutic tool.

Ethical statement

All experiments with commercial available human serum (Sigma Aldrich, H4522, from human male AB plasma) were conducted in accordance with the local law and national and institutional guidelines and ethics. The officer for biological safety has approved the performed experiments and informed consent was obtained for any experiment with commercial available human serum.

Acknowledgments

The authors thank the Max Planck Graduate Center, the Graduate School of the SFB 1066 and the Ci3Cluster of Excellence for supporting Kathrin Kettenbach.

REFERENCES

[1] Z. Miao, G. Ren, H. Liu, R. H. Kimura, L. Jiang, J. R. Cochran, S. S. Gambhir and Z. Chenz, "An engineered knottin peptide labeled with 18F for PET imaging of integrin expression. *Bioconjugate Chemistry*, 20 (12), 2342–2347.

[2] S. J. Moore, C. L. Leung, and J. R. Cochran, "Knottins: disulfide-bonded therapeutic and diagnostic peptides," *Drug Discovery Today*, vol. 9, no. 1, pp. e1-e70, 2012.

[3] L. Thorstholm, and D. J. Craik, "Discovery and applications of naturally occurring cyclic peptides," *Drug Discovery Today*, vol. 9, no. 1, pp. e1-e7, 2012.

[4] S. L. Carney, "Peptides or modified peptides as drug molecules," *Drug Discovery Today,* 9 (1), e1e70, 2012.

[5] N. Cox, J. R. Kintzing, M. Smith, G. A. Grant, J. R. and Cochran, "Integrin-Targeting Knottin Peptide-Drug Conjugates Are Potent Inhibitors of Tumor Cell Proliferation," *Angewandte Chemie International Edition*, vol. 55, no. 34, pp. 9894–7, 2016.

[6] R. Liu, H. Li, L. Liu, J. Yu, and X. Ren, "Fibroblast activation protein: A potential therapeutic target in cancer," *Cancer Biology & Therapy*, vol. 13, no. 3, pp. 123–9, 2012.

[7] P. Garin-Chesa, L. J. Old, and W. J. Rettig, "Cell surface glycoprotein of reactive stromal fibroblasts as a potential antibody target in humen epithelial cancers," *Proceedings of the National Academy of Science of the USA*, vol. 87, no. 18, pp. 7235-9, 1990.

[8] W. J. Rettig, P. Garin-Chesa, H. R. Beresford,H. F. Oettgen, M. R. Melamed, and L. J. Old, "Cellsurface glycoproteins of human sarcomas differential expression in normal and malignant tissues and cultured cells," *Proceedings of the National Academy of Science of the USA*, vol. 85, no. 9, pp. 3110-4, 1988.

[9] M. L. Pineiro-Sanchez, L. A. Goldstein, J. Dodt, L. Howard, Y. Yeh, H. Tran, W. S. Argraves, and W. T. Chen, "Identification of the 170-kDa Melanoma Membrane-bound Gelatinase (Seprase) as a Serine Integral Membrane Protease," The *Journal of Biological Chemistry*, vol. 272, no. 12, pp. 7595-601, 1997.

[10] S. Welt, C. R. Divgi, A. M. Scott, P. Garin-Chesa, R. D. Finn, M. Graham, E. A. Carswell, A. Cohen, S. M. Larson, and L. J. Old, "Antibody Targeting in Metastatic Colon Cancer: A Phase I Study of Monoclonal Antibody F19 Against a Cell-Surface Protein of Reactive Tumor Stromal Fibroblasts," *Journal of Clinical Oncology*, vol. 12, no. 6, pp. 1193-203, 1994.

[11] P. Tanswell, P. Garin-Chesa, W. Rettig, S. Welt, C. R. Dicgi, E. S. Casper, R. D. Finn, S. M. Larson, L. J. Old, and A. M. Scott, "Population pharmacokinetics of antifibroblast activation protein monoclonal antibody F19 in cancer patients," *British Journal of Clinical Pharmacology*, vol. 51, no. 2, pp.177-80, 2001.

[12] R. D. Hofheinz, S. E. al-Batran, F. Hartmann, G. Gartung, D. Jäger, C. Renner, P. Transwell, U. Kunz, A. Amelsberg, H. Kuthan, and G. Stehle, "Stromal antigen targeting by a humanised monoclonal antibody: an early phase II trial of sibrotuzumab in patients with metastatic colorectal cancer," *Onkologie*, vol. 26, no. 1, pp. 44–8, 2003.

[13] A. Heitz, O. Avrutina, D. Le-Nguyen, U. Diederichsen, J.-F. Hernandez, J. Gracy, H. Kolmar, and L. Chiche, "Knottin cyclization: impact on structure and dynamics," *BMC structural biology*, 8, 5473, 2008.

[14] L. Le Nguyen, A. Heitz, L. Chiche, B. Castro, R. A. Boigegrain, A. Favel, and M. A. Coletti-Previero, " Molecular recognition between serine proteases and new bioactive microproteins with a knotted structure," *Biochimie*, vol. 72, no. 6-7, pp. 431-5, 1990.

[15] R. H. Kimura, A. M. Levin, F. V. Cochran, and J. R. Cochran,"Engineered cystine knot peptides that bind $alpha_v beta_3$, $alpha_v beta_5$, and $alpha_5 beta_1$ integrins with low-nanomolar affinity," *Proteins*, vol. 77, no. 2, pp. 359–69, 2009.

[16] A. P. Silverman, A. M. Levin, J. L. Lahti, and J. R. Cochran, "Engineered cystine-knot peptides that bind alpha(v)beta(3) integrin with antibody-like affinities," *Journal of Molecular Biology*, vol. 385, no. 4, pp. 1064–75, 2009.

[17] R. H. Kimura, Z. Cheng, S. S. Gambhir, and J. R. Cochran, "Engineered Knottin Peptides: A New Class of Agents for Imaging Integrin Expression in Living Subjects," *Cancer Research*, vol. 69, no. 6, pp. 2435–42, 2009.

[18] L. Jiang, R. H. Kimura, Z. Miao, A. P. Silverman, G. Ren, H. Liu, P. Li, S. S. Gambhir, J. R. Cochran, and Z. Chenz, "Evaluation of a (64)Cu-labeled cystine-knot peptide based on agouti-related protein for PET of tumors expressing alphavbeta3 integrin," *Journal of Nuclearl Medicine*, vol. 51, no. 2, pp. 251–8, 2010.

[19] R. H. Kimura, Z. Miao, Z. Cheng, S. S. Gambhir, and J. R. Cochran, "A Dual-labeled knottin pepdtide for PET and Near-infrared fluorescence imaging of intregrin expression in living subjects," *Bioconjugate Chemistry*, vol. 21, no. 3, pp. 436-44, 2010.

[20] S. Liu, H. Liu, G. Ren, R. H. Kimura, J. R. Cochran, and Z. Cheng, "PET Imaging of Integrin Positive Tumors Using ^{18} F Labeled Knottin Peptides," *Theranostics*, vol. 1, pp. 403–12, 2011.

[21] L. Jiang, Z. Miao, R. H. Kimura, H. Liu, J. R. Cochran, C. S. Culter, A. Bao, P. Li, and Z. Cheng, "Preliminary evaluation of (177)Lu-labeled knottin peptides for integrin receptor-targeted radionuclide therapy," *European Journal of Nuclear Medicine and Molecular Imaging*, vol. 38, no. 4, pp. 613–22, 2011.

[22] Y. Hiller, J. M. Gershoni, E. A. Bayer, and M. Wilcheck, "Biotin binding to avidin. Oligosaccharide side chain not required for ligand association," *Biochemical Journal*, vol. 248, no. 1, pp. 167-71, 1987.

[23] A. T. Marttila, O. H. Laitinen, K. J. Airenne, T. Kulik, E. A. Bayer, M. Wilchek, and M. S. Kulomaa, "Recombinant NeutraLite Avidin: a non-glycosylated, acidic mutant of chicken avidin that exhibits high affinity for biotin and low non-specific binding properties," *FEBS* Letters, vol. 467, no. 1, pp. 31-6, 2000.

6. List of publications

6. List of publications

"^{18}F-labeling using click cycloaddtions"

K. Kettenbach, H. Schieferstein, T. L. Ross, BioMed Research International, 2014, dx.doi.org/10.1155/2014/361329

"Synthesis and evaluation of boron folates for Boron-Neutron-Capture-Therapy (BNCT)"

K. Kettenbach, H. Schieferstein, C. Grunewald, D. Iffland, L. M. Reffert, G. Hampel, C. L. Schütz, N. H. Bings, T. L. Ross, Radiochimica Acta, 2015, 103, 11, 799-809

"A ^{18}F-labeled Dibenzocyclooctyne(DBCO)-Derivative for Copper-free Clicj Labeling of Biomolecules"

K. Kettenbach, T.L. Ross, MedChemComm, 2016, 7, 654-657

"Orthogonal Click Conjugation to the Liposomal Surface Reveals the Stability of the Lipid Anchorage as Crucial for Targeting"

T. Fritz, M. Voigt, M. Worm, I. A. Negwer, S. S. Müller, K. Kettenbach, T. L. Ross, F. Rösch, K. Koynov, H. Frey, M. Helm, Chemistry – A European Journal, 2016, 22, 33, 11578-11586.